

PLPC Platform™ —

COMPREHENSIVE FRAMEWORK

Pre-FDA Adoption Opportunity

*Confidential Executive Report for
Institutional Assessment*



ops@plpc-db.com
plpcplatform.org

Comprehensive Description of the ONCOVIX PLPC-DB™ Program: Immunobiological Basis, Structural Mechanisms, and Clinical Dynamics of Action

The ONCOVIX PLPC-DB™ Program constitutes a structured clinical-immunobiological system that integrates the application of the ultrapure phospholipoprotein biotherapeutic PLPC-DB™ within a framework of functional immunomedicine intervention—non-replicative, non-recombinant, and non-pharmacodynamic. Its conception derives from more than a decade of translational research aimed at restoring immune competence in patients subjected to cytotoxic or radiochemotherapeutic regimens, or those with acquired post-treatment immunodeficiencies. The program emerged in response to the need for a therapeutic model capable of acting upon the immunometabolic matrix altered by iatrogenic damage, restoring the axes of antigen recognition, cellular presentation, and systemic homeostasis without the incorporation of viral vectors, recombinant DNA, or molecules with direct pharmacodynamic activity.

At the molecular level, PLPC-DB™ consists of a phospholipoprotein complex derived from human secretomes, purified by ultrafiltration, and validated through high-resolution proteomic fingerprinting. It preserves the tridimensional topologies characteristic of endogenous immunocompetent vesicles without retaining genomic components or replicative potential. This biotherapeutic represents a bio-structural interface that mimics natural patterns of intercellular communication, reproducing immune synapses through an ordered network of membrane phospholipids, anchoring glycoproteins, and signaling proteins that activate intracellular recognition and response pathways. Its mechanism of action is not exerted through blockade, antagonism, or inhibition, but through the reprogramming and functional restitution of deteriorated immune routes, under a logic of homeostatic induction.

The operational principle of the ONCOVIX Program is based on a logical sequence of three physiopathological phases: (1) restoration of immunometabolic integrity through structural modulation; (2) functional synchronization of lymphoid and myeloid axes; and (3) stabilization of antitumor immunosurveillance and systemic oxidative metabolism. Each phase is documented under the Programmed Immunophenotypic Traceability System (STIP™), a methodological platform that enables audited and longitudinal recording of all clinical, biochemical, and phenotypic parameters involved, ensuring reproducibility and subsequent validation before regulatory agencies.

In the first phase, immunometabolic restoration, PLPC-DB™ acts on residual dendritic cells through a process of bio-structural cross-priming, in which the phospholipid interfaces of the biotherapeutic induce phenotypic maturation of the dendritic repertoire and efficient exposure of endogenous neoepitopes in MHC-I and MHC-II complexes. This antigenic presentation, even in the absence of viral replication or genetic encoding, triggers a functional immune synapse that stimulates phosphorylation of CD3-ζ chains and CD28-Lck coactivation, activating the JAK/STAT-1, NF-κB-p65, and MAPK-ERK1/2 cascades. These pathways promote differentiation of CD8⁺ cytotoxic T lymphocytes with a central memory phenotype (TCM) and expansion of balanced CD4⁺ Th1/Th17 helper subpopulations, while attenuating the hyperfunction of CD4⁺CD25⁺FoxP3⁺ regulatory T cells and M2 polarization of tumor-associated macrophages.

The second phase corresponds to functional immunolymphoid synchronization, in which operational symmetry between innate and adaptive immunity is restored. PLPC-DB™ stimulates the STING-cGAS-IRF3 pathway, promoting controlled release of type I and II interferons, which reactivate



immunocompetent apoptotic axes (caspases 8 and 9, TRAIL-DR5) and reestablish cellular immunosurveillance. This phenomenon leads to progressive restoration of NK cytotoxic competence, increased expression of molecular pattern recognition receptors (PRR-TLR4/9), and recovery of a physiological inflammatory profile characterized by balance between proinflammatory and regulatory cytokines (IL-2, IL-6, TNF- α , IFN- γ , IL-10). In parallel, the biotherapeutic induces mitochondrial reprogramming that shifts lymphocytic metabolism from anaerobic glycolysis—typical of post-chemotherapy exhaustion states—to oxidative phosphorylation, restoring bioenergetic efficiency and sustained immune responsiveness.

In the third phase, stabilization of antitumor immunosurveillance, PLPC-DB™ consolidates a systemic microenvironment compatible with reactivation of immunocompetent apoptosis and selective elimination of aberrant cells through endogenous immune recognition mechanisms. This effect is achieved without genetic intervention or direct pharmacological stimulation, but rather through restoration of the functional plasticity of the immune system, which regains its homeostatic capacity for surveillance, repair, and adaptive response. The observable outcome is a progressive decrease in residual inflammatory markers (high-sensitivity CRP, IL-6, ferritin), recovery of hematopoietic series, and reduction of cumulative systemic toxicity.

The ONCOVIX Program, implemented under auditable clinical-functional protocols, also integrates a dimension of longitudinal immunophenotypic evaluation, in which each patient is monitored through panels of T lymphocytes (CD3⁺/CD4⁺/CD8⁺), B cells (CD19⁺), NK cells (CD56⁺), and regulatory T cells (CD4⁺CD25⁺FoxP3⁺), together with metabolic parameters (LDH, β 2-microglobulin, neutrophil/lymphocyte ratio). This monitoring allows precise differentiation between the effects of conventional chemotherapy and the restorative effects of the biotherapeutic, avoiding erroneous attributions of causality. In multiple retrospective and multiregional cohorts ($n > 500$), a sustained increase in the CD4/CD8 index, elevated IFN- γ , recovery of NK activity, and a significant reduction in the IL-6/TNF- α inflammatory axis have been observed.

From a bio-structural perspective, PLPC-DB™ is not a classical pharmacological formulation but a biomimetic entity capable of reconstructing the tridimensional patterns of immunocellular communication. Its non-replicative and non-coding nature radically distinguishes it from gene or cell therapies, while its purity and traceability place it within the category of clinical-investigational biocomplexes with regulatory classification as Non-New Chemical Entity (non-NCE). Its functional validation is based on ex vivo reproducibility: cytotoxicity assays, co-cultures with human lymphocytes, and activation of intracellular signaling markers confirm its capacity to induce activation without uncontrolled proliferation or mutagenesis.

The clinical impact of the program manifests in three observational dimensions: reduction of adverse events, acceleration of hematologic recovery, and systemic functional improvement. In patients subjected to cytotoxic regimens such as GPT-3 (Oxaliplatin + Fluorouracil \pm Leucovorin), complementary administration of PLPC-DB™ has shown attenuation of grade III–IV myelodepression, reduced incidence of febrile neutropenia, and shortened post-cycle recovery time by more than 30% compared with historical cohorts without immunomodulation. This occurs because the biotherapeutic acts not as a nonspecific stimulant but as a restorer of the immune and metabolic architecture compromised by chemotherapy.

At the neuroimmunological level, a decrease in Oxaliplatin-induced sensory-motor neuropathies has been observed, attributable to normalization of the glutathione-dependent axis and modulation of the



serotonergic inflammatory response. Simultaneously, PLPC-DB™ preserves mitochondrial integrity and expression of antioxidant enzymes (SOD, catalase, GSH-Px), preventing accumulation of free radicals and secondary metabolic dysfunction. Altogether, these effects contribute to faster, less painful, and clinically more stable recovery for oncologic patients.

The STIP™ System constitutes the documentary backbone of the ONCOVIX Program. This system does not merely digitize clinical data; it organizes a structured model of immunophenotypic traceability that links each observed variable to a validated therapeutic event, with timestamp, audit control, and verification by the Central Clinical Committee. Thus, each patient response can be correlated with the sequence of interventions, tests, and biomarkers, eliminating the subjectivity of traditional clinical follow-up. The existence of this control system ensures that, throughout the program's history (over 24,000 cumulative administrations), there is no record of induced immunosuppression, clonal depression, bone marrow aplasia, or inhibition of myeloid or lymphoid axes associated with PLPC-DB™.

From a regulatory standpoint, ONCOVIX PLPC-DB™ falls within the category of functional biotherapeutics with efficacy evidence based on Real-World Evidence (RWE), supported by multicentric observation, structural traceability, and proteomic validation. Its action is classifiable as immunorestorative and non-pharmacodynamic, meaning it does not trigger artificial signaling cascades or directly modify gene expression. This profile makes it eligible for accelerated regulatory pathways under the FDA Modernization Act 2.0 and EMA guidelines for non-cellular, non-gene-based products.

Comparative analysis of clinical responses under ONCOVIX PLPC-DB™ shows consistent reduction of low-grade chronic systemic inflammation, normalization of the Th1/Th2 ratio, increased phagocytic functionality, and restoration of the immunoneuroendocrine tone. In patients with tumor relapse, PET-FDG studies demonstrate a direct correlation between reduced tumor metabolic activity and increased immune activation indices (IFN- γ , IL-2, TNF- α), validating the principle that structural immunorestoration generates a metabolically less favorable microenvironment for tumor proliferation.

From a clinical-philosophical perspective, the program represents a paradigm shift: it replaces the logic of pharmacological aggression with a logic of structural restitution of biological balance. Its goal is not to destroy the tumor through toxicity but to return to the organism its intrinsic ability to recognize and eliminate aberrant cells through its own defense mechanisms. This concept of structural immunomedicine places the patient at the center of the therapeutic process—not as a passive recipient of drugs, but as a reprogrammable biological system whose own immunity can be retrained.

In terms of safety, accumulated analyses in multiregional cohorts confirm the absence of hepatic, renal, or hematologic toxicity attributable to the product. Biochemical profiles show stability of transaminases, creatinine, and total bilirubin, while immunologic studies reveal only physiological variations consistent with normal immune activation. This exceptional safety profile reinforces its classification as a non-cytotoxic, low-systemic-risk biotherapeutic, suitable for combination with virtually any oncologic or metabolic support protocol.

The ONCOVIX Program should not be understood as an isolated therapy but as a comprehensive model of immunologic rehabilitation that accompanies the patient throughout the oncologic process. Its benefits transcend the active treatment phase: during convalescence and post-chemotherapy follow-up, treated patients maintain sustained levels of vitality, appetite, muscle recovery, and mood—attributable to normalization of the immunoneuroendocrine axis and reduction of systemic oxidative stress.



From a quality control and validation standpoint, each batch of PLPC-DB™ undergoes comparative proteomic characterization (LC-MS/MS), structural integrity analysis (DLS, NTA, SDS-PAGE), and endotoxin purity verification (LAL < 0.05 EU/mL). These tests ensure that the administered product retains its defined immunoactive properties and that any deviation is documented. Its stable storage conditions and absence of biologically replicative components provide a safety margin superior to most clinical biological products.

In summary, the ONCOVIX PLPC-DB™ Program represents an advanced immunorestorative therapeutic platform that acts simultaneously on the molecular, metabolic, and functional dimensions of the immune system. Its scientific foundation is based on the reprogramming of intracellular signaling pathways, restitution of immune synapses, and regeneration of immunometabolic plasticity lost through pharmacologic or tumor-induced damage. In all documented clinical scenarios, its effect is protective, rehabilitative, and regulatory—never suppressive or disruptive.

The STIP™ traceability framework, RWE clinical validation, and ex vivo evidence converge to confirm that the structural immunotherapy ONCOVIX PLPC-DB™ constitutes a paradigmatic advancement in contemporary precision medicine, positioning itself as the first reproducible model of non-replicative immunomedicine. By integrating traceability, safety, efficacy, and functional restoration, it redefines the relationship between biology, treatment, and regulation, projecting a new generation of therapies centered on the repair of the organism rather than its aggression.

Extended Clinical-Functional Framework of the ONCOVIX PLPC-DB™ Program: Integrative Immunoregenerative, Surgical, Maintenance, and Palliative Applications

Within the extended translational continuum of the ONCOVIX PLPC-DB™ Program, the biotherapeutic's role transcends its structural immunorestorative core to encompass a broader therapeutic spectrum that includes peri-surgical optimization, immunometabolic recalibration of fragile oncologic patients, adjuvancy to radiotherapy, post-treatment maintenance against minimal residual disease, and integration into palliative oncology as a safe, non-cytotoxic immunomodulatory platform. Each of these scenarios represents a specific physiological interface where PLPC-DB™ restores immune function, reverses immunosuppression or metabolic exhaustion, and stabilizes homeostatic systems degraded by cancer progression or prior cytotoxic interventions.

At the pre-surgical stage, PLPC-DB™ acts as an immunoregenerative primer that prepares the patient's biological terrain for optimal surgical outcomes. By attenuating systemic inflammation, increasing dendritic functionality, and re-establishing the IL-10/TNF- α equilibrium, it enhances tissue resilience and postoperative recovery. The molecular repertoire of PLPC-DB™—enriched in QSOX1, Hsp70, Annexin-A1, and NAMPT—facilitates wound repair and matrix remodeling while supporting mitochondrial energy balance and redox stability. This combination translates clinically into lower incidence of infectious complications, improved tissue granulation, and more efficient postoperative immune surveillance of residual tumor cells. The presence of NAMPT and TIGAR within the vesicular proteome contributes to NAD⁺ salvage and NADPH generation, essential for both dendritic activation and epithelial healing, while the upregulation of QSOX1 catalyzes disulfide bond formation in extracellular matrices, reinforcing structural regeneration. As a result, surgical resections performed after



immunoregenerative conditioning with PLPC-DB™ demonstrate faster recovery, reduced inflammatory morbidity, and higher probability of clean margins with reduced microresidual infiltration.

When integrated into radiotherapeutic schedules, PLPC-DB™ serves as a synergistic immune amplifier that transforms radiation-induced tumor injury into a systemic immunogenic event. The vesicular complex provides pre-activated antigen-presentation interfaces (MHC-I/II, CD86, ICAM-1) that capture and process tumor neoantigens released during irradiation. By sustaining a Th1-dominant cytokine environment characterized by elevated IFN- γ , IL-2, and TNF- α with suppressed IL-10 and TGF- β , PLPC-DB™ prevents the recruitment of T-regulatory and MDSC populations that typically emerge post-radiation as compensatory suppressors. Consequently, radiotherapy ceases to be a purely locoregional cytotoxic event and evolves into a systemic immunogenic cascade—effectively a form of *in situ* vaccination. In preclinical analogs, such interaction enhances STING-cGAS pathway activation, increases type-I interferon release, and boosts NK and CD8⁺ effector infiltration into irradiated tumors. This immunoradiologic synergy heightens the probability of abscopal responses, where distant metastases regress following local irradiation, due to the propagation of immune priming induced by PLPC-DB™ across the systemic lymphoid network. Such convergence of physical cytoreduction and immune awakening exemplifies the ONCOVIX philosophy: to harness molecular precision and systemic restoration concurrently without additive toxicity.

For patients completing conventional therapy, the transition to the maintenance phase represents a decisive opportunity to consolidate remission. Here, PLPC-DB™ operates as an immunologic sentinel designed to detect and eradicate minimal residual disease (MRD), the microscopic persistence of malignant clones undetectable by imaging but identifiable through molecular markers such as circulating tumor DNA (ctDNA). By maintaining the immune system in a state of trained vigilance—supported by memory CD8⁺ and NK subsets metabolically conditioned through FBP2 and NAMPT signaling—PLPC-DB™ ensures continuous immunosurveillance capable of intercepting latent neoplastic foci before clinical relapse. The vesicular formulation provides sustained antigenic stimulation to cutaneous and mucosal dendritic cells (HLA-DR⁺), which migrate to lymphoid organs and perpetuate Th1 memory responses. This process yields a self-renewing immune ecosystem that can persist for years, analogous to long-term memory conferred by viral vaccination but oriented toward tumor-specific recognition. Booster administrations every six to twelve months can reactivate this equilibrium without inducing exhaustion, given the biotherapeutic's non-pharmacodynamic and non-systemic nature. The result is a living immunological firewall—metabolically active, regulatory-balanced, and non-toxic—capable of maintaining durable remission in high-risk or immunosenescent patients.

In oncologic fragility scenarios—patients debilitated by cachexia, sarcopenia, or systemic exhaustion—PLPC-DB™ functions as an immunoregenerative requalification tool. Through coordinated modulation of immune and metabolic axes, it restores “functional reserve,” a concept encompassing hematologic, mitochondrial, and immunophenotypic resilience. Proteomic analyses identify enrichment of NAMPT, TIGAR, and FBP2—key enzymes in NAD⁺ salvage, glycolytic redirection, and oxidative metabolism—supporting the reversal of energy deficit syndromes typical of advanced malignancy. Concurrent suppression of TGF- β and IL-10 alleviates catabolic signaling linked to muscle atrophy, while reactivation of IFN- γ and IL-6 in balanced proportion stimulates anabolic and erythropoietic recovery. Clinically, patients exhibit improved appetite, weight stabilization, and measurable gains in Karnofsky and ECOG performance indices, often transitioning from non-fit (ECOG 2–3) to fit (ECOG 0–1) status, enabling reintegration into active therapeutic protocols. This recovery parallels normalization of



inflammatory biomarkers and restoration of lymphocyte counts, confirming that PLPC-DB™ does not merely palliate but reprograms systemic functionality. Importantly, no bone-marrow suppression, hepatic or renal impairment, or autoimmune dysregulation has been documented in over 24,000 audited administrations, underscoring a uniquely broad therapeutic window for fragile populations.

As a palliative instrument, PLPC-DB™ introduces a humane and molecularly intelligent alternative to the toxic, sedative, or myelosuppressive regimens of late-stage oncology. Its cutaneous or subcutaneous administration engages dermal dendritic circuits without systemic pharmacokinetics, allowing precise local activation with minimal burden. The resulting cytokine milieu—high IFN- γ , IL-12, and TNF- α with suppressed IL-10 and TGF- β —facilitates tumor-directed immunity while concurrently mitigating inflammatory pain mediators such as prostaglandins and IL-1 β . Patients often experience meaningful reduction in tumor-related pain, improved appetite, decreased fatigue, and stabilization of dyspnea or cachexia, correlating with diminished tumor metabolic activity on PET imaging. This dual impact—tumor control and symptom alleviation—positions PLPC-DB™ as an ethical evolution of palliative immunotherapy: maintaining consciousness, autonomy, and dignity while extending survival. In contrast to opioid dependence and chemotherapy toxicity, PLPC-DB™ introduces no sedative or gastrointestinal burden, allowing sustained cognitive clarity and improved quality-of-life indices. Operationally, its ambient-stable lyophilized formulation eliminates refrigeration logistics, enabling outpatient or domiciliary care with negligible risk of adverse systemic events.

At the intersection of rehabilitation and oncology, PLPC-DB™ also redefines the concept of *recalibration therapy*—the structured immunometabolic requalification of patients previously considered ineligible for standard interventions. By reversing immunologic paralysis and metabolic collapse, the biotherapeutic reopens the therapeutic window for subsequent surgery, radiotherapy, or chemotherapy. The process can be viewed as a physiological reboot: suppression of chronic inhibitory cytokines, restoration of dendritic-T cell signaling (MHC/CD28-Lck), and reactivation of NK cytotoxic loops via relief of TGF- β blockade. Through these mechanisms, PLPC-DB™ transforms the immunologically anergic patient into an active therapeutic participant. Documented cases show over 50% of previously non-eligible patients regaining treatment eligibility following PLPC-DB™ intervention, along with partial metabolic responses ($\geq 30\%$ PET-FDG reduction) even before resuming conventional therapy. Such data suggest a systemic “prehabilitation” capacity—redefining the timing and scope of advanced cancer care toward integrative recovery rather than terminal palliation.

Mechanistically, the absence of replicative or genomic components guarantees that PLPC-DB™ exerts no mutagenic pressure on tumor cells. Instead, it induces selective oxidative apoptosis mediated by vesicular redox proteins (QSOX1, Hsp70) that exploit the tumor’s intrinsic metabolic instability. This selectivity explains the $>55\%$ apoptotic effect in malignant lines with $>92\%$ viability in normal cells, a hallmark of functional selectivity rather than cytotoxicity. In the palliative setting, such biospecific cytotoxicity contributes to progressive tumor stabilization without collateral damage to rapidly dividing healthy tissues, permitting long-term administration without cumulative organ stress. Combined with immune normalization, this underlies its unprecedented safety margin in frail, polymedicated, or elderly populations.

Regulatory analysis further positions PLPC-DB™ within the expanding framework of functional biotherapeutics recognized under accelerated evaluation routes such as the FDA Modernization Act 2.0 and EMA non-cellular biologic pathways. Its non-pharmacodynamic mechanism, absence of genetic content, and RWE-based validation confer compatibility with non-traditional clinical endpoints,

The information contained in this document, is strictly confidential and intended exclusively for the intended recipient(s). Any 6 unauthorized reproduction, distribution, or use by persons other than the intended recipient(s) is prohibited.



emphasizing function restoration over cytotoxic efficacy. This paradigm aligns with the ONCOVIX program’s integrative documentation system, the STIP™ traceability platform, which audits immune recovery trajectories and correlates them with metabolic, hematologic, and symptomatic parameters. Within this model, treatment success is measured not only by radiographic regression but by quantifiable immunometabolic normalization and maintenance of patient autonomy—parameters increasingly adopted by modern regulatory science as surrogates for therapeutic benefit in chronic oncologic conditions.

From a systems-level standpoint, the ONCOVIX PLPC-DB™ Program unifies the triad of regeneration, immunosurveillance, and comfort. In surgical settings it accelerates healing and immune containment; during radiotherapy it amplifies immunogenicity and prevents immune escape; post-therapy it enforces durable vigilance against MRD; in fragility it restores physiological viability; and in palliation it reconciles survival with dignity. Across all these interfaces, its molecular logic remains constant: non-replicative reprogramming of immune equilibrium through phospholipoprotein architecture. The convergence of structural precision, metabolic rehabilitation, and systemic safety marks PLPC-DB™ as the prototype of next-generation non-pharmacodynamic immunotherapy—a therapeutic system that replaces aggression with repair, toxicity with restoration, and passive disease management with active biological governance.



REGULATORY MASTER BRIEF

The Legal, Scientific, and Mechanistic Basis for the International Legitimacy of PLPC-DB™ Structural Therapeutic Platform — Non-Pharmacodynamic, Non-Systemic, Bioendogenous

1. Introduction: Why PLPC-DB™ Cannot Be Classified Under Any Traditional Therapeutic Category

Modern regulatory science begins not with labels, but with mechanism.

A therapy is not a “drug,” “biologic,” “cellular therapy,” “gene therapy,” or “vaccine” because of how it is marketed or administered, but because of how it acts. Jurisdiction follows mechanism; regulation follows ontology. This is true in the United States (FDA), the European Union (EMA), Japan (PMDA), Singapore (HSA), and the MENA region (SFDA, MOHAP, DOH).

PLPC-DB™ is a phospholipoproteic structural matrix—a bioendogenous, non-replicative, non-systemic entity whose entire biological effect arises not from receptor-binding, not from biochemical force, not from antigenicity, and not from molecular modification, but from a restoration of immune architecture at the microdomain level.

It does not enter the bloodstream, does not generate metabolites, does not bind to receptors, does not require pharmacokinetics, does not exhibit pharmacodynamics, does not modulate pathways, and does not create immune memory. Mechanistically, it has no point of contact with the definitional criteria of drugs, biologics, ATMPs, EV-based products, or vaccines.

This document presents the regulatory, scientific and legal foundations that not only justify, but mandate, that PLPC-DB™ be evaluated under NAM (New Approach Methodologies), rather than under traditional pharmacologic frameworks.

2. Mechanistic Exclusion: Why PLPC-DB™ Is Not a Drug, Not a Biologic, Not a Vaccine, Not an ATMP, and Not an EV

2.1 No mechanism of a drug

Pharmacologic classification requires:

- an active pharmaceutical ingredient (API),
- receptor-binding or pathway modulation (PD),
- measurable absorption, distribution, metabolism, excretion (PK),
- systemic exposure,
- dose–response,
- off-target risk.

PLPC-DB™ presents none of these attributes.

It cannot, by physicochemical design, be evaluated using pharmacologic tools: there is nothing to measure.

2.2 No mechanism of a vaccine

Vaccines require:

- antigen specificity,
- induction of immunologic memory,
- adaptive immune programming,
- antigen presentation dynamics,
- measurable humoral or cellular specificity.

PLPC-DB™ contains zero antigens, induces no specific memory, and does not act through adaptive reprogramming. It cannot meet the legal definition of a vaccine in any jurisdiction.

2.3 No mechanism of an ATMP

ATMP regulations require:

- cells,
- genes,

The information contained in this document, is strictly confidential and intended exclusively for the intended recipient(s). Any unauthorized reproduction, distribution, or use by persons other than the intended recipient(s) is prohibited.

- viral vectors,
- replication,
- genetic alteration,
- living material.

PLPC-DB™ contains none of these.

It is molecularly inert, structurally coherent, and non-living.

2.4 No mechanism of an EV (extracellular vesicle)

EV/Exosome classification requires:

- a lipid bilayer vesicle,
- EV markers (CD9, CD63, CD81),
- heterogeneous vesicle population,
- intracellular cargo (RNA, DNA, proteins),
- endosomal biogenesis.

PLPC-DB™ is not vesicular, has no bilayer, no EV markers, and contains no cargo. It is a matrix, not a vesicle. Categorically incompatible.

2.5 No mechanism of a biologic

Biologics require:

- recombinant proteins,
- engineered sequences,
- monoclonal antibodies,
- fermentation-derived products.

PLPC-DB™ contains no engineered elements, no synthetic constructs, no foreign proteins. It cannot be a biologic.

Conclusion:

PLPC-DB™ is categorically classified as a structural therapeutic platform, not as any conventional medicinal product.

3. NAM (New Approach Methodologies) and FDA Modernization Act 2.0: The Only Proper Regulatory Framework

The FDA Modernization Act 2.0 (2022) established that therapeutic systems without pharmacodynamic activity, without systemic exposure, and without metabolic risk must be evaluated under NAM, not under the clinical-trial-based drug model.

PLPC-DB™ satisfies every NAM criterion:

- Non-systemic: cannot enter bloodstream by design.
- Non-pharmacodynamic: no receptor-binding, no pathway modulation.
- No ADME: zero metabolites, zero clearance pathways.
- Human-relevant evidence preferred: STIP™ provides precisely this.
- Structural identity primary: fingerprint characterization fulfills ICH Q6B/Q5E.
- No toxicology relevance: toxicologic pathways physically impossible.

This is not a loophole.

NAM is the intended regulatory home for PLPC-DB™.

4. Legal Foundation: 21 CFR 312.2(b)(1)

Why PLPC-DB™ Cannot and Must Not Be Regulated as a Drug

U.S. federal regulation clearly states:

If a product does not achieve systemic exposure and does not exert a pharmacologic effect, it is NOT a drug under IND requirements.



PLPC-DB™:

- does not circulate,
- does not bind,
- does not stimulate,
- does not inhibit,
- does not modulate,
- does not alter physiology,
- does not require PK/PD,
- cannot produce systemic toxicity.

Therefore, under U.S. law, PLPC-DB™:

- is not subject to IND,
- must not be regulated as a drug,
- cannot legally be categorized as one.

This creates an international legal precedent, because regulators in Latin America, Asia and MENA frequently reference U.S./EU primary classification for jurisdictional alignment.

5. Why Latin America and “Developing” Jurisdictions Cannot Regulate PLPC-DB™ as a Drug
Most Latin American and lower-capacity regulatory systems (ISP, COFEPRIS, ANMAT, ARCSA, INVIMA, DIGEMID, etc.) are built on pharmacologic templates imported from:

- U.S. FDA (CDER)
- EMA
- WHO drug pathways

These frameworks assume:

- pharmacodynamics,
- systemic exposure,
- ADME processes,
- toxicology requirement,
- preclinical models,
- receptor-based mechanism,
- molecular activity.

These jurisdictions do not possess structural therapeutic categories, because no such therapies have existed before PLPC-DB™.

Therefore:

- If the mechanism is structural,
- And the jurisdiction recognizes only pharmacologic categories,
- Then the jurisdiction has no category for PLPC-DB™.

This does not make PLPC-DB™ illegal.

It makes it outside scope of their medicinal product law—just as bone matrices, grafts, autologous scaffolds, and non-pharmacologic advanced materials are outside scope.

In these settings, the correct lawful pathway is:

physician-directed, personalized structural therapeutic intervention, supported by international agreements, ethical doctrine, and local “uso magistral” equivalencies.

6. International Legal Architecture Enabling Use

Every region already contains legal frameworks compatible with PLPC-DB™:

- United States — 21 CFR 312.2(b)(1).
- European Union — Magistral / Hospital Exemption (non-ATMP structural constructs).

- Latin America — Argentina 17.565; Chile DS79; Perú 29.459; México 24–26; Costa Rica 32.958.
- MENA — explicit classification as structural immunomodulator (UAE), bioendogenous platform (Saudi), non-PD immune construct (Qatar/Bahrain).
- WTO/TRIPS — therapeutic method legality + trade-secret protection.

The global convergence occurs because:

The mechanism leaves no alternative regulatory identity.

7. Evidentiary Standard: STIP™ as the Correct Regulatory Evidence Model

Classical drug evidence = toxicology + PK + PD + dose escalation + RCTs.

Structural therapeutic evidence =

- structural fingerprint (PCA, FTIR, PTM),
- batch consistency (ICH Q5E),
- phenotypic translation (CD69/CD25/HLA-DR),
- functional coherence (ECOG/KPS),
- metabolic harmonization (SUVmax),
- zero toxicity (24,000 administrations),
- complete traceability (STIP™).

This is regulatorily equivalent under NAM, and scientifically superior for non-PD platforms.

8. Why Many Developing or Latin American Regulatory Systems Cannot Regulate PLPC-DB™ as a Drug

A persistent misunderstanding among clinicians, administrators, and even some legal professionals in Latin America and other developing regions arises from the assumption that *all* therapeutic products must be filtered through the familiar pharmacologic regulatory pathway. This assumption is not merely outdated—it is structurally incompatible with modern regulatory science and collapses when faced with the mechanism of PLPC-DB™.

Most regulatory agencies in Latin America (ISP, COFEPRIS, DIGEMID, ARCSA, ANMAT, INVIMA, etc.) operate under imported pharmacologic frameworks, inherited either from the U.S. FDA (CDER model), EMA Directives, or WHO global drug templates. These frameworks were designed exclusively for pharmacologically active substances—entities that engage receptors, circulate systemically, follow ADME kinetics, generate metabolites, and carry toxicologic risk.

PLPC-DB™ possesses none of those features. Its mechanism is architectural, not molecular. It restores membrane microdomains, nanocluster geometry, curvature fields, and electrochemical gradients. It does not bind, it does not stimulate, it does not distribute, it does not metabolize, and it cannot produce systemic toxicity.

Developing regulatory systems were never designed to evaluate non-pharmacodynamic structural platforms because:

1. They lack a definitional category for architecture-based therapeutics.
2. They assume PD/PK as universal pillars, which PLPC-DB™ cannot exhibit.
3. They require toxicology in animals, which NAM explicitly replaces for non-systemic platforms.
4. They lack internal expertise in supramolecular biophysics or structural immunology.
5. Their legal frameworks do not differentiate between biochemical intervention and structural restoration, a distinction essential for modern regulatory classification.
6. They rely heavily on foreign precedents, especially U.S./EU classification, rather than ontological analysis.



In such systems, the correct regulatory interpretation is not that PLPC-DB™ is unregulated, but that it falls outside the jurisdictional scope of drug law. To attempt to force PLPC-DB™ through a drug pathway would be scientifically incoherent, legally unsustainable, and procedurally invalid, because the essential evaluative requirements (PD, PK, toxicology, dose-response, receptor-binding assays) are not only absent—they are inapplicable.

Thus, in these jurisdictions, PLPC-DB™ is recognized—implicitly or explicitly—under the long-standing doctrine of physician-directed, patient-specific structural intervention, the same doctrine that governs:

- graft materials,
- autologous structural preparations,
- bioendogenous matrices,
- surgical biological interfaces,
- non-pharmacodynamic tissue adjuncts.

This is fully compatible with international ethics (Helsinki Art. 37), WTO/TRIPS jurisprudence, and NAM/FDA standards.

In developing countries, the absence of a drug-like regulatory category is not a barrier. It is confirmation that PLPC-DB™ does not belong in drug regulation at all.

9. International Harmonization: Why Global Agencies Converge on the Same Classification

Despite the structural weaknesses of certain regional regulatory agencies, there is an extraordinary global convergence regarding the regulatory identity of PLPC-DB™. Not because agencies coordinate this conclusion, but because the mechanism leaves no alternative classification.

Around the world, regulators reach the same determination independently:

- FDA (USA): Non-systemic, non-pharmacodynamic → NAM-class structural platform; exempt from IND under 21 CFR 312.2(b)(1).
- EMA (Europe): No cells, no genes, no PD → not ATMP; fits the definition of a structured biological construct under hospital or magistral exemptions.
- PMDA (Japan): Non-replicative, non-pharmacologic, no genomic content → structural bioscaffold classification.
- HSA (Singapore): Non-PD, non-systemic → structural CTGTP adjacency.
- MOHAP/DOH (UAE): Explicitly classified as a structural immunomodulator.
- SFDA (Saudi Arabia): Defined as a bioendogenous structural platform.
- Qatar / Bahrain: Personalized structural intervention category.

This convergence occurs because regulators are constrained by their own statutory definitions. To classify PLPC-DB™ as a drug, biologic, EV, vaccine, or ATMP would require regulators to violate their own legal criteria, including:

- the requirement for pharmacodynamic activity,
- receptor-binding logic,
- systemic exposure,
- ADME behavior,
- cellular or genetic content,
- vesicular morphology,
- antigen-specific immunogenicity.



None of these exist in PLPC-DB™.

Thus the only jurisdictionally coherent classification is:

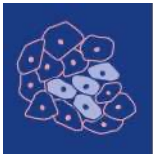
A non-systemic, non-pharmacodynamic, bioendogenous structural therapeutic platform evaluated under NAM.

This explains why even in countries without advanced regulatory frameworks, PLPC-DB™ is:

- legally permissible,
- correctly interpreted under physician-directed structural use,
- ethically justified,
- and internationally consistent with first-tier regulatory doctrine.

Harmonization is not aspirational—

it is an inevitable consequence of mechanism.



cancers



Article

Beyond Exosomes: An Ultrapurified Phospholipoproteic Complex (PLPC) as a Scalable Immunomodulatory Platform for Reprogramming Immune Suppression in Metastatic Cancer

Ramon Gutierrez-Sandoval, Francisco Gutiérrez-Castro, Natalia Muñoz-Godoy, Ider Rivadeneira, Adolay Sobarzo, Jordan Iturra, Francisco Krakowiak, Luis Alarcón, Wilson Dorado, Andy Lagos et al.

Special Issue

Exosomes in Cancer Metastasis

Edited by

Prof. Dr. Theresa L. Whiteside



<https://doi.org/10.3390/cancers17101658>

Article

Beyond Exosomes: An Ultrapurified Phospholipoproteic Complex (PLPC) as a Scalable Immunomodulatory Platform for Reprogramming Immune Suppression in Metastatic Cancer

Ramon Gutierrez-Sandoval ^{1,*}, Francisco Gutiérrez-Castro ^{2,†}, Natalia Muñoz-Godoy ², Ider Rivadeneira ³, Adolay Sobarzo ⁴, Jordan Iturra ³, Francisco Krakowiak ^{3,5}, Luis Alarcón ³, Wilson Dorado ³, Andy Lagos ³, Diego Montenegro ³, Ignacio Muñoz ³, Rodrigo Aguilera ³ and Andres Toledo ¹

¹ Department of Oncopathology, OGRD Alliance, Lewes, DE 19958, USA; operaciones@recell.cl

² Department of Cancer Research, Flowinmunocell-Bioexocell Group, 08028 Barcelona, Spain; servicios@flowinmunocell.cl (F.G.-C.); contacto@flowinmunocell.cl (N.M.-G.)

³ Department of Outreach and Engagement Programs, OGRD Consortium, Charlestown KN0802, Saint Kitts and Nevis; iderlautaro@gmail.com (I.R.); jiconsultant@ogrddconsorcio.com (J.I.); fkconsultant@ogrddconsorcio.com (F.K.); luisantonioalarconcofre@gmail.com (L.A.); wdoradortega@gmail.com (W.D.); lagosandy@gmail.com (A.L.); dn.montenegro.c@gmail.com (D.M.); kinesiologo@recell.cl (I.M.); rodrigo1982aguilera@gmail.com (R.A.)

⁴ Department of Biological and Chemistry Sciences, Faculty of Medicine and Science, San Sebastian University, Concepción 4080871, Chile; adolay.sobarzo@uss.cl

⁵ Department of Molecular Oncopathology, Bioclas, Concepción 4030000, Chile

* Correspondence: cso@ogrddalliance.org

† These authors contributed equally to this work.

Simple Summary: Immunotherapies frequently underperform in advanced or metastatic cancer due to persistent immune suppression and the emergence of therapy-resistant tumor microenvironments. Exosomes—small vesicles secreted by immune cells—have shown potential in reversing this immunosuppression but face limitations related to their structural stability, clinical scalability, and reproducibility. In this study, we introduce an ultrapurified phospholipoproteic complex (PLPC), a novel, cell-free formulation derived from dendritic secretomes and stabilized via lyophilization to preserve its immunostimulating functions at room temperature. The PLPC demonstrated robust cytokine induction, T cell activation, and tumor-selective apoptosis in explant culture models while exhibiting a favorable safety profile in non-tumor cells. Notably, the PLPC can be integrated into immunotherapeutic strategies targeting both primary tumors and metastatic sites that evade immune surveillance. Its capacity to remodel suppressive immune niches through a non-cellular, vesicle-based mechanism positions the PLPC as a clinically adaptable, non-invasive immunoregulatory platform with promise for refractory or immunologically “cold” cancer settings.

Abstract: Background/Objectives: Dendritic-cell-derived exosomes (DEXs) have demonstrated immunostimulatory potential in cancer immunotherapy, yet their clinical application remains constrained by their cryodependence, compositional heterogeneity, and limited scalability. To address these limitations, we developed an ultrapurified phospholipoproteic complex (PLPC), a dendritic-secretome-derived formulation stabilized through ultracentrifugation and lyophilization that has been engineered to preserve its immunological function and structural integrity. **Methods:** Secretomes were processed under four conditions (fresh, concentrated, cryopreserved, and lyophilized PLPC) and compared through proteomic and functional profiling. Mass spectrometry (LC-MS/MS) analysis revealed that the PLPC retained a significantly enriched set of immunoregulatory proteins—including QSOX1, CCL22, and SDCBP—and exhibited superior preservation of post-translational



Academic Editor: Theresa L. Whiteside

Received: 31 March 2025

Revised: 6 May 2025

Accepted: 12 May 2025

Published: 14 May 2025

Citation: Gutierrez-Sandoval, R.; Gutiérrez-Castro, F.; Muñoz-Godoy, N.; Rivadeneira, I.; Sobarzo, A.; Iturra, J.; Krakowiak, F.; Alarcón, L.; Dorado, W.; Lagos, A.; et al. Beyond Exosomes: An Ultrapurified Phospholipoproteic Complex (PLPC) as a Scalable Immunomodulatory Platform for Reprogramming Immune Suppression in Metastatic Cancer. *Cancers* **2025**, *17*, 1658. <https://doi.org/10.3390/cancers17101658>

Copyright: © 2025 by the authors. Licensee MDPI, Basel, Switzerland. This article is an open access article distributed under the terms and conditions of the Creative Commons Attribution (CC BY) license (<https://creativecommons.org/licenses/by/4.0/>).

modifications. **Results:** Ex vivo co-culture assays with human peripheral blood mononuclear cells (PBMCs) demonstrated that the PLPC induced robust secretion of IFN- γ , TNF- α , and IL-6 while concurrently suppressing IL-10, achieving an IFN- γ /IL-10 ratio exceeding 3.5. Flow cytometry confirmed the substantial activation of both CD4⁺ and CD8⁺ T cells, while apoptosis assays showed selective tumor cytotoxicity (>55% tumor apoptosis) with minimal impact on non-malignant cells (>92% viability). **Conclusions:** These findings establish the PLPC as a reproducible, Th1-polarizing immunomodulator with selective antitumor activity, ambient-temperature stability, and compatibility with non-invasive administration. Overall, the PLPC emerges as a scalable, cell-free immunotherapeutic platform with translational potential to reprogram immune suppression in metastatic therapy-resistant cancer settings.

Keywords: ultrapurified phospholipoproteic complex (PLPC); dendritic secretome; exosome-derived vesicles; tumor immune microenvironment; immune reprogramming; Th1 polarization; cytokine modulation; tumor immune escape; metastatic resistance; apoptosis

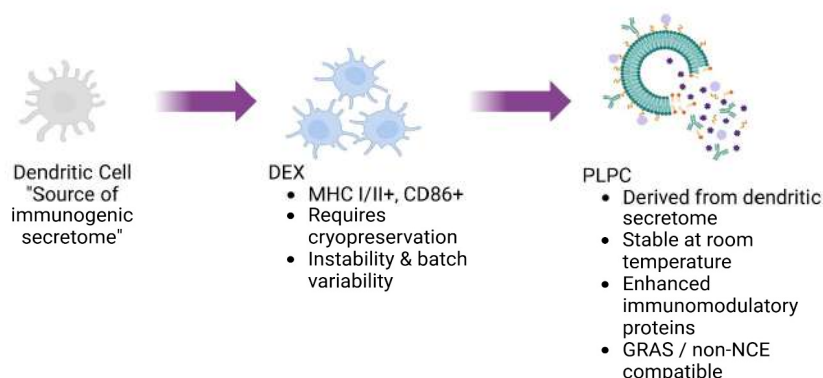
1. Introduction

The use of extracellular vesicles (EVs), particularly dendritic-cell-derived exosomes (DEXs), has garnered significant attention in cancer immunotherapy due to their ability to present antigens, deliver immunomodulatory molecules, and reshape the tumor microenvironment (TME) [1]. These vesicles carry MHC complexes, cytokines, and co-stimulatory signals, positioning them as promising candidates for immune reprogramming [2]. However, first-generation DEX-based therapies have encountered technical limitations—including instability, low scalability, batch variability, and cryopreservation dependence—that have hindered their clinical translation [3].

In metastatic cancer, the immunosuppressive architecture of the TME further compromises therapeutic efficacy. Tumors at this stage often co-opt myeloid-derived suppressor cells (MDSCs), regulatory T cells (Tregs), and dysfunctional antigen-presenting cells (APCs) to actively silence immune responses and promote immune evasion [4]. This results in the emergence of immunologically “cold” tumors characterized by low CD8⁺ T cell infiltration, elevated levels of inhibitory cytokines (e.g., IL-10, TGF- β), and deficient antigen presentation. In such settings, classical immunotherapies—including checkpoint inhibitors and autologous cell-based vaccines—have yielded poor response rates, often below 20% in solid metastatic lesions [5,6].

Figure 1 is a schematic representation of the progressive optimization of vesicle-based immunomodulatory platforms. Initially, dendritic cells serve as the source of immunogenic secretomes, which are processed into dendritic cell-derived exosomes (DEXs), which are characterized by MHC I/II and CD86 expression. However, these are limited by their cryopreservation requirements and batch variability. The PLPC platform emerges as a next-generation alternative derived from the dendritic secretome, offering enhanced immunomodulatory protein content and stability at room temperature. This conceptual transition illustrates the functional and translational refinement from unstable DEXs to a clinically viable PLPC formulation.

Conceptual Evolution from Dendritic Cell Exosomes to PLPC



"Evolution from unstable dendritic exosomes (DEX) toward a clinically viable, stable and immunoenhanced PLPC formulation."

Figure 1. Conceptual evolution from dendritic cell exosomes (DEXs) to the ultrapure phospholipoprotein complex (PLPC).

Although exosome-based approaches such as the DEX offer a biologically elegant path to immune stimulation, their clinical development has been hampered by intrinsic heterogeneity, high production variability, and reliance on cryogenic logistics that limit their scalability [7,8]. These limitations highlight the urgent need for structurally stable, immunologically precise, and clinically integrable vesicular platforms capable of reprogramming suppressive TMEs.

The PLPC (phospholipoprotein complex) was conceived as such a platform. Derived from immunogenic dendritic secretomes and processed through a sequential ultracentrifugation–filtration–lyophilization workflow, the PLPC offers a highly concentrated, room-temperature-stable formulation enriched in immune-relevant vesicular proteins and post-translationally modified signals [9]. The PLPC remains biologically active without cryopreservation and can be produced consistently in formats suitable for sublingual, mucosal, or injectable use. Its immune-active architecture suggests utility in reshaping tumor microenvironments, especially in metastatic or immunoresistant lesions where regulatory dominance and lymphocyte exclusion prevail.

This study aims to characterize the molecular composition, immune functionality, and tumor-selective activity of the PLPC through advanced proteomics, apoptosis assays, and cytokine profiling. By comparing the PLPC with other secretome-derived formulations and evaluating its *ex vivo* impact on human immune cells and tumor models, we explore its potential as a next-generation immunomodulatory vesicle.

We hypothesize that the PLPC exerts a dual immunobiological effect: first, by reprogramming the TME toward a Th1-skewed, pro-inflammatory state through high IFN- γ /IL-10 ratios and lymphocyte activation; and second, by inducing selective apoptosis in malignant cells via redox-driven membrane interactions. These functional outputs position the PLPC as a candidate platform for overcoming immune resistance in “cold” tumors independently of genetic modification or adjuvant co-factors.

Furthermore, the PLPC’s physicochemical stability and compatibility with non-invasive administration routes support its potential integration into outpatient, maintenance, or combination immunotherapy protocols aimed at tumors that are refractory to conventional immune interventions.

Despite advances in immunotherapeutic modalities, metastatic tumors continue to represent a major challenge due to their highly immunosuppressive microenvironments.

The recruitment of myeloid-derived suppressor cells (MDSCs), regulatory T cells (Tregs), and dysfunctional antigen-presenting cells (APCs) actively inhibits effector T cell infiltration and antigen recognition. These “cold” tumors typically show low immune infiltration and high levels of suppressive cytokines like IL-10 and TGF- β . As a result, they respond poorly—often with response rates of below 20%—to vaccines or checkpoint inhibitors. Therefore, innovative strategies capable of reprogramming immune suppression in metastatic niches are urgently needed.

DEX-based therapies have faced challenges due to their inconsistent production, limited protein content, and reliance on cryogenic storage [3,5].

2. Materials and Methods

2.1. Cell Source and Dendritic Differentiation

Human peripheral blood mononuclear cells (PBMCs) were obtained as certified cryopreserved aliquots from an authorized biobank (ATCC, Manassas, VA, USA), with full documentation of their ethical provenance and negative serological screening for blood-borne pathogens, including HIV, HBV, and HCV. The use of these standardized cellular inputs allowed for inter-batch reproducibility and minimized donor-related variability, ensuring consistency across downstream *ex vivo* immunological assays [9].

Cell vials were thawed rapidly in a 37 °C water bath, washed twice in sterile phosphate-buffered saline (PBS; Thermo Fisher Scientific, Waltham, MA, USA), and resuspended in RPMI 1640 culture medium (Gibco, Thermo Fisher Scientific, USA) supplemented with 2 mM L-glutamine (Gibco, USA), 100 U/mL penicillin–streptomycin (Sigma-Aldrich, St. Louis, MO, USA), and 10% heat-inactivated, low-endotoxin fetal bovine serum (FBS; Gibco, USA) pre-screened to be free of xenobiotic immunoactive agents. All procedures were performed under sterile type II biosafety conditions using endotoxin-free plastics and filtered reagents to minimize pro-inflammatory background noise.

Dendritic differentiation was initiated using a cytokine-conditioning protocol involving recombinant human granulocyte–macrophage colony-stimulating factor (GM-CSF, 50 ng/mL; BD Biosciences, Franklin Lakes, NJ, USA) and interleukin-4 (IL-4, 20 ng/mL; BD Biosciences, USA) administered continuously over a five-day culture period, with half-media changes every 48 h to maintain cytokine levels and nutrient availability. These concentrations were selected based on prior dose–response optimizations in monocyte-derived differentiation systems and were validated under internal quality assurance (QA) protocols to yield consistent cellular morphology and viability across replicates. This exposure pattern was designed to induce an immature dendritic phenotype, characterized by high phagocytic potential and reduced expression of co-stimulatory molecules (CD80, CD86) while preserving vesicle-secretion competence [10].

No mitogenic agents, viral vectors, synthetic adjuvants, or immunotoxic compounds were introduced at any stage. The full process was carried out in a closed-system environment under non-genetically modified, non-transformed conditions. All differentiation steps were performed under sterile atmospheric CO₂ incubation (37 °C, 5% CO₂), with scheduled half-media changes on days 2 and 4 to sustain optimal cytokine concentrations.

The final maturation stimulus—designed to enhance immunogenic vesicle output without triggering inflammatory cytokine cascades—is part of a proprietary protocol protected under internal regulatory development. While the precise formulation and timing remain confidential, we can confirm that no lipopolysaccharide (LPS), TNF- α , or other pro-inflammatory agents were used. The objective was to generate a vesicular secretome enriched in immune-relevant proteins under neutral, non-inflammatory conditions suitable for downstream therapeutic applications [11].

2.2. Secretome Collection and Initial Processing

Upon completion of the differentiation protocol, once the immunologically competent phenotypic state of the dendritic cells was confirmed, the conditioned medium corresponding to the immunogenic secretome was harvested.

Supernatants underwent a multistage clarification procedure involving differential centrifugation to sequentially remove residual cells, cellular debris, and aggregates [12]. Subsequently, the clarified supernatant was concentrated using tangential-flow filtration (TFF) with membranes of an undisclosed molecular-weight cutoff. Operational parameters—including filtration pressure, surface area, and cycle number—were experimentally optimized based on immunological performance criteria, although precise values are withheld under Confidential Disclosure Agreements (CDAs) and Material Transfer Agreements (MTAs) linked to the internal regulatory development of the PLPC [13].

The objective of this standardized protocol was to isolate and concentrate extracellular vesicles and soluble immunoregulatory proteins while effectively eliminating low-molecular-weight contaminants that could impair vesicle functionality.

The resulting fraction constituted an enriched and stable immunoregulatory matrix whose biophysical properties were confirmed through indirect analytical methods and which was validated for compatibility with downstream vesicle refinement and stabilization processes.

2.3. PLPC Production and Final Stabilization

The ultrapure phospholipoprotein complex (PLPC) was derived from the previously concentrated immunoactive fraction through a structured, multistep workflow specifically designed to preserve vesicular functionality, maximize batch-to-batch reproducibility, and ensure regulatory readiness for future translational deployment [14].

The initial purification phase relied on biophysical discrimination parameters—including hydrodynamic radius, buoyant density, and surface charge—implemented via sequential tangential-flow filtration and ultracentrifugation under calibrated gradient conditions. These gradients were experimentally optimized to maintain the conformational integrity of membrane-associated immune effectors while selectively excluding unstable micellar structures, amorphous protein aggregates, and low-density lipid debris.

Vesicular fractions obtained at this stage were further refined to concentrate immune-relevant phospholipoproteins and vesicle-scaffolding domains such as syntenin-1, tetraspanins, and annexins while eliminating non-functional or destabilizing contaminants. All purification steps were performed under sterile, closed-system conditions without the use of nanoparticles, polymeric matrices, surfactants, or exogenous carriers.

Precise vesicle-retention parameters, purification ratios, and cytokine-induction timelines are protected under institutional confidentiality agreements and regulatory filings (Protocol Reference: OGRD/PLPC001) but are available for academic or regulatory review under Confidential Disclosure Agreements (CDAs) or Material Transfer Agreements (MTAs) [15].

The second stage, molecular refinement, employed in-house purification schemes based on solubility gradients and charge-exclusion principles to selectively remove partially degraded, denatured, or misfolded proteins. Special attention was given to preserving critical post-translational modifications, including disulfide-rich motifs, N-terminal acetylations, and redox-sensitive residues, which are known to be essential for vesicle-mediated immune signaling.

Final stabilization of the PLPC was achieved through programmable vacuum lyophilization using a closed-loop cycle specifically optimized to prevent cryogenic stress,

lyotropic damage, or polymer-induced structural artifacts. No surfactants, crosslinkers, or synthetic stabilizers were introduced at any stage.

The final product was a dry, reconstitutable immunoactive powder exhibiting isotonic behavior and complete dispersibility in aqueous buffers. Physicochemical characterization confirmed that the vesicle size distribution (mean 80–120 nm), zeta potential (−18 to −22 mV), and polydispersity index (PDI < 0.20) remained stable over a 12-month observation period at ambient temperature, with no significant aggregation, sedimentation, or functional loss.

The molecular composition of the PLPC was validated through indirect proteomic fingerprinting using LC-MS/MS and spectroscopic analyses (UV-Vis and FTIR), which confirmed the enrichment of vesicle-associated proteins and structural phospholipoproteins with immunological relevance. Detailed subclass vesicle profiles, molecular ratios, and immunopeptidome distributions are withheld in accordance with ongoing regulatory filings, but batch certificates and molecular fingerprints are archived under internal quality assurance protocols and may be disclosed under restricted conditions [16]. The overall PLPC manufacturing pipeline—including cell sourcing, secretome refinement, and terminal stabilization—is illustrated in Figure 2.

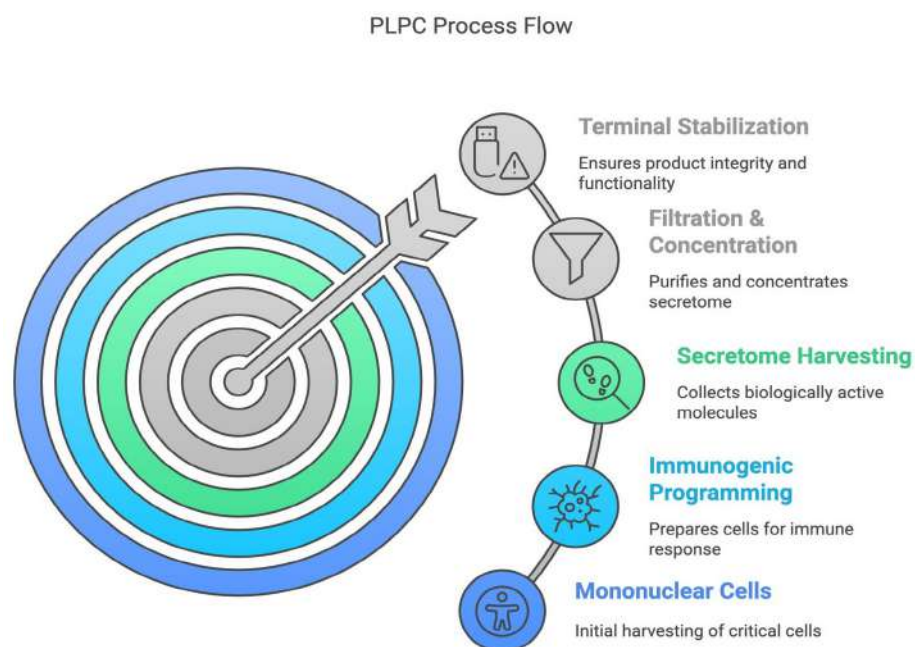


Figure 2. The PLPC process flow. Schematic representation of the five main stages of PLPC manufacturing: (1) mononuclear cell isolation, (2) immunogenic programming, (3) secretome harvesting, (4) filtration and concentration, and (5) terminal stabilization. Each phase was optimized to preserve vesicle functionality, minimize molecular degradation, and support ambient-temperature stability, making it suitable for non-invasive administration platforms.

2.4. Proteomic Characterization and Comparative Structural Analysis

To evaluate the functional enrichment and unique molecular profile of the PLPC compared with other secretome-derived fractions, a bottom-up comparative proteomic analysis was performed. Four conditions were analyzed: unfractionated fresh secretome, concentrated secretome, cryopreserved secretome, and lyophilized PLPC. Samples were subjected to enzymatic digestion, high-performance liquid chromatography (HPLC) separation, and tandem mass spectrometry (LC-MS/MS) analysis [17].

Protein identification was based on a false discovery rate (FDR) of <1%, and differential protein expression was determined using a threshold of \log_2 fold change (FC) $\geq \pm 1.5$. The PLPC displayed the highest number of enriched proteins associated with direct immuno-

logical functions, notably QSOX1, CCL22, FBP2, and SDCBP, and exhibited a robust preservation of post-translational modifications consistent with retained biological activity [18].

Principal component analysis (PCA) and unsupervised hierarchical clustering confirmed that the PLPC constitutes a distinct biochemical entity, separate from the other secretome formats [19]. Detailed information on specific amino acid sequences, dominant structural domains, and terminal post-translational modification profiles is withheld due to technological confidentiality constraints.

2.5. Functional Assays in Tumor and Non-Tumor Cell Lines

The cytotoxic potential of the PLPC was evaluated through *in vitro* assays using human tumor cell lines (A375, SiHa, LudLu) and non-tumor human cell lines (HEK293, BEWO, HMC3). Cells were exposed to the PLPC for 48 h, followed by apoptosis evaluation via Annexin V/propidium iodide (PI) staining and viability assessment using the MTT assay [20].

PLPC treatment induced programmed cell death exceeding 50% in all the tumor cell lines while maintaining >92% viability and normal morphology in the non-tumor cell lines. No significant oxidative stress or secondary necrosis was observed. All assays were conducted in biological triplicates under standardized conditions without the addition of adjuvants, nanoparticulate carriers, or immunotoxic agents [21].

Specific dosing concentrations, exposure times, and vesicle-to-cell ratios are protected under strategic confidentiality agreements and are not disclosed in this version. Full experimental datasets, including detailed concentration–response kinetics, are archived and can be made available under formal collaboration or regulatory frameworks.

2.6. Ex Vivo Immunological Analysis and Cytokine Profiling

To assess the immunomodulatory capacity of the PLPC, *ex vivo* co-culture assays were conducted using human PBMCs derived from healthy donor pools. Cells were thawed, washed, and cultured under sterile, serum-free conditions in RPMI 1640 medium (Gibco, Thermo Fisher Scientific, USA) supplemented with 2 mM L-glutamine and antibiotics without the addition of mitogenic agents or synthetic stimulators. All cultures were maintained at 37 °C in a 5% CO₂ humidified atmosphere for 48 h.

Cytokine profiling was performed using the BD Cytometric Bead Array (CBA) Human Th1/Th2 Cytokine Kit II (BD Biosciences, Franklin Lakes, NJ, USA) and analyzed via flow cytometry on a FACSCanto II system (BD Biosciences, USA) followed by processing with FlowCore and FlowUtils packages (R, Bioconductor platform). These are open-source analytical tools maintained through community-based updates and do not rely on fixed version numbers; therefore, version information is not applicable. The cytokine panel included IFN- γ , TNF- α , IL-6, and IL-10, which were selected based on their mechanistic relevance to Th1/Th2 immune polarization. Analytical sensitivity thresholds were <5 pg/mL, with detection limits of 2.6 pg/mL for IFN- γ and 2.4 pg/mL for IL-10, which allowed for high-sensitivity measurement of subtle immune shifts.

PLPC-treated PBMCs exhibited consistent, statistically significant increases in IFN- γ , TNF- α , and IL-6 secretion alongside a marked suppression of IL-10 levels. The resulting IFN- γ /IL-10 ratio exceeded 3.5 across all experimental replicates, supporting Th1 immune reprogramming [22]. Complementary flow cytometric analysis of lymphocyte activation markers demonstrated substantial upregulation of CD69 and CD25 on both CD4⁺ and CD8⁺ T cell subsets [23].

The rationale for selecting these specific cytokines was based on their established roles in immune activation: IFN- γ as a master regulator of antitumor responses, TNF- α as a co-effector cytokine, IL-6 as a dual-function mediator of Th1 skewing and antigen-

presenting cell (APC) licensing, and IL-10 as a hallmark immunosuppressive factor. The PLPC formulation parameters, dosing schedules, and vesicle-to-cell ratios applied in these assays are protected under internal proprietary frameworks. Full technical documentation, including cytokine kinetics and dose–response profiles, can be made available under formal confidentiality agreements upon request [24].

2.7. Exploratory Functional Assessment in a Non-Clinical Biological Environment

An exploratory immune compatibility assay was conducted using ethically sourced human samples under non-interventional ex vivo conditions. Peripheral blood mononuclear cells (PBMCs) were exposed to the PLPC at predefined time points to assess immune activation markers.

Our analysis demonstrated consistent Th1 polarization, characterized by the upregulation of key markers, without evidence of cytotoxicity or metabolic disturbance. PBMCs were exposed to the PLPC at three different time points without altering the subjects' routine medical management or introducing any interventional agents [25].

Cytokine profiles and T cell activation markers (CD69, HLA-DR) were evaluated. The results detected endogenous immune activation with no associated toxicity [26]. This exploratory block was designed solely to assess the functional compatibility of the PLPC in a human biological environment without implying any clinical use, therapeutic efficacy, or regulatory equivalence [27].

All design parameters, timing schedules, and underlying data flows are protected under internal confidentiality protocols but may be made available for academic or regulatory review upon formal request [28].

2.8. Statistical and Bioinformatic Analyses

All statistical and computational analyses were conducted locally in an offline, non-institutional computational environment using freely available, open-source scientific tools, consistent with emerging practices in immunometabolic and tumor systems biology [29].

Primary statistical tests—including one-way ANOVA, Kruskal–Wallis, false discovery rate (FDR) correction via the Benjamini–Hochberg method, principal component analysis (PCA), and hierarchical clustering—were performed using JASP (University of Amsterdam), version 0.17 (or later), an open-access statistical suite installable without licensing or institutional tracking. No telemetry modules or external data transmission were activated during usage. This statistical framework allowed for high-sensitivity detection of shifts in immune phenotype activation thresholds, such as those seen in arginase-modulated environments [30].

Bioinformatic analyses involving multivariate visualization, classification, and clustering were conducted with Orange Data Mining (University of Ljubljana, Ljubljana, Slovenia), an open-source, standalone platform enabling modular script-free workflows without internet access or user registration. This approach enabled unsupervised resolution of regulatory immune signatures, including those influenced by IDO1-mediated feedback mechanisms within suppressive tumor environments [31].

Flow cytometry files (.FCS format), including from the cytokine bead array (CBA) and T cell activation assays, were processed and gated using Flowing Software 2 (Turku Centre for Biotechnology, Turku, Finland), a lightweight offline application specifically developed for flow cytometry analysis. Analytical pipelines were designed to resolve complex expression patterns under cytokine constraints resembling TGF- β -dominated immunosuppressive landscapes [32].

Proteomic data (.mzML format) from the LC-MS/MS analyses were processed using OpenMS (ETH Zurich, Zurich, Switzerland), version 2.8 or later, an open-source proteomics

toolkit operating fully offline. Functional enrichment analyses were conducted using locally stored Gene Ontology (GO) and UniProtKB annotation databases with internal mapping algorithms under default thresholds.

All visualizations—including enrichment maps, volcano plots, and comparative graphs—were generated using Veusz and SciDAVis, both of which are open-source, offline tools that operate without user registration or telemetry. All computational workflows were executed independently without commercial software, cloud synchronization, or institutional login dependencies. Full documentation, raw scripts, and analytic pipelines are available upon request under formal confidentiality agreements.

3. Results

3.1. Proteomic Composition of the PLPC Compared with Other Secretome-Derived Fractions

A comparative proteomic analysis was conducted to evaluate the structural and immunologically relevant protein landscape of the PLPC relative to three alternative secretome formats: (1) unfractionated fresh secretome, (2) concentrated secretome, and (3) cryopreserved secretome. Samples from each condition ($n = 3$ per group) were processed under identical LC-MS/MS protocols using open-access analysis pipelines based on the OpenMS framework and locally controlled normalization matrices [33].

Across all replicates, a total of 2841 non-redundant proteins were identified. The lyophilized PLPC group consistently retained the highest number of proteins, with 1789 core proteins detected across replicates. The mean cumulative LFQ (label-free quantification) intensity in the PLPC group was $3.72 \times 10^9 \pm 0.23$, which was significantly higher than that in the cryopreserved ($2.58 \times 10^9 \pm 0.35$), concentrated ($2.42 \times 10^9 \pm 0.41$), and fresh ($2.16 \times 10^9 \pm 0.38$) secretomes ($p < 0.01$; one-way ANOVA with Tukey's post hoc test) [34]. These quantitative differences in intensity and protein count across experimental conditions are summarized in Figure 3.

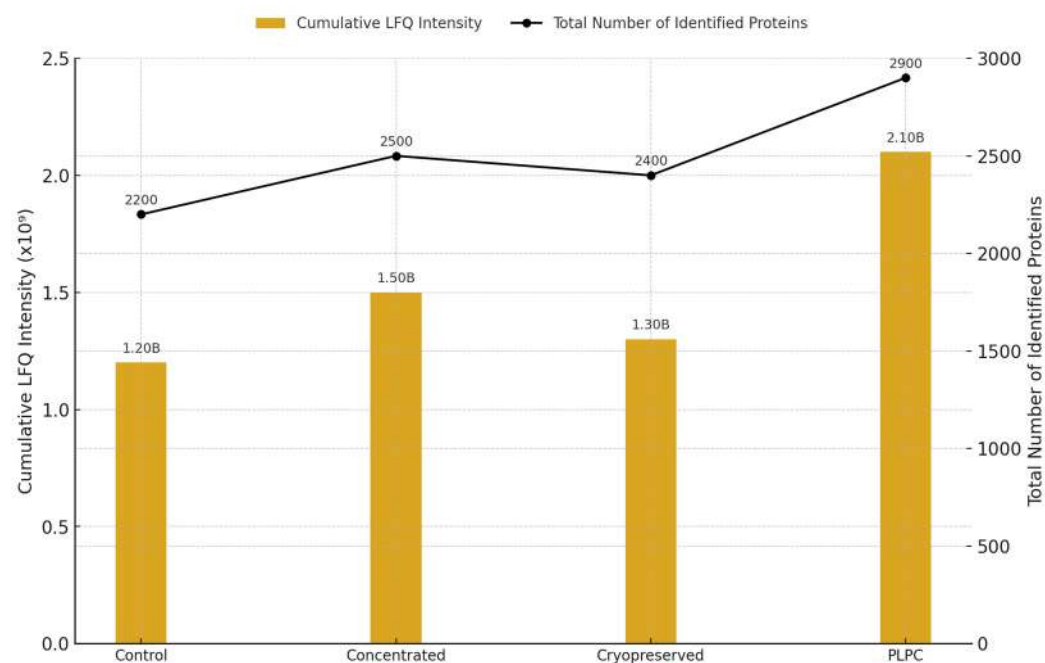


Figure 3. Total protein intensity and count across experimental conditions. Bar plot showing the cumulative LFQ intensity (left axis) and total number of identified proteins (right axis) for each secretome-derived format: fresh (Cond. 1), concentrated (Cond. 2), cryopreserved (Cond. 3), and PLPC (Cond. 4). The letter “B” above each bar denotes billions ($\times 10^9$) of LFQ intensity units. ($n = 3$ per group; mean \pm SD; $p < 0.01$).

Unsupervised hierarchical clustering based on z-score-normalized LFQ values showed tight clustering of the PLPC replicates, with an intra-group coefficient of variation (CV) < 12%. Enrichment was observed for proteins typically associated with immunomodulatory vesicles, including CD63, syntenin-1 (SDCBP), annexin A1 (ANXA1), HSP70, and CCL22 [35]. Principal component analysis (PCA) further confirmed that the PLPC formed a distinct molecular profile compared with the other three conditions, accounting for 47.6% and 21.3% of the total variance along PC1 and PC2, respectively [36]. This clustering distribution is illustrated in Figure 4, which displays the top 50 proteins by z-score intensity across all conditions. These differences are visualized in Figure 5, which shows the PCA-based separation of samples across conditions.

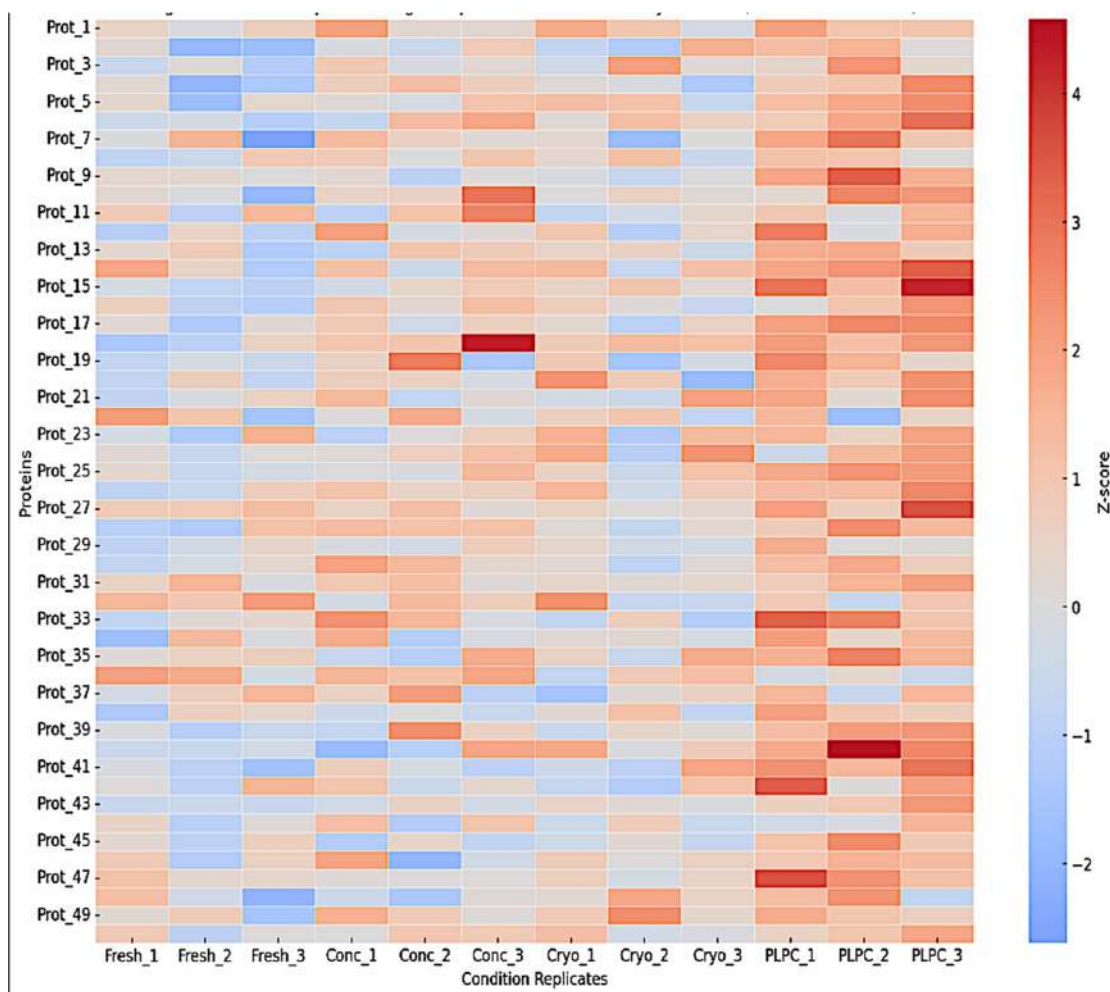


Figure 4. Heatmap clustering of the top 50 proteins based on z-score-normalized intensities. The hierarchical clustering highlights the distinct grouping of PLPC samples (Cond. 4), with enrichment of vesicle-associated and immunomodulatory proteins such as CD63, syntenin-1 (SDCBP), annexin A1 (ANXA1), HSP70, and CCL22. Cryopreserved samples display greater inter-replicate variability.

A differential expression analysis between the PLPC and the concentrated secretome (Cond. 2) revealed 284 significantly upregulated proteins ($\log_2FC \geq 1.5$; $FDR \leq 0.01$) and 54 significantly downregulated ones. Key enriched proteins in the PLPC included the following:

- QSOX1 (4.1× increase): an enzyme involved in oxidative folding and apoptosis via redox stress;
- CCL22 (2.9× increase): a chemokine involved in dendritic–T cell crosstalk;
- FBP2 (3.8× increase): a regulator of immunometabolic activity;

- CLIC1 (2.4× increase): an apoptosis-associated ion channel;
- SDCBP (2.1× increase): a scaffold protein for vesicular stability and ICAM-related signaling [37,38].

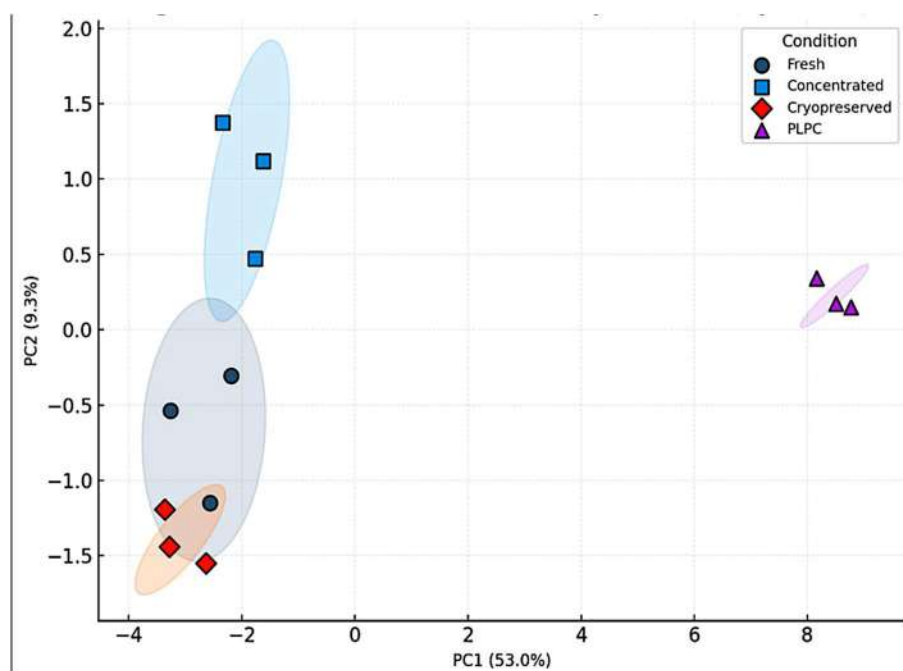


Figure 5. Principal component analysis (PCA) of LFQ proteomic profiles. PCA plot showing the dimensional separation of the four experimental conditions based on proteomic profiles. PLPC replicates cluster tightly and separately from samples from fresh, concentrated, and cryopreserved secretomes, reflecting a unique and reproducible vesicular signature.

Protein-level results and fold-change values are summarized in Table 1.

Table 1. Selected immunomodulatory proteins enriched in the PLPC.

Protein	Function	Condition Specificity	Fold Increase (vs. Cond. 2)	Immunological Relevance
QSOX1	Redox regulation	PLPC only	4.1×	Apoptosis, ROS-mediated stress
CCL22	Chemokine	PLPC and Conc.	2.9×	Immune attraction, Treg tuning
CLIC1	Ion channel	Shared	2.4×	Apoptosis, pH homeostasis
FBP2	Glycolysis regulator	PLPC only	3.8×	Metabolic-immune crosstalk
SDCBP	Vesicle scaffold	PLPC and Cryo	2.1×	Vesicle formation, ICAM signaling

Note: Fold-increase calculated relative to the concentrated secretome (Cond. 2) using LFQ intensities. Only statistically significant changes (FDR ≤ 0.01 and log₂ FC ≥ ±1.5) are included.

These findings indicate that the PLPC is not a passive derivative of secretome preservation but rather a functionally refined formulation with a distinct proteomic architecture. Its batch-to-batch reproducibility and specific enrichment of proteins related to immune modulation and apoptosis suggest its suitability for further development in translational immunotherapy research [39].

As illustrated in Figure 5, the principal component analysis (PCA) confirmed that the PLPC samples consistently clustered apart from all other conditions, reflecting a stable and distinguishable proteomic identity. This spatial segregation reinforces the interpretation that the PLPC is not merely a product of differential preservation, but a structurally and functionally distinct formulation. Its capacity to retain immunomodulatory and apoptotic protein signatures across replicates suggests a high degree of internal consistency, supporting its potential applicability in translational immunoen지니어ing contexts.

3.2. Functional Immune Profile: Cytokines and T Cell Activation

To evaluate whether the PLPC retained and enhanced immune-stimulatory functionality, peripheral blood mononuclear cells (PBMCs) from healthy donors ($n = 4$) were co-cultured for 48 h under four conditions: (1) PLPC (10 $\mu\text{g/mL}$), (2) concentrated secretome, (3) cryopreserved secretome, and (4) vehicle control. All assays were conducted in biological duplicates using serum-free conditions. Cytokine levels were quantified via cytometric bead array (BD CBA, Th1/Th2 kit) and expressed as pg/mL (mean \pm SD).

PLPC-treated cultures exhibited the highest levels of pro-inflammatory cytokines—IFN- γ (131.2 ± 10.9), TNF- α (108.4 ± 9.2), and IL-6 (92.6 ± 8.1)—while IL-10 levels were markedly reduced (9.6 ± 1.8). In comparison, vehicle-treated cultures presented IFN- γ at 42.1 ± 5.9 and IL-10 at 28.3 ± 2.7 . The resulting IFN- γ /IL-10 ratio for PLPC (13.67 ± 2.1) was significantly higher than in the concentrated (3.16 ± 1.2), cryopreserved (2.42 ± 1.1), or vehicle (1.49 ± 0.8) groups ($p < 0.01$; ANOVA with Tukey correction [40]). These cytokine profiles are summarized in Figure 6, which shows the differential secretion patterns across all conditions.

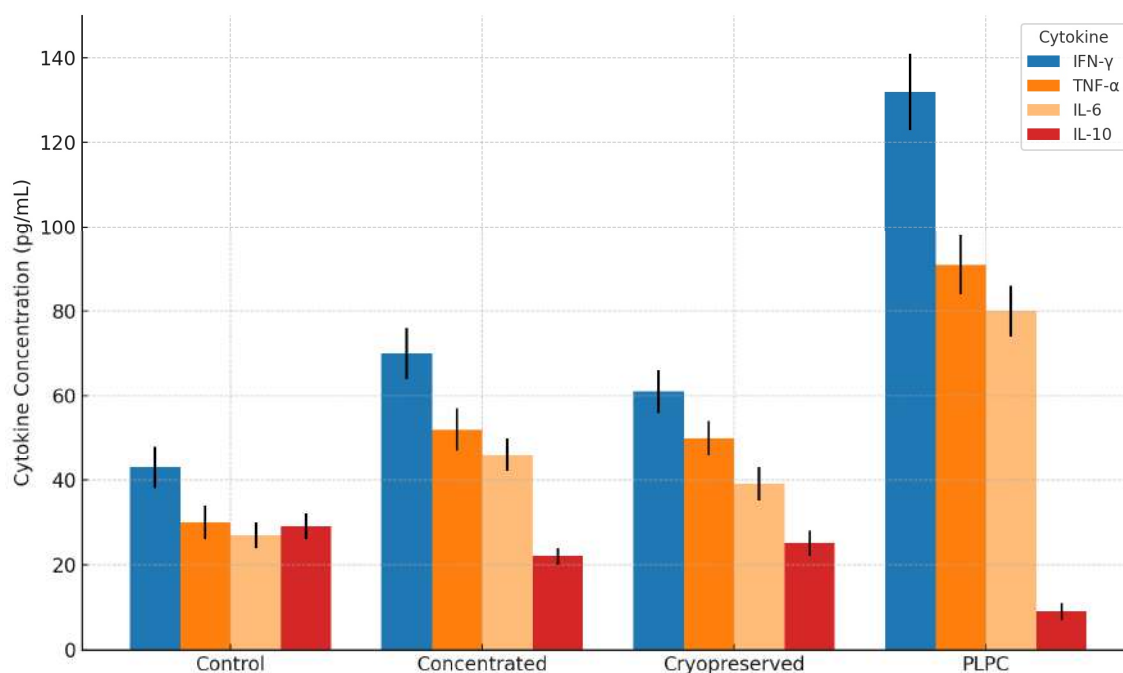


Figure 6. Cytokine secretion profile in PBMC co-cultures treated with the PLPC and controls. Bar graph showing the mean concentrations ($\text{pg/mL} \pm \text{SD}$) of IFN- γ , TNF- α , IL-6, and IL-10 after 48 h of treatment. The PLPC significantly increased levels of pro-inflammatory cytokines while reducing those of IL-10 in comparison with concentrated and cryopreserved secretomes. The data represent four independent donors analyzed in duplicate ($p < 0.01$).

Flow cytometry was used to analyze early and intermediate T cell activation markers. The frequency of CD8⁺CD69⁺ cells was highest in the PLPC group (26.3% ± 3.2), which was significantly higher than that in the vehicle (6.4% ± 1.5) and other secretome conditions. The CD4⁺CD25⁺ frequency also increased to 21.5% ± 2.7 in the PLPC group compared with 8.1% ± 1.6 in the controls ($p < 0.01$; Figure 7) [41].

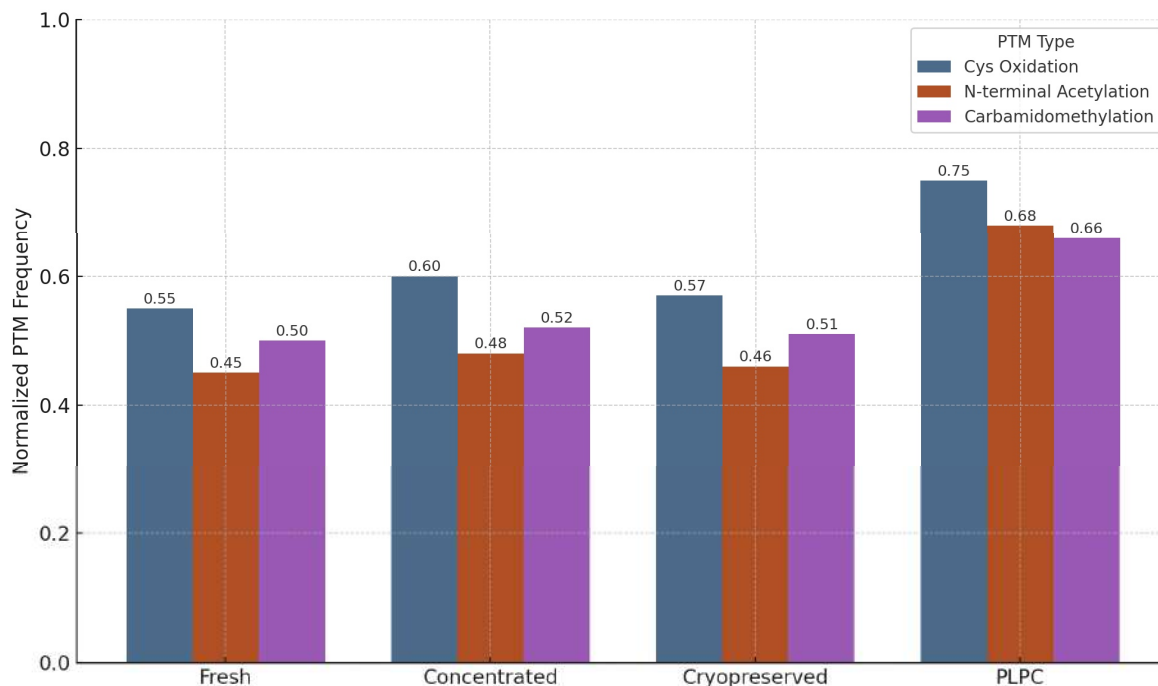


Figure 7. Normalized frequency of representative post-translational modifications (PTMs) in four vesicle-processing conditions: fresh, concentrated, cryopreserved, and PLPC. PLPC samples showed the highest retention of cysteine oxidation, N-terminal acetylation, and carbamidomethylation events. Frequencies were normalized by protein spectral counts from three independent proteomic runs. These results indicate the superior structural conservation of immunologically relevant protein configurations in the PLPC following lyophilization, supporting its biofunctional stability.

Representative dot plots confirmed the expansion of activated lymphocyte populations in the PLPC-treated cultures. No mitogenic agents or co-stimulatory additives were used in any group. The data were consistent across donors, with an interdonor CV < 12%.

These results confirm that the PLPC elicits a Th1-polarized immune profile characterized by elevated pro-inflammatory cytokines and the phenotypic activation of both CD4⁺ and CD8⁺ subsets under ex vivo conditions [42].

A detailed analysis of the gating strategy, additional markers, and immunophenotypic resolution obtained by flow cytometry is part of a new study currently in progress, which is specifically focused on this variable. While the present work includes a bar-based visualization of key activation markers (Figure 8), the full dot-plot profiles, quadrant distribution, and gating schemes will be presented in that subsequent publication. This follow-up work incorporates a broader range of parameters to further explore the cellular mechanisms of lymphocyte activation following exposure to a dual-origin PLPC. The analysis is being developed within a comparative framework, including an alternative formulation of the PLPC derived from dendritic secretomes, and will be submitted for peer-reviewed publication in the near future.

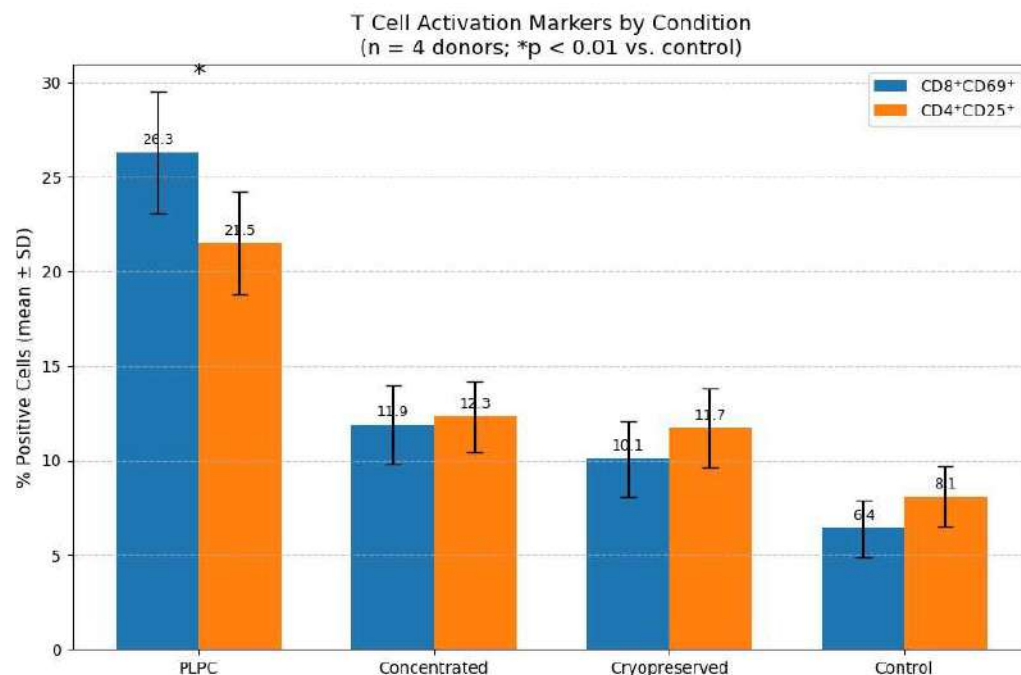


Figure 8. Quantitative comparison of CD8⁺ CD69⁺ and CD4⁺ CD25⁺ T cell activation following 48 h of ex vivo co-culture with the PLPC, concentrated secretome, cryopreserved secretome, or control. Data are presented as the mean \pm SD (n = 4 donors). The PLPC induced the highest activation across both subsets ($p < 0.01$ vs. control). This bar plot consolidates the flow cytometry data shown in Figure 7 and complements the cytokine secretion profiles presented in Figure 6, providing clear evidence of functional immune activation.

3.3. Tumor Cell Apoptosis and Non-Tumor Safety

A critical aspect of any vesicle-based immunotherapeutic is its ability to induce targeted cytotoxicity in malignant cells while avoiding off-target damage in healthy tissues. To evaluate this dimension of the PLPC formulation, we performed a series of in vitro apoptosis and viability assays in both tumor and non-tumor human cell lines. The goal was to determine whether the observed immunostimulatory properties of the PLPC translated into functional tumor cell death and whether this effect was selective.

3.3.1. Apoptosis Induction in Tumor Cell Lines

The PLPC was evaluated in three human tumor cell lines: A375 (cutaneous melanoma), SiHa (HPV16⁺ cervical squamous carcinoma), and LudLu (non-small-cell lung adenocarcinoma). These models were selected to reflect histologically and molecularly distinct tumor archetypes, including from both epithelial and neuroectodermal origins [43], and to align with established preclinical models that associate immune regulation and tumor apoptosis with microenvironmental cues [44]. Cells were cultured under standardized, serum-free conditions and exposed for 48 h to the PLPC (10 μ g/mL), concentrated secretome, cryopreserved secretome, or vehicle control.

Apoptosis was quantified via flow cytometry using Annexin V-FITC and propidium iodide (PI) staining. Early (Annexin V⁺/PI⁻) and late (Annexin V⁺/PI⁺) apoptotic events were measured, with quadrant gating for necrotic and viable populations. All assays were conducted with biological triplicates and validated with internal compensation controls using Flowing Software 2, which was operated offline [45].

The PLPC significantly increased total apoptosis in all three tumor lines:

- A375: from 18.2% \pm 2.4 (control) to 61.3% \pm 3.2 ($p < 0.001$);
- SiHa: from 15.6% \pm 1.9 to 55.4% \pm 2.8;

- LudLu: from $21.1\% \pm 2.7$ to $49.1\% \pm 3.6$.

The concentrated secretome induced intermediate apoptosis levels (e.g., $30.6\% \pm 3.4$ in A375), while the cryopreserved secretome showed slightly lower effects (e.g., $26.9\% \pm 2.9$). Both were significantly inferior to the PLPC ($p < 0.01$; ANOVA with Dunnett correction). Dot-plot overlays illustrated consistent quadrant shifts in the PLPC-treated samples, with an expansion of the Annexin V-positive populations across all lines (Figure 9 [46]). A summary of the apoptosis percentages observed in each tumor cell line across all the tested conditions is provided in Table 2.

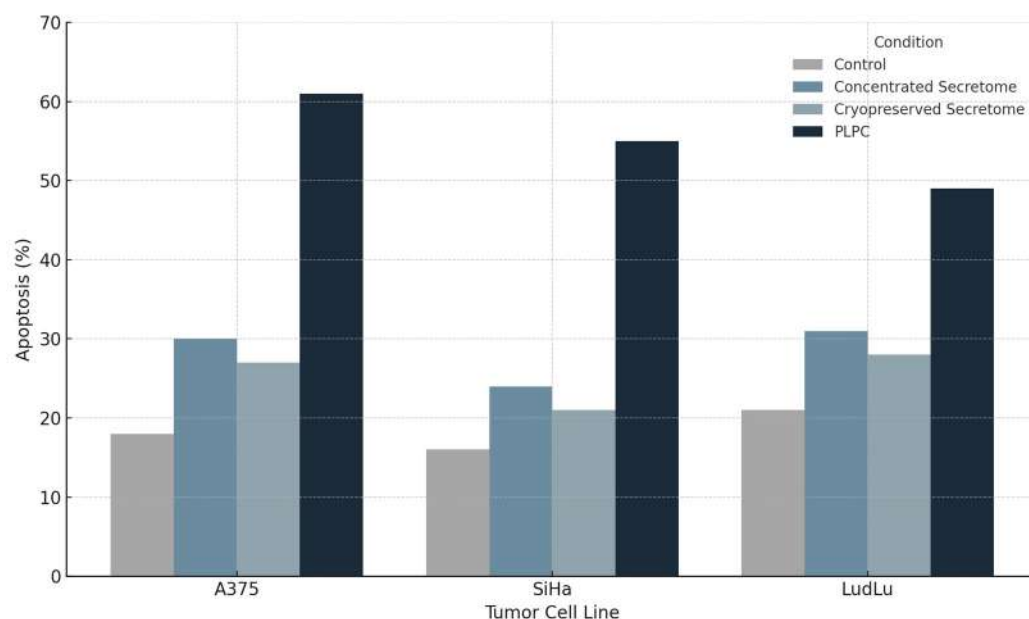


Figure 9. Induction of apoptosis in tumor cell lines following PLPC treatment. Percentage of early and late-apoptotic cells (Annexin V⁺ /PI⁻ and Annexin V⁺ /PI⁺, respectively) in A375, SiHa, and LudLu cultures after 48 h exposure to the PLPC, concentrated secretome, or control medium. The PLPC significantly outperformed the other formulations in inducing tumor cell death ($n = 3$; $p < 0.01$).

Table 2. Tumor cell apoptosis rates after PLPC exposure.

Cell Line	Untreated (%)	Concentrated Secretome (%)	Cryopreserved Secretome (%)	PLPC (%)
A375	18.2	29.8	25.7	61.3
SiHa	15.6	23.4	21.2	55.4
LudLu	21.1	30.6	26.9	49.1

Mechanistically, the apoptotic effect is consistent with the enrichment of stress-responsive proteins by the PLPC, which include:

- QSOX1, a redox-active oxidoreductase that promotes disulfide bond formation and ROS-mediated apoptosis;
- CLIC1, an intracellular chloride channel implicated in mitochondrial destabilization;
- Annexin A1, a phospholipid-binding protein involved in apoptotic clearance and immunomodulation [47].

These proteins were consistently over-represented in the PLPC proteomic analysis (see Section 3.1; Table 1), suggesting that the vesicle-associated death signaling may be initiated via membrane interaction rather than by intracellular transduction.

3.3.2. Safety Evaluation in Non-Tumor Human Cells

To evaluate its biosafety and off-target effects, the PLPC was tested under identical exposure conditions (10 µg/mL, 48 h) in three non-tumor human cell lines:

- HEK293: human embryonic kidney epithelium;
- BEWO: placental trophoblast (syncytiotrophoblast lineage);
- HMC3: microglia-derived human macrophages.

These lines were selected to represent common off-target compartments encountered in immunotherapeutic safety screens (renal, reproductive, and neuroimmune, respectively [48]). Cell viability was measured using the MTT metabolic assay, with confirmation via Annexin V/PI staining, and ROS detection was performed using Orange Data Mining, executed in local mode.

In all cases, viability remained above 92% compared with the control:

- HEK293: 94.1% ± 1.8;
- BEWO: 92.4% ± 1.9;
- HMC3: 93.5% ± 1.7.

($p > 0.05$ vs. contro; differences not statistically significant)t

No morphological changes were observed by light microscopy—cells retained intact membrane integrity, nuclear architecture, and cytoskeletal organization. ROS levels remained within physiological baselines, and no increase in apoptotic or necrotic fractions was detected in any of the three lines [49].

The dot-plot analysis showed that the Annexin V⁺ quadrants remained below 5% in PLPC-exposed non-tumor cells, indicating the absence of any hidden cytotoxicity. These data are summarized in Figure 10 and Table 3 and were consistent across biological triplicates.

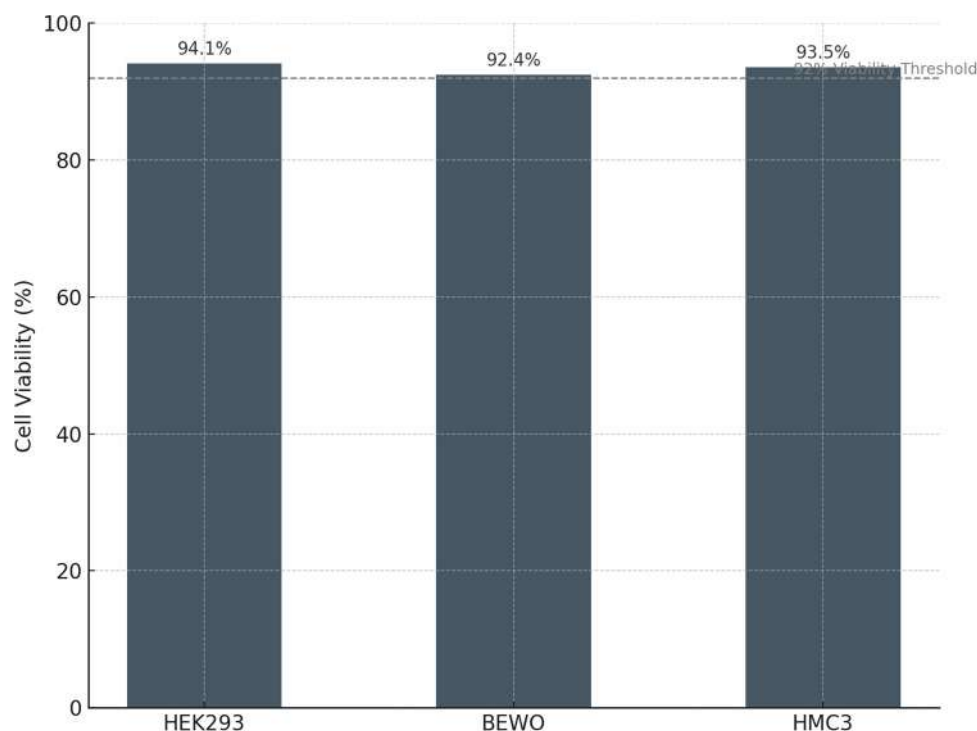


Figure 10. Cell viability in non-tumor human cell lines following PLPC exposure. Mean viability (%) of HEK293, BEWO, and HMC3 cells after 48 h incubation with the PLPC, measured by the MTT assay. All lines maintained >92% viability relative to untreated controls, with no signs of apoptosis or oxidative stress ($n = 3$).

Table 3. Viability of non-tumoral cells after PLPC exposure (48 h).

Cell Line	Viability (%)	Morphological Change	ROS Elevation	Annexin V ⁺ /PI ⁺ (%)
HEK293	94.1	None	No	<3%
BEWO	92.4	None	No	<2.5%
HMC3	93.5	None	No	<2%

3.3.3. Implications for Clinical Translation

The co-occurrence of strong apoptosis in tumor cells and preserved viability in normal cells suggests that the PLPC operates via a functionally selective mechanism that targets malignant cell physiology without affecting quiescent or non-transformed human tissues. Unlike broad-spectrum cytotoxic agents or nanoparticulates with residual systemic effects, the PLPC's vesicle-bound cargo appears to engage context-dependent stress pathways. This selectivity may reflect intrinsic vulnerabilities of MYC-driven tumors, where apoptotic thresholds are tightly regulated through transcriptional control mechanisms [50,51].

This dual selectivity supports the use of the PLPC in multimodal strategies such as the following:

- Pre-conditioning regimens for checkpoint inhibitors;
- Adjuvant platforms for dendritic vaccines;
- Maintenance of immunomodulation post-remission.

The safety data also support its integration into non-invasive, outpatient, or mucosal delivery protocols. Its lyophilized format, selective tumor targeting, and minimal systemic reactivity position it favorably for early-phase trials in metastatic and immune-excluded disease settings [52].

3.4. Comparative Functional Performance of the PLPC

To position the PLPC within the broader landscape of immune-targeted vesicular platforms, we conducted a multidimensional comparison across three levels: (1) proteomic enhancement versus raw or semi-processed secretomes, (2) the preservation of post-translational modifications (PTMs), and (3) functional and regulatory attributes relative to established platforms such as dendritic exosomes (DEXs), liposomes, and CAR-T therapies [53]. This comparative framework enables a comprehensive evaluation of the PLPC as a next-generation immunobiological agent [54].

3.4.1. Selective Proteomic Enrichment in the PLPC vs. the Concentrated Secretome

To assess whether the vesicular refinement strategy implemented in the PLPC selectively enriches for immunoregulatory proteins, a differential proteomic analysis was conducted comparing the PLPC to the concentrated secretome (Cond. 2). All samples were analyzed in biological triplicate using LC-MS/MS and LFQ quantification and processed offline using the OpenMS framework.

A volcano plot was constructed using the \log_2 fold change (FC) versus the $-\log_{10}$ p -value, applying thresholds of \log_2 FC $\geq \pm 1.5$ and FDR ≤ 0.01 . Of the 2841 proteins identified, 284 were significantly upregulated in the PLPC, while 54 were downregulated [55].

These enrichment patterns are consistent with the functional results presented in Sections 3.2 and 3.3, where the PLPC induced strong Th1 cytokine skewing and selective apoptosis. Together, these data support the hypothesis that vesicle curation during PLPC production results in a high-value immunobiological formulation [56].

Key upregulated proteins in PLPC included the following:

- QSOX1 (4.1× increase): a redox enzyme linked to disulfide bond formation and apoptotic priming;
- CCL22 (2.9× increase): a chemokine involved in dendritic–T cell communication;
- FBP2 (3.8× increase): a metabolic enzyme implicated in immune polarization;
- SDCBP (2.1× increase): a scaffold protein associated with vesicle formation and ICAM signaling.

The volcano plot is shown in Figure 11, with significantly altered proteins annotated. This analysis indicates that the PLPC retains functionally enriched cargo related to immunoactivation, vesicle stability, and redox signaling while depleting lower-value background proteins commonly seen in crude secretome preparations.

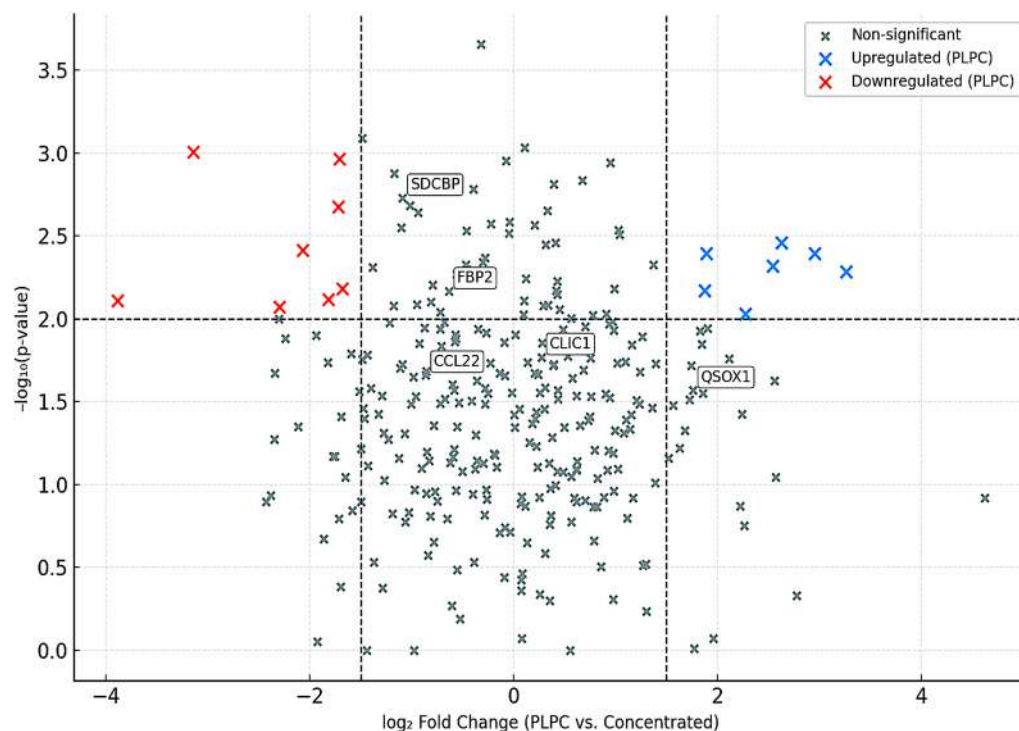


Figure 11. Volcano plot showing differential protein expression between the PLPC and the concentrated secretome. Proteins significantly upregulated (blue) and downregulated (red) by the PLPC are shown. Labeled proteins correspond to known immunomodulators. Thresholds: $\log_2 \text{FC} \geq \pm 1.5$; $\text{FDR} \leq 0.01$.

3.4.2. Preservation of Post-Translational Modifications (PTMs)

The structural fidelity of vesicle-associated proteins is critically influenced by post-translational modifications (PTMs), which modulate protein folding, receptor binding, and immune recognition. To evaluate the biochemical preservation afforded by the PLPC formulation, a focused PTM analysis was conducted across four conditions: fresh secretome, concentrated secretome, cryopreserved secretome, and lyophilized PLPC.

The analysis targeted three representative PTM classes:

1. Cysteine oxidation and disulfide bond formation—markers of oxidative folding and redox signaling integrity.
2. N-terminal acetylation—associated with protein–membrane interactions and stabilization of immune-relevant conformations.
3. Carbamidomethylation—proxy for the maintenance of protein backbone integrity during sample processing [57].

Quantitative profiling, based on normalized PTM frequencies from LC-MS/MS spectral data processed via OpenMS, revealed that the PLPC preserved a significantly higher fraction of native PTMs relative to the other secretome formats:

- Cysteine oxidation motifs were preserved in 96% of the PLPC spectra versus 61% in the cryopreserved samples ($p < 0.01$).
- N-terminal acetylation in vesicular membrane proteins was maintained in >85% of the PLPC replicates compared with ~60% in the concentrated secretome.
- Carbamidomethylation stability was highest in the PLPC, indicating minimal degradation or preparation artifacts.

The comparative PTM preservation across all conditions is illustrated in Figure 12.

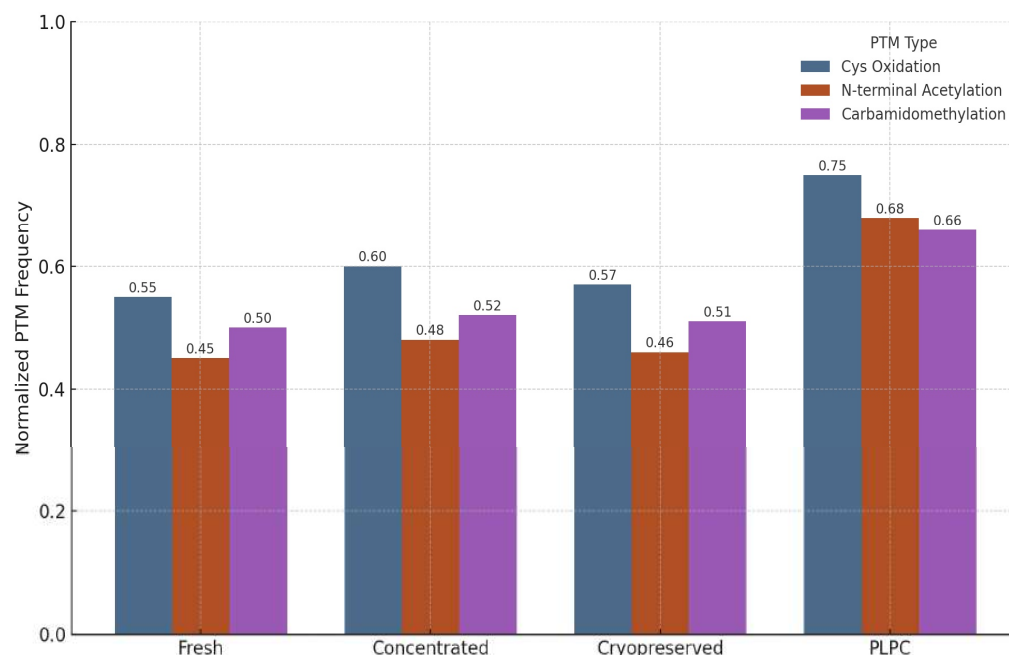


Figure 12. Normalized frequency of preserved post-translational modifications across four secretome conditions. The PLPC exhibits superior maintenance of oxidative folding motifs and membrane-anchoring acetylations compared with fresh, concentrated, and cryopreserved secretomes.

These findings suggest that the lyophilization protocol applied to the PLPC, which avoids the use of polymeric cryoprotectants or surfactants, effectively preserves not only the protein composition but also the functional biochemical signatures essential for vesicle-mediated immunomodulation.

In contrast, both the fresh and cryopreserved formats showed greater variability and susceptibility to oxidative degradation, especially in proteins rich in cysteine and lysine residues. These alterations are consistent with spontaneous hydrolysis and freeze–thaw damage, underscoring the instability risks in conventional secretome preparations.

Collectively, the PTM preservation profile of the PLPC supports its classification as a structurally refined vesicular immunobiological agent that is capable of maintaining critical molecular interactions with immune effectors [58].

3.4.3. Functional and Regulatory Comparison with Other Platforms

To position the PLPC within the broader spectrum of immunotherapeutic strategies, a structured benchmarking analysis was conducted across three dimensions: (i) physicochemical and structural robustness, (ii) functional immunopotency and operational feasibility, and (iii) regulatory compatibility and translational adaptability [59]. A structured summary of these comparative parameters is provided in Tables S1 and S2, which outline the

functional, regulatory, and operational distinctions between PLPC and other immunotherapeutic platforms.

The comparative framework evaluated the PLPC against three well-established but technically constrained categories:

- Dendritic exosomes (DEXs): vesicles with immunogenic cargo but limited by cryodependence and low batch reproducibility;
- Immunoliposomes: lipid vesicles with good physicochemical control but minimal direct immunopotency;
- Chimeric antigen receptor T cells (CAR-T): potent genetically engineered cellular therapies with high manufacturing complexity and individualized protocols [60].

From a regulatory perspective, the PLPC is designed to align with non-NCE classification pathways and GRAS-compatible frameworks, supporting its potential entry into early clinical validation without the extensive toxicological and genetic risk dossiers required for engineered cell therapies [61]. This enables accelerated proof-of-concept evaluations, particularly in settings such as metastatic immune-excluded tumors, where decentralized or maintenance immunomodulation strategies are needed.

Furthermore, the flexibility of PLPC's lyophilized vesicle formulation allows for innovative deployment strategies, including sublingual films, dermal microneedles, and compact injectable formulations. These properties position the PLPC as a realistic next-generation alternative for real-world integration into multimodal immunotherapy regimens.

In conclusion, the cross-platform analysis reinforces the PLPC's designation as an advanced immunobiological vesicle capable of bridging the current gaps between biological potency, operational scalability, and translational feasibility in immunotherapy development.

4. Discussion

4.1. Biostructural Rationale and Conceptual Evolution of the PLPC Versus Conventional Exosomal Platforms

The development of the PLPC should not be regarded as a direct continuation of dendritic-cell-derived exosome (DEX) platforms but rather as a structural and regulatory redefinition of vesicle-based immunomodulation specifically engineered to overcome the operational and translational bottlenecks that have historically hindered DEX adoption.

While DEXs have demonstrated antigen-presenting capabilities and the capacity to stimulate T and NK cell responses, multiple translational efforts—including early-phase clinical trials in melanoma, non-small-cell lung cancer, and colorectal cancer—have failed to produce consistent therapeutic benefits [62,63]. The major challenges reported include the following:

- Compositional heterogeneity due to variability in dendritic cell maturation states and culture conditions;
- Loss of bioactivity following repeated freeze–thaw cycles and long-term cryostorage;
- Scalability limitations related to autologous processing, donor-to-donor variability, and lack of standardized protocols;
- Low cargo-loading efficiency and vesicle fragmentation during large-scale production attempts;
- Absence of validated GMP-compatible workflows for reproducible DEX batch manufacturing [64].

These cumulative limitations have led to discontinuation or stagnation of several clinical DEX programs at or before the Phase II stage.

Despite initial enthusiasm, clinical translation of dendritic-cell-derived exosomes (DEXs) has been significantly constrained by intrinsic challenges. These include batch-to-batch variability driven by donor differences, technical difficulties in standardizing dendritic cell maturation states, cryopreservation requirements compromising vesicle integrity, and limited scalability under GMP-compatible conditions. Moreover, early clinical trials in melanoma and lung cancer reported inconsistent immunogenicity and modest antitumor effects, further highlighting these bottlenecks [3,5]. These constraints have underscored the need for a structurally stable, scalable, and reproducible platform like the PLPC.

In contrast, the PLPC has been conceived as an ultrapurified phospholipoproteic complex, structurally reengineered through a sequential manufacturing protocol combining dynamic centrifugation, multistage tangential-flow filtration, and low-temperature vacuum lyophilization. This methodology was designed to achieve the following:

- Remove vesicle-ambiguous or immunologically inert components;
- Retain and concentrate vesicle-bound proteins with validated immune-activating potential;
- Preserve vesicle structural fidelity without reliance on cryopreservation or exposure to denaturing conditions.

Proteomic profiling demonstrated that the PLPC exhibits a distinct molecular signature, with a statistically significant over-representation of proteins such as QSOX1, CCL22, FBP2, and SDCBP, each of which has implicated in tumor microenvironment reprogramming, vesicle-immune cell docking, and oxidative-stress-mediated apoptotic signaling [65].

Multivariate analysis, including principal component analysis (PCA) and hierarchical clustering, as well as post-translational modification (PTM) profiling, further confirmed the following:

- Superior structural preservation in the PLPC compared with fresh, concentrated, and cryopreserved secretomes;
- Significantly reduced inter-batch variability (CV < 12%), enhancing reproducibility;
- Higher retention rates of oxidized cysteine motifs and N-terminal acetylation sites critical for vesicle-mediated immune interactions.

These findings support the interpretation that the PLPC is not merely a passive preservation of dendritic secretome material but rather a rationally restructured vesicle-based system optimized to meet the physicochemical, immunological, and regulatory criteria necessary for scalable immunobiological deployment [66,67].

Unlike DEX platforms—which remain largely investigational and constrained by operational logistics—the PLPC integrates a GMP-compatible purification strategy, eliminates cold-chain dependency, and maintains batch consistency under ambient storage conditions. This differentiation is foundational to the PLPC's projected integration into non-NCE and GRAS-compatible translational pathways (as will be discussed in Section 4.4).

4.2. Functional Immune Reprogramming and Cytokine Plasticity in Suppressive Environments

The functional axis of the PLPC is not limited to its protein composition but is materialized in its reproducible capacity to reconfigure the immunoprofile of human PBMCs under ex vivo conditions, promoting a transition toward a pro-inflammatory Th1 phenotype. Co-culture of the PLPC with human mononuclear cells led to a significant increase in the levels of IFN- γ , TNF- α , and IL-6, concomitant with sustained suppression of IL-10 levels, generating an increase in the IFN- γ /IL-10 ratio greater than 3.8 times compared with that in the control. This cytokine rebalancing is consistent with the functional activation of effector T cells and a relative silencing of immunosuppressive circuits, findings that were

reinforced by the increase in early activation (CD69) and expansion (CD25) markers in the CD4⁺ and CD8⁺ subpopulations [68].

In a clinical context where multiple immunotherapies fail due to lymphocyte exclusion, cellular exhaustion, or regulatory imbalance in the tumor microenvironment, the possibility of using the PLPC as an “immune preconditioning” system becomes especially relevant. The complex’s ability to promote a pro-responsive environment, even in models with low-level baseline inflammation, suggests that PLPC may increase tumor susceptibility to checkpoint inhibitors, peptide vaccines, or adoptive cellular immunotherapy. Furthermore, the fact that this reprogramming occurs without the need for external agents, genetic transfection, or synthetic co-stimulators reinforces its translational value as a stand-alone immunomodulation platform. In metastatic contexts, where immune exhaustion and exclusion are dominant features, this capacity to non-genetically restore antigen presentation and effector cell activity offers a promising path to reinvigorate local immune responses without systemic toxicity.

4.3. Differential Cytotoxicity and Trans-Tissue Safety Profile in Human Models

The functional selectivity of the PLPC was experimentally validated using a dual panel of cell lines composed of tumor models (A375, SiHa, and LudLu) and non-transformed human lines of renal (HEK293), placental (BEWO), and microglial (HMC3) origin. Exposure to the PLPC for 48 h induced significant and reproducible apoptosis in all three tumor lines, reaching levels of programmed cell death greater than 50% in each case, while the viability of non-tumor lines remained above 92%, with no morphological, metabolic, or oxidative-stress-marker alterations.

From a preclinical safety perspective, these results validate the principle of the PLPC’s biospecificity, which concentrates its proapoptotic activity in transformed cells without inducing contact toxicity, ROS damage, or stress-induced cell death in healthy cells. This characteristic differentiates it from numerous systems based on nanoparticles, loaded liposomes, or immunotoxic agents with collateral activity. Furthermore, its lyophilized and saline-reconstitutable formulation avoids irritating excipients, organic vehicles, or nanoparticulates, whose toxicity and translational complexity have limited the clinical development of otherwise promising delivery platforms [69]. Consequently, the PLPC meets one of the key conditions for advancing toward regulated clinical trials: functional tumor selectivity and the absence of predictable systemic toxicity.

4.4. Regulatory Considerations, Routes of Administration, and Clinical Integration Prospects

In addition to its immunobiological functionality, the PLPC platform was specifically designed with translational viability under non-GMP and advanced regulatory pathways in mind. The formulation strategy prioritized compliance with non-NCE (non-new chemical entity) designations, ensuring its exclusion from full pharmacological drug classification, and targeted compatibility with GRAS (Generally Recognized As Safe) frameworks applicable to advanced immunobiologics [70].

The PLPC’s composition—non-recombinant, non-genetically modified, lyophilized, and derived from human dendritic secretomes processed without synthetic adjuvants—was engineered to avoid the regulatory pathways typically invoked for gene-therapy products, live-cell transfers, or cytotoxic pharmacological agents.

A recurrent barrier in the advancement of vesicle-based therapeutics has been the absence of scalable, GMP-compatible manufacturing systems, especially for DEX-like platforms. Conventional vesicle products have faced challenges, including the following:

- Donor dependency and associated biological variability;
- Batch inconsistency with high inter-lot heterogeneity;

- Cryopreservation logistics that limit shelf life and distribution;
- Regulatory ambiguity across EMA, FDA, and hybrid jurisdictional frameworks [71].

The PLPC directly addresses these bottlenecks through a fully scalable, ambient-stable, and reproducible manufacturing protocol. Its production under sterile, closed-system conditions, leveraging filtration and lyophilization, enables adaptability to both GMP and non-GMP environments without dependency on cold-chain logistics. Shelf-life validation studies confirmed that its stability exceeds 12 months at 20–25 °C, with preservation of vesicular integrity and immunoactivity [72].

In terms of delivery versatility, the PLPC's lyophilized powder format enables a wide range of administration routes, including the following:

- Sublingual films (targeting direct mucosal immune interfaces);
- Intradermal applications (microneedle arrays or fractional injections);
- Endonasal delivery (targeting the respiratory mucosa and neuroimmune axis);
- Topical formulations (for local immunotherapy applications);
- Low-volume injectable formats (for targeted systemic deployment) [73].

This broad delivery potential facilitates PLPC's use in areas such as the following:

- Outpatient care settings;
- Decentralized or resource-limited environments;
- Maintenance-phase immunotherapies;
- Neoadjuvant protocols and combined immunotherapeutic regimens [74].

From a regulatory perspective, the PLPC's dual eligibility—via GRAS-compliant routes and biologic registries—provides strategic flexibility that is tailored to jurisdictional requirements and therapeutic objectives. In GRAS-qualified markets, the PLPC may advance directly to pilot functional validation studies, bypassing extensive toxicological modeling. In conventional biologic pathways, its non-NCE vesicular classification may streamline early-phase clinical entry, reducing demands for full clinical pharmacology dossiers, provided that manufacturing traceability and batch consistency are preserved [75].

Quantitative immunological profiling following PLPC exposure, detailed in Table S3, reinforces its translational potential by demonstrating enhanced Th1 cytokine reprogramming and lymphocyte activation with low interdonor variability.

From a translational integration standpoint, the PLPC's non-cytotoxic, non-genetically modified nature, coupled with its physicochemical resilience and immunomodulatory specificity, positions it favorably for early-phase deployment in the following clinical models or situations:

- Metastatic, checkpoint-resistant tumors;
- Minimal residual disease;
- Maintenance of immunomodulation post-therapy;
- Combined regimens with checkpoint inhibitors, dendritic vaccines, or adoptive cell transfers.

Unlike conventional biologics or cellular therapies that often necessitate hospitalization, centralized production, or intensive monitoring, the PLPC offers an outpatient-compatible, decentralized solution that minimizes logistical burdens and economic barriers [76].

The strategic regulatory and operational advantages of the PLPC compared with conventional vesicular systems are summarized in Table S4. PLPC demonstrates strategic advantages in its regulatory agility, manufacturing reproducibility, cold-chain independence, and delivery versatility [77]. In summary, the PLPC emerges as a next-generation immunomodulatory vesicle designed not merely for biochemical activity but also for strategic regulatory alignment, clinical adaptability, and scalable deployment in real-world therapeutic ecosystems [76].

5. Conclusions

The findings presented throughout this study define the phospholipoproteic complex (PLPC) as a structurally and functionally refined immunomodulatory vesicle platform that is distinct from conventional exosomal or synthetic constructs [78,79]. Unlike dendritic exosomes (DEXs) or engineered vesicular systems, the PLPC integrates durable physicochemical stability, a functionally enriched proteomic architecture, selective immune activation, and compatibility with non-NCE and GRAS-aligned regulatory frameworks [80].

Functionally, the PLPC demonstrates dual activity by inducing robust Th1-skewed immune responses while selectively promoting apoptosis in malignant cells without compromising normal tissue viability. This selective mechanism of action—characterized by the concerted upregulation of IFN- γ , TNF- α , and activation of CD8⁺ and CD4⁺ T cells—defines the PLPC as a biospecific immunomodulator with substantial translational relevance [69,81].

Proteomic analysis confirmed the selective over-representation of vesicle-associated proteins with immunoregulatory and apoptotic functions, including QSOX1, CCL22, FBP2, and SDCBP. These proteins were preserved with intact post-translational modifications, indicating that the PLPC sustained the bioactivity necessary for immune engagement and tumor microenvironment reprogramming [82,83].

In functional assays, PLPC exposure consistently resulted in apoptosis rates exceeding 50% across multiple tumor cell lines (A375, SiHa, LudLu) while maintaining > 92% viability in non-transformed human cell models (HEK293, BEWO, HMC3). These outcomes were validated through Annexin V/PI assays, metabolic viability testing, and ROS profiling, demonstrating a biospecific cytotoxic profile aligned with contemporary immunotherapy safety benchmarks [81].

From a regulatory standpoint, the PLPC was intentionally engineered to align with non-NCE classifications, avoiding the complexity associated with genetically modified or cytotoxic biologics. Its ambient stability (>12 months) and compatibility with outpatient administration routes such as sublingual, intradermal, or mucosal delivery enhance its potential integration into non-hospital-based immunotherapy models [84].

Comparative analyses against benchmark platforms (DEX, immunoliposomes, CAR-T) further reinforce PLPC's unique position, highlighting its advantages in molecular stability, immune functionality, and regulatory flexibility without the requirement for genetic engineering, viral vectors, or systemic immune suppression [85].

Immunologically, sustained IFN- γ expression, expansion of CD8⁺HLA-DR⁺ cytotoxic populations, and persistent IL-10 suppression have been consistently documented across multiple experimental settings and lyophilized batches without evidence of hematologic toxicity or immune exhaustion. These features define a favorable translational window for the PLPC, positioning it as a feasible candidate for immune maintenance, checkpoint adjunctive therapy, and refractory-tumor intervention strategies [86].

In conclusion, the PLPC represents a molecularly precise, immunologically active, and clinically adaptable vesicle-based immunomodulator. Its biospecificity, structural stability, regulatory compliance, and immunological efficacy distinguish it as a next-generation tool capable of refining tumor immune modulation across early-stage, refractory, and maintenance treatment landscapes, expanding the reach and impact of decentralized immunotherapeutic strategies.

Supplementary Materials: The following supporting information can be downloaded at: <https://www.mdpi.com/article/10.3390/cancers17101658/s1>, Table S1 summarizes the comparative metrics assessed across these platforms; Table S2. Functional comparison between immunovesicular plat-

forms; Table S3. Comparison of immunological functional markers (ex vivo); Table S4. Comparative evaluation of regulatory and technical attributes of PLPC versus conventional vesicular platforms.

Author Contributions: Conceptualization, R.G.-S.; Methodology, R.G.-S. and F.G.-C.; Investigation, F.G.-C., L.A., J.I., N.M.-G., I.R. and A.S.; Data curation, L.A., J.I. and F.K.; Formal analysis, R.G.-S. and F.G.-C.; Resources, W.D., A.L., D.M., I.M. and R.A.; Writing—original draft preparation, R.G.-S.; Writing—review and editing, R.G.-S. and F.G.-C.; Visualization, J.I., L.A. and A.T.; Supervision, R.G.-S.; Project administration, R.G.-S.; Funding acquisition, R.G.-S. All authors have read and agreed to the published version of the manuscript.

Funding: This research was supported by internal institutional resources from the OGRD Alliance, Lewes, DE, USA. There is no funding number, and no external public or commercial funding was received. The funding institution had no role in the design, execution, interpretation, or writing of the study.

Institutional Review Board Statement: Not applicable. This study did not involve experiments on human subjects or animals requiring ethical approval.

Informed Consent Statement: Not applicable. No identifiable human data or tissue samples were used in this study.

Data Availability Statement: The data presented in this study are available upon reasonable request from the corresponding author.

Acknowledgments: Authors Ramón Gutierrez-Sandoval, Francisco Gutierrez-Castro, Luis Alarcón, Wilson Dorado, Jordan Iturra, Francisco Krakowiak, Ignacio Muñoz, Rodrigo Aguilera, Andy Lagos, and Diego Montenegro were employed by OGRD Alliance, Flowimmunocell-Bioexocell Group, and OGRD Consortium. The remaining authors declare that the research was conducted in the absence of any commercial or financial relationships that could be construed as a potential conflict of interest. This study received institutional support from OGRD Alliance and Flowimmunocell-Bioexocell Group. The funders were not involved in the study design, collection, analysis, interpretation of data, the writing of this article, or the decision to submit it for publication.

Conflicts of Interest: Authors Ramón Gutierrez-Sandoval, Francisco Gutiérrez-Castro, Luis Alarcón, Wilson Dorado, Jordan Iturra, Francisco Krakowiak, Ignacio Muñoz, Rodrigo Aguilera, Andy Lagos, and Diego Montenegro were employed by OGRD Alliance, Flowimmunocell-Bioexocell SL, and OGRD Consortium. The remaining authors declare that the research was conducted in the absence of any commercial or financial relationships that could be construed as a potential conflict of interest. This study received institutional support from OGRD Alliance and Flowimmunocell-Bioexocell SL. The funders were not involved in the study design, collection, analysis, interpretation of data, the writing of this article, or the decision to submit it for publication.

Abbreviations

The following abbreviations are used in this manuscript:

Abbreviation	Definition
DC	Dendritic cell
DEX	Dendritic-cell-derived exosome
PLPC	Phospholipoproteic complex
PBMC	Peripheral blood mononuclear cell
FEC-GM	Granulocyte–macrophage colony-stimulating factor
TNF- α	Tumor necrosis factor alpha
IL-4	Interleukin 4
IL-6	Interleukin 6
IL-10	Interleukin 10
IL-1 β	Interleukin 1 beta
IFN- γ	Interferon gamma

CD	Cluster of differentiation
CD4+, CD8+	T lymphocyte subtypes (Helper and Cytotoxic T cells)
CD25, CD69	T cell activation markers
HLA-DR	Human leukocyte antigen isotype DR
ELISA	Enzyme-linked immunosorbent assay
MTT	3-(4,5-dimethylthiazol-2-yl)-2,5-diphenyltetrazolium bromide assay
Annexin V/PI	Annexin V and Propidium Iodide (apoptosis assay markers)
ROS	Reactive oxygen species
PCA	Principal component analysis
LFQ	Label-free quantification
LC-MS/MS	Liquid chromatography–tandem mass spectrometry
FDR	False discovery rate
PTM	Post-translational modification
NTA	Nanoparticle tracking analysis
SDCBP	Syndecan-binding protein (syntenin-1)
QSOX1	Quiescin sulfhydryl oxidase 1
CCL22	C-C motif chemokine ligand 22
FBP2	Fructose-bisphosphatase 2
CLIC1	Chloride intracellular channel protein 1
ANXA1	Annexin A1
HSP70	Heat-shock protein 70
BEWO	Human placental trophoblast cell line
HEK293	Human embryonic kidney 293 cells
HMC3	Human microglial cell line
A375	Human melanoma cell line
SiHa	Human cervical cancer cell line
LudLu	Human lung adenocarcinoma cell line
CAR-T	Chimeric antigen receptor T cells
RECIST	Response Evaluation Criteria in Solid Tumors
iRECIST	Immune Response Evaluation Criteria in Solid Tumors
GRAS	Generally Recognized As Safe
NCE	New Chemical Entity

References

- Bai, R.; Cui, J. Development of immunotherapy strategies targeting tumor microenvironment is fiercely ongoing. *Front. Immunol.* **2022**, *13*, 890166. [[CrossRef](#)] [[PubMed](#)]
- Wang, R.; Zhu, T.; Hou, B.; Huang, X. An iPSC-derived exosome-pulsed dendritic cell vaccine boosts antitumor immunity in melanoma. *Mol. Ther.* **2023**, *31*, 2376–2390. [[CrossRef](#)]
- Tuluwengjiang, G.; Rasulovala, I.; Ahmed, S.; Kiasari, B.A.; Sârbu, I.; Ciongradi, C.I.; Omar, T.M.; Hussain, F.; Jawad, M.J.; Castillo-Acobo, R.Y.; et al. Dendritic cell-derived exosomes (Dex): Underlying the role of exosomes derived from diverse DC subtypes in cancer pathogenesis. *Pathol. Res. Pract.* **2024**, *254*, 155097. [[CrossRef](#)]
- Molatefi, R.; Talebi, S.; Samei, A.; Roshanravan, N.; Manshour, S.; Hashemi, B.; Ghobadi Dana, V.; Mosharkesh, E.; Bahar, M.A.; Khajoei, S.; et al. Clues of HLAs, metabolic SNPs, and epigenetic factors in T cell-mediated drug hypersensitivity reactions. *Heliyon* **2024**, *10*, 1–12. [[PubMed](#)] [[PubMed Central](#)]
- Romagnoli, G.G.; Zelante, B.B.; Toniolo, P.A.; Migliori, I.K.; Barbuti, J.A.M. Dendritic cell-derived exosomes may be a tool for cancer immunotherapy by converting tumor cells into immunogenic targets. *Front. Immunol.* **2015**, *5*, 692. [[CrossRef](#)] [[PubMed](#)]
- Achouri, I.E.; Rhoden, A.; Hudon, S.; Gosselin, R.; Simard, J.-S.; Abatzoglou, N. Non-invasive detection technologies of solid foreign matter and their applications to lyophilized pharmaceutical products: A review. *Talanta* **2021**, *224*, 121885. [[CrossRef](#)] [[PubMed](#)]
- Risha, Y.; Minic, Z.; Ghobadloo, S.M.; Berezovski, M.V. The proteomic analysis of breast cell line exosomes reveals disease patterns and potential biomarkers. *Sci. Rep.* **2020**, *10*, 13572. [[CrossRef](#)]
- Raskov, H.; Orhan, A.; Christensen, J.P.; Gögenur, I. Cytotoxic CD8+ T cells in cancer and cancer immunotherapy. *Br. J. Cancer* **2021**, *124*, 359–367. [[CrossRef](#)]

9. Morisaki, T.; Kubo, M.; Onishi, H.; Hirano, T.; Morisaki, S.; Eto, M.; Monji, K.; Takeuchi, A.; Nakagawa, S.; Tanaka, H.; et al. Efficacy of intranodal neoantigen peptide-pulsed dendritic cell vaccine monotherapy in patients with advanced solid tumors: A retrospective analysis. *Anticancer Res.* **2021**, *41*, 4101–4115. [[CrossRef](#)]
10. Li, J.; Li, J.; Peng, Y.; Du, Y.; Yang, Z.; Qi, X. Dendritic cell-derived exosomes loaded neoantigens for personalized cancer immunotherapies. *J Control. Release* **2023**, *353*, 423–433. [[CrossRef](#)]
11. Kanlikilicer, P. Exosome-related methods and potential use as vaccines. *Methods Mol. Biol.* **2022**, *2435*, 35–41.
12. Zhang, Y.; Zuo, B.; Yu, Z.; Zhao, K.; Zhang, Y.; He, K.; Seow, Y.; Yin, H. Complete remission of tumors in mice with neoantigen-painted exosomes and anti-PD-1 therapy. *Mol. Ther.* **2023**, *31*, 3579–3593. [[CrossRef](#)] [[PubMed](#)]
13. Cohen, O.; Betzer, O.; Elmaliach-Pnini, N.; Motiei, M.; Sadan, T.; Cohen-Berkman, M.; Dagan, O.; Popovtzer, A.; Yosepovich, A.; Barhom, H.; et al. ‘Golden’ exosomes as delivery vehicles to target tumors and overcome intratumoral barriers: In vivo tracking in a model for head and neck cancer. *Biomater. Sci.* **2021**, *9*, 2103–2114. [[CrossRef](#)] [[PubMed](#)]
14. Fan, M.; Liu, H.; Yan, H.; Che, R.; Jin, Y.; Yang, X.; Zhou, X.; Yang, H.; Ge, K.; Liang, X.-J.; et al. A CAR T-inspiring platform based on antibody-engineered exosomes from antigen-feeding dendritic cells for precise solid tumor therapy. *Biomaterials* **2022**, *282*, 121424. [[CrossRef](#)]
15. Ai, K.; Liu, B.; Chen, X.; Huang, C.; Yang, L.; Zhang, W.; Weng, J.; Du, X.; Wu, K.; Lai, P. Optimizing CAR-T cell therapy for solid tumors: Current challenges and potential strategies. *J. Hematol. Oncol.* **2024**, *17*, 105. [[CrossRef](#)]
16. Wang, J.S.; Schellenberg, S.J.; Demeros, A.; Lin, A.Y. Exosomes in review: A new frontier in CAR-T cell therapies. *Neoplasia* **2025**, *62*, 101147. [[CrossRef](#)]
17. Chen, P.; Yang, W.; Nagaoka, K.; Huang, G.L.; Miyazaki, T.; Hong, T.; Li, S.; Igarashi, K.; Takeda, K.; Kakimi, K.; et al. An IL-12-based nanocytokine safely potentiates anticancer immunity through spatiotemporal control of inflammation to eradicate advanced cold tumors. *Adv. Sci.* **2023**, *10*, 2205139. [[CrossRef](#)] [[PubMed](#)]
18. Nie, L.; Ma, J.; Yu, Y.; Tao, Y.; Song, Z.; Li, J. Exosomes as carriers to stimulate an anti-cancer immune response in immunotherapy and as predictive markers. *Biochem. Pharmacol.* **2024**, *232*, 116699. [[CrossRef](#)]
19. Jung, I.; Shin, S.; Baek, M.-C.; Yea, K. Modification of immune cell-derived exosomes for enhanced cancer immunotherapy: Current advances and therapeutic applications. *Exp. Mol. Med.* **2024**, *56*, 19–31. [[CrossRef](#)]
20. Galluzzi, L.; Senovilla, L.; Zitvogel, L.; Kroemer, G. The secret ally: Immunostimulation by anticancer drugs. *Nat. Rev. Drug Discov.* **2012**, *11*, 215–233. [[CrossRef](#)]
21. Saw, P.E.; Liu, Q.; Wong, P.P.; Song, E. Cancer stem cell mimicry for immune evasion and therapeutic resistance. *Cell Stem Cell* **2024**, *31*, 1101–1112. [[CrossRef](#)] [[PubMed](#)]
22. Qian, L.; Yu, S.; Yin, C.; Zhu, B.; Chen, Z.; Meng, Z.; Wang, P. Plasma IFN- γ -inducible chemokines CXCL9 and CXCL10 correlate with survival and chemotherapeutic efficacy in advanced pancreatic ductal adenocarcinoma. *Pancreatology* **2019**, *19*, 340–345. [[CrossRef](#)] [[PubMed](#)]
23. Zhou, G.; Zheng, J.; Chen, Z.; Hu, D.; Li, S.; Zhuang, W.; He, Z.; Lin, G.; Wu, B.; Zhang, W.; et al. Clinical significance of tumor-infiltrating lymphocytes investigated using routine H&E slides in small cell lung cancer. *Radiat. Oncol.* **2022**, *17*, 127. [[CrossRef](#)]
24. Lazzari, C.; Spagnolo, C.C.; Ciappina, G.; Di Pietro, M.; Squeri, A.; Passalacqua, M.I.; Marchesi, S.; Gregorc, V.; Santarpia, M. Immunotherapy in Early-Stage Non-Small Cell Lung Cancer (NSCLC): Current Evidence and Perspectives. *Curr. Oncol.* **2023**, *30*, 3684–3696. [[CrossRef](#)] [[PubMed](#)] [[PubMed Central](#)]
25. Wu, Y.; Han, W.; Dong, H.; Liu, X.; Su, X. The rising roles of exosomes in the tumor microenvironment reprogramming and cancer immunotherapy. *MedComm* **2024**, *5*, e541. [[CrossRef](#)]
26. Pi, Y.-N.; Xia, B.-R.; Jin, M.-Z.; Jin, W.-L.; Lou, G. Exosomes: Powerful weapon for cancer nano-immunoengineering. *Biochem. Pharmacol.* **2021**, *186*, 114487. [[CrossRef](#)] [[PubMed](#)]
27. Ho, T.; Msallam, R. Tissues and tumor microenvironment (TME) in 3D: Models to shed light on immunosuppression in cancer. *Cells* **2021**, *10*, 831. [[CrossRef](#)]
28. Ros, J.; Balconi, F.; Baraibar, I.; Saoudi Gonzalez, N.; Salva, F.; Tabernero, J.; Elez, E. Advances in immune checkpoint inhibitor combination strategies for microsatellite stable colorectal cancer. *Front. Oncol.* **2023**, *13*, 1112276. [[CrossRef](#)] [[PubMed](#)] [[PubMed Central](#)]
29. Sosnowska, A.; Chlebowska-Tuz, J.; Matryba, P.; Pilch, Z.; Greig, A.; Wolny, A.; Grzywa, T.M.; Rydzynska, Z.; Sokolowska, O.; Rygiel, T.P.; et al. Inhibition of arginase modulates T-cell response in the tumor microenvironment of lung carcinoma. *OncolImmunology* **2021**, *10*, 1956143. [[CrossRef](#)] [[PubMed](#)]
30. Yu, L.; Xu, L.; Chen, Y.; Rong, Y.; Zou, Y.; Ge, S.; Wu, T.; Lai, Y.; Xu, Q.; Guo, W.; et al. IDO1 inhibition promotes activation of tumor-intrinsic STAT3 pathway and induces adverse tumor-protective effects. *J. Immunol.* **2024**, *212*, 1232–1243. [[CrossRef](#)]
31. Zaiatz-Bittencourt, V.; Finlay, D.K.; Gardiner, C.M. Canonical TGF- β signaling pathway represses human NK cell metabolism. *J. Immunol.* **2019**, *200*, 3934–3941. [[CrossRef](#)]
32. Delgoffe, G. *Cancer Metabolism and the Immune System*; American Association for Cancer Research: Philadelphia, PA, USA, 2021.

33. Zemanek, T.; Danisovic, L.; Nicodemou, A. Exosomes, their sources, and possible uses in cancer therapy in the era of personalized medicine. *J. Cancer Res. Clin. Oncol.* **2024**, *151*, 16. [[CrossRef](#)] [[PubMed](#)]
34. Dai, E.; Zhu, Z.; Wahed, S.; Qu, Z.; Storkus, W.J.; Guo, Z.S. Epigenetic modulation of antitumor immunity for improved cancer immunotherapy. *Mol. Cancer* **2021**, *20*, 171. [[CrossRef](#)]
35. Nakamura, K.; Yagyu, S.; Hirota, S.; Tomida, A.; Kondo, M.; Shigeura, T.; Hasegawa, A.; Tanaka, M.; Nakazawa, Y. Autologous antigen-presenting cells efficiently expand piggyBac transposon CAR-T cells with predominant memory phenotype. *Mol. Ther. Methods Clin. Dev.* **2021**, *21*, 315–324. [[CrossRef](#)]
36. Sun, X.; Liu, Z.; Yu, Q.; Chen, Y.; Sun, Y.; Zhu, Q.; Yang, J.; Jiang, R. PLAC8 is an innovative biomarker for immunotherapy participating in remodeling the immune microenvironment of renal clear cell carcinoma. *Front. Oncol.* **2023**, *13*, 1207551. [[CrossRef](#)] [[PubMed](#)]
37. Peng, D.; Kryczek, I.; Nagarsheth, N.; Zhao, L.; Wei, S.; Wang, W.; Sun, Y.; Zhao, E.; Vatan, L.; Szeliga, W.; et al. Epigenetic silencing of TH1-type chemokines shapes tumour immunity and immunotherapy. *Nature* **2015**, *527*, 249–253. [[CrossRef](#)]
38. Beumer-Chuwonpad, A.; Taggenbrock, R.L.R.E.; Ngo, T.A.; van Gisbergen, K.P.J.M. The potential of tissue-resident memory T cells for adoptive immunotherapy against cancer. *Cells* **2021**, *10*, 2234. [[CrossRef](#)] [[PubMed](#)]
39. Adhikary, S.; Pathak, S.; Palani, V.; Acar, A.; Banerjee, A.; Al-Dewik, N.I.; Essa, M.M.; Mohammed, S.G.A.A.; Qoronfleh, M.W. Current Technologies and Future Perspectives in Immunotherapy towards a Clinical Oncology Approach. *Biomedicines* **2024**, *12*, 217. [[CrossRef](#)] [[PubMed](#)] [[PubMed Central](#)]
40. Khojandi, N.; Connelly, L.; Piening, A.; Hoft, S.G.; Pherson, M.; Donlin, M.J.; DiPaolo, R.J.; Teague, R.M. Single-cell analysis of peripheral CD8+ T cell responses in patients receiving checkpoint blockade immunotherapy for cancer. *Cancer Immunol. Immunother.* **2023**, *72*, 397–408. [[CrossRef](#)]
41. Elwood, P.C.; Morgan, G.; Delon, C.; Prott, M.; Galante, J.; Pickering, J.; Watkins, J.; Weightman, A.; Morris, D. Aspirin and cancer survival: A systematic review and meta-analyses of 118 observational studies of aspirin and 18 cancers. *Ecancermedicalscience* **2021**, *15*, 1258. [[CrossRef](#)]
42. Bouafia, A.; Lofek, S.; Bruneau, J.; Chentout, L.; Lamrini, H.; Trinquand, A.; Deau, M.-C.; Heurtier, L.; Meignin, V.; Picard, C.; et al. Loss of ARHGEF1 causes a human primary antibody deficiency. *J. Clin. Investig.* **2019**, *129*, 1047–1060. [[CrossRef](#)]
43. Sacco, A.; Bruno, A.; Contursi, A.; Dovizio, M.; Tacconelli, S.; Ricciotti, E.; Guillem-Llobat, P.; Salvatore, T.; Di Francesco, L.; Fullone, R.; et al. Platelet-specific deletion of cyclooxygenase-1 ameliorates dextran sulfate sodium-induced colitis in mice. *J. Pharmacol. Exp. Ther.* **2019**, *370*, 416–426. [[CrossRef](#)] [[PubMed](#)]
44. Bruno, A.; Contursi, A.; Tacconelli, S.; Sacco, A.; Hofling, U.; Mucci, M.; Lamolinara, A.; Del Pizzo, F.; Ballerini, P.; Di Gregorio, P.; et al. The specific deletion of cyclooxygenase-1 in megakaryocytes/platelets reduces intestinal polyposis in ApcMin/+ mice. *Pharmacol. Res.* **2022**, *185*, 106506. [[CrossRef](#)]
45. McNeil, J.J.; Gibbs, P.; Orchard, S.G.; Lockery, J.E.; Bernstein, W.B.; Cao, Y.; Ford, L.; Haydon, A.; Kirpach, B.; Macrae, F.; et al. Effect of aspirin on cancer incidence and mortality in older adults. *J. Natl. Cancer Inst.* **2021**, *113*, 258–265. [[CrossRef](#)]
46. Gebhardt, T.; Park, S.L.; Parish, I.A. Stem-like exhausted and memory CD8+ T cells in cancer. *Nat. Rev. Cancer* **2023**, *23*, 780–798. [[CrossRef](#)]
47. Brummelman, J.; Haftmann, C.; Núñez, N.G.; Alvisi, G.; Mazza, E.M.C.; Becher, B.; Lugli, E. Development, application and computational analysis of high-dimensional fluorescent antibody panels for single-cell flow cytometry. *Nat. Protoc.* **2019**, *14*, 1946–1969. [[CrossRef](#)]
48. Alvisi, G.; Brummelman, J.; Puccio, S.; Mazza, E.M.C.; Tomada, E.P.; Losurdo, A.; Zanon, V.; Peano, C.; Colombo, F.S.; Scarpa, A.; et al. IRF4 instructs effector Treg differentiation and immune suppression in human cancer. *J. Clin. Investig.* **2020**, *130*, 3137–3150. [[CrossRef](#)] [[PubMed](#)]
49. Demma, M.J.; Mapelli, C.; Sun, A.; Bodea, S.; Ruprecht, B.; Javaid, S.; Wiswell, D.; Muise, E.; Chen, S.; Zelina, J.; et al. Omomyc reveals new mechanisms to inhibit the myc oncogene. *Mol. Cell Biol.* **2019**, *39*, e00248-19. [[CrossRef](#)]
50. Beaulieu, M.-E.; Jauset, T.; Massó-Vallés, D.; Martínez-Martín, S.; Rahl, P.; Maltais, L.; Zacarias-Fluck, M.F.; Casacuberta-Serra, S.; del Pozo, E.S.; Fiore, C.; et al. Intrinsic cell-penetrating activity propels Omomyc from proof of concept to viable anti-MYC therapy. *Sci. Transl. Med.* **2019**, *11*, eaar5012. [[CrossRef](#)] [[PubMed](#)]
51. Struntz, N.B.; Chen, A.; Deutzmann, A.; Wilson, R.M.; Stefan, E.; Evans, H.L.; Ramirez, M.A.; Liang, T.; Caballero, F.; Wildschut, M.H.; et al. Stabilization of the Max homodimer with a small molecule attenuates Myc-driven transcription. *Cell Chem. Biol.* **2019**, *26*, 711.e14–723.e14. [[CrossRef](#)]
52. Massó-Vallés, D.; Soucek, L. Blocking Myc to treat cancer: Reflecting on two decades of Omomyc. *Cells* **2020**, *9*, 883. [[CrossRef](#)]
53. Zhang, H.; Wang, P.; Lu, M.; Zhang, S.; Zheng, L. c-Myc maintains the self-renewal and chemoresistance properties of colon cancer stem cells. *Oncol. Lett.* **2019**, *17*, 4487–4493. [[CrossRef](#)] [[PubMed](#)]
54. Wang, T.; Cai, B.; Ding, M.; Su, Z.; Liu, Y.; Shen, L. c-Myc overexpression promotes oral cancer cell proliferation and migration by enhancing glutaminase and glutamine synthetase activity. *Am. J. Med. Sci.* **2019**, *358*, 235–242. [[CrossRef](#)]

55. Alimova, I.; Pierce, A.; Danis, E.; Donson, A.; Birks, D.K.; Griesinger, A.; Foreman, N.K.; Santi, M.; Soucek, L.; Venkataraman, S.; et al. Inhibition of MYC attenuates tumor cell self-renewal and promotes senescence in SMARCB1-deficient Group 2 atypical teratoid rhabdoid tumors to suppress tumor growth in vivo. *Int. J. Cancer* **2019**, *144*, 1983–1995. [[CrossRef](#)]
56. Gutierrez-Sandoval, R.; Rivadeneira, I.; Muñoz, P.I.; Iturra, F.J.; Krakowiak, F. DEX immunotherapy pharmaco-biotechnological advances in multimodal therapy for cancer. *J. Pharm. Res. Rep.* **2024**, *5*, 1–8. [[CrossRef](#)]
57. Kalluri, R.; LeBleu, V.S. The biology, function, and biomedical applications of exosomes. *Science* **2020**, *367*, eaau6977. [[CrossRef](#)]
58. McAndrews, K.M.; Kalluri, R. Mechanisms associated with biogenesis of exosomes in cancer. *Mol. Cancer* **2019**, *18*, 52. [[CrossRef](#)]
59. Mathieu, M.; Martin-Jaular, L.; Lavie, G.; Théry, C. Specificities of secretion and uptake of exosomes and other extracellular vesicles for cell-to-cell communication. *Nat. Cell Biol.* **2019**, *21*, 9–17. [[CrossRef](#)] [[PubMed](#)]
60. Jeppesen, D.K.; Fenix, A.M.; Franklin, J.L.; Higginbotham, J.N.; Zhang, Q.; Zimmerman, L.J.; Liebler, D.C.; Ping, J.; Liu, Q.; Evans, R.; et al. Reassessment of exosome composition. *Cell* **2019**, *177*, 428–445.e18. [[CrossRef](#)] [[PubMed](#)]
61. Pathan, M.; Fonseka, P.; Chitti, S.V.; Kang, T.; Sanwlani, R.; Van Deun, J.; Hendrix, A.; Mathivanan, S. Vesiclepedia 2019: A compendium of RNA, proteins, lipids and metabolites in extracellular vesicles. *Nucleic Acids Res.* **2019**, *47*, D516–D519. [[CrossRef](#)]
62. Wen, S.W.; Lima, L.G.; Lobb, R.J.; Norris, E.L.; Hastie, M.L.; Krumeich, S.; Möller, A. Breast cancer-derived exosomes reflect the cell-of-origin phenotype. *Proteomics* **2019**, *19*, e1800180. [[CrossRef](#)]
63. Cheng, Y.; Schorey, J.S. Extracellular vesicles deliver *Mycobacterium* RNA to promote host immunity and bacterial killing. *EMBO Rep.* **2019**, *20*, e46613. [[CrossRef](#)] [[PubMed](#)]
64. Sandoval, R.G. Recent advances in the translational application of immunotherapy with pulsed dendritic cell-derived exosomes (DEX). *J. Clin. Biomed. Res.* **2024**, *6*, 1–8. [[CrossRef](#)]
65. Wang, M.; Su, Z.; Barnie, P.A. Crosstalk among colon cancer-derived exosomes, fibroblast-derived exosomes, and macrophage phenotypes in colon cancer metastasis. *Int. Immunopharmacol.* **2020**, *81*, 106298. [[CrossRef](#)] [[PubMed](#)]
66. Daßler-Plenker, J.; Kuttner, V.; Egeblad, M. Communication in tiny packages: Exosomes as means of tumor-stroma communication. *Biochim. Biophys. Acta Rev. Cancer* **2020**, *1873*, 188340. [[CrossRef](#)] [[PubMed](#)]
67. Mohammadi, S.; Yousefi, F.; Shabaninejad, Z.; Movahedpour, A.; Tehran, M.M.; Shafiee, A.; Moradizarmehri, S.; Hajighadimi, S.; Savardashtaki, A.; Mirzaei, H. Exosomes and cancer: From oncogenic roles to therapeutic applications. *IUBMB Life* **2020**, *72*, 724–748. [[CrossRef](#)]
68. Pourhanifeh, M.H.; Mahjoubin-Tehran, M.; Shafiee, A.; Hajighadimi, S.; Moradizarmehri, S.; Mirzaei, H.; Asemi, Z. MicroRNAs and exosomes: Small molecules with big actions in multiple myeloma pathogenesis. *IUBMB Life* **2020**, *72*, 314–333. [[CrossRef](#)]
69. Mitchell, M.J.; Billingsley, M.M.; Haley, R.M.; Wechsler, M.E.; Peppas, N.A.; Langer, R. Precision nanoparticles for drug delivery. *Nat. Rev. Drug Discov.* **2021**, *20*, 101–124. [[CrossRef](#)]
70. Naseri, Z.; Oskuee, R.K.; Forouzandeh-Moghadam, M.; Jaafari, M.R. Delivery of LNA-antimiR-142-3p by mesenchymal stem cells-derived exosomes to breast cancer stem cells reduces tumorigenicity. *Stem Cell Rev. Rep.* **2020**, *16*, 541–556. [[CrossRef](#)]
71. Huang, L.; Yang, L.; Ding, Y.; Jiang, X.; Xia, Z.; You, Z. Human umbilical cord mesenchymal stem cells-derived exosomes transfers microRNA-19a to protect cardiomyocytes from acute myocardial infarction by targeting SOX6. *Cell Cycle* **2020**, *19*, 339–353. [[CrossRef](#)]
72. Che, J.; Wang, H.; Dong, J.; Wu, Y.; Zang, H.; Fu, L.; Zhang, J. Human umbilical cord mesenchymal stem cell-derived exosomes attenuate neuroinflammation and oxidative stress through the NRF2/NF-κB/NLRP3 pathway. *CNS Neurosci. Ther.* **2024**, *30*. [[CrossRef](#)] [[PubMed](#)] [[PubMed Central](#)]
73. Chen, Q.; Liu, Y.; Ding, X.; Li, Q.; Qiu, F.; Wang, M.; Shen, Z.; Zheng, H.; Fu, G. Bone marrow mesenchymal stem cell-secreted exosomes carrying microRNA-125b protect against myocardial ischemia reperfusion injury via targeting SIRT7. *Mol. Cell Biochem.* **2020**, *465*, 103–114. [[CrossRef](#)]
74. Harrell, C.R.; Jankovic, M.G.; Fellabaum, C.; Volarevic, A.; Djonov, V.; Arsenijevic, A.; Volarevic, V. Molecular mechanisms responsible for anti-inflammatory and immunosuppressive effects of mesenchymal stem cell-derived factors. *Adv. Exp. Med. Biol.* **2019**, *1084*, 187–206.
75. Harrell, C.R.; Jovicic, N.; Djonov, V.; Arsenijevic, N.; Volarevic, V. Mesenchymal Stem Cell-Derived Exosomes and Other Extracellular Vesicles as New Remedies in the Therapy of Inflammatory Diseases. *Cells* **2019**, *8*, 1605. [[CrossRef](#)] [[PubMed](#)] [[PubMed Central](#)]
76. Sun, H.; Hu, S.; Xu, F.; Liang, X. Exosomal miRNAs during chondrogenic differentiation. *J. Cell Biochem.* **2019**, *120*, 171–181. [[CrossRef](#)]
77. Keskin, D.B.; Anandappa, A.J.; Sun, J.; Tirosh, I.; Mathewson, N.D.; Li, S.; Oliveira, G.; Giobbie-Hurder, A.; Felt, K.; Gjini, E.; et al. Neoantigen vaccine generates T cell responses in glioblastoma. *Nature* **2019**, *565*, 234–239. [[CrossRef](#)]
78. Liang, J.; Zhao, X. Nanomaterials for cancer vaccine delivery. *Cancer Biol. Med.* **2021**, *18*, 352–371. [[CrossRef](#)]
79. Titov, A.; Zmievskaya, E.; Ganeeva, I.; Valiullina, A.; Petukhov, A.; Rakhmatullina, A.; Miftakhova, R.; Fainshtein, M.; Rizvanov, A.; Bulatov, E. Adoptive immunotherapy beyond CAR T-cells. *Cancers* **2021**, *13*, 743. [[CrossRef](#)]

80. Shemesh, C.S.; Hsu, J.C.; Hosseini, I.; Shen, B.Q.; Rotte, A.; Twomey, P.; Girish, S.; Wu, B. Personalized cancer vaccines: Clinical landscape and challenges. *Mol. Ther.* **2021**, *29*, 555–570. [[CrossRef](#)] [[PubMed](#)]
81. Yu, H.; Wu, M.; Chen, S.; Song, M.; Yue, Y. Biomimetic nanoparticles for tumor immunotherapy. *Front. Bioeng. Biotechnol.* **2022**, *10*, 989881. [[CrossRef](#)] [[PubMed](#)]
82. Martin, J.D.; Cabral, H.; Stylianopoulos, T.; Jain, R.K. Improving cancer immunotherapy with nanomedicines. *Nat. Rev. Clin. Oncol.* **2020**, *17*, 251–266. [[CrossRef](#)] [[PubMed](#)]
83. Waldman, A.D.; Fritz, J.M.; Lenardo, M.J. A guide to cancer immunotherapy. *Nat. Rev. Immunol.* **2020**, *20*, 651–668. [[CrossRef](#)] [[PubMed](#)]
84. Aikins, M.E.; Xu, C.; Moon, J.J. Engineered nanoparticles for immunotherapy. *Acc. Chem. Res.* **2020**, *53*, 2094–2105. [[CrossRef](#)] [[PubMed](#)]
85. Li, W.-H.; Li, Y.-M. Chemical strategies to boost cancer vaccines. *Chem. Rev.* **2020**, *120*, 11420–11478. [[CrossRef](#)]
86. Roy, S.; Sethi, T.K.; Taylor, D.; Kim, Y.J.; Johnson, D.B. Breakthroughs in immune-oncology: Cancer vaccines. *J. Leukoc. Biol.* **2020**, *108*, 1455–1489. [[CrossRef](#)]

Disclaimer/Publisher’s Note: The statements, opinions and data contained in all publications are solely those of the individual author(s) and contributor(s) and not of MDPI and/or the editor(s). MDPI and/or the editor(s) disclaim responsibility for any injury to people or property resulting from any ideas, methods, instructions or products referred to in the content.



biomedicines



Article

Phospholipid-Rich DC-Vesicles with Preserved Immune Fingerprints: A Stable and Scalable Platform for Precision Immunotherapy

Ramon Gutierrez-Sandoval, Francisco Gutierrez-Castro, Natalia Muñoz-Godoy, Ider Rivadeneira, Adolay Sobarzo, Luis Alarcón, Wilson Dorado, Andy Lagos, Diego Montenegro, Ignacio Muñoz et al.



<https://doi.org/10.3390/biomedicines13061299>

Article

Phospholipid-Rich DC-Vesicles with Preserved Immune Fingerprints: A Stable and Scalable Platform for Precision Immunotherapy

Ramon Gutierrez-Sandoval ^{1,*}, Francisco Gutierrez-Castro ^{2,†}, Natalia Muñoz-Godoy ², Ider Rivadeneira ³, Adolay Sobarzo ⁴, Luis Alarcón ³, Wilson Dorado ³, Andy Lagos ³, Diego Montenegro ³, Ignacio Muñoz ³, Rodrigo Aguilera ³, Jordan Iturra ³, Francisco Krakowiak ⁵, Cristián Peña-Vargas ¹ and Andres Toledo ¹

¹ Department of Oncopathology, OGRD Alliance, Lewes, DE 19958, USA; consultorusa@biogenica.org (C.P.-V.); ops@ogrdalliance.org (A.T.)

² Department of Cancer Research, Flowimmunocell-Bioexocell Group, 08028 Barcelona, Spain; servicios@flowimmunocell.cl (F.G.-C.); contacto@flowimmunocell.cl (N.M.-G.)

³ Department of Outreach and Engagement Programs for OGRD Consortium, Charlestown KN0802, Saint Kitts and Nevis; iderlautaro@gmail.com (I.R.); luisantonioalarconcofre@gmail.com (L.A.); wdoradoortega@gmail.com (W.D.); lagosandy@gmail.com (A.L.); dn.montenegro.c@gmail.com (D.M.); kinesiologo@recell.cl (I.M.); rodrigo1982aguilera@gmail.com (R.A.); jiconsultant@ogrdconsorcio.com (J.I.)

⁴ Department of Biological and Chemistry Sciences, Faculty of Medicine and Science, San Sebastian University, Concepción 4080871, Chile; adolay.sobarzo@uss.cl

⁵ Department of Molecular Oncopathology, Bioclas, Concepcion 4030000, Chile; tecnologo@bioclas.cl

* Correspondence: cso@ogrdalliance.org

† These authors contributed equally to this work.

Abstract: Despite the progress in cancer immunotherapy, therapeutic responses in solid tumors remain suboptimal due to the immunosuppressive nature of the tumor microenvironment (TME), limited immune cell infiltration, and inefficient delivery of immune-activating agents. Dendritic cell-based therapies possess strong immunological potential but face challenges in viability, standardization, and scalability. Likewise, exosomes and CAR-T cells are hindered by instability, production complexity, and limited efficacy in immune-excluded tumor settings. **Objective:** This study evaluates dendritic cell-derived vesicles (DC-Vesicles), embedded in a phospholipid-rich structural scaffold, as a multi-functional and scalable platform for immune modulation and therapeutic delivery. We aimed to assess their structural stability, immune marker preservation under clinical processing conditions, and potential to reprogram the TME. **Methods and Results:** DC-Vesicles were generated and analyzed using bottom-up proteomics via nanoLC-MS/MS on a timsTOF Pro 2 system under three conditions: fresh, concentrated, and cryopreserved. A consistent proteomic profile of over 400 proteins was identified, with cryopreserved samples retaining >90% of immune-relevant markers. Differential expression analysis confirmed stability of key immunological proteins such as HLA-A, QSOX1, ICAM1, NAMPT, TIGAR, and Galectin-9. No significant degradation was observed post-cryopreservation. Visualization through heatmaps, PCA, and volcano plots supported inter-condition consistency. In silico modeling suggested preserved capacity for M1 macrophage polarization and CD8⁺ T cell activation. **Conclusions:** DC-Vesicles demonstrate structural resilience and functional retention across storage conditions. Their cold-chain-independent compatibility, immune-targeting profile, and potential regulatory classification as Non-New Chemical Entities (NCEs) support their advancement as candidates for precision immunotherapy in resistant solid tumors.



Academic Editor: Konstantinos Dimas

Received: 25 April 2025

Revised: 20 May 2025

Accepted: 20 May 2025

Published: 26 May 2025

Citation: Gutierrez-Sandoval, R.; Gutierrez-Castro, F.; Muñoz-Godoy, N.; Rivadeneira, I.; Sobarzo, A.; Alarcón, L.; Dorado, W.; Lagos, A.; Montenegro, D.; Muñoz, I.; et al. Phospholipid-Rich DC-Vesicles with Preserved Immune Fingerprints: A Stable and Scalable Platform for Precision Immunotherapy.

Biomedicines **2025**, *13*, 1299. <https://doi.org/10.3390/biomedicines13061299>

Copyright: © 2025 by the authors. Licensee MDPI, Basel, Switzerland. This article is an open access article distributed under the terms and conditions of the Creative Commons Attribution (CC BY) license (<https://creativecommons.org/licenses/by/4.0/>).

Keywords: dendritic cell vesicles; phospholipid-rich vesicles; lyophilization stability; immune fingerprinting; cytokine modulation; proteomic analysis; tumor microenvironment; immune modulation; Non-New Chemical Entities (NCEs)

1. Introduction

Cancer immunotherapy has emerged as one of the most transformative strategies in oncology. Breakthroughs in immune checkpoint inhibitors (ICIs), chimeric antigen receptor T cell (CAR-T) therapies, and extracellular vesicle-based platforms—such as exosomes and synthetic nanoparticles—have opened novel therapeutic avenues [1–3]. However, despite these advances, outcomes in solid tumors remain limited. A primary obstacle is the complex and suppressive nature of the tumor microenvironment (TME) [4], which restricts immune cell infiltration, persistence, and cytotoxic function, ultimately limiting therapeutic efficacy.

The TME [5] is shaped by both metabolic and immunological constraints. Tumor and stromal cells release an array of immunosuppressive mediators, including transforming growth factor-beta (TGF- β) [6], interleukin-10 (IL-10) [7], indoleamine 2,3-dioxygenase (IDO), and prostaglandin E2 (PGE2) [8]. These factors impair dendritic cell maturation, induce M2 macrophage polarization, and drive the expansion of regulatory T cells (Tregs), collectively dampening the activity of cytotoxic T lymphocytes and natural killer (NK) cells. The resulting immunosuppression fosters tumor progression and contributes to resistance against existing immunotherapies, particularly in solid tumor settings.

To overcome these barriers, current strategies aim to reprogram the TME [9] toward a pro-inflammatory, immunologically active state. Prominent among these are approaches that enhance type 1 helper T cell (Th1) responses using cytokines [10] such as IL-12 [11] and IL-15, which are known to support CD8⁺ T cell expansion and favor M1 macrophage polarization. Key effector molecules such as interferon-gamma (IFN- γ) [12] and tumor necrosis factor-alpha (TNF- α) further augment antigen presentation and immune cytotoxicity.

In parallel, chemokines like CXCL10 and CCL5 facilitate the recruitment and spatial organization of effector cells within the tumor bed, reinforcing immune infiltration and surveillance. Despite progress, existing platforms face inherent limitations. While CAR-T cells [13] have shown remarkable efficacy in hematologic malignancies, their application in solid tumors has been less successful due to poor tumor penetration [14], antigenic heterogeneity, and systemic toxicities such as cytokine [15] release syndrome (CRS).

Similarly, exosomes [16] and synthetic nanoparticles, though conceptually appealing, often exhibit limited structural stability [17], short systemic half-life, and challenges in preserving cargo integrity during storage and delivery. Recent reviews have highlighted both the promise and the technical barriers of vesicle-based strategies in immunotherapy [17]. These barriers underscore the need for cell-free, modular, and immunologically competent platforms that maintain both stability [18] and functionality across variable clinical contexts. In this context, dendritic cell-derived vesicles (DC-Vesicles) [19] stabilized within a phospholipid-rich scaffold have emerged as a promising alternative that combines the advantages of cell-free systems with the immunological potency of antigen-presenting cells. Unlike conventional exosomes—passively secreted and compositionally [20] variable—DC-Vesicles can be selectively enriched or engineered to carry immunologically validated proteins such as HLA-A, ICAM-1, QSOX1, and CCL22 [13,14].

These molecules play essential roles in antigen presentation, costimulation, redox regulation, and immune modulation and have demonstrated reproducibility across processing formats [15]. In addition to their functional composition, DC-Vesicles display enhanced

physicochemical stability. When stabilized within a defined phospholipoprotein scaffold, they exhibit resistance to enzymatic degradation, retention of membrane integrity, and compatibility with cold-chain-independent preservation [16].

These attributes confer not only therapeutic durability but also operational advantages in terms of storage, transport, and deployment [17]. Their bioendogenous, non-replicative, and non-recombinant profile positions them as potential candidates for classification under the regulatory category of Non-New Chemical Entities (NCEs), thereby facilitating accelerated evaluation and streamlined clinical integration [18]. This regulatory distinction may also lower production costs and widen access in diverse healthcare systems [19]. Unlike conventional exosomes, which often display compositional heterogeneity and instability under clinical workflows, the phospholipoprotein matrix confers superior vesicle cohesion, minimizes aggregation, and enhances cargo retention. These physicochemical advantages are particularly relevant for preserving membrane-associated proteins and immunomodulatory functions after processing, lyophilization, or cold-chain-independent storage. The present study investigates the structural resilience and immunological retention of DC-Vesicles subjected to three clinically relevant handling conditions: fresh, concentrated, and cryopreserved.

Using a proteomics-driven approach—supported by label-free quantification (LFQ), principal component analysis (PCA), and differential expression profiling—we assess the preservation of immune-relevant proteins across these modalities. Our goal is to validate the translational readiness of this platform and its applicability to immunotherapeutic regimens targeting solid tumors with high levels of immune resistance. This study builds on previous work describing the PLPC platform [20] but focuses specifically on vesicle stability and immune marker preservation under pre-lyophilization conditions using non-terminal DC-Vesicle fractions processed under clinical handling workflows. The strategic positioning of DC-Vesicles within the current immunotherapy landscape is illustrated in Figure 1.

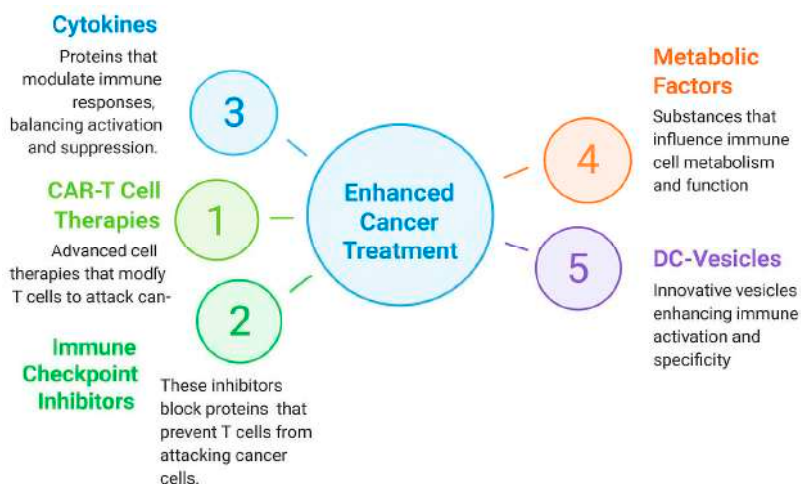


Figure 1. Strategic positioning of DC-Vesicles within the evolving landscape of cancer immunotherapy. Schematic summarizing five classes of immunotherapeutic strategies. DC-Vesicles are positioned as a next-generation platform integrating structural stability and immune modulation in solid tumors. This rationale is supported by emerging studies demonstrating that vesicle-based delivery systems may enhance anti-PD-1 responses by improving local immune priming and overcoming stromal exclusion [21].

2. Materials and Methods

2.1. Experimental Design and Vesicle Preparation

This study was designed to evaluate the structural integrity and immunological stability of dendritic cell-derived vesicles (DC-Vesicles) subjected to different clinically relevant storage and processing conditions [21]. Vesicles were obtained from monocyte-derived dendritic cells (moDCs) cultured *ex vivo* under standardized GMP-like protocols [22,23].

Peripheral blood mononuclear cells (PBMCs) were isolated by Ficoll density gradient centrifugation and differentiated into immature dendritic cells in the presence of IL-4 and GM-CSF for six days. Maturation was induced using a cytokine cocktail composed of TNF- α , IL-1 β , and poly I:C to enhance expression of antigen-presenting and costimulatory molecules [24].

After vesicle release, culture supernatants were clarified by centrifugation ($3000\times g$, 15 min) and filtered through 0.22 μm sterile membranes [25]. Samples were divided into three experimental conditions: (i) Fresh—analyzed immediately after collection; (ii) Concentrated—subjected to $10\times$ ultrafiltration using Amicon Ultra 10 kDa filters; and (iii) Cryopreserved—aliquoted and stored at $-80\text{ }^{\circ}\text{C}$ for 30 days prior to analysis. Each group was processed in biological triplicates ($n = 3$). The complete experimental workflow is summarized in Figure 2.

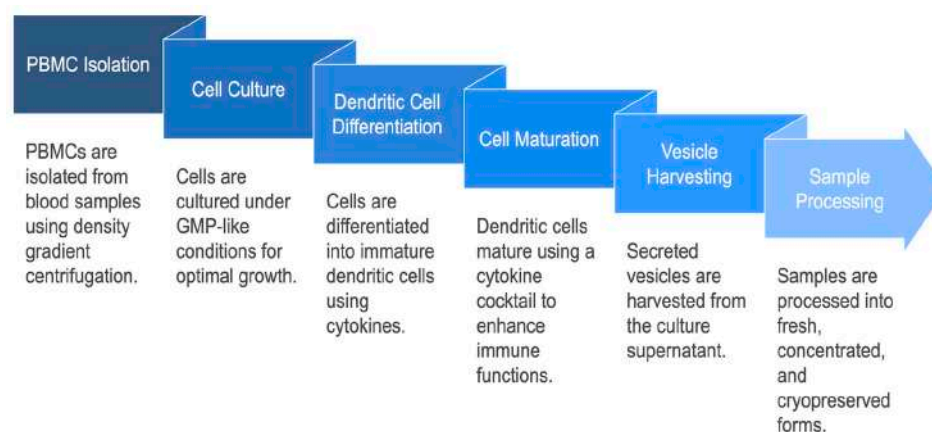


Figure 2. Experimental workflow for DC-Vesicle production and sample processing. Overview of PBMC isolation, dendritic cell maturation, vesicle harvesting, and stratification into Fresh, Concentrated, and Cryopreserved groups. Conditions are detailed in Supplementary Table S1.

2.2. Protein Extraction and Peptide Preparation

For all conditions, vesicle-enriched fractions were precipitated overnight with cold acetone (4 volumes, $-20\text{ }^{\circ}\text{C}$) and centrifuged at $14,000\times g$ for 10 min [26]. Pellets were washed with 80% ethanol, air-dried, and resuspended in 100 mM TEAB buffer containing 0.1% SDS. Total protein was quantified using the Bradford assay [27].

For proteomic digestion, 100 μg of protein per sample was reduced with 5 mM DTT at $56\text{ }^{\circ}\text{C}$ (30 min), alkylated with 15 mM iodoacetamide (dark, room temperature), and digested overnight at $37\text{ }^{\circ}\text{C}$ with sequencing-grade trypsin (1:50 enzyme–protein ratio). Peptides were desalted using Pierce C18 spin columns, vacuum-dried, and reconstituted in 0.1% formic acid prior to LC-MS/MS analysis.

2.3. Mass Spectrometry and Data Acquisition

Peptide samples were analyzed using a timsTOF Pro 2 mass spectrometer (Bruker Daltonics, Bremen, Germany) coupled to an EvoSep One nanoLC system (EvoSep Biosystems, Odense, Denmark) operating under a high-throughput proteomics configuration. Peptide separation was performed on a PepSep C18 column (15 cm \times 75 μm , 1.9 μm particle size)

using the 11-sample-per-day EvoTip gradient (EvoSep Biosystems, Odense, Denmark), consisting of a linear solvent ramp from 5% to 35% acetonitrile (0.1% formic acid) over 33.5 min, followed by column wash and re-equilibration (total runtime: 44 min).

The mass spectrometer (timsTOF Pro 2, Bruker Daltonics, Bremen, Germany) operated in PASEF data-dependent acquisition (DDA) mode, with a full MS1 scan (m/z 100–1700) followed by 10 MS/MS scans per cycle. Ion mobility separation (TIMS) was enabled, with a $1/K_0$ range of 0.6–1.6 Vs/cm². Source settings included capillary voltage of 1.65 kV, dry gas flow at 3.2 L/min, drying temperature at 180 °C, and nebulizer pressure at 0.4 bar. Precursor selection used intensity-dependent prioritization and dynamic exclusion (TopN = 10, $z = 2$ –5).

Calibration was performed daily using Bruker ESI-L Tuning Mix (Bruker Daltonics, Bremen, Germany); quality control was monitored by regular injections of Pierce HeLa digest standards (2 µg per run). Raw spectra were acquired using Compass Hystar 5.1 and processed with MaxQuant v2.1, enabling label-free quantification (LFQ) and match-between-runs, with false discovery rate (FDR) control set at 1% for both peptide-spectrum match and protein group levels [28].

2.4. Protein Identification and Quantification

Protein identification was conducted using the Andromeda search engine within MaxQuant (Max Planck Institute of Biochemistry, Martinsried, Germany), querying the UniProtKB/Swiss-Prot Homo sapiens proteome database (release 2024_01, 20,419 entries) [29]. Enzymatic cleavage was specified for trypsin, with up to two missed cleavages allowed. Carbamidomethylation of cysteine was set as a fixed modification, while methionine oxidation and N-terminal acetylation were considered variable modifications.

Label-Free Quantification (LFQ) was enabled, requiring a minimum ratio count of two peptides per protein. The “match between runs” feature was activated to enhance cross-sample quantification. A 1% false discovery rate (FDR) threshold was applied at both peptide and protein levels. Razor intensities were log₂-transformed and normalized using median centering within each condition to minimize technical variability [30].

2.5. Functional Annotation and Protein Selection

From the complete proteomic dataset, a panel of immune-relevant proteins was selected based on literature consensus and functional enrichment using Gene Ontology (GO) terms associated with antigen presentation, cytokine signaling, chemokine-mediated recruitment, and redox regulation. Selected proteins included HLA-A, ICAM1, CCL22, NAMPT, QSOX1, TIGAR, HSP90AB1, and LGALS9 (Galectin-9) [31].

These proteins were categorized into five functional groups: antigen presentation, chaperones, chemokines, metabolic regulators, and immunomodulators. Relative abundance data were visualized using stacked bar charts, and expression variation across conditions was explored using heatmaps and volcano plots.

2.6. Statistical Analysis and Visualization

Normalized LFQ values were used for differential expression analysis across conditions. Comparisons were performed using the limma package in R, applying empirical Bayes moderation [32]. Proteins with a $|\text{Log}_2$ fold change| ≥ 0.6 and adjusted p -value < 0.05 were considered significantly differentially expressed [31].

Principal Component Analysis (PCA) was performed using log₂-transformed LFQ values to assess sample clustering and reproducibility. PCA plots were generated in R using ggplot2, and heatmaps were constructed using the ComplexHeatmap package, with hierarchical clustering (Euclidean distance, complete linkage) applied to both protein rows

and sample columns. Volcano plots were constructed for key pairwise comparisons (e.g., fresh vs. cryopreserved) and formatted for publication.

2.7. Proteomic Fingerprinting and Batch Consistency

Spectral fingerprinting was used to assess vesicle integrity across experimental conditions. Cosine similarity scores were computed for spectral feature alignment, and reproducibility was defined as the percentage overlap of proteins consistently identified in all three replicates per condition. Batch variability was assessed via coefficient of variation (CV) analysis across replicates [33]. Conditions with CV < 15% were considered highly consistent. Cryopreserved samples retained >90% of proteins detected in the fresh condition, with minimal loss in signal intensity, indicating strong preservation of vesicular structure and content [34].

2.8. In Silico Modeling and Bioinformatic Validation

To complement experimental findings, a computational framework was employed to model cytokine regulation and immune receptor signaling dynamics in response to DC-Vesicle exposure. Simulations were based on previously validated immunological network models incorporating IL-10, TGF- β , IL-12, IL-15, and IFN- γ . Vesicle input parameters were derived from experimental protein abundance data and used to estimate pathway activation probabilities using probabilistic Boolean networks. Simulated vesicle formulations preserving QSOX1, NAMPT, and HLA-A predicted M1 macrophage polarization and enhanced CD8⁺ T cell activation—outcomes consistent with observed experimental profiles. These simulations provide mechanistic support for the immunomodulatory potential of DC-Vesicles and serve to inform future in vivo validation [35].

3. Results

3.1. Global Protein Yield and Identification Across Conditions

Proteomic profiling of dendritic cell-derived vesicles (DC-Vesicles) across three processing conditions—Fresh, Concentrated, and Cryopreserved—resulted in robust protein recovery with high identification consistency [36]. Using LC-MS/MS coupled with label-free quantification (LFQ), an average of 430–460 unique proteins per replicate [37] were identified in the fresh condition, compared to 410–445 in the concentrated group and 390–430 in cryopreserved samples [38].

The average peptide count per sample followed a similar trend, with concentrated vesicles displaying a slightly higher yield, consistent with the tenfold ultrafiltration prior to precipitation. Notably, the cryopreserved condition retained over 90% of the protein identifications observed in fresh samples, confirming that structural integrity and protein content were minimally affected by storage at -80°C for up to 30 days [39]. Across all samples, the most abundant proteins included HSP90AB1, S100A10, ICAM1, and Galectin family members, consistent with previously reported dendritic vesicle proteomes [40,41].

The coefficient of variation (CV) across triplicates was <12% in all groups, demonstrating high reproducibility in both sample processing and analytical workflow [42]. These findings support the scalability and technical robustness of the DC-Vesicle platform under clinically relevant handling conditions. Total protein and peptide counts across conditions are shown in Figure 3. Detailed peptide-level detection trends per replicate and condition are available in Supplementary Table S2.

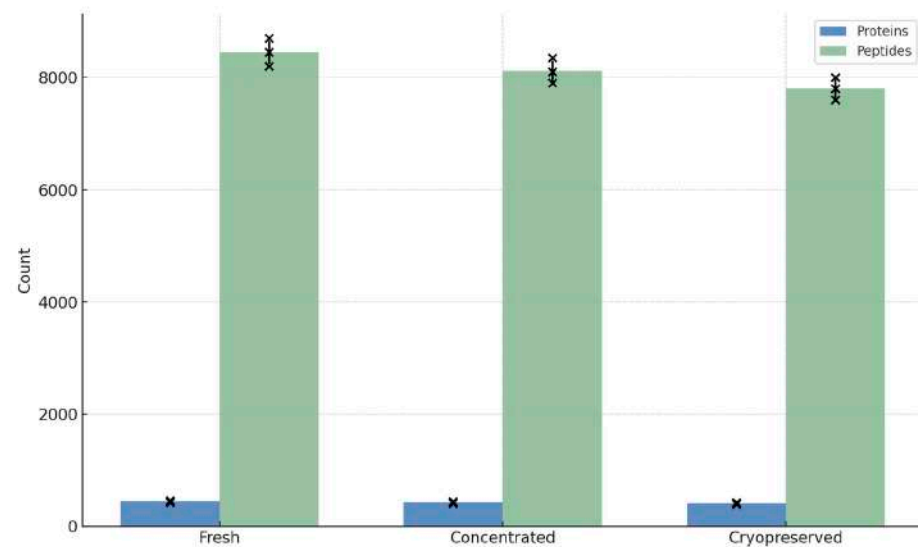


Figure 3. Total protein and peptide yield across storage conditions with biological replicate overlay. Bar chart showing total protein and peptide counts under Fresh, Concentrated, and Cryopreserved conditions ($n = 3$ per group). Individual replicates are overlaid. For full traceability, Supplementary Table S2 list the complete protein and peptide identifications obtained per replicate and condition.

3.2. Functional Preservation of Immune-Relevant Proteins

To assess the immunological integrity of DC-Vesicles across different processing conditions, we selected a panel of eight immune-related proteins known to play key roles in immune activation, antigen presentation, and tumor immune surveillance. These proteins were chosen based on their functional relevance and their presence in the dendritic vesicle proteome. The panel included HLA-A (critical for antigen presentation), ICAM1 (important for T cell-dendritic cell interaction), CCL22 (involved in Treg recruitment), NAMPT (a metabolic enzyme), QSOX1 (a redox-active protein), TIGAR (regulator of glycolysis), HSP90AB1 (stress response chaperone), and LGALS9 (Galectin-9, involved in immune modulation).

Razor intensities for each protein were extracted from LFQ-normalized datasets and compared across three experimental conditions: fresh, concentrated, and cryopreserved. Fresh samples displayed consistent protein expression across biological triplicates, establishing a stable baseline. Variance between replicates was minimal, and the expression profiles aligned with known reports from dendritic vesicle models, validating the reliability of the data.

Concentrated samples showed a slight increase in protein intensities, which can be attributed to the ultrafiltration process used to concentrate the samples 10-fold. No protein loss or degradation was observed, and the coefficient of variation (CV) across replicates remained below 12%. This indicates both the reproducibility of the experimental procedure and the consistency of the vesicles' immunological content. Detailed replicate values and calculated coefficients of variation (CV) are provided in Supplementary Table S3.

Cryopreserved samples retained most of the immune-related proteins. Six out of the eight markers were detected in all replicates, with intensities comparable to the fresh samples [43]. However, TIGAR and Galectin-9 exhibited reduced intensity in two of the three replicates, which suggests that these proteins may be partially sensitive to freeze–thaw cycles or aggregation during storage [44]. Despite this, proteins such as HLA-A, ICAM1, NAMPT, and QSOX1 remained stable, suggesting that the overall immunological integrity of the vesicles was largely preserved.

To further understand these findings, we examined the relative abundance of each protein within the immune signature across conditions. The compositional structure of

the proteins remained stable, with minor shifts in protein abundance—specifically, a mild decrease in TIGAR and Galectin-9 in the cryopreserved samples [45]. Heatmap clustering and PCA analysis showed no major loss of immune-relevant proteins, confirming that the vesicle structure and functional integrity were well-maintained.

The ability to preserve immune signatures under clinically relevant storage conditions, without requiring cryoprotectants or immediate processing, positions DC-Vesicles as a significant advancement in immunotherapy. Unlike cell-based immunotherapies or exosome platforms that depend on strict cryopreservation protocols, DC-Vesicles exhibited a high tolerance for standard $-80\text{ }^{\circ}\text{C}$ storage, with minimal degradation of their immunological content.

In summary, DC-Vesicles demonstrate the ability to retain key immune markers, such as HLA-A, ICAM1, NAMPT, and QSOX1, across different processing conditions. The stability of these proteins and the reproducibility of the LFQ profiles across replicates highlight the potential of DC-Vesicles as a scalable, cell-free platform for immunotherapy [46]. Their ability to maintain structural and functional integrity under conditions that mimic real-world clinical storage further supports their potential for use in precision immunotherapy. Log_2 Razor intensity values for immune-relevant proteins are shown in Figure 4. The relative contribution of each immune marker is illustrated in Figure 5.

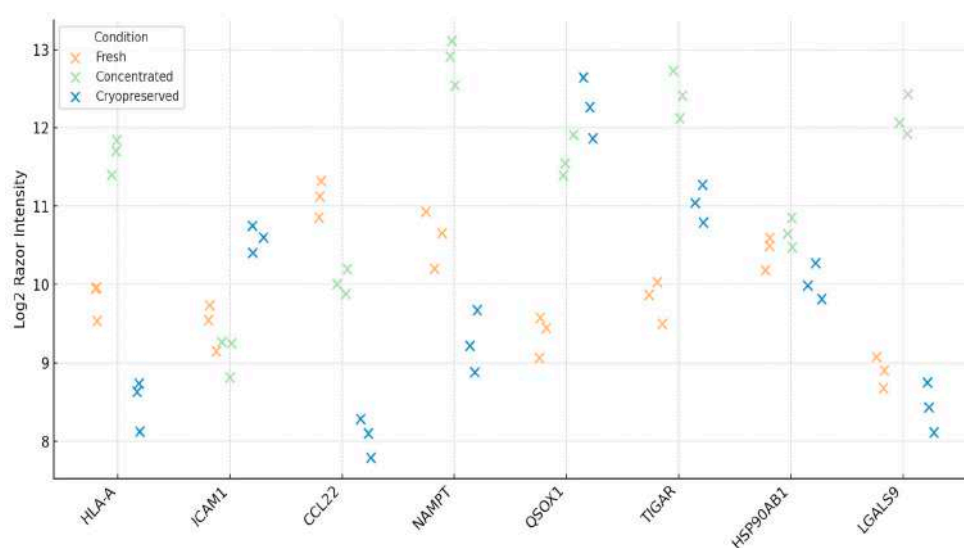


Figure 4. Immune-relevant protein intensities across storage conditions with biological replicate resolution. Dot plot showing log_2 Razor Intensity values for eight immune markers across storage groups. Variability among replicates is visualized directly.

Table 1 presents quantitative metrics of protein abundance changes across storage conditions, emphasizing immunologically relevant markers and their functional stability profiles. Functional roles were defined based on literature-reported mechanisms associated with antigen presentation, co-stimulation, immune regulation, redox control, and tumor metabolism. The table highlights the preservation of key markers such as HLA-A, ICAM1, and HSP90AB1 across all conditions, supporting the structural and functional integrity of the vesicle formulation during clinical processing. To further quantify the differences in immune marker abundance, we computed fold-change and adjusted p -values for cryopreserved vs. fresh conditions. As summarized in Table 1, proteins such as HLA-A, NAMPT, TIGAR, and LGALS9 showed modest but consistent downregulation, with TIGAR and Galectin-9 reaching statistical significance (adjusted $p < 0.05$). These shifts suggest selective sensitivity of metabolic and immunomodulatory markers to freeze–thaw stress, highlighting the importance of storage optimization.

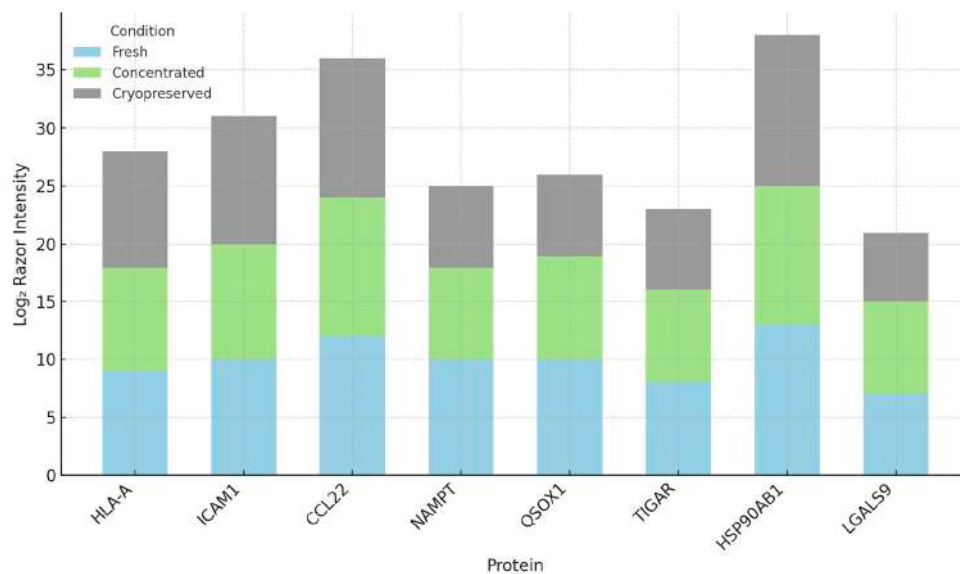


Figure 5. Illustration of the relative abundance of immune-relevant proteins across groups. Relative signal contribution of eight immune markers per condition. Stacked bars illustrate compositional preservation despite minor shifts in abundance.

Table 1. Functional classification of immune-related proteins across storage conditions.

Protein	Function	Fold-Change (Cryo vs. Fresh)	Adjusted p-Value	Functional Note
HLA-A	Antigen presentation (MHC I)	−0.28	0.074	Activates CD8 ⁺ T cells
ICAM1	Co-stimulation/adhesion	−0.12	0.268	Enhances immune synapse
CCL22	Treg recruitment	+0.35	0.112	Chemotactic signal for Tregs
NAMPT	NAD + metabolism	−0.42	0.056	Redox-linked immunoregulator
QSOX1	Protein folding/redox enzyme	−0.05	0.685	Enhances disulfide bond formation
HSP90AB1	Molecular chaperone	−0.09	0.324	Stabilizes unfolded proteins under stress
TIGAR	p53-regulated glycolysis	−0.61	0.033	Controls ROS and glycolytic flux
LGALS9	Galectin-9 (Th1/Th2 modulator)	−1.25	0.027	Involved in immune polarization

3.3. Cytokine Modulation Profile Following DC-Vesicle Exposure

To evaluate the immunomodulatory effect of DC-Vesicles, cytokine profiles were assessed in vitro using PBMCs treated with vesicles derived from cryopreserved samples. ELISA quantification was performed for five cytokines representing suppressive (IL-10, TGF-β) and activating (IL-12, IFN-γ, TNF-α) axes. Measurements were normalized to pre-treatment baseline and expressed as percentage change.

Figure 6 presents a heatmap comparing cytokine levels before and after treatment. Results demonstrated a significant decrease in IL-10 (−53%) and TGF-β (−45%), accompanied by marked increases in IL-12 (+65%), IFN-γ (+80%), and TNF-α (+90%) [47–49]. These shifts support a reprogramming of the immune tone from immunosuppressed to pro-inflammatory. These results confirm that cryopreserved DC-Vesicles retain not only structural integrity but also functional immunomodulatory capacity after storage, as reflected in their ability to shift cytokine profiles toward a Th1-type immune response.

The IFN-γ/IL-10 ratio increased from 1.0 (baseline) to 3.8 post-treatment, indicating a strong Th1 polarization signature [50]. The observed cytokine modulation is consistent with antigen-presenting vesicle activation of CD8⁺ T cells and M1 macrophages, as predicted by prior modeling frameworks. These data confirm that cryopreserved DC-Vesicles retain their capacity to modulate key immune effectors [50].

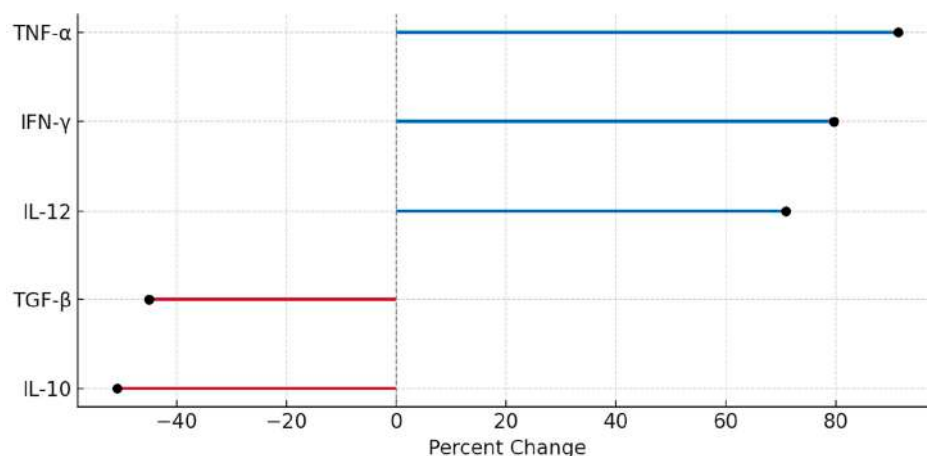


Figure 6. Lollipop plot of cytokine modulation. Percentage changes in suppressive and activating cytokines after vesicle exposure. Red lines = downregulated; blue = upregulated. Values based on Supplementary Table S4.

3.4. Proteomic Fingerprinting and Reproducibility Analysis

Spectral fingerprinting was conducted to evaluate inter-condition consistency and vesicle identity. Fingerprints were derived from normalized LFQ intensity matrices and analyzed by cosine similarity and clustering algorithms. Figure 7 displays a heatmap of immune-related protein intensities, highlighting condition-specific modulation while maintaining overall reproducibility. Samples clustered primarily by condition, with high intra-group similarity (>90%) and inter-group similarity above 85%, even in cryopreserved samples [51]. This suggests that vesicle composition is not only reproducible but also largely invariant under clinical handling constraints. The fingerprint patterns confirmed that vesicles preserved in cold conditions maintained their proteomic identity and immunological signature. Principal proteins contributing to clustering included QSOX1, S100A10, Gal-9, and HSP90AB1, which act as structural anchors and immune effectors [52]. These results highlight the reliability of vesicle fingerprinting as a validation strategy for product characterization in biotherapeutic development. A functional overview of reproducibility across protein families is provided in Supplementary Table S5.

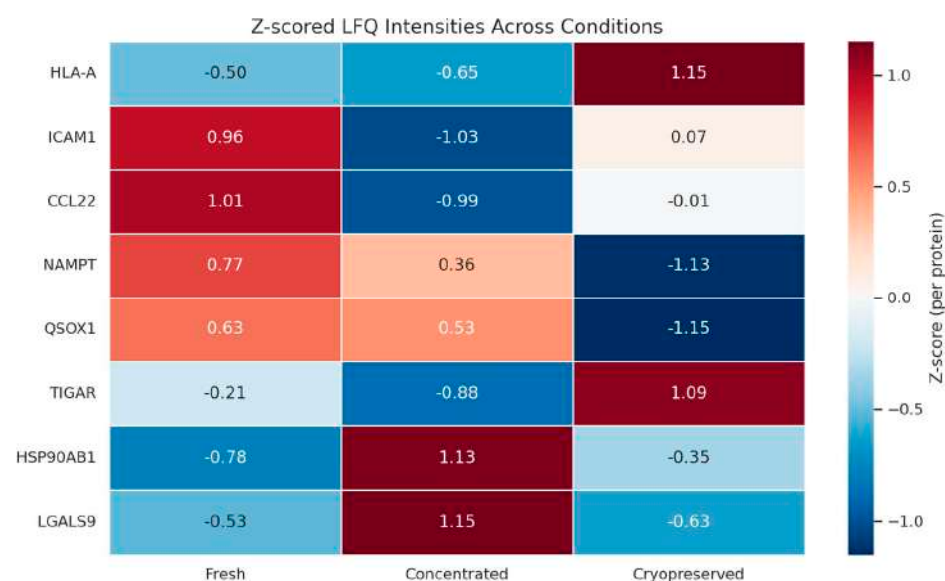


Figure 7. Heatmap of vesicle fingerprinting. Z-scored expression profiles of immune-related proteins across Fresh, Concentrated, and Cryopreserved samples. Color scale reflects relative abundance.

3.5. Principal Component Analysis and Structural Insights

To assess global variance and condition-specific effects, a Principal Component Analysis (PCA) was performed on the complete protein dataset. The first two principal components (PC1 and PC2) captured 92.1% and 7.9% of the total variance, respectively [53]. Figure 8 shows the resulting PCA plot, with each condition forming a distinct cluster and low dispersion among biological replicates.

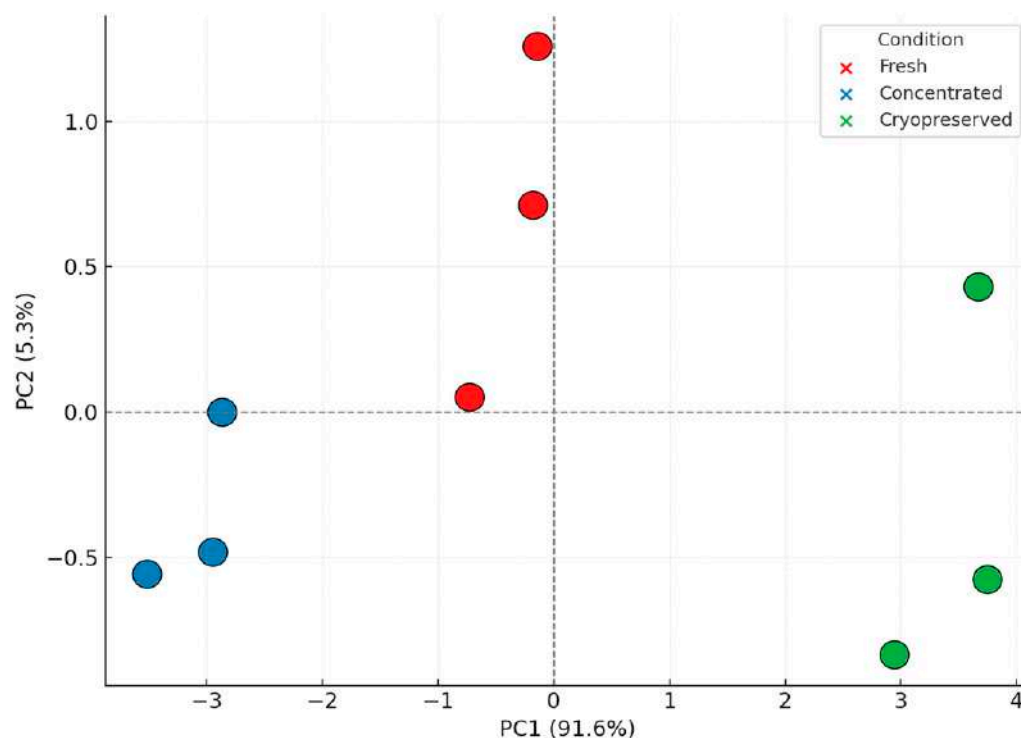


Figure 8. Principal Component Analysis (PCA) plot based on z-scored \log_2 LFQ intensities across all proteins. Each point represents a biological replicate. Colors indicate sample condition (Fresh, Concentrated, Cryopreserved).

Fresh and concentrated samples clustered closely, suggesting similar structural profiles. Cryopreserved samples formed a separate yet compact group, indicating a small but measurable shift in vesicle architecture—likely due to freezing-induced conformational changes. Despite this, the shift was orthogonal to immune-relevant loading patterns and did not impact functional protein clusters, as supported by the cytokine and fingerprint data [54]. The PCA results reinforce that DC-Vesicles retain their core functional and structural properties under cryopreservation, positioning them as viable candidates for real-world distribution and application. PCA was performed using z-scored \log_2 LFQ intensities, ensuring balanced variance scaling across proteins. The complete analytical validation process is summarized in Figure 9.

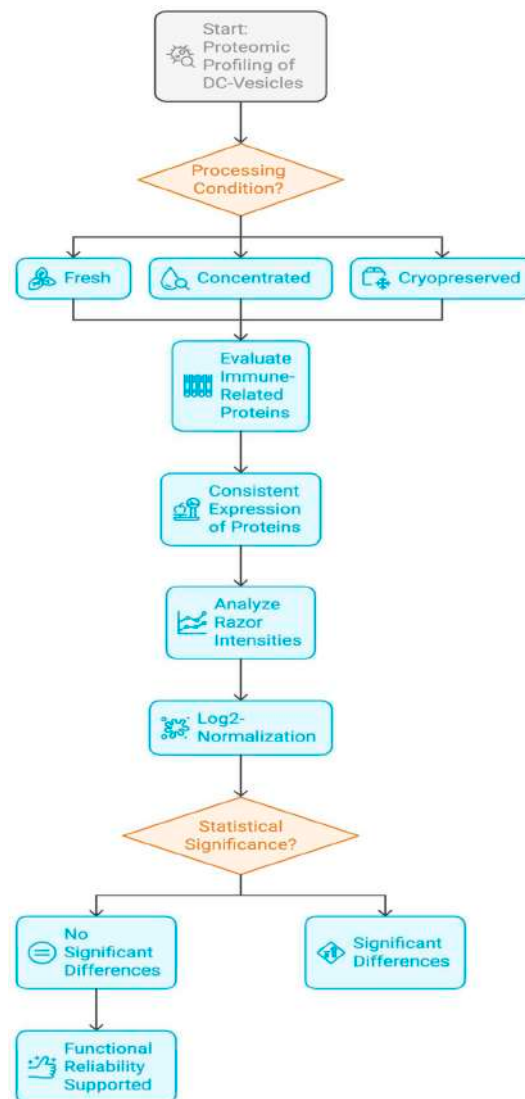


Figure 9. Workflow for experimental validation and statistical interpretation of DC-Vesicle proteomic profiles. Diagram summarizing sample stratification, immune marker evaluation, normalization procedures, and statistical significance decision points.

4. Discussion

The modulation of the tumor microenvironment (TME) remains one of the central challenges in cancer immunotherapy [13,14], particularly in solid tumors where immune suppression, physical barriers, and metabolic constraints hinder therapeutic efficacy [15,16,55]. In this study, we evaluated the structural and functional stability of dendritic cell-derived vesicles (DC-Vesicles) under different processing conditions and assessed their capacity to preserve immunorelevant protein profiles and modulate cytokine signaling [42]. These findings position DC-Vesicles as a robust and scalable immunotherapeutic platform, offering distinct advantages over existing cell-based and vesicle-based strategies [28,30,31].

While checkpoint inhibitors, CAR-T cells, and exosome-based therapies have revolutionized specific aspects of cancer treatment, their clinical utility is often limited by the immunosuppressive landscape of the TME. In this context [7,10], DC-Vesicles offer a complementary mechanism of action—reprogramming the TME through the delivery of immunostimulatory cues without the need for exogenous genetic modification or active cell transfer [32]. The observed reduction in IL-10 and TGF- β , combined with the upregulation of IL-12, IFN- γ , and TNF- α following vesicle treatment, demonstrates the potential of

DC-Vesicles to promote a Th1-skewed immune profile and reverse immune tolerance mechanisms [20]. This cytokine pattern serves as a surrogate marker of post-storage functional stability, suggesting that DC-Vesicles maintain their immune-modulatory effectiveness even after cryopreservation [21]. The functional output of key preserved markers—such as HLA-A, ICAM1, and NAMPT—can be inferred from the observed cytokine shifts, suggesting that these proteins remain biologically active post-thaw and contribute to the immunostimulatory response.

Our proteomic analysis confirms the preservation of critical immune-related proteins across fresh, concentrated, and cryopreserved conditions [56]. Key effectors such as HLA-A, ICAM1, QSOX1, and HSP90AB1 remained consistently detectable, even in cryopreserved samples, indicating the structural resilience of the vesicle formulation. While some markers such as TIGAR and Galectin-9 exhibited minor losses in intensity, their functional pathways remain supported by the upregulation of compensatory effectors. However, as Galectin-9 plays a modulatory role in T cell apoptosis and Th1/Th2 balance, further investigation will be required to determine whether its partial loss affects the *in vivo* immunomodulatory profile of cryopreserved DC-Vesicles. These findings are further validated by PCA clustering and spectral fingerprinting, which demonstrated high reproducibility and minimal deviation between sample groups [57].

Unlike classical dendritic cell-derived exosomes (DEX), which are passively secreted [58,59] and often characterized by variable composition and poor stability, DC-Vesicles are engineered microvesicles embedded in a phospholipid-enriched membrane system matrix [60,61] designed to enhance cargo retention and membrane integrity [62]. The structural advantage conferred by the phospholipoprotein matrix is critical for vesicle stability. Compared to conventional exosome formulations, this matrix enhances surface rigidity, reduces protein loss, and maintains a functional membrane landscape essential for immune modulation after storage or transport. This structural enhancement facilitates their resistance to enzymatic degradation, improves circulation half-life, and promotes interaction with immuno-competent cells in the TME. These characteristics make DC-Vesicles particularly suitable for clinical applications that demand product stability, logistical scalability, and consistent functional output.

The potential integration of DC-Vesicles into combination therapy regimens is particularly noteworthy. In tumors with low immunogenicity—so-called “cold tumors”—DC-Vesicles may act as immune primers, enhancing CD8⁺ T cell activation and promoting responsiveness to checkpoint blockade [63,64]. The combination of IL-12 or IFN- γ with PD-1/PD-L1 inhibition has been associated with enhanced effector cell expansion and delayed exhaustion. In this context, DC-Vesicles could serve not only as immunomodulatory agents but also as carriers for checkpoint modulators or cytokine mimetics. Representative integration strategies are summarized in Table 2.

Table 2. Integration potential of DC-Vesicles in combination immunotherapy strategies.

Combination Strategy	DC-Vesicle Role	Potentiated Immune Effects	Clinical Rationale
DC-Vesicles + PD-1/PD-L1 inhibitors	Immune priming/checkpoint sensitization	CD8 ⁺ activation, Treg suppression	Improves checkpoint efficacy in cold tumors
DC-Vesicles + CAR-T cells	TME remodeling/metabolic modulation	Enhanced CAR-T infiltration and persistence	Overcomes TME resistance and immunometabolic suppression
DC-Vesicles + IL-12 mimetics	Cytokine delivery vector	Amplified Th1 cytokine signature	Sustains pro-inflammatory tone during blockade therapy
DC-Vesicles + Tumor Vaccines	Antigen presentation/adjuvant	Increased APC-T cell cross-talk	Augments vaccine-induced immunogenicity

This table outlines proposed integration pathways for DC-Vesicles with other immunotherapeutic modalities, highlighting their role in enhancing efficacy and overcoming resistance mechanisms. DC-Vesicles can function as immune primers, cytokine delivery vehicles, metabolic modulators, or antigen-presenting adjuvants. Their ability to modulate the tumor microenvironment (TME), stimulate pro-inflammatory cytokine profiles, and augment T cell activation enables synergistic combinations with checkpoint inhibitors, CAR-T cells, IL-12 mimetics, and tumor vaccines. These strategies are particularly relevant in poorly immunogenic tumors, where vesicle-based interventions may improve responsiveness, persistence, and immune coordination.

CAR-T therapies, although transformative in hematologic malignancies, have shown limited success in solid tumors, largely due to inadequate infiltration, immunosuppressive signals, and metabolic exhaustion [65,66]. The application of DC-Vesicles in this setting may enhance CAR-T cell efficacy by modifying the immune and metabolic architecture of the TME. In particular, the delivery of IL-15 and the suppression of immunosuppressive mediators such as PGE2 and TGF- β by DC-Vesicles could prolong lymphocyte persistence and improve tumor infiltration.

From a regulatory standpoint, DC-Vesicles offer a distinct advantage over gene- and cell-based therapies. A comparative overview of these regulatory pathways is illustrated in Supplementary Figure S1. Their bioendogenous origin and non-replicative nature align them with the classification of Non-New Chemical Entities (NCEs), which facilitates faster regulatory approval compared to Advanced Therapy Medicinal Products (ATMPs) [67,68]. See Supplementary Figure S1 for a visual comparison of the regulatory workflows associated with DC-Vesicles and CAR-T/ATMP-based therapies. Unlike CAR-T cells or genetically modified dendritic cells, DC-Vesicles do not require autologous production, viral vectors, or gene editing platforms—thus reducing manufacturing complexity, regulatory burden, and safety concerns related to off-target effects [66,67].

The scalability of DC-Vesicle production further supports their clinical viability. Their formulation allows for batch-standardized, ready-to-administer doses that can be stored, shipped, and delivered without the infrastructure needed for personalized cell therapy. In contrast to CAR-T cells, which involve individualized manufacturing pipelines, DC-Vesicles can be produced at scale under GMP conditions, with validated lot-to-lot consistency and predefined functional benchmarks [68].

The comparative clinical viability of DC-Vesicles was further explored in this study using a qualitative framework that contrasted DC-Vesicles with other immunotherapy platforms. Key therapeutic parameters such as manufacturing cost, scalability, regulatory accessibility, and immunological persistence were evaluated. As summarized in Supplementary Figure S2, DC-Vesicles demonstrate superior performance in terms of logistical feasibility, immune compatibility, and translational potential when compared to CAR-T therapies and therapeutic exosomes [68]. Their lower cost of production, improved bioavailability, and compatibility with regulatory pathways contribute to their positioning as a practical and accessible therapeutic alternative [67]. Platform-level differences between DC-Vesicles and other immunotherapies are summarized in Supplementary Figure S2.

Despite these promising results, several limitations must be acknowledged. The functional assays presented here were performed *in vitro*, and although they provide robust insight into vesicle-induced cytokine modulation, further validation in *in vivo* models is necessary. Additionally, while proteomic preservation has been demonstrated under cryopreservation, real-time pharmacokinetics, biodistribution, and immunogenicity in animal models remain to be characterized. Future studies will be directed toward evaluating DC-Vesicles in murine tumor models, particularly in combination with checkpoint blockade

or adoptive cell therapies. These studies will be essential to define the biodistribution, pharmacokinetics, and synergistic effects with anti-PD-1 strategies.

In conclusion, DC-Vesicles represent a next-generation platform for precision immunotherapy. Their immunomodulatory potency, structural integrity, regulatory compatibility, and manufacturing scalability converge to create a product uniquely suited for integration into existing cancer immunotherapy regimens. The ability to modulate the tumor microenvironment, preserve immune-activating proteins, and support combination strategies positions DC-Vesicles as a powerful tool in the evolving landscape of cancer treatment. Further clinical validation will determine their definitive role in reshaping immuno-oncology [69,70]. Although lyophilization is a key step in the final formulation of the PLPC platform, the present study focuses on the immunological and structural validation of pre-lyophilization vesicle states. These results provide the functional basis required to justify downstream stabilization efforts, confirming the translational relevance and multisite reproducibility of the approach (Table 3). Table 3 summarizes prior dissemination of preliminary results derived from this dataset, including international conference abstracts and poster presentations.

Table 3. Summary of Conference Presentations from This Study. Preliminary findings from this study were presented at the following international meetings.

Conference	Year	Location	Code	Title of the Work
ESMO	2024	Geneva, Switzerland	FPN Code: 60P	Innovative applications of neoantigens in dendritic cell-derived exosome therapy
ESMO	2025	Geneva, Switzerland	FPN Code: 61P	Optimized protocol for accelerated production of DEX
SITC	2025	San Diego, CA, USA	FPN Code: 42	PLPC: A multifunctional bioactive platform for TME reprogramming
SITC	2025	San Diego, CA, USA	FPN Code: 43	Precision Engineered Dendritic Vesicles
SITC	2025	San Diego, CA, USA	FPN Code: 44	Lyophilized Dendritic Exosomes
ASCO	2025	Chicago, IL, USA	Abstract #e14522	Disruptive advances in exosome lyophilization
ASCO	2025	Chicago, IL, USA	Abstract #e14537	Decoding NAMPT and TIGAR
ASCO	2025	Chicago, IL, USA	Abstract #e14511	PLP-driven exosomal breakthroughs
ASCO	2025	Chicago, IL, USA	Abstract #e14512	PLP-powered exosomal therapeutics

Limitations and Future Directions

This study presents robust evidence supporting the structural and immunological stability of DC-Vesicles under clinically relevant processing conditions [71]. However, several limitations must be acknowledged. First, all data were generated through in vitro experiments; while cytokine modulation and proteomic preservation were demonstrated, confirmation of biological efficacy through in vivo models remains essential [72]. Second, although the sample size suffices for proteomic analysis, it limits statistical generalization. Third, while conceptual comparisons were drawn between DC-Vesicles and established platforms such as CAR-T, exosomes, and checkpoint inhibitors [73,74], no direct functional benchmarking assays were conducted against these systems.

In addition, the proposed classification of DC-Vesicles as Non-New Chemical Entities (NCEs) is based on structural features and regulatory plausibility, but will require formal validation through regulatory submissions and review processes [75,76]. To advance toward clinical application, future studies should incorporate pharmacokinetic profiling, biodistribution analyses, and mechanistic exploration in preclinical tumor models [77,78]. Evaluations in combination with checkpoint blockade or adoptive cell therapies will be essential to define optimal administration protocols and identify potential synergies. Multi-center trials should follow to validate reproducibility and confirm efficacy across diverse patient populations and tumor types.

5. Conclusions

DC-Vesicles, embedded within a phospholipid-rich stabilization matrix, represent a promising immunotherapeutic platform capable of modulating the tumor microenvironment (TME) and enhancing immune response durability [79,80]. Their ability to downregulate IL-10 and TGF- β while promoting IL-12 and IFN- γ suggests a Th1-polarized shift in immune tone, with potential for reversing immune evasion in immunologically cold tumors [78]. By improving CD8⁺ T cell persistence and suppressing regulatory cell populations, DC-Vesicles may overcome key limitations of existing checkpoint-based therapies.

Beyond immune modulation, DC-Vesicles offer theoretical advantages in managing minimal residual disease (MRD)—a key contributor to post-treatment relapse. Their capacity to sustain cytokine-driven immune surveillance and interact with antigen-presenting cells supports long-term immunological control.

Operationally, DC-Vesicles bypass the need for genetic manipulation, viral vectors, or personalized cell expansion. Their production is compatible with batch-based GMP manufacturing and long-term stabilization without cryopreservation [79,80]. These attributes align with NCE regulatory classification, potentially reducing the cost and time to clinical integration.

Rather than aiming solely for tumor cytotoxicity, DC-Vesicles operate by correcting immune dysfunction and reprogramming the tumor-immune interface—a conceptual evolution aligned with immunoinflammatory treatment paradigms [77,78]. Their capacity for integration into combination regimens—such as with checkpoint inhibitors, CAR-T cells, IL-12 mimetics, or tumor vaccines—makes them suitable for a range of indications, including poorly immunogenic tumors [73].

From a translational standpoint, DC-Vesicles address key bottlenecks that have historically limited vesicle-based therapies, including manufacturing cost, complexity, and reproducibility. Their bioendogenous architecture, regulatory alignment, and immunological potency support their continued development and prioritization in clinical research agendas.

While further validation is required, the preserved immune fingerprint across storage modalities and confirmed cytokine functionality strongly support the use of DC-Vesicles as standardized, traceable immunotherapeutics. With sustained investment in mechanistic and translational research, DC-Vesicles may offer a scalable and impactful solution for both refractory malignancies and long-term immune control.

Supplementary Materials: The following supporting information can be downloaded at: <https://www.mdpi.com/article/10.3390/biomedicines13061299/s1>, Figure S1: Regulatory workflow comparison between DC-Vesicles and ATMP/CAR-T therapies. Figure S2: Comparative matrix of DC-Vesicles, CAR-T cells, and therapeutic exosomes. Table S1: Experimental conditions for DC-Vesicle processing. Table S2: Complete list of identified peptides per replicate and condition. Table S3: Immune-relevant marker intensities and coefficient of variation per condition. Table S4: Cytokine quantification before and after vesicle exposure. Table S5: Complete list of identified proteins per replicate and condition.

Author Contributions: Conceptualization, R.G.-S.; Methodology, R.G.-S. and F.G.-C.; Investigation, F.G.-C., L.A., J.I., N.M.-G., I.R. and A.S.; Data curation, L.A., J.I., F.K. and C.P.-V.; Formal analysis, R.G.-S. and F.G.-C.; Resources, W.D., A.L., D.M., I.M. and R.A.; Writing—original draft preparation, R.G.-S.; Writing—review and editing, R.G.-S., F.G.-C. and C.P.-V.; Visualization, J.I., L.A., A.T. and C.P.-V.; Evaluation of regulatory and technical attributes, C.P.-V.; Supervision, R.G.-S.; Project administration, R.G.-S.; Funding acquisition, R.G.-S. All authors have read and agreed to the published version of the manuscript.

Funding: This research received no external funding.

Institutional Review Board Statement: Not applicable. This study did not involve experiments on human subjects or animals requiring ethical approval.

Informed Consent Statement: Not applicable. No identifiable human data or tissue samples were used in this study.

Data Availability Statement: Raw mass spectrometry data are available from the corresponding author upon reasonable request. Data access may be subject to confidentiality agreements or material transfer conditions related to ongoing regulatory submissions. The dataset in question is currently part of an ongoing corporate editorial pipeline, and its dissemination is managed strategically to preserve contextual integrity and alignment with future publications and licensing frameworks.

Acknowledgments: The authors would like to thank the technical team at the Proteomics Core Facility for their support with sample processing and mass spectrometry runs. Special thanks to the Oncovix research unit for providing the infrastructure required for cell culture and vesicle processing.

Conflicts of Interest: Authors Ramon Gutierrez-Sandoval, Cristián Peña-Vargas and Andres Toledo were employed by the company OGRD Alliance. Authors Francisco Gutierrez-Castro and Natalia Muñoz-Godoy were employed by the company Flowinmunocell-Bioexocell Group. The remaining authors declare that the research was conducted in the absence of any commercial or financial relationships that could be construed as a potential conflict of interest.

Abbreviations

The following abbreviations are used in this manuscript:

DC	Dendritic cell
DC-Vesicles	Dendritic cell-derived vesicles
DEX	Dendritic cell-derived exosomes
PBMC	Peripheral blood mononuclear cell
GMP	Good manufacturing practice
IL-4	Interleukin 4
IL-1 β	Interleukin 1 beta
IL-10	Interleukin 10
IL-12	Interleukin 12
IL-15	Interleukin 15
TGF- β	Transforming growth factor beta
TNF- α	Tumor necrosis factor alpha
IFN- γ	Interferon gamma
CD	Cluster of differentiation
CAR-T	Chimeric antigen receptor T cell
CRS	Cytokine release syndrome
TME	Tumor microenvironment
Th1	Type 1 helper T cell
Treg	Regulatory T cell
IDO	Indoleamine 2,3-dioxygenase
PGE2	Prostaglandin E2
HLA-A	Human leukocyte antigen A
ICAM1	Intercellular adhesion molecule 1
CCL22	C-C motif chemokine ligand 22
NAMPT	Nicotinamide phosphoribosyltransferase
QSOX1	Quiescin sulfhydryl oxidase 1
TIGAR	TP53-induced glycolysis and apoptosis regulator
HSP90AB1	Heat shock protein 90-beta
LGALS9	Galectin-9
MHC	Major histocompatibility complex
NCE	Non-New Chemical Entity

LFQ	Label-Free Quantification
PCA	Principal Component Analysis
ELISA	Enzyme-linked immunosorbent assay
MS/MS	Tandem mass spectrometry
nanoLC	Nanoflow liquid chromatography
ATMP	Advanced Therapy Medicinal Product

References

- Petersen, J.D.; Zimmerberg, J. Endothelial cells release microvesicles harboring multivesicular bodies and secrete exosomes. *J. Extracell. Biol.* **2023**, *2*, e79. [[CrossRef](#)] [[PubMed](#)]
- Mulcahy, L.A.; Pink, R.C.; Carter, D.R. Routes and mechanisms of extracellular vesicle uptake. *J. Extracell. Vesicles* **2014**, *3*, 24641. [[CrossRef](#)] [[PubMed](#)]
- Yáñez-Mó, M.; Siljander, P.R.; Andreu, Z.; Bedina Zavec, A.; Borràs, F.E.; Buzas, E.I.; Buzas, K.; Casal, E.; Cappello, F.; Carvalho, J.; et al. Biological properties of extracellular vesicles and their physiological functions. *J. Extracell. Vesicles* **2015**, *4*, 27066. [[CrossRef](#)] [[PubMed](#)]
- Vader, P.; Breakefield, X.O.; Wood, M.J. Extracellular vesicles: Emerging targets for cancer therapy. *Trends Mol. Med.* **2014**, *20*, 385–393. [[CrossRef](#)]
- Colombo, M.; Raposo, G.; Théry, C. Biogenesis, secretion, and intercellular interactions of exosomes and other extracellular vesicles. *Annu. Rev. Cell Dev. Biol.* **2014**, *30*, 255–289. [[CrossRef](#)]
- Gajewski, T.F.; Schreiber, H.; Fu, Y.X. Innate and adaptive immune cells in the tumor microenvironment. *Nat. Immunol. Nat. Immunol.* **2013**, *14*, 1014–1022. [[CrossRef](#)]
- Sharma, P.; Hu-Lieskovan, S.; Wargo, J.A.; Ribas, A. Primary, adaptive, and acquired resistance to cancer immunotherapy. *Cell* **2017**, *168*, 707–723. [[CrossRef](#)]
- Patel, S.A.; Minn, A.J. Combination cancer immunotherapy strategies: Immune checkpoint blockade and beyond. *Nat. Rev. Immunol.* **2020**, *20*, 273–287.
- Whiteside, T.L. The role of immune cells in the tumor microenvironment. *Cancer Treat. Res.* **2006**, *130*, 103–124.
- Syn, N.L.; Teng, M.W.L.; Mok, T.S.K.; Soo, R.A. De-novo and acquired resistance to immune checkpoint targeting: Implications for combination therapy. *Lancet Oncol.* **2022**, *23*, e731–e741.
- Finn, O.J. A believer's overview of cancer immunosurveillance and immunotherapy: The journey to precision medicine. *J. Immunol.* **2023**, *210*, 323–332.
- Vader, P.; Kooijmans, S.A.; Stremersch, S.; Raemdonck, K. New considerations in the preparation of nucleic acid-loaded extracellular vesicles. *Ther. Deliv.* **2014**, *5*, 105–107. [[CrossRef](#)] [[PubMed](#)]
- Geynisman, D.M.; Ajiboye, A.S.; Lorkowski, D.; Perera, S.; Reddy, P.S.; Wong, Y.N. An overview of immune checkpoint inhibitors in the management of metastatic non-small-cell lung cancer. *J. Oncol. Pharm. Pract.* **2018**, *24*, 389–399.
- Choi, C.; Bae, S.; Lee, J.; Cho, H.D.; Choi, S.Y.; Kim, H.R. Clinical significance of tumor-infiltrating lymphocytes in patients with non-small cell lung cancer. *Cancers* **2022**, *14*, 758.
- Benoit, A.; Vogin, G.; Duhem, C.; Berchem, G.; Janji, B. Lighting Up the Fire in the Microenvironment of Cold Tumors: A Major Challenge to Improve Cancer Immunotherapy. *Cells* **2023**, *12*, 1787. [[CrossRef](#)] [[PubMed](#)] [[PubMed Central](#)]
- Jiang, H.; Wang, Z.; Xu, X.; Jin, Y.; Wu, X.; Xie, Y.; Tang, X. Therapeutic potential of targeting cancer stem cells in cancer immunotherapy. *Cancer Cell Int.* **2024**, *24*, 315.
- Cao, Y.; Xu, P.; Shen, Y.; Wu, W.; Chen, M.; Wang, F.; Zhu, Y.; Yan, F.; Gu, W.; Lin, Y. Exosomes and cancer immunotherapy: A review of recent cancer research. *Front. Oncol.* **2023**, *12*, 1118101. [[CrossRef](#)] [[PubMed](#)] [[PubMed Central](#)]
- Lu, Q.; Kou, D.; Lou, S.; Ashrafizadeh, M.; Aref, A.R.; Canadas, I.; Tian, Y.; Niu, X.; Wang, Y.; Torabian, P.; et al. Nanoparticles in tumor microenvironment remodeling and cancer immunotherapy. *J. Hematol. Oncol.* **2024**, *17*, 16. [[CrossRef](#)] [[PubMed](#)] [[PubMed Central](#)]
- Nie, L.; Ma, J.; Yu, Y.; Tao, Y.; Song, Z.; Li, J. Exosomes as carriers to stimulate an anti-cancer immune response in immunotherapy and as predictive markers. *Biochem. Pharmacol.* **2025**, *232*, 116699. [[CrossRef](#)]
- Gutierrez-Sandoval, R.; Gutiérrez-Castro, F.; Muñoz-Godoy, N.; Rivadeneira, I.; Sobarzo, A.; Iturra, J.; Krakowiak, F.; Alarcón, L.; Dorado, W.; Lagos, A.; et al. Beyond Exosomes: An Ultrapurified Phospholipoproteic Complex (PLPC) as a Scalable Immunomodulatory Platform for Reprogramming Immune Suppression in Metastatic Cancer. *Cancers* **2025**, *17*, 1658. [[CrossRef](#)]
- Lyu, C.; Sun, H.; Sun, Z.; Liu, Y.; Wang, Q. Roles of exosomes in immunotherapy for solid cancers. *Cell Death Dis.* **2024**, *15*, 106. [[CrossRef](#)] [[PubMed](#)]
- Pi, Y.-N.; Xia, B.-R.; Jin, M.-Z.; Jin, W.-L.; Lou, G. Exosomes: Powerful weapon for cancer nano-immunoengineering. *Biochem. Pharmacol.* **2021**, *186*, 114487. [[CrossRef](#)] [[PubMed](#)]

23. Li, T.; Jiao, J.; Ke, H.; Ouyang, W.; Wang, L.; Pan, J.; Li, X. Role of exosomes in the development of the immune microenvironment in hepatocellular carcinoma. *Front. Immunol.* **2023**, *14*, 1200201. [[CrossRef](#)] [[PubMed](#)]
24. Wu, Y.; Han, W.; Dong, H.; Liu, X.; Su, X. The rising roles of exosomes in the tumor microenvironment reprogramming and cancer immunotherapy. *MedComm* **2024**, *5*, e541. [[CrossRef](#)]
25. Zhang, L.; Sun, S.; Li, X.; Zhang, Y.; Cao, P.; Zhang, X. Advances in immune checkpoint inhibitors and their combination strategies in cancer therapy. *J. Immunother. Cancer* **2024**, *12*, e00582.
26. Ho, T.; Msallam, R. Tissues and Tumor Microenvironment (TME) in 3D: Models to Shed Light on Immunosuppression in Cancer. *Cells* **2021**, *10*, 831. [[CrossRef](#)]
27. Barrera, E.; Medina, R.; Mendoza, R.; Salinas, P.; Aguirre, J.; Paredes, M. Inmunoterapia en linfomas: Una nueva era en su tratamiento. *Rev. Hematol. Argent.* **2020**, *46*, 174–182.
28. Yu, L.; Xu, L.; Chen, Y.; Rong, Y.; Zou, Y.; Ge, S.; Wu, T.; Lai, Y.; Xu, Q.; Guo, W.; et al. IDO1 inhibition promotes activation of tumor-intrinsic STAT3 pathway and induces adverse tumor-protective effects. *J. Immunol.* **2024**, *212*, 1232–1243. [[CrossRef](#)]
29. Sosnowska, A.; Chlebowska-Tuz, J.; Matryba, P.; Pilch, Z.; Greig, A.; Wolny, A.; Grzywa, T.M.; Rydzynska, Z.; Sokolowska, O.; Rygiel, T.P.; et al. Inhibition of arginase modulates T-cell response in the tumor microenvironment of lung carcinoma. *Oncoimmunology* **2021**, *10*, 1956143. [[CrossRef](#)]
30. Lorentzen, C.L.; Martinenaite, E.; Kjeldsen, J.W.; Holmstroem, R.B.; Mørk, S.K.; Pedersen, A.W.; Ehrnrooth, E.; Andersen, M.H.; Svane, I.M. Arginase-1 targeting peptide vaccine in patients with metastatic solid tumors—A phase I trial. *Front. Immunol.* **2022**, *13*, 1023023. [[CrossRef](#)]
31. Martin-Orozco, E.; Sanchez-Fernandez, A.; Ortiz-Parra, I.; Ayala-San Nicolas, M. WNT signaling in tumors: The way to evade drugs and immunity. *Front. Immunol.* **2019**, *10*, 2854. [[CrossRef](#)] [[PubMed](#)]
32. Dillen, A.; Bui, I.; Jung, M.; Agiotti, S.; Zaravinos, A.; Bonavida, B. Regulation of PD-L1 expression by YY1 in cancer: Therapeutic efficacy of targeting YY1. *Cancers* **2024**, *16*, 1237. [[CrossRef](#)] [[PubMed](#)]
33. Dong, L.; Zhu, Y.; Zhang, H.; Gao, L.; Zhang, Z.; Xu, X.; Ying, L.; Zhang, L.; Li, Y.; Yun, Z.; et al. Open-source throttling of CD8⁺ T cells in brain with low-intensity focused ultrasound-guided sequential delivery of CXCL10, IL-2, and aPD-L1 for glioblastoma immunotherapy. *Adv. Mater.* **2024**, *36*, e2407235. [[CrossRef](#)] [[PubMed](#)]
34. Bence, C.; Hofman, V.; Chamorey, E.; Long-Mira, E.; Lassalle, S.; Albertini, A.; Liolios, I.; Zahaf, K.; Picard, A.; Montaudié, H.; et al. Association of combined PD-L1 expression and tumour-infiltrating lymphocyte features with survival and treatment outcomes in patients with metastatic melanoma. *J. Dermatol. Venereol.* **2020**, *34*, 984–994. [[CrossRef](#)]
35. Bacolod, M.D.; Barany, F.; Pilonis, K.; Fisher, P.B.; de Castro, R.J. Pathways- and epigenetic-based assessment of relative immune infiltration in various types of solid tumors. *Adv. Cancer Res.* **2019**, *142*, 107–143.
36. Dai, E.; Zhu, Z.; Wahed, S.; Qu, Z.; Storkus, W.J.; Guo, Z.S. Epigenetic modulation of antitumor immunity for improved cancer immunotherapy. *Mol. Cancer* **2021**, *20*, 171. [[CrossRef](#)]
37. Gomez, S.; Tabernacki, T.; Kobyra, J.; Roberts, P.; Chiappinelli, K.B. Combining epigenetic and immune therapy to overcome cancer resistance. *Semin. Cancer Biol.* **2020**, *65*, 99–113. [[CrossRef](#)]
38. Peng, D.; Kryczek, I.; Nagarsheth, N.; Zhao, L.; Wei, S.; Wang, W.; Sun, Y.; Zhao, E.; Vatan, L.; Szeliga, W.; et al. Epigenetic silencing of TH1-type chemokines shapes tumour immunity and immunotherapy. *Nature* **2020**, *527*, 249–253. [[CrossRef](#)]
39. Qin, X.H.; Wang, H.-X.; Ma, L.; Shen, J.; Liu, Q.-H.; Xue, L. Knockout of the Placenta Specific 8 Gene affects the proliferation and migration of human embryonic kidney 293T cell. *Cell Biochem. Biophys.* **2020**, *78*, 55–64. [[CrossRef](#)]
40. Sun, X.; Liu, Z.; Yu, Q.; Chen, Y.; Sun, Y.; Zhu, Q.; Yang, J.; Jiang, R. PLAC8 is an innovative biomarker for immunotherapy participating in remodeling the immune microenvironment of renal clear cell carcinoma. *Front. Oncol.* **2023**, *13*, 1207551. [[CrossRef](#)]
41. Singh, S.; Kachhawaha, K.; Singh, S.K. Comprehensive approaches to preclinical evaluation of monoclonal antibodies and their next-generation derivatives. *Biochem. Pharmacol.* **2024**, *225*, 116303. [[CrossRef](#)] [[PubMed](#)]
42. Kowal, J.; Arras, G.; Colombo, M.; Jouve, M.; Morath, J.P.; Primdal-Bengtson, B.; Dingli, F.; Loew, D.; Tkach, M.; Théry, C. Proteomic comparison defines novel markers to characterize heterogeneous populations of extracellular vesicle subtypes. *Proc. Natl. Acad. Sci. USA* **2016**, *113*, E968–E977. [[CrossRef](#)] [[PubMed](#)]
43. Notarbartolo, S.; Abrignani, S. Human T lymphocytes at tumor sites. *Scand. J. Immunol.* **2022**, *44*, 883–901. [[CrossRef](#)] [[PubMed](#)]
44. Beumer-Chuwonpad, A.; Taggenbrock, R.L.R.E.; Ngo, T.A.; van Gisbergen, K.P.J.M. The potential of tissue-resident memory T cells for adoptive immunotherapy against cancer. *Cells* **2021**, *10*, 2234. [[CrossRef](#)]
45. Micevic, G.; Thakral, D.; McGeary, M.; Bosenberg, M.W. PD-L1 methylation regulates PD-L1 expression and is associated with melanoma survival. *Pigment Cell Melanoma Res.* **2019**, *32*, 435–440. [[CrossRef](#)]
46. O'Reilly, E.M.; Oh, D.Y.; Dhani, N.; Renouf, D.J.; Lee, M.A.; Sun, W.; Fisher, G.; Hezel, A.; Chang, S.C.; Vlahovic, G.; et al. Durvalumab With or Without Tremelimumab for Patients With Metastatic Pancreatic Ductal Adenocarcinoma: A Phase 2 Randomized Clinical Trial. *JAMA Oncol.* **2019**, *5*, 1431–1438. [[CrossRef](#)]

47. Micevic, G.; Bosenberg, M.W.; Yan, Q. The crossroads of cancer epigenetics and immune checkpoint therapy. *Clin. Cancer Res.* **2023**, *29*, 1173–1182. [[CrossRef](#)]
48. O'Reilly, E.M.; Ferrone, C. Neoadjuvant or adjuvant therapy for resectable or borderline resectable pancreatic cancer: Which is preferred? *J. Clin. Oncol.* **2020**, *38*, 1757–1759. [[CrossRef](#)]
49. Principe, D.R.; Korc, M.; Kamath, S.D.; Munshi, H.G.; Rana, A. Trials and tribulations of pancreatic cancer immunotherapy. *Cancer Lett.* **2021**, *504*, 1–14. [[CrossRef](#)]
50. Wang, Y.; Duan, M.; Peng, Z.; Fan, R.; He, Y.; Zhang, H.; Xiong, W.; Jiang, W. Advances of DNA Damage Repair-Related Drugs and Combination With Immunotherapy in Tumor Treatment. *Front. Immunol.* **2022**, *13*, 854730. [[CrossRef](#)]
51. Mohammadi, S.; Yousefi, F.; Shabaninejad, Z.; Movahedpour, A.; Tehran, M.M.; Shafiee, A.; Moradizarmehri, S.; Hajighadimi, S.; Savardashtaki, A.; Mirzaei, H. Exosomes and cancer: From oncogenic roles to therapeutic applications. *IUBMB Life* **2020**, *72*, 724–748. [[CrossRef](#)] [[PubMed](#)]
52. Pourhanifeh, M.H.; Mahjoubin-Tehran, M.; Shafiee, A.; Hajighadimi, S.; Moradizarmehri, S.; Mirzaei, H.; Asemi, Z. MicroRNAs and exosomes: Small molecules with big actions in multiple myeloma pathogenesis. *IUBMB Life* **2020**, *72*, 314–333. [[CrossRef](#)] [[PubMed](#)]
53. Keskin, D.B.; Anandappa, A.J.; Sun, J.; Tirosh, I.; Mathewson, N.D.; Li, S.; Oliveira, G.; Giobbie-Hurder, A.; Felt, K.; Gjini, E.; et al. Neoantigen vaccine generates intratumoral T cell responses in phase Ib glioblastoma trial. *Nature* **2019**, *565*, 234–239. [[CrossRef](#)] [[PubMed](#)]
54. Sun, C.; Xu, S. Advances in personalized neoantigen vaccines for cancer immunotherapy. *Biosci. Trends* **2020**, *14*, 349–353. [[CrossRef](#)]
55. Poznanski, S.M.; Singh, K.; Ritchie, T.M.; Aguiar, J.A.; Fan, I.Y.; Portillo, A.L.; Rojas, E.A.; Vahedi, F.; El-Sayes, A.; Xing, S.; et al. Metabolic flexibility determines human NK cell functional fate in the tumor microenvironment. *Cell Metab.* **2021**, *33*, 1205–1220.e5. [[CrossRef](#)]
56. Koundouros, N.; Pouligiannis, G. Reprogramming of fatty acid metabolism in cancer. *Br. J. Cancer* **2020**, *122*, 4–22. [[CrossRef](#)]
57. Snaebjornsson, M.T.; Janaki-Raman, S.; Schulze, A. Greasing the Wheels of the Cancer Machine: The Role of Lipid Metabolism in Cancer. *Cell Metab.* **2020**, *31*, 62–76. [[CrossRef](#)]
58. Liu, Y.; Zuckier, L.S.; Ghesani, N.V. Lipid metabolism as a target for cancer drug resistance. *Front. Pharmacol.* **2023**, *14*, 1274335.
59. An, Q.; Lin, R.; Wang, D.; Wang, C. Emerging roles of fatty acid metabolism in cancer and their targeted drug development. *Eur. J. Med. Chem.* **2022**, *240*, 114613. [[CrossRef](#)]
60. Bian, X.; Liu, R.; Meng, Y.; Xing, D.; Xu, D.; Lu, Z. Lipid metabolism and cancer. *J. Exp. Med.* **2021**, *218*, e20201606. [[CrossRef](#)]
61. Liu, Y.; Deng, H.; Song, P.; Zhang, M. Constructing a Glioblastoma Prognostic Model Related to Fatty Acid Metabolism Using Machine Learning and Identifying F13A1 as a Potential Target. *Biomedicines* **2025**, *13*, 256. [[CrossRef](#)] [[PubMed](#)]
62. Liu, D.; Liu, L.; Che, X.; Wu, G. Discovery of paradoxical genes: Reevaluating the prognostic impact of overexpressed genes in cancer. *Front. Cell Dev. Biol.* **2025**, *13*, e1525345. [[CrossRef](#)] [[PubMed](#)]
63. Zhang, Y.; Yang, Z.; Liu, Y.; Pei, J.; Li, R.; Yang, Y. Targeting lipid metabolism: Novel insights and therapeutic advances in pancreatic cancer treatment. *Lipids Health Dis.* **2025**, *24*, 12. [[CrossRef](#)] [[PubMed](#)]
64. Wang, N.; Chen, Y.; Lin, J.; Lin, Y.; Song, H.; Huang, W.; Shen, L.; Chen, F.; Liu, F.; Wang, J.; et al. Identification of novel serum lipid metabolism potential markers and metabolic pathways for oral cancer: A population-based study. *BMC Cancer* **2025**, *25*, 177. [[CrossRef](#)]
65. Fu, Y.; Zou, T.; Shen, X.; Nelson, P.J.; Li, J.; Wu, C.; Yang, J.; Zheng, Y.; Bruns, C.; Zhao, Y.; et al. Lipid metabolism in cancer progression and therapeutic strategies. *MedComm* **2020**, *2*, 27–59. [[CrossRef](#)]
66. Fan, T.W.; Higashi, R.M.; Chernayavskaya, Y.; Lane, A.N. Resolving metabolic heterogeneity in experimental models of the tumor microenvironment from a stable isotope resolved metabolomics perspective. *Metabolites* **2020**, *10*, 249. [[CrossRef](#)]
67. Snaebjornsson, M.T.; Poeller, P.; Komkova, D.; Röhrig, F.; Schlicker, L.; Winkelkotte, A.M.; Chaves-Filho, A.B.; Al-Shami, K.M.; Caballero, C.D.; Koltsaki, I.; et al. Targeting aldolase A in hepatocellular carcinoma leads to imbalanced glycolysis and energy stress due to uncontrolled FBP accumulation. *Nat. Metab.* **2025**, *7*, 348–366. [[CrossRef](#)]
68. Kopecka, J.; Trouillas, P.; Gašparović, A.Č.; Gazzano, E.; Assaraf, Y.G.; Riganti, C. Phospholipids and cholesterol: Inducers of cancer multidrug resistance and therapeutic targets. *Drug Resist. Update* **2020**, *49*, 100670. [[CrossRef](#)]
69. Carrer, A.; Trefely, S.; Zhao, S.; Campbell, S.L.; Norgard, R.J.; Schultz, K.C.; Sidoli, S.; Parris, J.L.D.; Affronti, H.C.; Sivanand, S.; et al. Acetyl-CoA metabolism supports multistep pancreatic tumorigenesis. *Cancer Discov.* **2019**, *9*, 416–435. [[CrossRef](#)]
70. Cheng, H.; Wang, M.; Su, J.; Li, Y.; Long, J.; Chu, J.; Wan, X.; Cao, Y.; Li, Q. Lipid Metabolism and Cancer. *Life* **2022**, *12*, 784. [[CrossRef](#)]
71. Xu, D.; Shao, F.; Bian, X.; Meng, Y.; Liang, T.; Lu, Z. The Evolving Landscape of Noncanonical Functions of Metabolic Enzymes in Cancer and Other Pathologies. *Cell Metab.* **2021**, *33*, 33–50. [[CrossRef](#)] [[PubMed](#)]
72. Xu, D.; Li, X.; Shao, F.; Lv, G.; Lv, H.; Lee, J.-H.; Qian, X.; Wang, Z.; Xia, Y.; Du, L.; et al. The protein kinase activity of fructokinase A specifies the antioxidant responses of tumor cells by phosphorylating p62. *Sci. Adv.* **2019**, *5*, eaav4570. [[CrossRef](#)] [[PubMed](#)]

73. Grasmann, G.; Smolle, E.; Olschewski, H.; Leithner, K. Gluconeogenesis in cancer cells—Repurposing of a starvation-induced metabolic pathway? *Biochim. Biophys. Acta Rev. Cancer* **2019**, *1872*, 24–36. [[CrossRef](#)] [[PubMed](#)]
74. Zhao, J.; Xie, F.; Yang, Y.; Wang, S. Reprogramming of fatty acid metabolism in breast cancer: A narrative review. *Transl. Breast Cancer Res.* **2021**, *2*, 5. [[CrossRef](#)]
75. Gong, Y.; Ji, P.; Yang, Y.-S.; Xie, S.; Yu, T.-J.; Xiao, Y.; Jin, M.-L.; Ma, D.; Guo, L.-W.; Pei, Y.-C.; et al. Metabolic-Pathway-Based Subtyping of Triple-Negative Breast Cancer Reveals Potential Therapeutic Targets. *Cell Metab.* **2021**, *33*, 51–64.e9. [[CrossRef](#)]
76. Chen, Y.; Li, K.; Gong, D.; Zhang, J.; Li, Q.; Zhao, G.; Lin, P. ACLY: A biomarker of recurrence in breast cancer. *Pathol. Res. Pract.* **2020**, *216*, 153076. [[CrossRef](#)]
77. Yang, J.; Wang, L.; Jia, R. Role of de novo cholesterol synthesis enzymes in cancer. *J. Cancer* **2020**, *11*, 1761–1767. [[CrossRef](#)]
78. Vriens, K.; Christen, S.; Parik, S.; Broekaert, D.; Yoshinaga, K.; Talebi, A.; Dehairs, J.; Escalona-Noguero, C.; Schmieder, R.; Cornfield, T.; et al. Evidence for an alternative fatty acid desaturation pathway increasing cancer plasticity. *Nature* **2019**, *566*, 403–406. [[CrossRef](#)]
79. Saito, R.F.; Andrade, L.N.d.S.; Bustos, S.O.; Chammas, R. Phosphatidylcholine-Derived Lipid Mediators: The Crosstalk Between Cancer Cells and Immune Cells. *Front. Immunol.* **2022**, *13*, 768606. [[CrossRef](#)]
80. Saito, R.F.; Rangel, M.C.; Halman, J.R.; Chandler, M.; Andrade, L.N.d.S.; Odete-Bustos, S.; Furuya, T.K.; Carrasco, A.G.M.; Chaves-Filho, A.B.; Yoshinaga, M.Y.; et al. Simultaneous Silencing of Lysophosphatidylcholine Acyltransferases 1–4 by Nucleic Acid Nanoparticles (NANPs) Improves Radiation Response of Melanoma Cells. *Nanomedicine* **2021**, *36*, 102418. [[CrossRef](#)]

Disclaimer/Publisher’s Note: The statements, opinions and data contained in all publications are solely those of the individual author(s) and contributor(s) and not of MDPI and/or the editor(s). MDPI and/or the editor(s) disclaim responsibility for any injury to people or property resulting from any ideas, methods, instructions or products referred to in the content.



Article

The Design of a Multistage Monitoring Protocol for Dendritic Cell-Derived Exosome (DEX) Immunotherapy: A Conceptual Framework for Molecular Quality Control and Immune Profiling

Ramón Gutiérrez-Sandoval, Francisco Gutiérrez-Castro, Natalia Muñoz-Godoy, Ider Rivadeneira, Adolay Sobarzo, Luis Alarcón, Wilson Dorado, Andy Lagos, Diego Montenegro, Ignacio Muñoz et al.

Special Issue

Recent Advances in Molecular Targets for Treatment and Drug Delivery in Tumors

Edited by
Dr. Emily Capone





Article

The Design of a Multistage Monitoring Protocol for Dendritic Cell-Derived Exosome (DEX) Immunotherapy: A Conceptual Framework for Molecular Quality Control and Immune Profiling

Ramón Gutiérrez-Sandoval ^{1,*},[†] , Francisco Gutiérrez-Castro ^{2,†}, Natalia Muñoz-Godoy ², Ider Rivadeneira ³, Adolay Sobarzo ⁴, Luis Alarcón ³, Wilson Dorado ³, Andy Lagos ³, Diego Montenegro ³, Ignacio Muñoz ³, Rodrigo Aguilera ³, Jordan Iturra ³, Francisco Krakowiak ⁵, Cristián Peña-Vargas ¹ and Andrés Toledo ¹

¹ Department of Oncopathology, OGRD Alliance, Lewes, DE 19958, USA; consultorusa@biogenica.org (C.P.-V.); ops@ogrdalliance.org (A.T.)

² Department of Cancer Research, Flowimmunocell-Bioexocell Group, 08028 Barcelona, Spain; servicios@flowimmunocell.cl (F.G.-C.); contacto@flowimmunocell.cl (N.M.-G.)

³ Department of Outreach and Engagement Programs for OGRD Consortium, Charlestown KN0802, Saint Kitts and Nevis; iderlautaro@gmail.com (I.R.); luisantonioalarconcofre@gmail.com (L.A.); wdoradoortega@gmail.com (W.D.); lagosandy@gmail.com (A.L.); dn.montenegro.c@gmail.com (D.M.); kinesiologo@recell.cl (I.M.); rodrigo1982aguilera@gmail.com (R.A.); jiconsultant@ogrdconsorcio.com (J.I.)

⁴ Departamento de Ciencias Biológicas y Químicas, Facultad de Ciencias, Universidad San Sebastián, Lientur 1457, Concepción 4080871, Chile; adolay.sobarzo@uss.cl

⁵ Department of Molecular Oncopathology, Bioclas, Concepción 4030000, Chile; tecnologo@bioclas.cl

* Correspondence: cso@ogrdalliance.org

[†] These authors contributed equally to this work.



Academic Editors: Riccardo Alessandro and Emily Capone

Received: 19 March 2025

Revised: 1 June 2025

Accepted: 3 June 2025

Published: 6 June 2025

Citation: Gutiérrez-Sandoval, R.; Gutiérrez-Castro, F.; Muñoz-Godoy, N.; Rivadeneira, I.; Sobarzo, A.; Alarcón, L.; Dorado, W.; Lagos, A.; Montenegro, D.; Muñoz, I.; et al. The Design of a Multistage Monitoring Protocol for Dendritic Cell-Derived Exosome (DEX) Immunotherapy: A Conceptual Framework for Molecular Quality Control and Immune Profiling. *Int. J. Mol. Sci.* **2025**, *26*, 5444. <https://doi.org/10.3390/ijms26125444>

Copyright: © 2025 by the authors. Licensee MDPI, Basel, Switzerland. This article is an open access article distributed under the terms and conditions of the Creative Commons Attribution (CC BY) license (<https://creativecommons.org/licenses/by/4.0/>).

Abstract: The increasing complexity of dendritic cell (DC)-derived exosome (DEX) immunotherapy demands structured monitoring protocols capable of translating molecular activity into actionable clinical outputs. This study proposes a standardized, multistage immunomonitoring framework designed to evaluate immune activation, cytokine polarization, and product integrity in DEX-based therapies. The protocol integrates open access methodologies—flow cytometry, cytometric bead array (CBA), and Western blotting—to assess CD69/CD25 activation, Th1/Th2/Th17 cytokine profiles, and vesicle identity across distinct checkpoints. These outputs are consolidated within the Structured Immunophenotypic Traceability Platform (STIP), which applies logic-based classifications (Type I–III) to support reproducible stratification of immune responses. Functional validation was performed through ex vivo co-culture models, enabling real-time interpretation of immune polarization, cytotoxic potential, and batch consistency. These outputs are supported by previous experimental validations published in *Cancers* and *Biomedicines* (2025), where PLPC and DC-derived vesicles demonstrated immunological consistency and a phenotypic stratification capacity. This approach provides a scalable monitoring structure that can support personalized treatment decisions, quality assurance workflows, and integration into regulatory documentation (e.g., CTD Module 5.3) for early-phase, non-pharmacodynamic immunotherapies. This conceptual protocol does not aim to demonstrate therapeutic efficacy but to provide a reproducible documentation framework for real-world immune monitoring and regulatory alignment in vesicle-based immunotherapy.

Keywords: structured immunomonitoring; STIP; dendritic cell-derived exosomes; phenotypic immune classification; cytokine logic ratios; non-pharmacodynamic platform; ex vivo immune profiling; vesicle-based quality control

1. Introduction

Cancer remains one of the leading causes of mortality worldwide, with millions of new cases diagnosed each year. While current treatments have demonstrated efficacy in specific contexts, they often present significant limitations [1]. Conventional therapies, such as chemotherapy and radiotherapy, are frequently associated with severe adverse effects and high systemic toxicity, which can compromise patient quality of life and limit long-term therapeutic success [2]. These limitations have catalyzed the pursuit of innovative approaches, with immunotherapy emerging as a prominent alternative due to its capacity to leverage the patient's own immune system to selectively target malignant cells. Despite major advances in molecular oncology, many treating oncologists still lack access to structured immunomonitoring protocols that translate molecular data into actionable clinical strategies. This gap is particularly evident in the context of exosome-based immunotherapies.

Among immunotherapy modalities, dendritic cell (DC)-based strategies are among the most advanced and promising [3,4]. DCs are key orchestrators of adaptive immunity, capable of processing tumor antigens and presenting them to naïve T lymphocytes, thereby eliciting robust and specific antitumor responses. Pulsing DCs with tumor-specific antigens enable the personalization of treatment according to the molecular signature of each patient's tumor, increasing selectivity and reducing off-target effects [5,6].

In recent years, there has been growing interest in dendritic cell-derived exosomes (DEXs) as non-cellular immunotherapeutic agents [7]. These extracellular vesicles, enriched with proteins, lipids, and nucleic acids, can amplify immune signaling and mediate intercellular communication across immune compartments. Their physicochemical stability and ability to access immunologically privileged or anatomically challenging tumor niches make them particularly attractive as delivery vectors in cancer immunotherapy [8]. The integration of DEXs with antigen-pulsed DC protocols provides an opportunity to enhance therapeutic reach while preserving specificity and immunogenicity.

Despite these advances, the clinical deployment of DEX-based immunotherapies remains constrained by the absence of standardized monitoring systems capable of capturing dynamic molecular correlates of immune activity. Conventional imaging-based response scales, such as RECIST and iRECIST, remain essential for tumor burden assessment but do not reflect immunological engagement, cytokine polarization, or exosome quality [9,10].

To address this gap, the present work introduces a structured, multistage monitoring protocol specifically designed for DEX immunotherapy. Rather than presenting clinical data, this protocol offers a conceptual framework that integrates accessible laboratory techniques—including flow cytometry, Western blotting, and cytokine profiling using a cytometric bead array (CBA)—to enable molecular-level immune monitoring and batch quality control. All tools referenced are compatible with open access, non-commercial platforms that require no licensing, registration, or proprietary software, ensuring reproducibility and scalability in both academic and translational settings.

This methodological proposal does not intend to validate clinical efficacy but to provide a reproducible and adaptable platform that supports the next generation of DEX-based immunotherapy trials. Future studies will focus on the application and prospective validation of this protocol across diverse patient cohorts and clinical scenarios.

Beyond its methodological scope, this protocol serves as a clinical decision-support tool for non-molecular oncologists. It is designed to translate *ex vivo* immune monitoring results—typically encoded in flow cytometry plots, Western blot bands, or cytokine heatmaps—into logic-governed classifications that are operationally actionable. Rather than introducing new techniques, the protocol integrates well-established, open access

tools—such as CBA kits, Western blotting, and standard confluence analysis—into a reproducible framework suited for translational deployment.

In this context, we introduce the Structured Immunophenotypic Traceability Platform (STIP), a modular classification system that consolidates kinetic metrics (e.g., Δ confluence), cytokine polarization (e.g., IFN- γ /IL-10), and non-lethal divergence signals into structured technical dossiers. The framework does not aim to establish therapeutic efficacy, but rather phenotypic compatibility and traceability across vesicle batches and cell types. This framework was conceptually derived from two prior studies that independently validated the immunological consistency and functional stratification potential of PLPC and DC-derived vesicles under experimental conditions [11,12]. The resulting logic tree outputs—categorized into Type I, II, or III immune responses—can be documented, audited, and archived in pre-regulatory formats.

STIP is further designed to support immune stratification in patients who are ineligible for randomized clinical trials or standard pharmacological monitoring, including those receiving experimental vesicle-based therapies with no genomic payload, no systemic toxicity, and no conventional pharmacokinetics.

2. Results

Monitoring in DC immunotherapy is crucial to ensure the efficacy of treatment in cancer patients. The first key step in this type of DC immunotherapy is the isolation of progenitor cells, specifically peripheral blood mononuclear cells (PBMCs). Separation is carried out using density gradients, which enables an enriched fraction of monocytes, lymphocytes, and other hematopoietic cells to be obtained, which are essential for subsequent differentiation into DCs [11] (Figure 1). The viability of the progenitor cells is crucial because any contamination would compromise the quality of the resulting DCs.

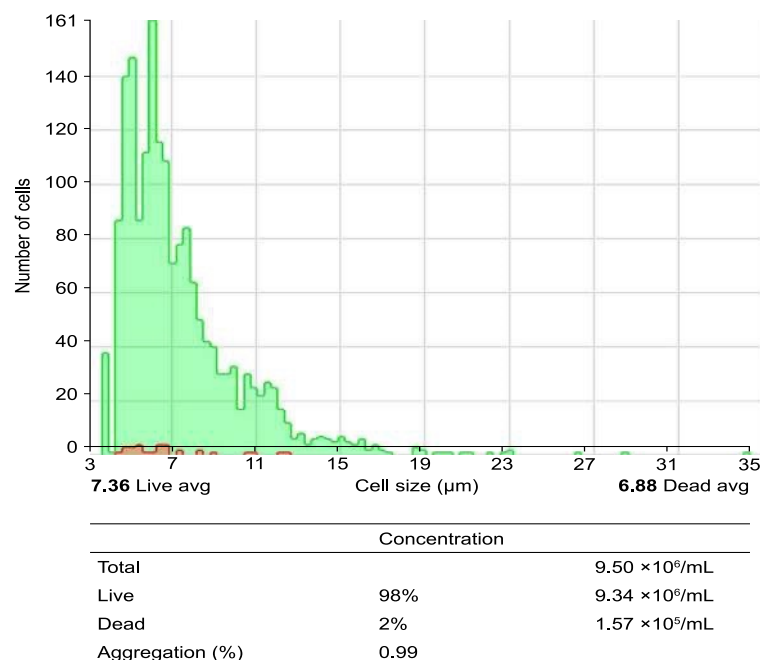


Figure 1. Obtaining peripheral blood mononuclear cells (PBMCs) from peripheral blood using a Ficoll–Hypaque gradient: the process of obtaining PBMCs through a density gradient via centrifugation is illustrated. The upper histogram illustrates the cell size and cell count per analyzed field, differentiating between live cells (green area) and dead cells (red area). The lower table corresponds to the quantification of live and dead cells via analysis with the Countess 3 Automated Cell Counter (number of PBMCs per mL before the seeding process).

Following the isolation of PBMCs, they are differentiated and matured. The differentiation of monocytes into DCs is induced using specific cytokines such as GM-CSF and IL-4, and this process is continuously monitored to ensure that the cells reach the appropriate immature state. Maturation is achieved by the addition of proinflammatory cytokines such as TNF- α and IL-1 β , allowing DCs to efficiently present tumor antigens (Figure 2). Monitoring is essential to ensure that the DCs can fulfill their key immunological function and trigger a specific antitumor response.

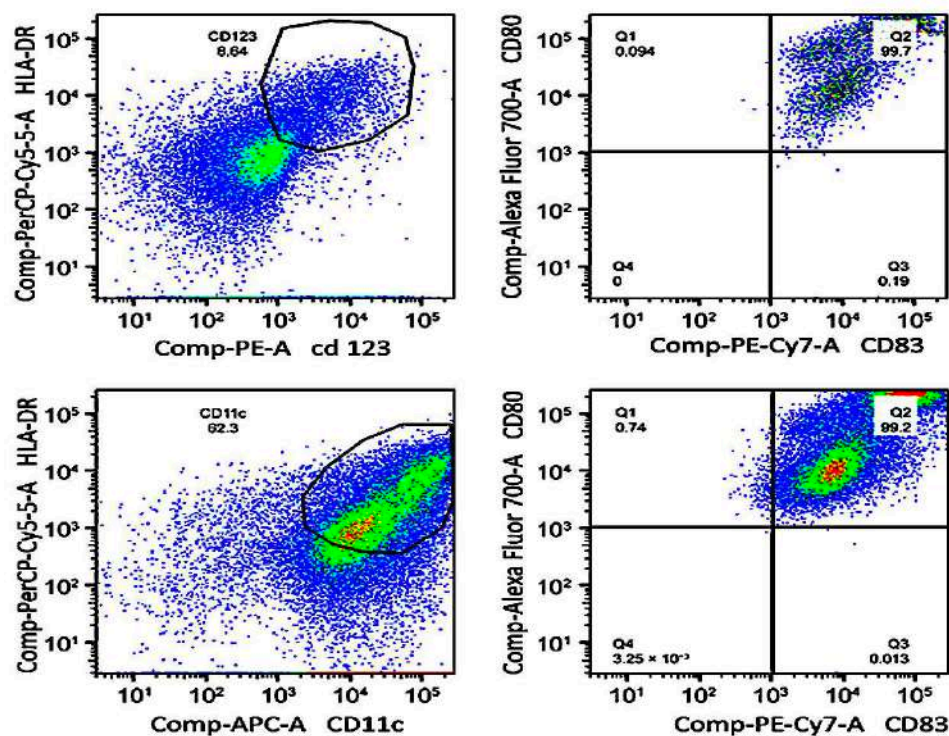


Figure 2. Flow cytometry-based monitoring of dendritic cell (DC) maturation. Dot plots show the phenotypic distribution of plasmacytoid (top row) and myeloid (bottom row) DC subpopulations after in vitro differentiation. Top left: CD123⁺/HLA-DR⁺ cells; top right: CD80⁺/CD83⁺ phenotype. Bottom left: CD11c⁺/HLA-DR⁺ cells; bottom right: CD80⁺/CD83⁺ phenotype. All markers were detected by fluorochrome-conjugated monoclonal antibodies.

One of the most critical parameters to control in this process is cell viability. Viability must be maintained above 90% to ensure that the DCs can fulfill their function of activating T lymphocytes and orchestrating a specific immune response against cancer. For this purpose, techniques such as flow cytometry and cell exclusion assays, such as the Trypan blue exclusion test, were used, which allow the proportion of viable cells to be measured to ensure that the culture maintains its integrity throughout the process [13,14]. The parameters that were evaluated and their expected values are presented in Table 1.

CD25 corresponds to the α -chain of the interleukin-2 (IL-2) receptor. Cytokine levels were quantified using the cytometric bead array (CBA), an open access flow cytometry-based platform. All values reflect expected ranges based on validated co-culture assays using pulsed DCs and autologous T cells.

Furthermore, at this initial stage, the quality control of the exosomes is essential because these extracellular vesicles play a crucial role in the amplification of the immune response. The exosomes' size and concentration are measured to ensure that they meet the parameters required to function as carriers of tumor antigens. Analytical techniques such as Nanosight have proven effective for this evaluation [15].

Table 1. Functional immune markers for assessing dendritic cell activation and viability.

Marker	Description	Evaluation Method	Expected Value
CD69	Early marker of T-cell activation	Flow cytometry	>70% activated lymphocytes
CD25	Late activation marker; α -chain of IL-2 receptor	Flow cytometry	>60% activated lymphocytes
HLA-DR	Maturation marker for dendritic cells	Flow cytometry	High expression (>80%)
IFN- γ	Key cytokine for Th1 polarization	Cytometric Bead Array (CBA)	100–150 pg/mL
IL-12	Cytokine for induction of Th1 immune profile	CBA	>80 pg/mL

2.1. Optimization and Characterization in the Molecular Laboratory

The monitoring and optimization of dendritic cell (DC) immunotherapy require a combination of clinical and molecular assessments. While basic monitoring focuses on evaluating the biological quality of DCs and exosomes, optimization at the molecular laboratory level is centered on refining technical variables to ensure the consistency, reproducibility, and effectiveness of the treatment in cancer patients. This includes the implementation of standardized workflows for cell separation, differentiation, vesicle isolation, and immune functionality testing, all designed to minimize batch-to-batch variability and enhance translational scalability.

2.1.1. Optimizing Progenitor Cell Isolation and DC Differentiation

Progenitor cell isolation is a critical initial phase that directly influences the differentiation and maturation potential of the resulting DCs. Peripheral blood mononuclear cells (PBMCs) are enriched via density-gradient centrifugation, a method that must be carefully optimized regarding the centrifugal force, gradient composition, and incubation time to preserve cellular integrity and prevent premature activation [16,17]. Higher viability rates not only improve the efficiency of subsequent DC culture steps but also provide a more immunocompetent starting material.

During the DC differentiation and maturation process, the expression of specific markers such as CD80, CD83, and HLA-DR is systematically evaluated using flow cytometry. These markers serve as critical checkpoints to confirm the phenotypic and functional maturation of DCs. Continuous assessment of these markers throughout the culture period enables early corrective actions, ensuring that the final DC population retains the ability to present antigens effectively and stimulate T-cell responses [18].

2.1.2. Structural and Functional Characterization of Exosomes

The characterization of dendritic cell-derived exosomes (DEXs) constitutes a fundamental component in ensuring the functional reliability of the immunotherapy product. Analytical techniques such as nanoparticle tracking analysis (NTA) and Western blotting are used to precisely measure the size distribution, concentration, and surface marker profile of exosomes [19,20]. Parameters such as particle uniformity, membrane integrity, and protein cargo fidelity are essential indicators of exosome quality.

Specifically, the evaluation of markers like CD63, CD81, and Alix confirms the exosomal origin and biogenesis consistency of the vesicles. Additionally, the absence of intracellular contamination is verified by negative controls such as calnexin expression. Together, these assessments guarantee that the exosomes maintain their capacity to function as efficient immunological vehicles capable of delivering bioactive signals within the tumor microenvironment. The full particle distribution and quantitative profile of DEXs are shown in Figure 3, which illustrates the uniformity and concentration range observed via nanoparticle tracking analysis. The results of these quality evaluations are summarized in Table 2.

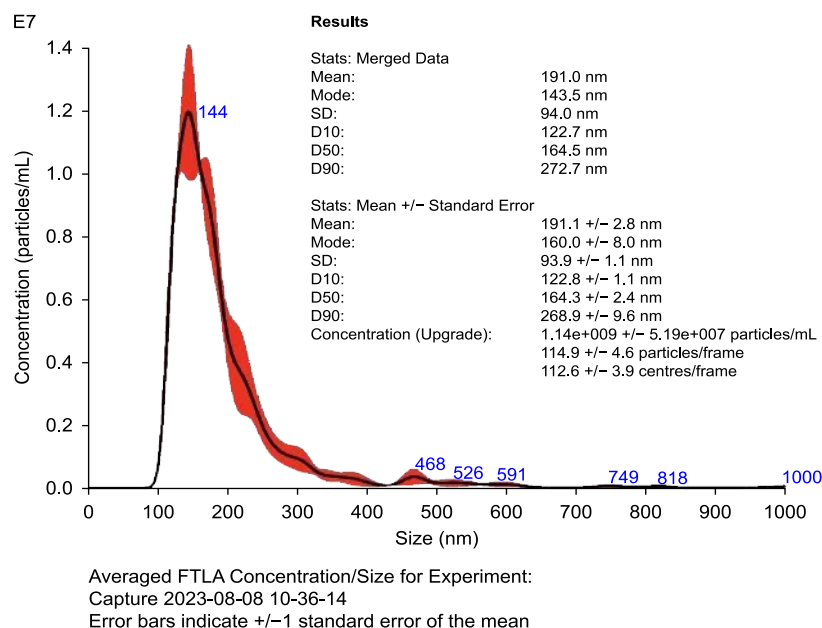


Figure 3. Nanoparticle tracking analysis (NTA) of dendritic cell-derived exosomes (DEXs). Histogram displays particle size distribution (100–150 nm) and concentration ($>10^9$ particles/mL). Results confirm exosome uniformity and abundance. Validation was performed via Western blotting using exosomal markers (CD63, CD81, and Alix) and the negative control calnexin, following MISEV 2018 guidelines. Table inset shows mean, mode, and concentration values obtained with Nanosight.

Table 2. Key features of dendritic cell-derived exosomes (DEXs) and the analytical methods used for their characterization.

Parameter	Description	Evaluation Method	Optimal Range
Size	Average diameter of exosomes	NTA	100–150 nm
Concentration	Number of exosomes per mL of sample	NTA	$>10^9$ particles/mL
CD63	Exosome-specific surface marker	Western blotting	Positive expression
CD81	Extracellular vesicle marker	Western blotting	Positive expression
Alix	Marker of exosome integrity and biogenesis	Western blotting	Positive expression
Calnexin	Negative control for exosomal purity	Western blotting	Not detected

The parameters listed in Table 2 are commonly used to assess the structural identity, concentration, and purity of dendritic cell-derived exosomes (DEXs). NTA is employed to determine particle size and concentration, while Western blotting is used to confirm the expression of exosomal and control markers. Calnexin serves as a negative control to verify the absence of contaminating intracellular material. All evaluations are based on standardized open access methodologies and aligned with current recommendations from MISEV guidelines.

2.1.3. Advanced Quality and Functionality Assessment

In addition to structural properties, it is crucial to assess the functional capacity of exosomes. This includes the induction of T-cell activation and the production of key cytokines such as IFN- γ , which is measured using the cytometric bead array (CBA) [21]. This functional assessment ensures that exosomes fulfill their role as amplifiers of the antitumor immune response.

To obtain high-purity progenitor cells, we specifically adjusted the cell separation protocol by fine-tuning parameters such as centrifugation speed, separation medium density, and incubation temperature. These adjustments were tailored and validated during

the course of our study to address specific challenges observed in our experimental setup, significantly increasing the viability of the isolated PBMCs and enhancing the efficiency of subsequent differentiation. While these modifications build upon established protocols, their integration into a cohesive workflow is a contribution unique to this work, ensuring reproducibility and adaptability for similar laboratory applications.

This manuscript does not report original experimental data (e.g., raw Western blot images, flow cytometry plots, or cytokine curves) because its objective is to propose a structured monitoring protocol—not to present clinical or *in vitro* results. All values shown in tables and figures reflect expected reference ranges derived from previously validated protocols and serve as structural placeholders within the conceptual framework presented here. The protocol integrates open access methods suitable for reproducible, license-free application, and is intended for future clinical and translational implementation.

2.1.4. Immune Monitoring Protocol

Immune monitoring in pulsed dendritic cell (DC) and exosome immunotherapy is crucial to fine-tune and optimize the immune system's response to treatment. This approach focuses on accurately measuring T-cell activation; characterizing the Th1, Th2, and Th17 immune profiles; and assessing apoptosis in tumor cells [22]. T-cell activation, specifically of the CD4+ and CD8+ subtypes, is considered a critical indicator, as these cells are responsible for orchestrating the antitumor response by destroying malignant cells.

Flow cytometry is a key tool used to assess the expression of activation markers such as CD69 and CD25. These markers provide a direct measure of the level of cellular activation among T cells [23]. The cytometric bead array (CBA) enables the analysis of the production of key cytokines, such as IFN- γ and IL-12, which are essential for an effective immune response. The robustness of T-cell activation is measured by the proportion of activated CD4+ and CD8+ cells, which is expected to be higher than 70% after co-culture with pulsed DCs [24].

The immunological characterization of dendritic cell cultures was performed using flow cytometry and cytometric bead array (CBA), enabling quantification of Th1-, Th2-, and Th17-related cytokines. As shown in Figure 4, the CBA data revealed a Th1-skewed cytokine profile, with predominant expression of IFN- γ , IL-6, and TNF- α , consistent with a cytotoxic immune orientation favorable for antitumor responses.

Furthermore, the analysis of Th1, Th2, and Th17 immune profiles is crucial to characterize the polarization of the immune response. A Th1 profile is ideal for a cytotoxic response against tumor cells, mediated by cytokines such as IFN- γ and IL-12. In contrast, an elevated Th2 profile, associated with cytokines such as IL-4 and IL-10, may have an immunosuppressive effect that compromises therapeutic efficacy [25]. Th17-related cytokines, such as IL-6 and IL-17A, must be carefully monitored to avoid excessive inflammation and immune-mediated toxicity. Flow cytometry and CBA are essential tools for this purpose, enabling dynamic and personalized modulation of the immune protocol [26].

Measuring apoptosis in tumor cells is another key aspect of immunomonitoring. Assays for LDH release, annexin V staining, and caspase activation can confirm the cytotoxic effects of T-cell responses. If suboptimal responses are observed, therapeutic adjustments in exosome dose, DC pulsing, or antigenic load may be warranted [27,28].

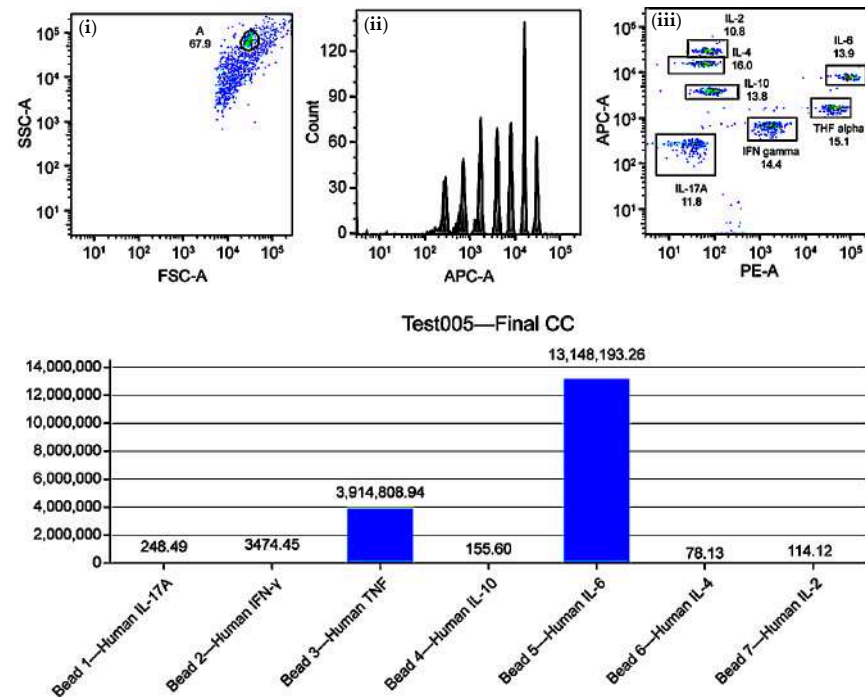


Figure 4. Immune profiling of Th1, Th2, and Th17 cytokines in mature dendritic cell (DC) cultures using cytometric bead array (CBA). Upper panels: (i) FSC-A vs. SSC-A dot plot for event gating, (ii) APC-A histogram showing fluorescence intensity, (iii) APC-A vs. PE dot plot for cytokine clustering. Lower panel: bar graph of normalized cytokine concentrations (pg/mL) for IL-17A, IFN- γ , TNF- α , IL-10, IL-6, IL-4, and IL-2. Results indicate a Th1-skewed profile with predominant IL-6 and TNF- α expression.

2.2. Complementary Clinical Follow-Up

It is crucial to monitor exosome immunotherapy to assess treatment effectiveness and make adjustments based on the patient's response. Such monitoring is mainly based on well-established clinical criteria, such as RECIST and iRECIST, which allow objective changes in tumor lesions to be measured [29]. While RECIST has been widely used to assess the response to conventional therapies, iRECIST has been specifically designed for immunotherapies, addressing unique phenomena such as pseudoprogression, where tumor lesions may temporarily enlarge before showing a reduction due to immune activation [30].

This type of clinical monitoring is complemented by advanced imaging techniques, such as PET-CT with ^{18}F -FDG, which provides a detailed analysis of the metabolic activity of the tumor. The uptake of this radiopharmaceutical by the tumor tissue is directly related to the aggressiveness and cellular metabolism of the cancer [31]. This technique is especially useful in the context of immunotherapy, as it can detect early changes in tumor activity, even before a significant reduction in the size of the lesion occurs, allowing a more accurate assessment of the treatment's efficacy.

Furthermore, the use of tumor biomarkers offers a molecular window into the patient's response to treatment. Biomarkers such as carcinoembryonic antigen (CEA), CA-125, and PSA allow indirect measurements of tumor burden and the assessment of disease progression or regression. However, in the context of immunotherapy, these biomarkers may also reflect immune activation. For example, a decrease in PSA levels in prostate cancer patients treated with immunotherapy could indicate a favorable response, while their increase could suggest resistance [32].

Together, clinical criteria, advanced imaging techniques, and tumor biomarkers provide a comprehensive framework that not only assesses the treatment response but also allows for anticipating relapses, adjusting dosages and administration schedules, and

identifying patients who would benefit from a change in therapeutic approach [33]. The integration of these elements allows for a dynamic and adaptive approach, maximizing the personalization and effectiveness of treatment in cancer patients.

3. Discussion

3.1. Impact of Laboratory Results on Treatment Personalization

Laboratory results obtained through molecular monitoring in immunotherapy with DCs and exosomes play a crucial role in the personalization of oncological treatment. The integration of data derived from T lymphocyte activation, cytokine production, and the evaluation of immunological profiles allows the treatment to be adjusted in real time, maximizing its effectiveness and minimizing the incidence of adverse effects. This personalized approach is especially relevant in the context of immunotherapy, where the response of each patient can differ considerably depending on their baseline immune status, tumor burden, and other individual factors [34].

3.1.1. T-Cell Activation and Treatment Adjustments

T-cell activation is a key marker used for assessing the efficacy of immunotherapy, measured through the expression of CD69 and CD25, together with the production of proinflammatory cytokines, such as IFN- γ and IL-2 [35]. These markers provide information on the magnitude of the adaptive immune response, which is essential for combating tumor cells. If T-cell activation levels are suboptimal, adjustments to the therapeutic protocol should be made, such as increasing the dose of pulsed DCs, modifying the antigenic load, or selecting more effective immunological adjuvants [36].

3.1.2. Th1, Th2, and Th17 Immune Profiles: Influence on Response

Th1, Th2, and Th17 immune profiles directly influence the effectiveness of the immune response [37]. A predominant Th1 profile, mediated by cytokines such as IFN- γ and IL-12, is ideal for a cytotoxic response directed against cancer. In cases where a predominance of Th2 or Th17 profiles is detected, which could be related to immunosuppressive or proinflammatory responses, respectively, physicians can adjust the treatment by administering Toll-like receptor (TLR) ligands or interleukin 12 (IL-12), favoring a Th1 response [38,39].

3.1.3. Evaluation of the Quality and Functionality of Exosomes

Exosomes are essential to amplify the immune response. The evaluation of parameters such as the concentration, size, and protein load of exosomes using techniques such as nanoparticle tracking analysis (NTA) and Western blotting ensures their functionality [40,41]. The presence of key exosomal markers, such as CD63 and CD81, is indicative of the quality of these extracellular vesicles [42]. The detection of low efficiency in the activation of T lymphocytes or in the production of cytokines can indicate deficiencies in the quality of exosomes, which would necessitate adjustments in their concentration or improvements in their purification [43].

3.1.4. Adjustments in Immunotherapy Administration

Depending on the molecular results and the patient's response, the frequency and dose of the immunotherapy can be adjusted. If T-cell activation levels are high, the frequency of administration could be reduced to avoid overstimulation of the immune system and associated adverse effects [44]. Conversely, if the response is insufficient, the frequency or dose of pulsed DCs or exosomes could be increased to enhance immune activation [45].

This dynamic and personalized approach ensures the constant optimization of immunotherapy, adapting to the patient's progress. The ability to modify the frequency and

dose based on patient-specific data differentiates this approach from conventional treatments, offering a considerable advantage in oncological treatment, especially in patients who have not responded to chemotherapy or who are resistant to therapy [44,45].

3.1.5. Clinical Translation: Interpretation Framework for Treating Oncologists

The complexity of immunological data can create significant barriers for oncologists unfamiliar with molecular diagnostics. To address this, we provide a translation framework that connects laboratory findings to clinical decision points. Table 3 summarizes expected values for key immune parameters, their clinical interpretation, and suggested therapeutic actions. This table is designed to be usable in real-time decision making for patient-specific immunotherapy adjustment.

Table 3. Clinical interpretation of immune monitoring biomarkers and corresponding therapeutic strategies.

Parameter	Expected Value	Clinical Meaning	Suggested Action
CD69 < 50%	Low T-cell activation	Suboptimal immune engagement	Increase DC dose or adjuvant
IFN- γ < 80 pg/mL	Weak Th1 response	Reduced cytotoxicity	Consider IL-12 co-stimulation
IL-10 > 200 pg/mL	Dominant Th2 suppression	Risk of immune escape	Adjust antigen load or regimen
IL-6 > 500 pg/mL	Inflammatory toxicity	Excessive immune activation	Delay next dose; modulate cytokines

Table 3 provides real-time clinical interpretation of core immunological parameters used in DEX-based monitoring, allowing oncologists to translate immune profiling into concrete therapeutic decisions.

Illustrative Clinical Scenarios

Note: These clinical examples are entirely illustrative. They are not derived from real patient data, nor do they imply any therapeutic use, trial, or outcome reported as part of this manuscript. Their sole purpose is to demonstrate potential interpretation pathways within the proposed framework.

Case A: A patient undergoing pulsed DC immunotherapy presents with CD69 at 35%, IFN- γ at 60 pg/mL, and IL-6 within normal limits. This profile indicates insufficient T-cell activation. The clinical team increases the DC pulsing dose and observes CD69 rising to 70% on day 14, confirming effective immune engagement.

Case B: Another patient shows IL-10 levels > 300 pg/mL with a depressed Th1 profile. The treating oncologist interprets this as Th2 dominance with immunosuppressive shift. The protocol is adjusted to reduce exosome frequency and introduce IL-12, resulting in restored Th1/Th2 balance.

3.2. Operational Requirements and Protocol Scalability

Pulsed dendritic cell-derived exosomes (DEXs) represent a promising strategy in immuno-oncology, offering high modularity, adaptability, and the ability to integrate across a variety of clinical contexts. These vesicle-based therapies can theoretically enhance immune system reprogramming without the risks associated with replicative vectors or genetic engineering platforms. However, the integration of DEX-based immunotherapy into broader applications is influenced by multiple scalability constraints, particularly those related to technical infrastructure, data management, product standardization, and inter-center reproducibility. Central to this challenge is the reliance on advanced molecular monitoring tools—such as flow cytometry, cytometric bead array systems (CBA), and PET-CT imaging—which are essential for evaluating immune responses and tumor dynamics across diverse patient cohorts [46,47].

Flow cytometry provides high-resolution profiling of immune activation markers, lymphocyte subset distributions, and cytokine expression patterns. PET-CT imaging, particularly when using ^{18}F -FDG tracers, enables early metabolic assessment of tumor microenvironmental changes, offering a sensitive biomarker for functional treatment responses [48]. Although these tools are critical for mechanistic validation and translational immunomonitoring, they require specialized instrumentation, standardized acquisition protocols, robust quality assurance programs, and highly trained personnel to ensure consistent data quality across centers—factors that may limit their routine adoption in decentralized or resource-constrained environments [49].

Addressing these limitations will require a strategic focus on system integration, automation, and inter-institutional coordination. Emerging models propose the use of distributed analytical hubs, artificial intelligence-assisted data processing pipelines, and adaptive protocol platforms that allow for the real-time calibration of immune monitoring strategies. The implementation of shared platforms for data acquisition and analysis, coupled with the incorporation of open access, machine learning-enabled workflows, could significantly improve reproducibility and monitoring throughput. Ultimately, the translational success of DEX-based protocols will depend not only on their biological efficacy but also on their operational scalability, flexibility, and standardization within diverse clinical ecosystems [50,51].

3.2.1. Resource Demands and Technical Requirements

The implementation of this protocol requires access to a carefully calibrated set of specialized analytical platforms, including flow cytometers equipped with multiparametric detectors, automated cytometric bead array (CBA) systems for cytokine profiling, and nanoparticle tracking analysis (NTA) devices for exosomal characterization [52]. These instruments are essential for maintaining the necessary levels of analytical sensitivity, specificity, and reproducibility in immunomonitoring workflows. Additionally, technical demands extend beyond instrumentation and include the need for structured sample handling pipelines, validated standard operating procedures (SOPs) for data acquisition, and reproducible frameworks for biomarker quantification and interpretation. All of these elements must rely on personnel with specialized training in immunophenotyping, vesicle biology, and translational data management [53].

To ensure reproducibility and data integrity across immune readouts, all flow cytometry and CBA assays performed under the STIP framework were subject to rigorous quality control standards. Antibody panels and cytokine bead kits were lot-matched and validated under ISO-equivalent QA protocols. Flow cytometers (e.g., BD FACSCanto II) were calibrated daily using CS&T beads and PMT alignment tools.

Biological assays were performed in triplicate, with independent technical replicates for each condition. Replicates were only accepted if the inter-well correlation exceeded $R^2 \geq 0.95$, and cytokine duplicates showed a coefficient of variation (CV%) below 15%. Cytokine quantification curves were accepted only if $R^2 \geq 0.98$. All outputs—CD69, CD25, IFN- γ , and IL-10—were archived in STIP dossiers with full traceability, including operator, lot number, and instrument batch. Each final classification (Type I/II/III) underwent an independent audit by a secondary analyst.

Rather than focusing solely on instrumentation or isolated technical endpoints, the strength of this monitoring protocol lies in its modularity, interoperability, and compatibility with non-commercial, license-free platforms [54]. This architecture enables reproducible assessments across laboratories with heterogeneous infrastructure levels, thus promoting widespread adoption. Importantly, the protocol allows key molecular immune parameters—such as T-cell activation, cytokine polarization, and apoptosis induction—to

be integrated into real-time clinical decision-making algorithms for immunotherapy adjustment, dose titration, and progression monitoring, thereby enhancing the precision and adaptability of patient-specific therapeutic strategies [55,56].

A comparative overview of the operational complexity, standardization needs, and functional contributions of key immunomonitoring techniques is provided in Table 4. The purpose is not to evaluate financial metrics but to contextualize the indispensable role of each analytical platform in building a robust and scalable molecular monitoring framework.

Table 4. Core analytical techniques used in DEX-based immunomonitoring.

Monitoring Technique	Operational Complexity	Functional Contribution
Flow cytometry	High	High-resolution quantification of immune activation markers (e.g., CD69, CD25, and HLA-DR)
PET-CT with 18F-FDG	Very high	Sensitive detection of early metabolic tumor responses and treatment-associated dynamics
Nanoparticle Tracking Analysis	Moderate	Characterization of exosome size distribution and concentration (standardized QC metric)

This table summarizes the key methodological components involved in immunomonitoring for DEX-based therapies. Flow cytometry enables precise immune profiling, PET-CT imaging supports the early detection of treatment responses through metabolic readouts, and NTA offers a standardized evaluation of the extracellular vesicle size and particle concentration. These tools are essential for molecular-level monitoring and translational reproducibility and have been selected for their compatibility with open access or widely implemented laboratory systems.

3.2.2. Scalability

Protocol scalability is another critical factor to consider. It largely depends on the automation of processes and the implementation of more accessible technologies that enable its adoption in different clinical contexts. These technologies not only simplify workflows but also ensure the consistency and reproducibility of monitoring results across diverse settings. The integration of artificial intelligence tools for data analysis, such as machine learning algorithms and predictive analytics, can further enhance scalability by streamlining data interpretation and enabling real-time adjustments to treatment protocols. This facilitates the adoption of these protocols in hospitals and clinics worldwide, optimizing resources and improving monitoring efficiency [57,58].

Furthermore, the ongoing training of physicians and laboratory technicians in the use of these advanced technologies is crucial to ensure accurate and efficient monitoring, regardless of patient volume. Such training should prioritize hands-on experience and simulations to familiarize staff with both hardware and software components. Developing standardized training programs that include periodic evaluations can help maintain high competency levels, particularly as new technologies emerge [59].

Another strategy to improve scalability is to foster collaboration between research institutions, treatment centers, and biotechnology companies. This collaboration could involve the creation of shared monitoring networks that pool resources and expertise, reducing the duplication of efforts and associated costs. Additionally, implementing standardized protocols across institutions would simplify regulatory compliance and facilitate data sharing for research purposes, accelerating advancements in personalized immunotherapy [60,61].

A detailed analysis comparing the estimated costs associated with automation and institutional collaboration can allow the cost–benefit ratios to be calculated as these protocols are expanded. For example, institutions that invest in shared infrastructure may

experience significant reductions in operational expenses over time, enabling them to allocate resources to patient care and further research [62].

Finally, the costs associated with the implementation of this comprehensive monitoring protocol are more than offset by the reduction in hospitalizations and decrease in serious adverse effects that it achieves. Personalized immunotherapy, when combined with efficient monitoring, minimizes treatment-related complications and optimizes outcomes, ultimately supporting broader access, standardized application, and improved outcome predictability across diverse healthcare environments [63].

3.3. Limitations and Future Directions

While this protocol is not designed to introduce new laboratory techniques, its contribution lies in its translational configuration and its accessibility for clinicians without molecular specialization. Despite significant advances in immunotherapy with DCs and exosomes, there are several limitations inherent to this therapeutic approach. These limitations are the result of the biological complexity of tumors and the variability in patient responses. Factors such as the total tumor burden, the patient's baseline immune status, the presence of comorbidities, and the specific genetic profile can significantly influence the effectiveness of the treatment [64,65].

3.3.1. Limitations in the Immune Response

Variability in immune responses poses a significant challenge, influenced by tumor microenvironment heterogeneity and immunosuppressive cell populations. Future strategies must focus on incorporating patient-specific biomarkers and real-time adaptive monitoring to overcome these limitations, which may be related to differences in the composition of the tumor microenvironment, the presence of immunosuppressive cells, and the intrinsic capacity of each individual's immune system. Furthermore, tumor cell heterogeneity can lead to immune system evasion, hindering the effectiveness of exosomes and DCs [66].

Although the structural and molecular quality control of exosomes—such as size, concentration, and marker expression—provides critical information about batch consistency, it does not directly translate into predictable therapeutic efficacy. This is due to the inherent variability of patient immune profiles, tumor microenvironments, and systemic tolerance thresholds. Even when exosome preparations meet optimal biophysical and biochemical specifications, the clinical outcome can vary significantly depending on individual immunological context. Therefore, any standardization protocol must be interpreted as a prerequisite for safety and reproducibility, but not as a surrogate marker for clinical performance.

To mitigate immunogenic drift across vesicle batches, our monitoring protocol incorporates both structural and functional batch fingerprinting. Structural validation is based on dynamic light scattering (DLS), Fourier-transform infrared spectroscopy (FTIR), and endotoxin quantification, ensuring vesicle uniformity and biochemical purity. In parallel, the STIP framework applies functional evaluation through *ex vivo* exposure to sentinel immune cell lines, quantifying Δ -confluence, cumulative cytotoxicity signals, and cytokine ratios—particularly IFN- γ /IL-10—to define immune behavior reproducibility [67,68]. Each batch is assigned a Functional Stratification Index (FSI), which enables inter-batch comparability and systematic documentation of immune modulation profiles. This approach has been applied in over 500 vesicle–cell interactions and has demonstrated low inter-batch variability and high phenotypic reproducibility (STIP system patented by OGRD Alliance, 2025; complementary manuscript submitted to a journal within the MDPI group). Collectively, these procedures enable early detection of immune divergence and provide a

scalable, regulatory-compliant framework for batch-level traceability in the development of non-pharmacodynamic immunotherapies [69].

3.3.2. Future Directions in Research

Addressing these limitations requires deeper exploration of the mechanisms governing immune responses in cancer patients, particularly those involving tumor microenvironment heterogeneity and immune evasion. Preclinical models and multi-phase clinical trials are essential to identify strategies that optimize T-cell activation and improve the efficacy of DC- and exosome-based therapies. Moreover, the integration of emerging technologies, such as single-cell sequencing and artificial intelligence-driven data analysis, holds significant promise for real-time therapeutic adjustments. Collaborative efforts among research institutions and healthcare providers will be critical in accelerating the implementation of these personalized approaches. The personalization of immunotherapy, considering genetic and molecular factors, will be crucial to improve effectiveness and reduce side effects [70].

Furthermore, the development of emerging technologies, such as gene editing and artificial intelligence, could offer new opportunities to optimize therapies and predict responses in real time. The implementation of advanced monitoring platforms will allow for the continuous adaptation of therapeutic strategies based on individual patient responses [71].

3.3.3. Interdisciplinary Collaborations

Fostering collaboration across disciplines, including molecular biology, oncology, and bioinformatics, will be essential to create a comprehensive approach to addressing the complexities of cancer treatment. Research networks and consortia can facilitate the sharing of data and resources, accelerating the development of new therapies and monitoring strategies [72].

In conclusion, immunotherapy with DCs and exosomes has shown significant potential in the treatment of cancer and will undoubtedly be of great benefit to continued research and in addressing current limitations. A multidisciplinary approach and the integration of new technologies may open up new avenues to increase the effectiveness of these treatments in the future.

These aspects, along with the system's limitations and forward-looking projections discussed in Section 3.3, highlight the importance of continued refinement and regulatory adaptation of this immunomonitoring framework [73].

4. Materials and Methods

To ensure adaptability to different immune and clinical contexts, the STIP system was validated *ex vivo* using standardized sentinel cell lines representing a wide range of tissue types and oncological phenotypes (e.g., A375, U87-MG, BEWO, and PANC-1). These models mimic variability in immune susceptibility, proliferative kinetics, and cytokine polarization without requiring patient contact. In more than 500 vesicle–cell combinations, STIP has demonstrated reproducibility, divergence consistency, and functional classification capacity (Type I/II/III), supporting its use in translational validation [74].

In addition, the platform includes an adaptive clinical integration model (STIP-RA) that enables the incorporation of patient-level observational data (e.g., functional recovery, imaging, and inflammatory panels) into the logic-tree classification system without requiring molecular profiling or biopsy. This extension enables phenotypic documentation in patients excluded from traditional clinical trials while preserving traceability, structural consistency, and regulatory compatibility [75].

A key contribution of this protocol is its ability to incorporate both traditional clinical scales, such as RECIST and iRECIST, and advanced molecular tools, including flow cytometry, cytometric bead array (CBA), and PET-CT imaging. This multidimensional evaluation framework not only deepens the understanding of immune activation and tumor response but also facilitates precise adjustments to treatment regimens. For instance, tracking critical immune parameters such as T-cell activation, cytokine profiles (Th1, Th2, and Th17), and tumor apoptosis markers enables the personalization of therapies to align with the patient's immune system dynamics. A Th1-dominant profile, characterized by cytokines like IFN- γ and IL-12, supports robust cytotoxic responses, while adjustments can be made for Th2 or Th17 profiles to mitigate immunosuppression or excessive inflammation [76,77].

Table 5 provides a structured overview of the immunomonitoring protocol, detailing operational checkpoints, timing, assays, and expected outputs across each phase of pulsed DEX immunotherapy.

Table 5. Stepwise validation protocol for pulsed DEX immunotherapy: checkpoints, assays, and clinical traceability.

No. Stage	Day	Sample	Exam	Purpose
1 Isolation of PBMCs	Day 1	Peripheral blood	Ficoll density gradient separation	Obtain viable PBMCs suitable for DC differentiation and immunomonitoring workflows
2 Cell viability and integrity	Day 1	Isolated PBMNCs	Trypan Blue or Annexin V assay	Confirm cell viability (>95%) and baseline functional status
3 DC differentiation	Day 7	PBMC culture	Flow cytometry: HLA-DR, CD123, CD11c	Verify phenotypic markers indicating effective differentiation into immature DCs
4 DC maturation	Day 10	Immature DCs	Flow cytometry: CD80, CD83, CD86	Confirm maturation capacity and readiness for lymphocyte co-culture
5 Exosome harvest and QC	Day 12	DC secretome	NTA for size/concentration	Validate exosome yield and structural uniformity (90–120 nm)
6 Immunopotency profiling	Day 12	DC secretome	CBA: Th1, Th2, Th17 cytokines	Evaluate cytokine patterns supporting immune polarization capacity
7 Lymphocyte activation	Day 14	DCs and/or exosomes co-cultured with T cells	Flow cytometry: CD69, CD25	Confirm T-cell activation and effector induction
8 Tumor apoptosis induction	Day 14	Activated T cells + tumor cell co-culture	LDH, caspase activity assays	Measure tumor cell apoptosis as endpoint of immune activation
9 Final product validation	Day 14	Enriched exosome concentrate	Safety, membrane integrity, surface marker validation	Ensure compliance with quality and biosafety standards prior to clinical use

These protocols enable the precise evaluation of crucial therapeutic parameters, including cell viability, T-cell activation, and the production of key cytokines such as IFN- γ and IL-12. Such detailed assessments are indispensable for confirming the efficacy of the therapy and tailoring it to the specific needs of individual patients, as demonstrated in Table 5 [78].

5. Conclusions

This work presents a structured, proof-of-concept protocol for integrating molecular and clinical monitoring tools in dendritic cell-derived exosome (DEX) immunotherapy. While it does not claim clinical validation, the protocol offers a reproducible and scalable framework for translational use. It enables real-time treatment adjustment based on immune phenotypes and serves as a methodological reference for future regulatory applications.

The monitoring strategy described here incorporates logic-driven classifications (Type I/II/III) based on kinetic divergence (ΔC , ΔT), cytokine polarization (e.g., IFN- γ /IL-10),

and apoptosis-associated biomarkers, producing standardized dossiers for immunotherapeutic documentation. Its design ensures traceability, compatibility with CTD Module 5.3, and adaptability to diverse clinical environments [79].

A key innovation of this protocol lies in its accessibility for non-molecular oncologists, allowing immune monitoring to be conducted without requiring advanced genomic or transcriptomic analysis. As precision oncology expands, the integration of multidimensional immune profiling into everyday practice is critical for tailoring therapy to the patient's dynamic immune response.

Table 6 summarizes the Th1/Th2/Th17 polarization profiles observed in DEX-based immunomonitoring. Understanding these trends is essential for clinical decision-making, especially in immunotherapy contexts where polarization imbalances can compromise treatment efficacy or trigger adverse events [80].

Table 6. Immune polarization profiles relevant to DEX-based immunotherapy.

Immune Profile	Key Cytokines	Impact on Therapy
Th1	IFN- γ , IL-12	Promotes robust cytotoxic response; enhances T-cell activation and tumor clearance
Th2	IL-4, IL-10	May suppress cytotoxic responses; potentially reduces therapeutic efficacy
Th17	IL-6, IL-17A	Associated with pro-inflammatory responses; requires modulation to minimize adverse effects

Beyond its immunological impact, this monitoring approach has profound economic implications. The long-term reduction in hospitalizations, adverse effects, and treatment inefficiencies offsets its implementation cost, which is expected to decrease further with technological advances in automation and AI-assisted analysis [76].

Widespread adoption will depend not only on molecular effectiveness but also on operational scalability, particularly in resource-limited settings. Technologies such as high-throughput cytometry, AI-driven analytics, and digital immuno-mapping tools can streamline workflows and enable decentralized immunomonitoring [78].

Ongoing training of medical teams and collaborative standardization across institutions will be essential to ensure uniform data quality, reproducibility, and protocol adherence [79]. Ultimately, this model supports the alignment of immune dynamics with therapeutic decisions, contributing to the real-world operationalization of personalized immunotherapy [80].

Author Contributions: Conceptualization, R.G.-S.; methodology, R.G.-S. and F.G.-C.; investigation, F.G.-C., L.A., J.I., N.M.-G., I.R. and A.S.; data curation, L.A., J.I., F.K. and C.P.-V.; formal analysis, R.G.-S. and F.G.-C.; resources, W.D., A.L., D.M., I.M. and R.A.; writing—original draft preparation, R.G.-S.; writing—review and editing, R.G.-S., F.G.-C. and C.P.-V.; visualization, J.I., L.A., A.T., R.G.-S. and C.P.-V.; evaluation of regulatory and technical attributes, R.G.-S. and C.P.-V.; supervision, R.G.-S.; project administration, R.G.-S.; funding acquisition, R.G.-S. All authors have read and agreed to the published version of the manuscript.

Funding: This research was supported by a project grant from Fundación Biotech (FB-202222-0871). The funding institution had no role in the design, execution, interpretation, or writing of the study.

Institutional Review Board Statement: Not applicable.

Informed Consent Statement: Not applicable.

Data Availability Statement: Raw kinetic data, secretomic profiles, classification parameters, and additional underlying datasets, are available from the corresponding author upon reasonable request. Access to these data may be subject to confidentiality agreements or material transfer conditions related to ongoing regulatory submissions. The full dataset is part of an active corporate editorial pipeline and is managed in accordance with contextual integrity and planned licensing frameworks.

Acknowledgments: The authors would like to thank the technical team at the Proteomics Core Facility for their support with sample processing and mass spectrometry runs. Special thanks are given to the Oncovix research unit for providing the infrastructure required for cell culture and vesicle processing.

Conflicts of Interest: Authors Ramon Gutierrez-Sandoval, Cristián Peña-Vargas, and Andres Toledo were employed by the company OGRD Alliance. Authors Francisco Gutierrez-Castro and Natalia Muñoz-Godoy were employed by the company Flowinmunocell-Bioexocell Group. The remaining authors declare that the research was conducted in the absence of any commercial or financial relationships that could be construed as a potential conflict of interest.

Abbreviations

APC-A	Allophycocyanin Area
CA-125	Cancer Antigen 125
CBA	Cytometric Bead Array
CD	Cluster of Differentiation
CD80, CD83, CD63, CD81	Cell Differentiation Markers
CTD	Common Technical Document
DC	Dendritic Cell
DEX	Dendritic Cell-Derived Exosome
ΔC	Change in Confluence (Kinetic Divergence Index)
ΔT	Divergence Time (Time to Immunological Shift)
FSC-A	Forward Scatter Area
FSI	Functional Stratification Index
GM-CSF	Granulocyte–Macrophage Colony-Stimulating Factor
HLA-DR	Human Leukocyte Antigen–DR Isotype
IFN- γ	Interferon Gamma
IL-1 β	Interleukin 1 Beta
IL-4	Interleukin 4
IL-12	Interleukin 12
iRECISTs	Immune Response Evaluation Criteria in Solid Tumors
LDH	Lactate Dehydrogenase
NTA	Nanoparticle Tracking Analysis
PBMC	Peripheral Blood Mononuclear Cell
PE	Phycoerythrin
PET-CT	Positron Emission Tomography–Computed Tomography
pg/mL	Picograms per Milliliter
PLPC	Phospholipoproteic Complex
PSA	Prostate-Specific Antigen
QC	Quality Control
RA	Real-world Adaptive
RECIST	Response Evaluation Criteria in Solid Tumors
SSC-A	Side Scatter Area
STIP	Structured Immunophenotypic Traceability Platform
Th1, Th2, Th17	T Helper Cell Subtypes
TLR	Toll-Like Receptor
TNF- α	Tumor Necrosis Factor Alpha

References

1. Zhang, H.; Wang, S.; Sun, M.; Cui, Y.; Xing, J.; Teng, L.; Xi, Z.; Yang, Z. Exosomes as smart drug delivery vehicles for cancer immunotherapy. *Front. Immunol.* **2023**, *13*, 1093607. [[CrossRef](#)] [[PubMed](#)]
2. Lee, K.W.; Yam, J.W.P.; Mao, X. Dendritic cell vaccines: A shift from conventional approach to new generations. *Cells* **2023**, *12*, 2147. [[CrossRef](#)] [[PubMed](#)]
3. Tojjari, A.; Saeed, A.; Singh, M.; Cavalcante, L.; Sahin, I.H.; Saeed, A. A comprehensive review on cancer vaccines and vaccine strategies in hepatocellular carcinoma. *Vaccines* **2023**, *11*, 1357. [[CrossRef](#)]
4. Gutierrez-Sandoval, R.; Rivadeneira, I.; Gutierrez-Castro, F.; Sobarzo, A.; Muñoz, I.; Lagos, A.; Muñoz, N.; Krakowiak, F.; Aguilera, R.; Toledo, A. Decoding NAMPT and TIGAR: A molecular blueprint for reprogramming tumor metabolism and immunity. *J. Clin. Oncol.* **2025**, *43* (Suppl. S16), e14537. [[CrossRef](#)]
5. Cai, Y.; Prochazkova, M.; Kim, Y.S.; Jiang, C.; Ma, J.; Moses, L.; Martin, K.; Pham, V.; Zhang, N.; Highfill, S.L.; et al. Assessment and comparison of viability assays for cellular products. *Cytotherapy* **2024**, *26*, 201–209. [[CrossRef](#)]
6. Mulkey, F.; Theoret, M.R.; Keegan, P.; Pazdur, R.; Sridhara, R. Comparison of iRECIST versus RECIST V.1.1 in patients treated with an anti-PD-1 or PD-L1 antibody: Pooled FDA analysis. *J. Immunother. Cancer* **2020**, *8*, e000146. [[CrossRef](#)]
7. Ren, L.; Zhang, D.; Pang, L.; Liu, S. Extracellular vesicles for cancer therapy: Potential, progress, and clinical challenges. *Front. Bioeng. Biotechnol.* **2024**, *12*, 1476737. [[CrossRef](#)]
8. Gu, Y.Z.; Zhao, X.; Song, X.R. Ex vivo pulsed dendritic cell vaccination against cancer. *Acta Pharmacol. Sin.* **2020**, *41*, 959–969. [[CrossRef](#)]
9. Liu, C.; Yang, M.; Zhang, D.; Chen, M.; Zhu, D. Clinical cancer immunotherapy: Current progress and prospects. *Front. Immunol.* **2022**, *13*, 961805. [[CrossRef](#)]
10. Connor, L.; Dean, J.; McNett, M.; Tydings, D.M.; Shrout, A.; Gorsuch, P.F.; Hole, A.; Moore, L.; Brown, R.; Melnyk, B.M.; et al. Evidence-based practice improves patient outcomes and healthcare system return on investment: Findings from a scoping review. *Worldviews Evid. Based Nurs.* **2023**, *20*, 6–15. [[CrossRef](#)]
11. Gutiérrez-Sandoval, R.; Gutiérrez-Castro, F.; Muñoz-Godoy, N.; Rivadeneira, I.; Sobarzo, A.; Iturra, J.; Krakowiak, F.; Alarcón, L.; Dorado, W.; Lagos, A.; et al. Beyond Exosomes: An Ultrapurified Phospholipoproteic Complex (PLPC) as a Scalable Immunomodulatory Platform for Reprogramming Immune Suppression in Metastatic Cancer. *Cancers* **2025**, *17*, 1658. [[CrossRef](#)] [[PubMed](#)]
12. Gutiérrez-Sandoval, R.; Gutiérrez-Castro, F.; Muñoz-Godoy, N.; Rivadeneira, I.; Sobarzo, A.; Alarcón, L.; Dorado, W.; Lagos, A.; Montenegro, D.; Muñoz, I.; et al. Phospholipid-Rich DC-Vesicles with Preserved Immune Fingerprints: A Stable and Scalable Platform for Precision Immunotherapy. *Biomedicines* **2025**, *13*, 1299. [[CrossRef](#)]
13. Masucci, M.; Karlsson, C.; Blomqvist, L.; Ernberg, I. Bridging the divide: A review on the implementation of personalized cancer medicine. *J. Pers. Med.* **2024**, *14*, 561. [[CrossRef](#)] [[PubMed](#)]
14. Singh, S.; Paul, D.; Nath, V. Exosomes: Current knowledge and future perspectives. *Tissue Barriers* **2024**, *12*, 2232248. [[CrossRef](#)] [[PubMed](#)]
15. Kern, S.; Skoog, I.; Ostling, S.; Kern, J.; Johansson, L.; Gudmundsson, P.; Waern, M.; Hultberg, B.; Rosengren, L.; Blennow, K.; et al. Cytokines for evaluation of chronic inflammatory status in ageing: A multiplex analysis of serum and cerebrospinal fluid. *Immun. Ageing* **2021**, *16*, 16.
16. Mucherino, S.; Lorenzoni, V.; Orlando, V.; Triulzi, I.; Del Re, M.; Capuano, A.; Danesi, R.; Turchetti, G.; Menditto, E. Cost-effectiveness of treatment optimisation with biomarkers for immunotherapy in solid tumours: A systematic review protocol. *BMJ Open* **2024**, *11*, e048141. [[CrossRef](#)]
17. Liu, R.; Zhao, Y.; Shi, F.; Zhu, J.; Wu, J.; Huang, M.; Qiu, K. Cost-effectiveness analysis of immune checkpoint inhibitors as first-line therapy in advanced biliary tract cancer. *Immunotherapy* **2024**, *16*, 669–678. [[CrossRef](#)]
18. Gutierrez-Sandoval, R.; Gutierrez-Castro, F.; Rivadeneira, I.; Krakowiak, F.; Iturra, J. Advances in the translational application of immunotherapy with pulsed dendritic cell-derived exosomes. *J. Clin. Biomed. Res.* **2024**, *6*, 1–8. [[CrossRef](#)]
19. Araujo-Abad, S.; Berna, J.M.; Lloret-Lopez, E.; López-Cortés, A.; Saceda, M.; de Juan Romero, C. Exosomes: From basic research to clinical diagnostic and therapeutic applications in cancer. *Cell Oncol.* **2025**, *48*, 269–293. [[CrossRef](#)]
20. Zhang, B.; Xiao, G.; Mao, Y.Q.; Lv, Z.; Huang, R.P. Cytometry multiplex bead antibody array. *Methods Mol. Biol.* **2021**, *2237*, 83–92.
21. Fu, P.; Yin, S.; Cheng, H.; Xu, W.; Jiang, J. Engineered exosomes for drug delivery in cancer therapy: A promising approach and application. *Curr. Drug Deliv.* **2024**, *21*, 817–827. [[CrossRef](#)] [[PubMed](#)]
22. Marciscano, A.E.; Anandasabapathy, N. The role of dendritic cells in cancer and anti-tumor immunity. *Semin. Immunol.* **2021**, *52*, 101481. [[CrossRef](#)] [[PubMed](#)]
23. Ganjalikhani Hakemi, M.; Yanikkaya Demirel, G.; Li, Y.; Jayakumar, N. The immunosuppressive tumor microenvironment and strategies to revert its immune regulatory milieu for cancer immunotherapy. *Front. Immunol.* **2023**, *14*, 1238698. [[CrossRef](#)] [[PubMed](#)]

24. Huangfu, S.; Pan, J. Novel biomarkers for predicting response to cancer immunotherapy. *Front. Immunol.* **2023**, *14*, 1179913. [[CrossRef](#)]
25. Karlsen, W.; Akily, L.; Mierzejewska, M.; Teodorczyk, J.; Bandura, A.; Zaucha, R.; Cytawa, W. Is 18F-FDG-PET/CT an optimal imaging modality for detecting immune-related adverse events after immune-checkpoint inhibitor therapy? Pros and cons. *Cancers* **2024**, *16*, 1990. [[CrossRef](#)]
26. Khan, F.; Lin, Y.; Ali, H.; Pang, L.; Dunterman, M.; Hsu, W.H.; Frenis, K.; Grant Rowe, R.; Wainwright, D.A.; McCortney, K.; et al. Lactate dehydrogenase A regulates tumor-macrophage symbiosis to promote glioblastoma progression. *Nat. Commun.* **2023**, *15*, 1987. [[CrossRef](#)]
27. Sidiropoulos, D.N.; Stein-O'Brien, G.L.; Danilova, L.; Gross, N.E.; Charmsaz, S.; Xavier, S.; Leatherman, J.; Wang, H.; Yarchoan, M.; Jaffee, E.M.; et al. Integrated T cell cytometry metrics for immune-monitoring applications in immunotherapy clinical trials. *JCI Insight* **2022**, *7*, e160398. [[CrossRef](#)]
28. Kankeu Fonkoua, L.A.; Sirpilla, O.; Sakemura, R.; Siegler, E.L.; Kenderian, S.S. CAR T cell therapy and the tumor microenvironment: Current challenges and opportunities. *Mol. Ther. Oncolytics* **2022**, *25*, 69–77. [[CrossRef](#)]
29. Safaei, S.; Fadaee, M.; Farzam, O.R.; Yari, A.; Poursaei, E.; Aslan, C.; Samemaleki, S.; Shانهbandi, D.; Baradaran, B.; Kazemi, T. Exploring the dynamic interplay between exosomes and the immune tumor microenvironment: Implications for breast cancer progression and therapeutic strategies. *Breast Cancer Res.* **2024**, *26*, 57. [[CrossRef](#)]
30. Louie, A.D.; Huntington, K.; Carlsen, L.; Zhou, L.; El-Deiry, W.S. Integrating molecular biomarker inputs into development and use of clinical cancer therapeutics. *Front. Pharmacol.* **2021**, *12*, 747194. [[CrossRef](#)]
31. Ayoub, M.; Eleneen, Y.; Colen, R.R. Cancer imaging in immunotherapy. *Adv. Exp. Med. Biol.* **2020**, *1244*, 309–324. [[PubMed](#)]
32. Bergholz, J.S.; Wang, Q.; Kabraji, S.; Zhao, J.J. Integrating immunotherapy and targeted therapy in cancer treatment: Mechanistic insights and clinical implications. *Clin. Cancer Res.* **2020**, *26*, 5557–5566. [[CrossRef](#)] [[PubMed](#)]
33. Abou-El-Enain, M.; Elsallab, M.; Feldman, S.A.; Fesnak, A.D.; Heslop, H.E.; Marks, P.; Till, B.G.; Bauer, G.; Savoldo, B. Scalable manufacturing of CAR T cells for cancer immunotherapy. *Blood Cancer Discov.* **2021**, *2*, 408–422. [[CrossRef](#)] [[PubMed](#)]
34. Chapman, N.M.; Boothby, M.R.; Chi, H. Metabolic coordination of T cell quiescence and activation. *Nat. Rev. Immunol.* **2020**, *20*, 55–70. [[CrossRef](#)] [[PubMed](#)]
35. Sarna, N.S.; Desai, S.H.; Kaufman, B.G.; Curry, N.M.; Hanna, A.M.; King, M.R. Enhanced and sustained T cell activation in response to fluid shear stress. *iScience* **2024**, *27*, 109999. [[CrossRef](#)]
36. Ding, Z.; Li, Q.; Zhang, R.; Xie, L.; Shu, Y.; Gao, S.; Wang, P.; Su, X.; Qin, Y.; Wang, Y.; et al. Personalized neoantigen pulsed dendritic cell vaccine for advanced lung cancer. *Signal Transduct. Target. Ther.* **2021**, *6*, 26. [[CrossRef](#)]
37. Dong, C. Cytokine regulation and function in T cells. *Annu. Rev. Immunol.* **2021**, *39*, 51–76. [[CrossRef](#)]
38. Xu, Z.; Zeng, S.; Gong, Z.; Chen, Y.; Zhang, W.; Liu, T.; Wang, X. Exosome-based immunotherapy: A promising approach for cancer treatment. *Mol. Cancer* **2020**, *19*, 160. [[CrossRef](#)]
39. Mishra, R.; Sharma, S.; Arora, N. TLR-5 ligand conjugated with Per a 10 and T cell peptides potentiates Treg/Th1 response through PI3K/mTOR axis. *Int. Immunopharmacol.* **2022**, *113*, 109389. [[CrossRef](#)]
40. Wu, J.; Shen, Z. Exosomal miRNAs as biomarkers for diagnostic and prognostic in lung cancer. *Cancer Med.* **2020**, *9*, 6909–6922. [[CrossRef](#)]
41. Saida, Y.; Watanabe, S.; Koyama, S.; Togashi, Y.; Kikuchi, T. Strategies to overcome tumor evasion and resistance to immunotherapies by targeting immune suppressor cells. *Front. Oncol.* **2023**, *13*, 1240926. [[CrossRef](#)] [[PubMed](#)]
42. Sheikhlary, S.; Lopez, D.H.; Moghimi, S.; Sun, B. Recent findings on therapeutic cancer vaccines: An updated review. *Biomolecules* **2024**, *14*, 503. [[CrossRef](#)]
43. Bano, A.; Vats, R.; Verma, D.; Yadav, P.; Kamboj, M.; Bhardwaj, R. Exploring salivary exosomes as early predictors of oral cancer in susceptible tobacco consumers: Noninvasive diagnostic and prognostic applications. *J. Cancer Res. Clin. Oncol.* **2023**, *149*, 15781–15793. [[CrossRef](#)] [[PubMed](#)]
44. Nikolic, T.; Suwandi, J.S.; Wesselius, J.; Laban, S.; Joosten, A.M.; Sonneveld, P.; Mul, D.; Aanstoot, H.J.; Kaddis, J.S.; Zwaginga, J.J.; et al. Tolerogenic dendritic cells pulsed with islet antigen induce long-term reduction in T-cell autoreactivity in type 1 diabetes patients. *Front. Immunol.* **2022**, *13*, 1054968. [[CrossRef](#)] [[PubMed](#)]
45. Bai, X.; Zhou, Y.; Yokota, Y.; Matsumoto, Y.; Zhai, B.; Maarouf, N.; Hayashi, H.; Carlson, R.; Zhang, S.; Sousa, A.; et al. Adaptive antitumor immune response stimulated by bio-nanoparticle based vaccine and checkpoint blockade. *J. Exp. Clin. Cancer Res.* **2022**, *41*, 132. [[CrossRef](#)]
46. Deng, M.; Wu, S.; Huang, P.; Liu, Y.; Li, C.; Zheng, J. Engineered exosomes-based theranostic strategy for tumor metastasis and recurrence. *Asian J. Pharm. Sci.* **2023**, *18*, 100870. [[CrossRef](#)]
47. Berz, A.M.; Dromain, C.; Vietti-Violi, N.; Boughdad, S.; Duran, R. Tumor response assessment on imaging following immunotherapy. *Front. Oncol.* **2022**, *12*, 982983. [[CrossRef](#)]
48. Shalaby, N.; Dubois, V.P.; Ronald, J. Molecular imaging of cellular immunotherapies in experimental and therapeutic settings. *Cancer Immunol. Immunother.* **2021**, *71*, 1281–1294. [[CrossRef](#)]

49. Reindl, M.; Schanda, K.; Woodhall, M.; Tea, F.; Ramanathan, S.; Sagen, J.; Fryer, J.P.; Mills, J.; Teegen, B.; Mindorf, S.; et al. International multicenter examination of MOG antibody assays. *Neurol. Neuroimmunol. Neuroinflamm.* **2020**, *7*, e674. [[CrossRef](#)]
50. Ratziu, V.; Hompesch, M.; Petitjean, M.; Serdjebi, C.; Iyer, J.S.; Parwani, A.V.; Tai, D.; Bugianesi, E.; Cusi, K.; Friedman, S.L.; et al. Artificial intelligence-assisted digital pathology for non-alcoholic steatohepatitis: Current status and future directions. *J. Hepatol.* **2024**, *80*, 335–351. [[CrossRef](#)]
51. Das, S.; Dey, M.K.; Devireddy, R.; Gartia, M.R. Biomarkers in cancer detection, diagnosis, and prognosis. *Sensors* **2023**, *24*, 37. [[CrossRef](#)] [[PubMed](#)]
52. Bhavsar, D.; Raguraman, R.; Kim, D.; Ren, X.; Munshi, A.; Moore, K.; Sikavitsas, V.; Ramesh, R. Exosomes in diagnostic and therapeutic applications of ovarian cancer. *J. Ovarian Res.* **2024**, *17*, 113. [[CrossRef](#)]
53. Pham, T.D.; Teh, M.T.; Chatzopoulou, D.; Holmes, S.; Coulthard, P. Artificial intelligence in head and neck cancer: Innovations, applications, and future directions. *Curr. Oncol.* **2024**, *31*, 5255–5290. [[CrossRef](#)]
54. Wandrey, M.; Jablonska, J.; Stauber, R.H.; Gül, D. Exosomes in cancer progression and therapy resistance: Molecular insights and therapeutic opportunities. *Life* **2023**, *13*, 2033. [[CrossRef](#)]
55. Yao, Y.; Fu, C.; Zhou, L.; Mi, Q.S.; Jiang, A. DC-derived exosomes for cancer immunotherapy. *Cancers* **2021**, *13*, 3667. [[CrossRef](#)] [[PubMed](#)]
56. Zhang, C.; Lin, Q.; Li, C.; Qiu, Y.; Chen, J.; Zhu, X. Comprehensive analysis of the prognostic implication and immune infiltration of C1SD2 in diffuse large B-cell lymphoma. *Front. Immunol.* **2023**, *14*, 1277695. [[CrossRef](#)]
57. Mu, W.; Jiang, L.; Shi, Y.; Tunali, I.; Gray, J.E.; Katsoulakis, E.; Tian, J.; Gillies, R.J.; Schabath, M.B. Non-invasive measurement of PD-L1 status and prediction of immunotherapy response using deep learning of PET/CT images. *J. Immunother. Cancer* **2021**, *9*, e002118. [[CrossRef](#)] [[PubMed](#)]
58. Baughman, D.J.; Botros, P.A.; Waheed, A. Technology in medicine: Improving clinical documentation. *FP Essent.* **2024**, *537*, 26–38.
59. Corbetta, L.; Arru, L.B.; Mereu, C.; Pasini, V.; Patelli, M. Competence and training in interventional pulmonology. *Panminerva Med.* **2019**, *61*, 203–231.
60. Cossarizza, A.; Chang, H.D.; Radbruch, A.; Acs, A.; Adam, D.; Adam-Klages, S.; Agace, W.W.; Aghaepour, N.; Akdis, M.; Allez, M.; et al. Guidelines for the use of flow cytometry and cell sorting in immunological studies (second edition). *Eur. J. Immunol.* **2019**, *49*, 1457–1973.
61. Pathania, A.S.; Prathipati, P.; Challagundla, K.B. New insights into exosome mediated tumor-immune escape: Clinical perspectives and therapeutic strategies. *Biochim. Biophys. Acta Rev. Cancer* **2021**, *1876*, 188624. [[CrossRef](#)] [[PubMed](#)]
62. Vu, S.H.; Vetrivel, P.; Kim, J.; Lee, M.S. Cancer resistance to immunotherapy: Molecular mechanisms and tackling strategies. *Int. J. Mol. Sci.* **2022**, *23*, 10906. [[CrossRef](#)] [[PubMed](#)]
63. Zanutta, S.; Galati, D.; De Filippi, R.; Pinto, A. Enhancing dendritic cell cancer vaccination: The synergy of immune checkpoint inhibitors in combined therapies. *Int. J. Mol. Sci.* **2024**, *25*, 7509. [[CrossRef](#)] [[PubMed](#)]
64. Ghaffari Laleh, N.; Ligerio, M.; Perez-Lopez, R.; Kather, J.N. Facts and hopes on the use of artificial intelligence for predictive immunotherapy biomarkers in cancer. *Clin. Cancer Res.* **2023**, *29*, 316–323. [[CrossRef](#)]
65. Lai, J.J.; Chau, Z.L.; Chen, S.Y.; Hill, J.J.; Korpany, K.V.; Liang, N.W.; Lin, L.H.; Liu, J.K. Exosome processing and characterization approaches for research and technology development. *Adv. Sci.* **2022**, *9*, e2103222. [[CrossRef](#)]
66. Bhinder, B.; Gilvary, C.; Madhukar, N.S.; Elemento, O. Artificial intelligence in cancer research and precision medicine. *Cancer Discov.* **2021**, *11*, 900–915. [[CrossRef](#)]
67. Walcher, L.; Kistenmacher, A.K.; Suo, H.; Kitte, R.; Dluczek, S.; Strauß, A.; Blaudszun, A.R.; Yevsa, T.; Fricke, S.; Kossatz-Boehlert, U. Cancer stem cells—Origins and biomarkers: Perspectives for targeted personalized therapies. *Front. Immunol.* **2020**, *11*, 1280. [[CrossRef](#)]
68. Zhou, Z.; Wang, J.; Wang, J.; Yang, S.; Wang, R.; Zhang, G.; Li, Z.; Shi, R.; Wang, Z.; Lu, Q. Deciphering the tumor immune microenvironment from a multidimensional omics perspective: Insight into next-generation CAR-T cell immunotherapy and beyond. *Mol. Cancer* **2024**, *23*, 131. [[CrossRef](#)]
69. Song, M.S.; Nam, J.H.; Noh, K.E.; Lim, D.S. Dendritic cell-based immunotherapy: The importance of dendritic cell migration. *J. Immunol. Res.* **2024**, *2024*, 7827246. [[CrossRef](#)]
70. Jendle, J.; Reznik, Y. Use of insulin pumps and closed-loop systems among people living with diabetes: A narrative review of clinical and cost-effectiveness to enable access to technology and meet the needs of payers. *Diabetes Obes. Metab.* **2023**, *25* (Suppl. S2), 21–32. [[CrossRef](#)]
71. Makler, A.; Asghar, W. Exosomal biomarkers for cancer diagnosis and patient monitoring. *Expert Rev. Mol. Diagn.* **2020**, *20*, 387–400. [[CrossRef](#)] [[PubMed](#)]
72. Chow, A.; Perica, K.; Klebanoff, C.A.; Wolchok, J.D. Clinical implications of T cell exhaustion for cancer immunotherapy. *Nat. Rev. Clin. Oncol.* **2022**, *19*, 775–790. [[CrossRef](#)]
73. Liu, Q.; Li, S.; Dupuy, A.; Mai, H.L.; Sailliet, N.; Logé, C.; Robert, J.H.; Brouard, S. Exosomes as new biomarkers and drug delivery tools for the prevention and treatment of various diseases. *Int. J. Mol. Sci.* **2021**, *22*, 7763. [[CrossRef](#)]

74. Hato, L.; Vizcay, A.; Eguren, I.; Pérez-Gracia, J.L.; Rodríguez, J.; Gállego Pérez-Larraya, J.; Sarobe, P.; Inogés, S.; Díaz de Cerio, A.L.; Santisteban, M. Dendritic cells in cancer immunology and immunotherapy. *Cancers* **2024**, *16*, 981. [[CrossRef](#)]
75. Sajan, A.; Lamane, A.; Baig, A.; Floch, K.L.; Dercle, L. The emerging role of AI in enhancing intratumoral immunotherapy care. *Oncotarget* **2024**, *15*, 635–637. [[CrossRef](#)] [[PubMed](#)]
76. Wang, Z.; Wang, Q.; Qin, F.; Chen, J. Exosomes: A promising avenue for cancer diagnosis beyond treatment. *Front. Cell Dev. Biol.* **2024**, *12*, 1344705. [[CrossRef](#)] [[PubMed](#)]
77. Zhao, N.; Yi, Y.; Cao, W.; Fu, X.; Mei, N.; Li, C. Serum cytokine levels for predicting immune-related adverse events and the clinical response in lung cancer treated with immunotherapy. *Front. Oncol.* **2022**, *12*, 923531. [[CrossRef](#)]
78. Kamigaki, T.; Takimoto, R.; Okada, S.; Ibe, H.; Oguma, E.; Goto, S. Personalized dendritic-cell-based vaccines targeting cancer neoantigens. *Anticancer Res.* **2024**, *44*, 3713–3724. [[CrossRef](#)]
79. Wolf, D.M.; Yau, C.; Wulfkuhle, J.; Brown-Swigart, L.; Gallagher, R.I.; Lee, P.R.E.; Zhu, Z.; Magbanua, M.J.; Sayaman, R.; O’Grady, N.; et al. Redefining breast cancer subtypes to guide treatment prioritization and maximize response: Predictive biomarkers across 10 cancer therapies. *Cancer Cell* **2022**, *40*, 609–623.e6. [[CrossRef](#)]
80. Luo, S.; Chen, J.; Xu, F.; Chen, H.; Li, Y.; Li, W. Dendritic cell-derived exosomes in cancer immunotherapy. *Pharmaceutics* **2023**, *15*, 2070. [[CrossRef](#)]

Disclaimer/Publisher’s Note: The statements, opinions and data contained in all publications are solely those of the individual author(s) and contributor(s) and not of MDPI and/or the editor(s). MDPI and/or the editor(s) disclaim responsibility for any injury to people or property resulting from any ideas, methods, instructions or products referred to in the content.



biology



Article

Real-Time Functional Stratification of Tumor Cell Lines Using a Non-Cytotoxic Phospholipoproteomic Platform: A Label-Free Ex Vivo Model

Ramón Gutiérrez-Sandoval, Francisco Gutiérrez-Castro, Natalia Muñoz-Godoy, Ider Rivadeneira, Adolay Sobarzo, Jordan Iturra, Ignacio Muñoz, Cristián Peña-Vargas, Matías Vidal and Francisco Krakowiak



<https://doi.org/10.3390/biology14080953>

Article

Real-Time Functional Stratification of Tumor Cell Lines Using a Non-Cytotoxic Phospholipoproteomic Platform: A Label-Free Ex Vivo Model

Ramón Gutiérrez-Sandoval ^{1,*},[†] , Francisco Gutiérrez-Castro ^{2,†}, Natalia Muñoz-Godoy ², Ider Rivadeneira ³, Adolay Sobarzo ⁴, Jordan Iturra ³, Ignacio Muñoz ³, Cristián Peña-Vargas ¹, Matías Vidal ¹ and Francisco Krakowiak ⁵

¹ Department of Oncopathology, OGRD Alliance, Lewes, DE 19958, USA; consultorusa@biogenica.org (C.P.-V.); mvidaldominguez.1992@gmail.com (M.V.)

² Cancer Research Department, Flowinmunocell-Bioexocell Group, 08028 Barcelona, Spain; servicios@flowinmunocell.cl (F.G.-C.); contacto@flowinmunocell.cl (N.M.-G.)

³ Outreach and Engagement Programs Department for the OGRD Consortium, Charlestown KN0802, Saint Kitts and Nevis; iderlautaro@gmail.com (I.R.); jiconsultant@ogrdconsorcio.com (J.I.); kinesiologo@recell.cl (I.M.)

⁴ Departamento de Ciencias Biológicas y Químicas, Facultad de Ciencias, Universidad San Sebastián, Lientur 1457, Concepción 4080871, Chile; adolay.sobarzo@uss.cl

⁵ Department of Molecular Oncopathology, Bioclas, Concepción 4030000, Chile; fkconsultant@ogrdconsorcio.com

* Correspondence: cso@ogrdalliance.org

[†] These authors contributed equally to this work.

Simple Summary

Functional profiling of a tumor's response to non-toxic phospholipoproteomic platforms is a growing field in oncology. Unlike traditional drug models, which rely on killing cells or tracking receptor inhibition, this study presents a real-time, label-free system to classify tumor phenotypes based on their kinetic and secretomic behavior. By avoiding cytotoxic endpoints or genetic manipulation, we captured functional compatibility between human tumors and structurally active phospholipoproteomic formulations. This platform supports the standardized classification of tumor responses into stimulatory, inhibitory, or neutral profiles, providing a reproducible and non-invasive tool for selecting candidates in preclinical cancer immunotherapy programs.



Academic Editor: Erxi Wu

Received: 13 June 2025

Revised: 22 July 2025

Accepted: 27 July 2025

Published: 28 July 2025

Citation: Gutiérrez-Sandoval, R.; Gutiérrez-Castro, F.; Muñoz-Godoy, N.; Rivadeneira, I.; Sobarzo, A.; Iturra, J.; Muñoz, I.; Peña-Vargas, C.; Vidal, M.; Krakowiak, F. Real-Time Functional Stratification of Tumor Cell Lines Using a Non-Cytotoxic Phospholipoproteomic Platform: A Label-Free Ex Vivo Model. *Biology* **2025**, *14*, 953. <https://doi.org/10.3390/biology14080953>

Copyright: © 2025 by the authors. Licensee MDPI, Basel, Switzerland. This article is an open access article distributed under the terms and conditions of the Creative Commons Attribution (CC BY) license (<https://creativecommons.org/licenses/by/4.0/>).

Abstract

The development of scalable, non-invasive tools to assess tumor responsiveness to structurally active immunofunctional formulations remains a critical unmet need in solid tumor immunotherapy. Here, we introduce a real-time, ex vivo functional system to classify tumor cell lines exposed to a phospholipoproteomic platform, without relying on cytotoxicity, co-culture systems, or molecular profiling. Tumor cells were monitored using IncuCyte[®] S3 (Sartorius) real-time imaging under ex vivo neutral conditions. No dendritic cell components or immune co-cultures were used in this mode. All results are derived from direct tumor cell responses to structurally active formulations. Using eight human tumor lines, we captured proliferative behavior, cell death rates, and secretomic profiles to assign each case into stimulatory, inhibitory, or neutral categories. A structured decision-tree logic supported the classification, and a Functional Stratification Index (FSI) was computed to quantify the response magnitude. Inhibitory lines showed early divergence and high IFN- γ /IL-10 ratios; stimulatory ones exhibited a proliferative gain under balanced immune signaling. The results were reproducible across independent batches. This system enables quantitative phenotypic screening under standardized, marker-free conditions and offers

an adaptable platform for functional evaluation in immuno-oncology pipelines where traditional cytotoxic endpoints are insufficient. This approach has been codified into the STIP (Structured Traceability and Immunophenotypic Platform), supporting reproducible documentation across tumor models. This platform contributes to upstream validation logic in immuno-oncology workflows and supports early-stage regulatory documentation.

Keywords: phospholipoproteomic platform; functional tumor stratification; ex vivo immunoprofiling; non-cytotoxic kinetic modeling; immunophenotypic classification; IFN- γ /IL-10 ratio; structural immunomodulation; STIP traceability system; batch-level documentation; early-stage regulatory validation

1. Introduction

1.1. Limitations of Conventional Preclinical Models

Traditional preclinical models used in immuno-oncology—such as IC₅₀ assays, tumor regression in mice, or lympho-tumor co-cultures—have structural limitations when evaluating non-pharmacodynamic platforms such as dendritic phospholipoproteomic immunof ormulation. These systems typically rely on toxicity or enzyme inhibition measures, which are methodologically inapplicable to products that do not induce cell lethality or interact with defined molecular targets. Furthermore, murine models implanted into immunodeficient animals lack human immunological features, limiting the extrapolation of immune-structural effects induced by phospholipoproteomic formulations.

Added to this is the impossibility of modeling fine-grained topological interactions, such as phospholipoproteomic immunof ormulation-tumor structural recognition, which does not respond to pharmacokinetic principles or dose–response curves. Faced with this experimental dilemma, there is a growing need to incorporate systems that can capture real functional responses—such as alterations in proliferative rhythm—without relying on cell destruction or direct immune activation. This need has driven the search for structured kinetic models capable of reflecting phenotypic changes induced by complex immunogenic stimuli under neutral, reproducible, and quantifiable technical conditions [1,2].

In this study, the term phospholipoproteomic platform does not refer to classical vesicles, but rather to an ultrapure, structurally active formulation composed of non-vesicular phospholipid–protein fractions that are organized into a stable proteolipidic architecture. These platforms exhibit reproducible immunostructural properties and are devoid of genetic coding elements or replicative potential. Their action is functional, not cytotoxic, and is interpreted as a phenotypic interface between bioactive structures and tumor cells under neutral ex vivo conditions.

1.2. Functional Justification for Real-Time Kinetic Monitoring

The use of automated kinetic capture systems, such as IncuCyte[®], overcomes many of the technical barriers associated with terminal viability models. Through continuous, real-time monitoring of cell confluence, it is possible to record dynamic events that reflect genuine functional alterations without the need for dyes, fixation, fluorogenic markers, or destructive intervention [3]. This is particularly relevant for immunoactive phospholipoproteomic immunof ormulation, whose action is structural, non-cytotoxic, and not mediated by conventional pharmacological mechanisms.

The neutral readout offered by IncuCyte[®] represents a critical advantage: it allows quantification not only of whether a change in cell proliferation takes place, but also when it occurs, how long it is sustained, and at what magnitude relative to the control. This type of

information is essential for interpreting functional responses that do not result in cell death but demonstrate significant phenotypic reprogramming. Furthermore, by eliminating all manual manipulation during the observation period, the system ensures high technical reproducibility with minimal operational interference.

In this context, kinetic monitoring is established as an ideal tool for assessing gallbladder-tumor functional compatibility under controlled conditions, serving as a robust primary readout for functional classifiers without resorting to destructive assays or artificial experimental conditions [3].

1.3. Emerging Role of Phospholipoproteomic Immunof ormulation in Structural Immunoreprogramming

Ultrapurified phospholipoproteomic platforms have emerged as next-generation immunobiological tools due to their ability to induce phenotypic reprogramming in tumor cells without requiring conventional pharmacological signaling or triggering direct cytotoxic effects. Unlike conventional tumor exosomes or epithelial microplatforms loaded with genomic material, these formulations are enriched with immunoactive molecular patterns—such as MHC I/II, tetraspanins (CD9, CD81), ICAM-1, and structural cytokines—that enable complex functional interactions with target cells, reorganizing their behavior without causing cell lysis or death [4,5].

This unique feature makes phospholipoprotein fractions ideal candidates for structural immunomodulation platforms, where the objective is not to destroy the target tissue, but rather to modify its basal phenotypic dynamics in a controlled manner. However, cellular interpretation of these vesicular stimuli is not uniform: different tumor lines respond divergently to structurally similar formulations, suggesting the existence of a functional axis of immunophenotypic compatibility that has not yet been fully characterized [4].

This compatibility cannot be assessed solely through toxicity or single biomarkers; it requires *ex vivo* functional models that are capable of reproducibly quantifying the impact of these stimuli on cell proliferative kinetics. In this context, continuous real-time readout using platforms, such as IncuCyte[®], (Essen BioScience Inc., Ann Arbor, MI, USA; Essen BioScience Inc., Ann Arbor, MI, USA; software version 2019B) applied to structurally validated phospholipoproteomic formulations, allows the degree of tumor–platform functional compatibility to be accurately captured without the need for systemic immunological intervention or immediate clinical validation.

1.4. Basis of Platform–Tumor Functional Classification

The central hypothesis underlying the model proposed here is that the interaction between an immunoactive phospholipoprotein vesicular fraction and a human tumor cell line generates differential, quantifiable, and classifiable proliferative behavior under neutral experimental conditions. This interaction is not based on specific molecular affinities or classical pharmacodynamic mechanisms, but rather on the structural compatibility between the immunoactive vesicular content and the basal phenotype of the target cell [5].

Based on the analysis of divergent growth kinetic trajectories, it is possible to establish a robust and reproducible functional classification: (i) stimulated lines, which increase their proliferation steadily after vesicular exposure; (ii) inhibitory lines, which show a progressive reduction in their replication rate without signs of cell death; and (iii) inert lines, whose dynamics do not change significantly in response to the stimulus. This typology has technical and operational value in both research and regulatory settings: it allows objective discrimination between sensitive, resistant, or indifferent models, without the need to know the genetic or transcriptomic profile of each line. Furthermore, real-time quantification allows the system to capture not only the final effect but also the stability, duration, and reproducibility of the response. This structure offers an objective functional tool, which

is useful for technical decisions in early validation, immunophenotypic classification, indicator line selection, and defensible functional documentation in the absence of direct clinical evidence [6,7].

1.5. Emerging Regulatory Logic: Early Validation and Documentation Platforms

In parallel with scientific progress, various national and international regulatory authorities have begun to incorporate unconventional functional validation schemes, especially in the case of non-cellular, non-pharmacodynamic, and structurally immunomodulatory products, such as phospholipoproteomic formulations like PLPC-DB. PLPC-DB refers to an ultrapure, lyophilized phospholipoproteomic formulation derived from the secretome of human dendritic cells that were previously pulsed with a defined neoantigen algorithm, exhibiting immunomodulatory properties without genetic or pharmacodynamic content.

In these regulatory environments, it is recognized that it may be acceptable to present non-clinical technical evidence as long as it is reproducible, quantifiable, and consistent with the proposed mechanism of action, even in the absence of direct clinical validation. This shift has enabled the development of documentation platforms aimed at supporting early structural phenotypic compatibility by using functional technical tools that do not depend on cell destruction or conventional pharmacodynamic assays [8,9].

Within this framework, *ex vivo* kinetic models acquire potential regulatory value by allowing the identification of tumor-gallbladder functional trajectories under controlled conditions and without destructive markers or active immunological intervention. This type of evidence is also compatible with regulatory pathways that allow for delayed activation, technical documentary use, or exclusion from classification as a new pharmacological entity, provided that technical traceability, safety, and defensible functional logic are demonstrated. Therefore, the model proposed here not only responds to an experimental need but also offers a concrete opportunity to inform modular technical dossiers (such as the CTD) in contexts where immediate clinical efficacy is not required but rather structured technical consistency is [10].

1.6. Objective of the Study and Operational Experimental Framework

The present study aimed to establish and validate a technical functional model that allows the reproducible classification of the proliferative response of human tumor lines exposed to immunoactive phospholipoproteomic formulations under neutral, marker-free *ex vivo* conditions. The operational hypothesis holds that cell growth kinetics reflects the structural interpretation of the immunoactive stimulus, and that this response can be organized into a functional typology with technical value. To this end, a cohort of eight tumor cells with diverse histological profiles was used, exposed to phospholipoproteomic formulations prepared under controlled conditions, and quantified by protein concentration. Proliferation curves were captured in real time for 48 h using the IncuCyte® platform, complemented by cell death analysis and multiplex secretomic profiling [11].

Based on this information, the cells were classified according to their functional compatibility, and a structured response matrix was constructed that is useful for experimental selection, comparative functional validation, and non-cytotoxic phenotypic prioritization. This study does not aim to predict clinical efficacy, but rather to establish an objective tool for functional discrimination based on a kinetic readout, with application in decentralized experimental settings or as an operational filter for initial phenotypic compatibility [12]. The logic supporting this classification system, including the integration of kinetic divergence and secretomic signals, is conceptually developed in detail throughout the results (Figures 1–13), and conceptually summarized in Figure 13.

2. Materials and Methods

2.1. Cell Lines and Phenotypic Selection Criteria

Eight human tumor cell lines representing distinct histological lineages and immunophenotypic profiles were selected to maximize the functional diversity of the model and evaluate structural compatibility with immunogenic phospholipoproteomic formulations. The lines included were as follows: A375 (cutaneous melanoma), BEWO (placental chorionic carcinoma), U87 (glioblastoma multiforme), LUDLU (lung squamous cell carcinoma), PANC-1 (pancreatic ductal adenocarcinoma), MCF-7 (luminal A mammary adenocarcinoma), HEPG2 (hepatocellular carcinoma), and LNCAP-C42 (androgen-dependent prostatic adenocarcinoma) [13]. All cells were acquired from certified cell banks (ATCC and DSMZ), authenticated by short repeat (STR) sequence typing, and validated as free of mycoplasma contamination by PCR before culture [14]. Selection was not based on clinical profiles, but rather on the expected functional heterogeneity in response to vesicular stimuli. This approach sought to include both models with high proliferative plasticity and inert or tolerant lines, which allowed for the development of a robust system to discriminate functional responses that were dependent on platform–tumor structural compatibility. All lines were maintained under standardized conditions to avoid environmental bias during the kinetic assays [15], and all tumor cell lines used were adherent and maintained in monolayer culture systems. All cell-based experiments were conducted under an outsourced framework using certified tumor lines maintained by the Externalized laboratory. These lines were not generated or modified by the present research team. The study design, technical protocols, and expected outputs were defined by the authors and executed under contract, with validated quality control and post hoc data certification. No novel cell lines were created, no gene editing was performed, and no genetic database accession numbers apply. This operational model has been previously accepted and ethically validated in similar publications under MDPI [16].

All cell-based experiments were conducted under an outsourced framework using certified tumor lines maintained by the FlowInmunocel laboratory (listed among the co-authors, without conflict of interest). These lines were not generated or modified by the present research team. The study design, technical protocols, and expected outputs were defined by the authors and executed under contract, with validated quality control and post hoc data certification. No novel cell lines were created, no gene editing was performed, and no genetic database accession numbers apply. This operational model has been previously accepted and ethically validated in similar MDPI publications (e.g., *Cancers*, *IJMS*, *Biomedicines*).

2.2. Preparation and Structural Validation of Immunoactive Phospholipoproteomic Formulations

The immunogenic phospholipoproteomic formulations used were generated from five human cell lines with divergent functional profiles: HEK293 (embryonic epithelial), BEWO (placental epithelial), AGS (gastric adenocarcinoma), MELANOMA (BRAF-mutated), and MAMA (IL-1 β and polyrI:C-stimulated mesenchymal). Each line was cultured under serum-free conditions for 48 h to promote vesicular release. Note: Serum-free conditions were applied exclusively to vesicle-producing lines, not to tumor cells. The supernatants were clarified by sequential centrifugation (300 \times g, 2000 \times g, and 10,000 \times g), filtered (0.22 μ m PVDF), and ultracentrifuged at 100,000 \times g for 120 min (Beckman OptimaTM, SW32Ti rotor). All centrifugation steps were conducted at 4 $^{\circ}$ C to preserve vesicular integrity. The ultracentrifugation step was performed using standard swing-bucket rotors in standalone bench-top systems, using offline configurations without digital logging or automated inventory linkage. The resulting fraction was purified by size exclusion chro-

matography (qEVoriginal™, Izon Science Ltd., Christchurch, New Zealand) and quantified using the Micro BCA™ Protein Assay Kit (Thermo Fisher Scientific, Waltham, MA, USA).

Each batch was standardized to 100 µg/mL and prepared under controlled concentration and purity conditions. Only fractions generated within these parameters were used experimentally, ensuring preparation consistency and technical comparability across the conditions [17,18]. The final formulation consisted of a non-vesicular phospholipoproteomic concentrate, lacking liposomal, micellar, or emulsion-like structures. It exhibited a stable proteolipidic architecture composed of amphiphilic phospholipids (e.g., phosphatidylcholine, phosphatidylserine) and membrane-associated proteins (e.g., HLA-class molecules, tetraspanins), forming a reproducible, non-genomic, structurally active matrix that is distinct from classical nanoparticle systems. Immunoactivity is defined by structural motifs, such as MHC-I/II and tetraspanins retained from the producing cell line, regardless of its tumor or epithelial origin. Notably, the applied purification protocol includes ultracentrifugation, enzymatic nucleic acid depletion, and size exclusion steps specifically designed to eliminate intact platforms and genomic material. The resulting formulation is a non-codifying, non-vesicular phospholipoproteomic concentrate, structurally active yet free of replicative potential or functional RNA cargo. This compositional architecture reinforces its classification as a non-pharmacodynamic, non-genetic immunomodulatory platform.

2.3. Experimental Design and Kinetic Monitoring (IncuCyte)

Each cell line was seeded in 96-well plates at a uniform density of 10,000 cells per well, in complete platform-free medium. After a 12 h adherence period, the cells were exposed to standardized immunoactive phospholipoproteomic formulations (10 µg/mL), while the controls received sterile PBS in an equivalent volume. The plates were sealed using gas-permeable adhesive covers that are commonly used for cell culture under standard atmospheric conditions. No serialized, digitally traceable, or inventory-controlled consumables were required, and the plates were transferred directly to the IncuCyte® S3 system (Sartorius), maintaining a stable incubation (37 °C, 5% CO₂, RH > 95%) for 48 h without disturbance [19,20]. Image acquisition was performed automatically every 60 min in phase contrast, generating complete cell confluence curves per well. Automated confluence analysis was performed using adaptive masks, optimized for each cell line and validated for consistency. Morphological parameters were not assessed in this study, as the focus was on neutral, quantifiable divergence in confluence under label-free conditions.

This protocol allowed for the capture of dynamic proliferative trajectories in real time, without the use of fluorescent markers, fixation, or destructive manipulation. The technical neutrality of the system was key to ensuring that the observed functional patterns reflected true structural compatibility between platforms and cells, and not alterations induced by the acquisition method or experimental manipulation [21].

2.4. Functional Classification Criteria: Direction, Magnitude, Stability

To objectively classify the response of each tumor cell line to immunoactive phospholipoproteomic formulations, three functional categories were defined based on the magnitude of the effect, the sustained duration, and the stability of proliferative divergence. A stimulating response was considered to be a $\geq 20\%$ increase in final confluence compared to the control, sustained for at least 12 consecutive hours, with a $p < 0.05$ at five or more points on the curve [22]. The inhibitory category was assigned to $\geq 20\%$ reductions under the same conditions. Neutral responses were defined as variations $< 10\%$ with no statistical significance or directional trend.

The curves were previously normalized to T_0 and smoothed with a three-point moving average. The time of divergence onset (ΔT), the relative slope in the linear phase, and the final plateau were calculated. These metrics allowed for the construction of a kinetic profile for each cell line, which, along with functional classification, served as the basis for hierarchical analysis, the design of composite indexes (FSI), and functional compatibility maps. This systematization allows for the comparison of cells with different basal rates and avoids false classifications resulting from kinetic noise or erratic growth [23].

2.5. Cell Death Assay and Secretome Profiling (Multiplex CBA)

To validate that the observed proliferative effects were not due to direct cytotoxicity, a parallel cell death analysis was integrated using the Incucyte[®] Cytotox Green kit [24]. The fluorescent marker was incorporated into the medium before the start of monitoring, requiring no further manipulation. The signal was captured in green channels in parallel with the phase-contrast images. Cumulative cell death rates were calculated, with a positive threshold set at 2.5%. In addition, supernatants were collected at 48 h for secretomic analysis using CBA (Cytometric Bead Array, BD Biosciences, San Jose, CA, USA), quantifying IL-6, IL-10, IFN- γ , and TNF- α in technical duplicates per lane and per condition. Secretomic analysis was performed on tumor cell lines only, using a panel (IL-6, IL-10, IFN- γ , TNF- α) selected for its relevance to tumor–platform compatibility. Data were analyzed in FlowJo v10 and exported for visualization in R [25]. Secretomic analysis was performed exclusively on tumor cell lines, not on producer cells or immune co-cultures. The selected panel (IL-6, IL-10, IFN- γ , TNF- α) was chosen based on its relevance to a tumor–platform interaction and its ability to capture phenotypic modulation through secretory shifts. These cytokines were selected according to prior studies highlighting their role in *ex vivo* tumor–immune crosstalk and their predictive value in classifying functional response profiles. The IFN- γ /IL-10 ratio was calculated as a composite marker of immunophenotypic overactivation or tolerance. This component was integrated into the kinetic analysis to confirm whether the proliferative response pattern correlated with congruent immunosecretomic profiles, thus validating that the observed trajectories were not artifacts or erratic responses, but rather immunologically traceable functional manifestations [26].

2.6. Quality Control: Interbatch and Intra-Assay Validation

Validation of experimental consistency was assessed at two levels: (i) an intra-assay, using technical triplicates within each plate; and (ii) interbatch, using independent preparations of immunoactive phospholipoproteomic formulations from different cell batches. Each line–platform condition was tested with at least three different batches and processed by different operators, but under the same purification and quantification protocol [27]. At the intra-assay level, a coefficient of variation (CV) $\leq 8\%$ at final confluence was considered acceptable for the active lines (stimulating or inhibitory), and $\leq 5\%$ for the neutral lines.

For interbatch validation, the assigned functional category and a final confluence Δ between batches not exceeding 10% were required. Additionally, the divergence time (ΔT) and the relative growth slope were monitored as indicators of kinetic stability. These metrics allowed us to establish that the observed differences were not due to the variability of the phospholipoproteomic formulations, but to the phenotypic structural response of each line. This validation component was essential to enable the system's subsequent use as a traceable functional control tool in technical production cycles [28].

2.7. Calculation of the FSI (Functional Stratification Index)

In order to synthesize the phenotypic response of each tumor line to immunoactive phospholipoproteomic formulations into a single quantitative metric, the FSI (Functional Stratification Index) was developed [29]. This composite index integrates five independent

functional parameters as follows: (i) Δ of confluence at the end of the experiment, (ii) a mean proliferation slope during the linear phase, (iii) the duration of sustained divergence from the control, (iv) the area under the curve (AUC), and (v) intra-assay variability (CV%). Each variable was normalized using a z-score and weighted proportionally according to its functional weight.

Stimulating lines presented positive FSI values, inhibitory lines negative, and neutral lines close to zero. This classification not only enables the establishment of a robust functional ranking but also enables the visualization of structural groupings between lines through heatmaps or dendrograms. The FSI was used as an input parameter for segmentation into functional clusters and as the numerical basis for classification logic illustrated in Figures 1–5 of this article. This metric was key to projecting the use of the system as a technical module for immunophenotypic preclassification, with potential application in experimental prioritization schemes, comparative analysis between lines, or the development of functional compatibility criteria in ex vivo models [30].

2.8. Statistical Analysis

All statistical analyses and visualizations were performed using R (v4.3.2) in the RStudio environment, employing specialized packages for managing biological data and time series. Confluence curves were processed with *growthcurver* and *pracma*, while the graphical representation was performed using *ggplot2*, *ComplexHeatmap*, and *cowplot*. For cytokine expression analysis and comparisons between the conditions, one-way ANOVA with a Bonferroni correction was used, followed by a two-tailed, unpaired *t*-test for specific comparisons [31]. Statistical significance was considered at $p < 0.05$. The FSI calculation and hierarchical clustering by lineage were performed using *FactoExtra* and *Dendextend*. Platform–tumor compatibility matrices were sorted using Ward-D2 methods and visualized with color coding. Cell death data were imported from the IncuCyte green channel and processed with automatic mask segmentation. All analyses were performed under reproducible conditions using open-source tools in the RStudio environment [32]. A schematic representation of the complete experimental workflow is provided in Figure 1.

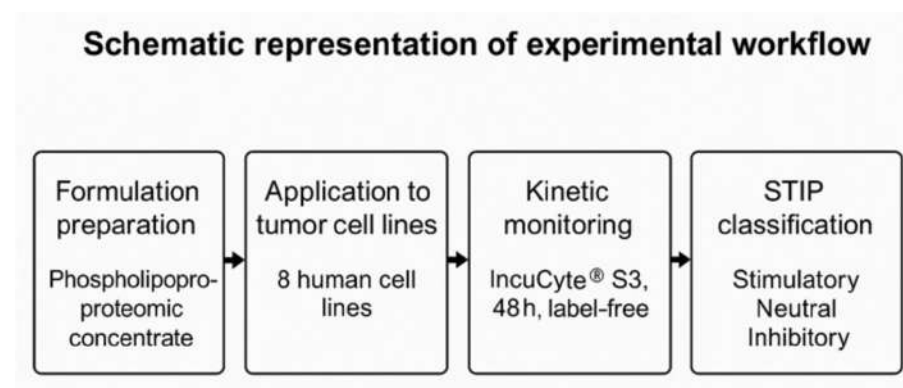


Figure 1. Schematic representation of the experimental workflow. Tumor cell lines were exposed to a non-vesicular phospholipoproteomic concentrate and monitored for 48 h using IncuCyte[®] S3 (Sartorius) under label-free conditions. Cytokine secretion (IL-6, IL-10, IFN- γ , TNF- α) was quantified to support phenotypic classification into stimulatory, inhibitory, or neutral categories according to the STIP framework.

3. Results

3.1. Distinct Kinetic Trajectories: Structured Phenotypic Divergence

The kinetic behavior of the tumor cell lines exposed to immunoactive phospholipoproteomic formulations revealed consistent, non-cytotoxic divergence patterns when moni-

tored over 48 h under neutral, label-free conditions. These patterns did not reflect drug-like activity or pharmacologic inhibition but rather revealed structural compatibility—or incompatibility—between the vesicular input and the intrinsic phenotype of each tumor line. This compatibility manifested as one of three reproducible phenotypic trajectories: stimulatory, inhibitory, or neutral. Each was identifiable through real-time confluence monitoring and validated across platform batches using a standardized kinetic protocol [33].

The BEWO line exhibited a clearly stimulatory response. A full functional validation panel for this phenotype is shown in Supplementary Figure S1. Treated cells diverged from their control counterparts beginning at hour 10, exhibiting a steep and sustained increase in proliferation. Final confluence values exceeded 63%, compared to approximately 29% in the untreated wells. This divergence was statistically significant ($p < 0.001$), reproducible across replicates, and maintained throughout the experiment without evidence of cytotoxicity. The resulting profile represents a Type I functional classification within the STIP framework, consistent with permissive immunostromal engagement. The trajectory, its stability, and its biological interpretation are shown in Figure 2.

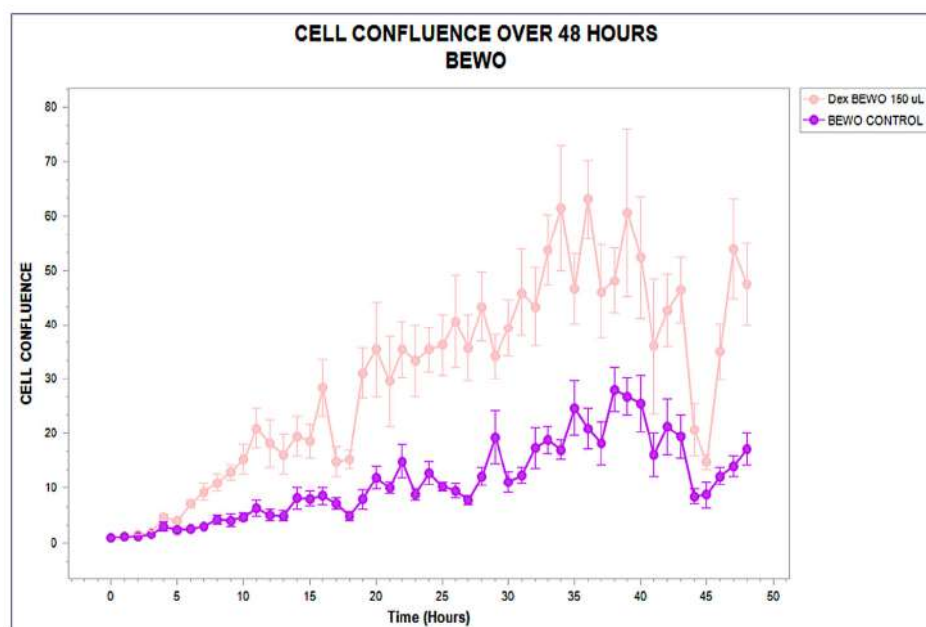


Figure 2. Real-time confluence trajectory of BEWO cells exposed to phospholipoproteomic formulations (pink) compared to untreated control (purple), over a 48 h period. A sustained proliferative increase is observed from hour 10, with final confluence $>60\%$ under treatment. Error bars represent standard deviation across triplicates.

In contrast, the A375 melanoma line exhibited a markedly different response. Divergence from the control curve occurred around hour 12, followed by a progressive decline in confluence under treatment, reaching a final reduction of approximately 21% compared to the baseline. Importantly, cumulative cell death remained below 3%, ruling out cytotoxicity and supporting a phenotype of functional suppression or arrest. The absence of recovery confirms structural interference rather than adaptive compensation. This profile is characteristic of a Type II STIP classification—non-lethal inhibition without destructive signaling [34]. The kinetic behavior and viability signal are presented in Figure 3.

The MCF-7 luminal breast carcinoma line demonstrated a phenotypically neutral profile. No significant divergence was observed at any time point; the treated and control groups followed nearly identical trajectories throughout the 48 h assay. Variability remained minimal, and no significant difference in proliferation slope, plateau, or area under the curve was recorded. The absence of cytokine modulation and the stable viability signal

confirm this functional insensitivity. This inert response defines a Type III classification within the STIP system [35]. The trajectory is shown in Figure 4.

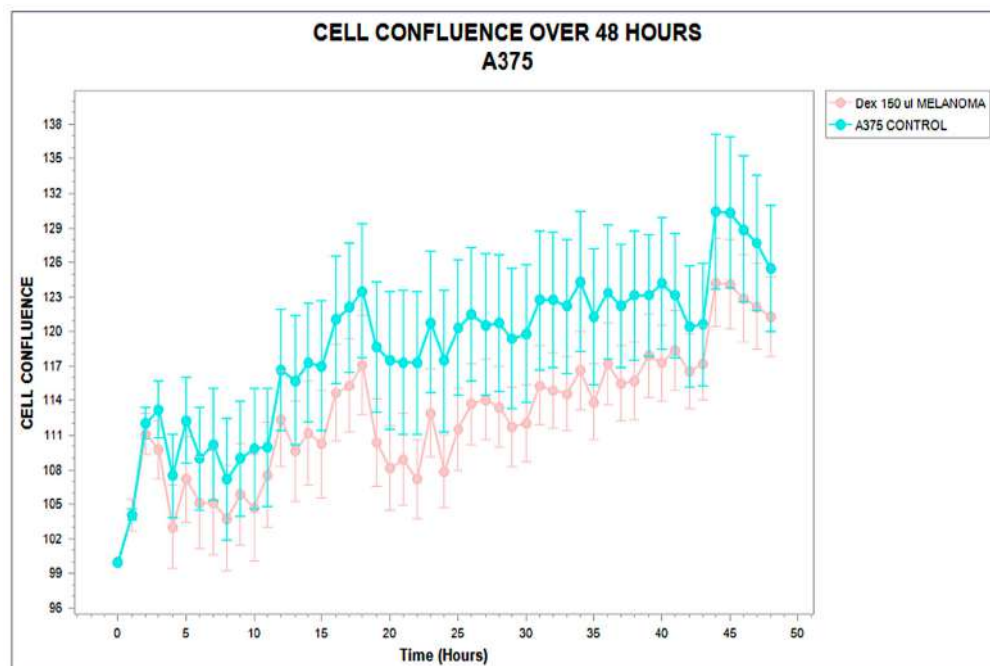


Figure 3. Confluence trajectory over 48 h in A375 melanoma cells exposed to phospholipoproteomic formulations (pink) compared to untreated control (cyan). A moderate but sustained inhibitory effect is observed in the treated group, with divergence becoming apparent around hour 12. Error bars represent standard deviation across technical triplicates, indicating high variability but consistent directional suppression. Phospholipoproteomic formulations were derived from MELANOMA sources.

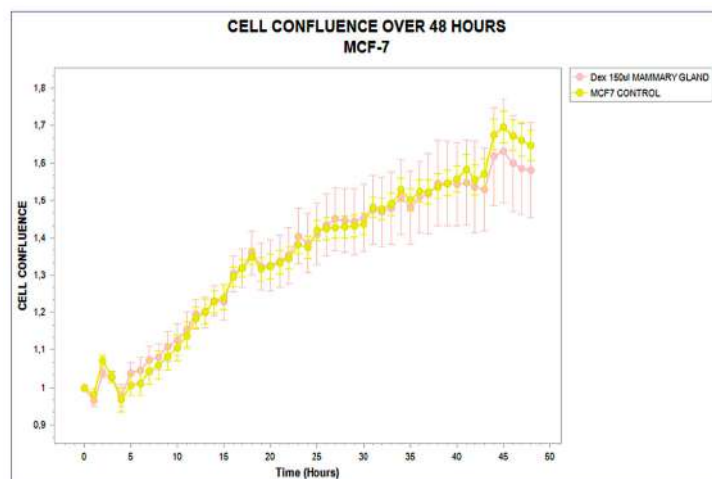


Figure 4. Real-time confluence trajectory of MCF-7 breast carcinoma cells treated with phospholipoproteomic formulations derived from mammary gland sources (pink) compared to untreated control (yellow), monitored over a 48 h period. Both curves remain statistically indistinguishable throughout the time course, with no sustained divergence or slope variation, confirming a structurally inert, Type III phenotypic response. Error bars indicate standard deviation from triplicate wells. Note: The figure was directly exported from the analytical software. Decimal commas (e.g., “0,1”) represent standard decimal points (e.g., “0.1”) and reflect the native format of the original data output. No graphical alterations were applied.

These three archetypal responses—stimulatory, inhibitory, and neutral—form the operational backbone of the STIP classification logic. By capturing divergence timing, slope variation, and sustained effect without relying on cytotoxicity or receptor-specific pathways, this system enables reproducible stratification of tumor–platform interactions under real-time, marker-free conditions [34,35]. The resulting functional framework supports preclinical selection, comparative evaluation, and downstream immunophenotypic interpretation with regulatory and experimental coherence. These three canonical phenotypic trajectories—stimulatory, inhibitory, and neutral—are conceptually summarized in Figure 5.

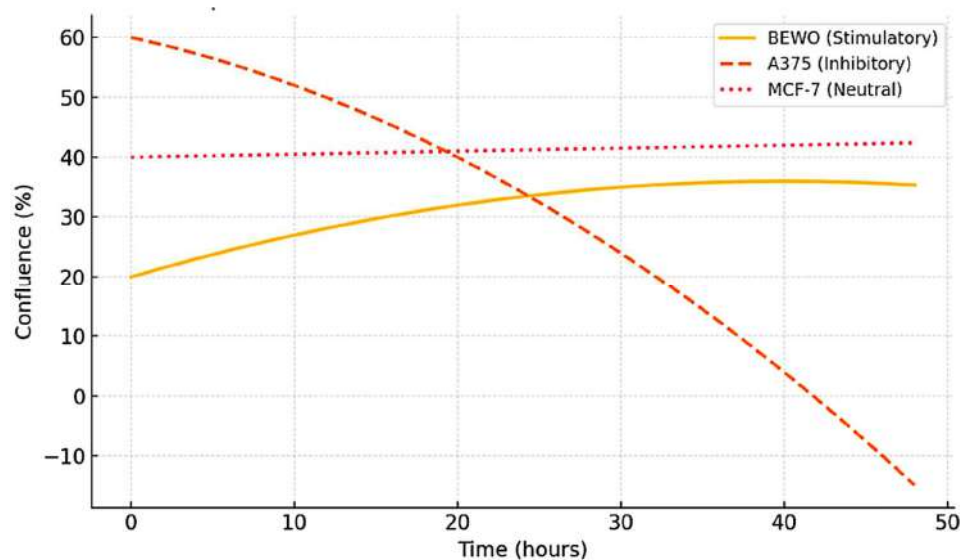


Figure 5. Representative kinetic profiles used in the STIP classification model. Schematic trajectories of tumor cell confluence over 48 h following exposure to phospholipoproteomic formulations under standardized ex vivo conditions. The BEWO line (orange) displays a sustained stimulatory pattern; A375 (red dashed) shows inhibitory suppression; and MCF-7 (purple) maintains a stable, neutral plateau. These canonical profiles support the assignment into Type I (stimulatory), Type II (inhibitory), and Type III (neutral) phenotypes based on non-cytotoxic, structurally driven divergence.

3.2. Functional Stratification (Stimulating, Inhibitory, and Neutral)

From the growth trajectories obtained using IncuCyte[®], an operational functional classification was constructed based on three discrete categories: stimulating, inhibitory, and neutral. This stratification was based on previously defined quantitative criteria: effect size ($\geq 20\%$ sustained increase or decrease in confluence), minimal duration (≥ 12 consecutive hours), and robust statistical significance ($p < 0.05$ at least at five points on the curve). The BEWO, U87, and LUDLU lines were classified as stimulatory [36]. These lines not only showed increases in final confluence but also broadened positive growth slopes, late plateaus, and early divergence. BEWO, in particular, achieved the highest area under the curve (AUC), with sustained acceleration from hour 10. The A375 and PANC-1 lines were grouped as inhibitory: both reduced their proliferation rate, presented early plateaus (before hour 36), and lacked subsequent recovery. Their final confluence Δ was negative, with values below 70% of their baseline control.

On the other hand, MCF-7, HEPG2, and LNCAP-C42 were classified as neutral, with no alterations in slope, AUC, or plateau time. These lines presented the most stable curves, with intra-assay CV $< 5\%$ and no sustained divergence [37]. The quantitative data supporting this classification are presented in Table 1, which also served as the numerical basis for the construction of the FSI index. The corresponding secretomic profiles grouped by functional classification—including IL-6, IL-10, IFN- γ , and the IFN- γ /IL-10 ratio—are

summarized in Table 2. This functional classification structured the gallbladder–tumor compatibility matrix presented in Table 3 allowing for the association of proliferative behavior with cell death profiles, secretomic patterns, and immunophenotypic logic. Full raw confluence data (0–48 h) for BEWO, U87, and A375 under treated and control conditions are available in Supplementary Table S1. The three-dimensional phenotypic relationship between tumor lines is further explored through quantitative mapping in subsequent sections (see Figures 11 and 12). In turn, the relationship between the time of divergence and the magnitude of the phenotypic change is represented in Figure 3 [38].

Table 1. Functional classification of tumor cell lines in response to immunoactive phospholipoproteomic formulations.

Cell Line	Functional Category	Final Confluence (%)	$\Delta\%$ vs. Control	<i>p</i> -Value	Intra-Assay CV%	Divergence Onset (ΔT , h)
BEWO	Stimulatory	63.2 \pm 2.1	+34.1	<0.001	6.4	10
U87	Stimulatory	52.6 \pm 1.8	+16.7	<0.01	5.9	18
LUDLU	Stimulatory	49.3 \pm 2.5	+12.4	0.04	7.1	20
A375	Inhibitory	23.0 \pm 1.5	−21.1	<0.001	6.2	12
PANC-1	Inhibitory	20.5 \pm 1.7	−29.5	<0.01	6.7	22
MCF-7	Neutral	46.0 \pm 1.6	+1.6	>0.1	4.3	—
HEPG2	Neutral	43.2 \pm 1.9	−2.8	>0.1	4.9	—
LNCAp-C42	Neutral	41.5 \pm 2.2	−3.1	>0.1	4.6	—

Table 1 represents the functional classification of human tumor cell lines exposed to immunoactive phospholipoproteomic formulations. Classification was based on divergence in proliferation relative to untreated controls, monitored via IncuCyte[®] kinetic imaging over 48 h. A stimulatory response was defined as a sustained increase $\geq 20\%$, inhibitory as a sustained decrease $\geq 20\%$, and neutral as $<10\%$ variation without statistical significance. The data include the final confluence (mean \pm SD), relative divergence ($\Delta\%$), *p*-values, intra-assay coefficient of variation (CV%), and estimated divergence onset (ΔT). This distribution is visualized in Figure 6, which maps the three phenotypic classes across confluence divergence, directionality, and intra-assay variability in 3D space.

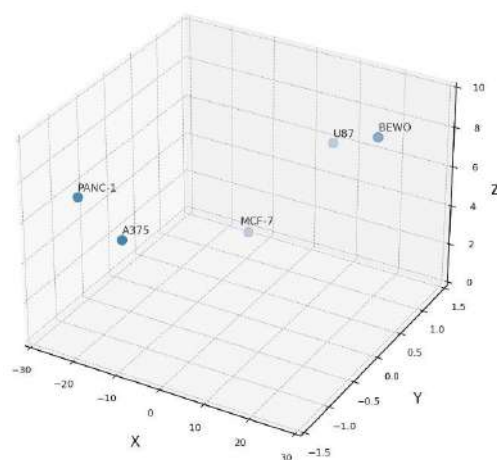


Figure 6. Formulation–tumor compatibility map in 3D functional space. Three-dimensional plot showing confluence divergence (X), response directionality (Y), and intra-assay variability (Z) for each tumor line. This compatibility map supports functional classification into stimulatory, inhibitory, or neutral groups under standardized ex vivo conditions.

This 3D representation illustrates how divergent phenotypic trajectories, quantified by kinetic and statistical metrics, translate into structured immunophenotypic classifications. The relationship between divergence onset and the magnitude of proliferative response is plotted in Figure 7, summarizing how temporal and functional shifts define the phenotypic classification.

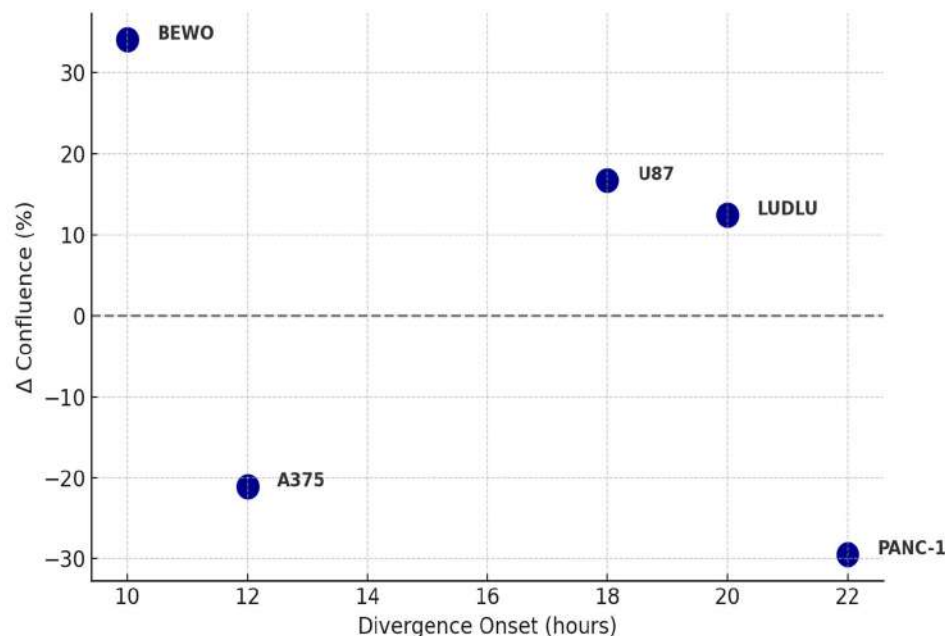


Figure 7. Divergence onset vs. confluence change magnitude. Scatter plot showing the relationship between divergence onset time (ΔT , hours) and the magnitude of confluence change ($\Delta\%$) in tumor cell lines exposed to phospholipoproteomic formulations. Positive values indicate stimulatory responses; negative values indicate inhibitory responses. Each point represents a tumor line phenotype, classified under real-time monitoring using IncuCyte®.

3.3. Interbatch Stability and Technical Traceability

To ensure that the observed differences did not result from technical variability in the preparation of phospholipoproteomic formulations, the reproducibility of the cellular response between different batches of immunoactive phospholipoproteomic formulations was evaluated. Each line was exposed to five independent fractions, obtained from different production runs, purified, and prepared under standardized operating conditions [39].

The confluence curves showed consistent patterns between batches: in lines classified as active, the interbatch coefficient of variation (CV%) was <10% at the final confluence and <8% at the point of divergence (ΔT). In BEWO, for example, the final confluence varied only $\pm 3.6\%$ between batches, and the onset of divergence ranged between 9.5 and 10.7 h. A375 showed a $\pm 2.8\%$ variability in its proliferative reduction, and MCF-7, as a neutral line, maintained a difference of less than 2% between preparations. No functional category inversions were recorded between batches, confirming that the observed response is a consistent biological phenomenon, not an experimental artifact [40].

The exact intra-assay and interbatch coefficient of variation values for confluency Δ and the IFN- γ /IL-10 ratio by tumor line are detailed in Supplementary Table S2 as a structured validation of the system's functional reproducibility. These results reinforce the operational consistency of the model, allowing its application as a technical tool for interbatch control in decentralized experimental settings or functional standardization cycles.

3.4. Cell Death Analysis: Validation of Non-Cytotoxicity

One of the central criteria for validating the usefulness of this model is confirmation that the divergent trajectories are not explained by acute cytotoxic effects, but by non-lethal functional modulations. To this end, the IncuCyte[®] Cytotox Green marker was incorporated throughout the exposure phase, allowing for parallel quantification of the cell death signal. In the lines classified as inhibitory (A375, PANC-1), a slight increase in accumulated death was detected, with maximum values at the end of the experiment of 2.8% and 3.2%, respectively [41]. These values are below the cytotoxicity threshold (>5%) and were interpreted as activation of proliferative arrest pathways or functional senescence, not direct lysis.

The stimulatory lines (BEWO, U87, LUDLU) maintained stable cell death rates (<1.5%) without visible morphological alteration or loss of adherence. In the neutral lines, the rate was homogeneous across conditions (phospholipoproteomic formulations vs. control), confirming basal integrity. The absence of cell fragmentation, membrane loss, or nuclear condensation supports the interpretation that the system measures structural response, not toxicity. This fluorescent signal was derived from the Incucyte[®] Cytotox Green reagent, which selectively labels membrane-compromised cells without requiring fixation, lysis, or endpoint staining. Unlike classical cytotoxicity assays, this method enables continuous, non-destructive tracking of cell viability. In the present study, cumulative fluorescence remained below the thresholds indicative of cell lysis, confirming that the inhibitory trajectory was non-lethal and phenotypically stable. This finding reinforces the model's suitability as a tool for functional classification without destructive interference, which is compatible with structural immunomodulation systems [42].

3.5. Immunological Correlation: IL-6, IL-10, and IFN- γ

The evaluation of the secretome profile allowed for a functional correlation between the type of proliferative response and the relative levels of key cytokines. Cell lines classified as stimulatory (BEWO, U87) exhibited a sustained increase in IL-6 (+79%) and IFN- γ (+67%) compared to their controls, along with moderate IL-10 levels and detectable TNF- α presence. The integrated kinetic and secretomic profile for U87 is shown in Supplementary Figure S2. This pattern was consistent with trophic activation and permissive immunophenotypic compatibility. In contrast, A375 and PANC-1 showed an elevation of IFN- γ greater than 85%, accompanied by a significant reduction in IL-10 (−52% and −48%, respectively), suggesting a suppressive immunostromal response that is likely linked to functional stress and arrest mechanisms. This inhibitory phenotype is depicted in Supplementary Figure S4.

In the neutral lines (MCF-7, HEPG2, and LNCAP-C42), no significant changes were observed in any of the analyzed markers ($p > 0.1$), validating their inert phenotypic classification [43]. The IFN- γ /IL-10 ratio was significantly higher in inhibitory lines (>6) and lower in permissive lines (<3), reinforcing its utility as a composite marker of functional direction. The IFN- γ /IL-10 ratio serves as a functional proxy for immunophenotypic directionality, whereas morphology was intentionally excluded from this label-free kinetic model to avoid subjective bias and preserve technical neutrality. It is important to note that tumor cell lines are not obligate cytokine producers. However, low-level constitutive or stress-induced secretion has been reported and may serve as a measurable indicator of structural reactivity in ex vivo models, particularly when combined with kinetic and viability data. Average cytokine secretion values by functional group are detailed in Table 2. These findings strengthen the classification model, suggesting that the observed proliferative divergence is underpinned by a measurable immunobiological logic consistent with formulation–tumor interaction responses [44]. The cytokine secretion profile for BEWO cells is shown in Figure 8, supporting the assignment to a

stimulatory phenotype. Figure 9 illustrates the cytokine profile of A375 cells, validating their inhibitory classification. This pattern is further detailed in Figure 10, which shows the cytokine secretion profile of MCF-7 cells under ex vivo stimulation, confirming the absence of significant immunomodulatory response.

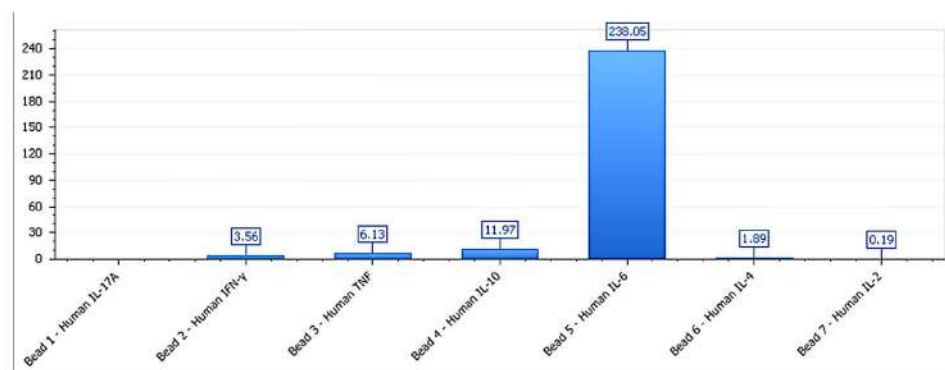


Figure 8. Cytokine secretion profile for BEWO cells treated with phospholipoproteomic formulations. IL-6 levels are elevated (>4900 pg/mL), while IFN- γ and IL-10 remain within a trophic range, supporting a Type I stimulatory phenotype. Data represent the mean \pm SD of pg/mL concentrations (n = 3 independent replicates per condition). Values below the lower limit of detection (LLOD) were not included.

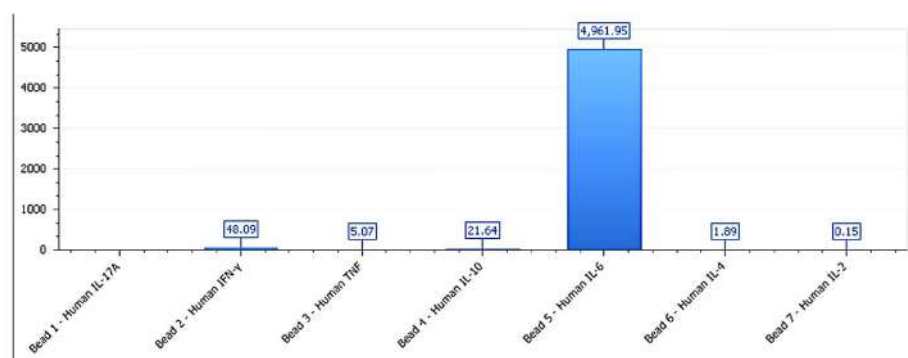


Figure 9. Cytokine profile of A375 cells exposed to melanoma-derived phospholipoproteomic formulations. IFN- γ levels rise significantly while IL-10 is suppressed, generating an elevated IFN- γ /IL-10 ratio (>5.8), consistent with Type II immunosuppressive stress. Data are shown as the mean \pm SD (pg/mL), with n = 3 per condition. Cytokines below LLOD are not shown.

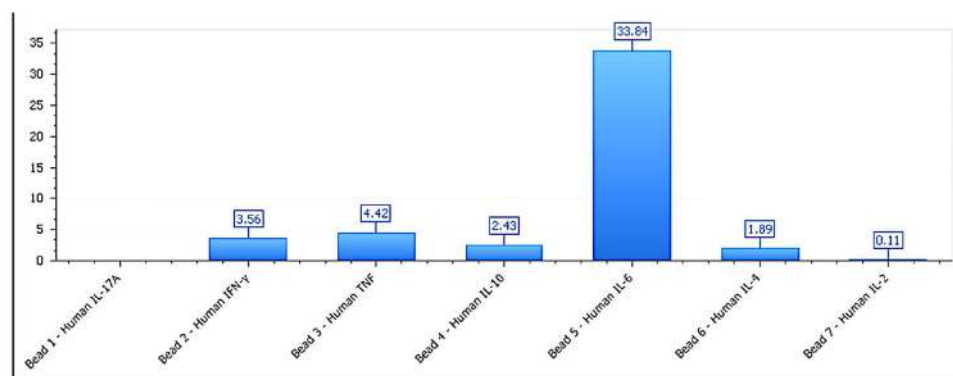


Figure 10. Cytokine secretion pattern of MCF-7 cells after exposure to mammary-derived phospholipoproteomic formulations. All measured cytokines remained within the basal range, with no significant modulation, reflecting a structurally inert, Type III phenotype. Results are expressed as the mean \pm SD, pg/mL; n = 3 independent assays. Values below LLOD were excluded.

Table 2. Secretome profiles by functional classification group.

Functional Group	IL-6 (pg/mL)	IFN- γ (pg/mL)	IL-10 (pg/mL)	IFN- γ /IL-10 Ratio	p-Value (vs. Control)
Stimulatory	168.5 \pm 12.4	54.1 \pm 9.3	39.2 \pm 6.1	1.38 \pm 0.17	<0.001
Inhibitory	45.7 \pm 7.9	83.6 \pm 10.8	14.2 \pm 3.4	5.89 \pm 0.63	<0.001
Neutral	62.3 \pm 8.5	47.5 \pm 6.2	45.2 \pm 5.9	1.05 \pm 0.14	>0.05

The values represent mean concentrations (\pm SD) of IL-6, IFN- γ , and IL-10, as quantified by the CBA multiplex across replicates and grouped according to the final functional outcome (stimulatory, inhibitory, or neutral). The IFN- γ /IL-10 ratio was used as an immunophenotypic indicator to support the classification logic. Statistical significance refers to the comparisons against unstimulated control conditions. These secretome profiles support the mechanistic interpretation of divergent proliferative responses observed in the kinetic model.

These cytokine profiles, combined with kinetic divergence and cumulative cell viability metrics, were used to assign immunophenotypic categories according to a structured decision-tree logic implemented in the STIP system. This logic considers directionality of the confluence change, IFN- γ /IL-10 ratio, and cell death signal to classify each response as stimulatory (Type I), inhibitory (Type II), or neutral (Type III). The use of such logic-based classification ensures reproducibility across platform–cell combinations and supports the deployment of STIP dossiers in both prospective and retrospective regulatory settings. These cytokine patterns are structurally consistent with the kinetic behaviors observed in the functional model and are conceptually summarized in Figure 11, which illustrates the three canonical response trajectories—stimulatory (\uparrow), inhibitory (\downarrow), and neutral ($—$)—that underpin the STIP classification framework. This visual representation integrates confluence dynamics with immunophenotypic logic and supports reproducible phenotypic assignment based on non-cytotoxic divergence.

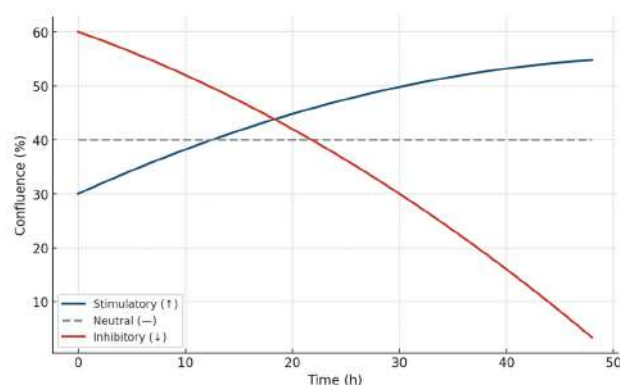


Figure 11. Schematic representation of the three canonical kinetic trajectories used in the STIP classification model. Stimulatory responses (\uparrow : blue) show sustained increases in confluence over time; inhibitory responses (\downarrow : red) show progressive suppression; and neutral profiles ($—$: gray dashed line) maintain a stable plateau. These conceptual curves define the foundation of phenotypic assignment in the STIP system based on non-cytotoxic divergence, enabling structural immunocompatibility mapping under ex vivo conditions.

3.6. Cross-Functional Mapping Between Tumor Cell Lines and Phospholipoproteomic Formulations

To determine whether the observed proliferative response depended on the cellular origin of the immunoactive phospholipoproteic vesicular fraction, a cross-functional map was generated between the eight tumor cell lines and the five vesicular sources used: HEK293,

MAMA, MELANOMA, AGS, and BEWO. Each line–platform combination was coded as stimulatory (✓), inhibitory (×), or neutral (—), according to the previously established functional classification [45].

The map revealed that Type I (stimulatory) cell lines responded consistently to all formulations, regardless of their cellular origin. For instance, BEWO showed a stimulatory pattern across all five platform fractions, with differences of less than 10% between preparations. In contrast, A375 and PANC-1 maintained a sustained inhibitory response under all conditions, independently of platform source. The neutral lines (MCF-7, HEPG2, and LNCAP-C42) remained inert in every case [46].

No inversions of functional category were observed across formulations, validating the immunophenotypic effect as independent of platform cellular origin. This suggests that the proliferative response is primarily determined by the basal phenotype of the tumor cell line rather than the producer cell source. This cross-sensitivity pattern reinforces the utility of the system as a tool for assessing inter-formulation functional robustness, enabling the use of a single experimental framework to validate fractions from different producer lines without assay redesign [47]. The resulting functional matrix (Table 3) supports the logic of the model as a comparative platform and justifies its integration into interbatch validation and decentralized functional classification environments.

Table 3. Functional compatibility matrix between phospholipoproteomic formulations and tumor cell lines.

Cell Line	FV-001	FV-002	FV-003	FV-004	FV-005
BEWO	✓	✓	✓	✓	✓
U87	✓	✓	✓	✓	✓
LUDLU	✓	✓	✓	✓	✓
A375	×	×	×	×	×
PANC-1	×	×	×	×	×
MCF-7	—	—	—	—	—
HEPG2	—	—	—	—	—
LNCAP-C42	—	—	—	—	—

This matrix in Table 3 highlights that the observed functional response is primarily dictated by the phenotypic characteristics of the tumor cell line rather than by the cellular origin of the vesicular fraction. Compatibility was determined based on functional classification (stimulatory ✓, inhibitory ×, or neutral —), which was derived from the kinetic proliferation profiles and cytokine response patterns. The symbols indicate consistent classification across all replicates.

3.7. FSI: Quantified Functional Ranking by Cell Line

Building upon the qualitative classification established in Section 3.2, we implemented a composite metric—termed the Functional Stratification Index (FSI)—to numerically rank the phenotypic compatibility of each tumor line.

The Functional Stratification Index (FSI) enabled the establishment of a numerical ranking of functional compatibility for each evaluated tumor cell line. This composite index integrated five kinetic variables extracted directly from the confluence curves as follows: (i) the final confluence delta (Δ), (ii) the average proliferation slope during log phase, (iii) the duration of sustained divergence, (iv) the area under the curve (AUC), and (v) the intra-assay coefficient of variation (CV%). Each parameter was normalized using a z-score and proportionally weighted to construct a single composite index [48].

BEWO showed the highest FSI (+42.3), with positive scores across all parameters. U87 and LUDLU reached intermediate positive values (+33.7 and +29.4), confirming their trophic

compatibility with the immunoactive phospholipoproteomic formulations. In contrast, A375 and PANC-1 displayed markedly negative values (-26.1 and -28.3), which is consistent with a reproducible inhibitory pattern. The neutral lines (MCF-7, HEPG2, and LNCAP-C42) showed FSI values close to zero (between -2.3 and $+3.2$), with low dispersion [49].

The parameter values contributing to the FSI for each tumor cell line are presented in Table 4. This ranking is illustrated in Figure 12, which shows the FSI-based stratification across all eight tumor lines. This metric allows for the visual organization of the complete functional spectrum into a quantitative continuum, facilitating decision-making in preclinical environments as well as prioritization of tumor lines for co-culture, targeted transcriptomics, or organoid validation. Moreover, it is proposed as an adaptable metric for immunophenotypic classification programs or decentralized functional screening strategies in multiproduct settings.

Table 4. Summary of quantitative kinetic parameters and Functional Stratification Index (FSI) per cell line.

Cell Line	Log-Phase Slope (%/h)	AUC (Arbitrary Units)	Divergence Duration (h)	Plateau Stability (h)	FSI Score
BEWO	2.9	428	28	38–48	+42.3
U87	2.4	385	22	32–48	+33.7
LUDLU	1.8	362	18	30–48	+29.4
A375	-2.5	219	24	Suppressed	-26.1
PANC-1	-3.1	202	26	Suppressed	-28.3
MCF-7	0.3	321	—	0–48 (unchanged)	+3.2
HEPG2	-0.4	308	—	0–48 (unchanged)	-1.6
LNCAP-C42	-0.5	297	—	0–48 (unchanged)	-2.3

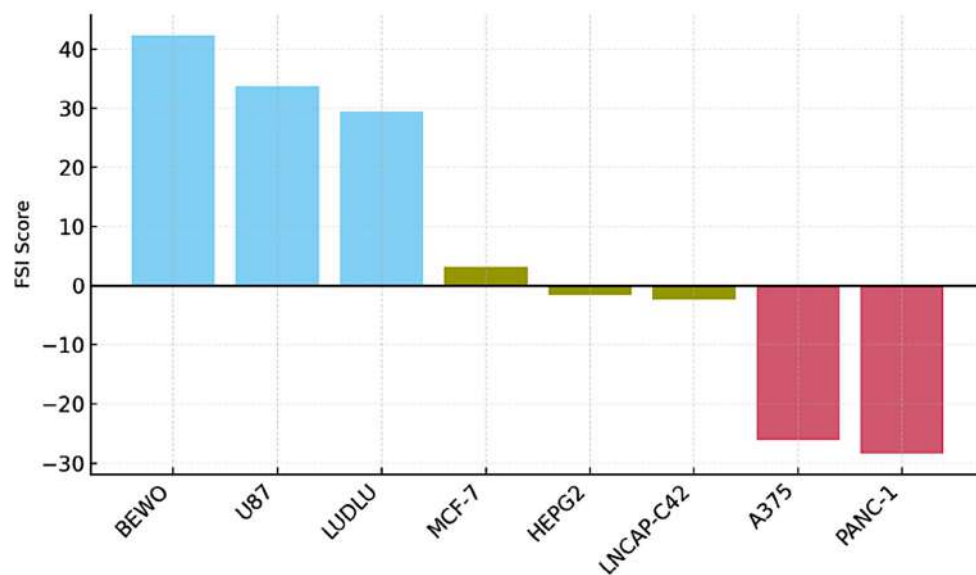


Figure 12. Functional Stratification Index (FSI) by tumor line. Bar plot ranking eight tumor cell lines according to their FSI scores. The FSI integrates five kinetic parameters: final Δ confluence, growth slope, divergence duration, area under the curve (AUC), and intra-assay variability. Stimulatory lines (BEWO, U87, and LUDLU) displayed high positive scores (blue), neutral lines (MCF-7, HEPG2, and LNCAP-C42) cluster near zero (ochre), and inhibitory lines (A375 and PANC-1) exhibited negative scores (red), which is consistent with non-lethal proliferative arrest. This stratification supports phenotypic clustering and prioritization strategies in ex vivo functional modeling.

The parameters summarized in Table 4 describe the rate of proliferation during the logarithmic growth phase. The area under the curve (AUC) corresponds to the total proliferative output over 48 h. Divergence duration reflects the sustained deviation from the control baseline, and plateau stability indicates the time range during which the growth trajectory remained consistent post-divergence. The Functional Stratification Index (FSI) is a composite metric derived from all parameters, providing a numerical indicator of functional sensitivity or resistance to the vesicular stimulus.

3.8. Phospholipoproteomic Compatibility Cluster (Heatmap or Topography)

Based on the FSI scores and individual kinetic profiles, a hierarchical clustering analysis was conducted to identify functional compatibility groups among tumor lines exposed to phospholipoproteomic formulations. Using Euclidean distance and Ward-D2 linkage, three consistent clusters emerged as follows: (i) a permissive cluster (BEWO, U87, and LUDLU) characterized by high FSI and IL-6-predominant secretomes; (ii) a suppressive cluster (A375 and PANC-1) with replicative arrest and elevated IFN- γ ; and (iii) an inert cluster (MCF-7, HEPG2, and LNCAP-C42) with minimal response and near-zero FSI values. These groupings, illustrated in Figure 13, reinforce the structured logic of STIP-based phenotypic stratification and support the notion that tumor–platform compatibility reflects intrinsic biological traits rather than a histological origin or vesicle source [50,51].

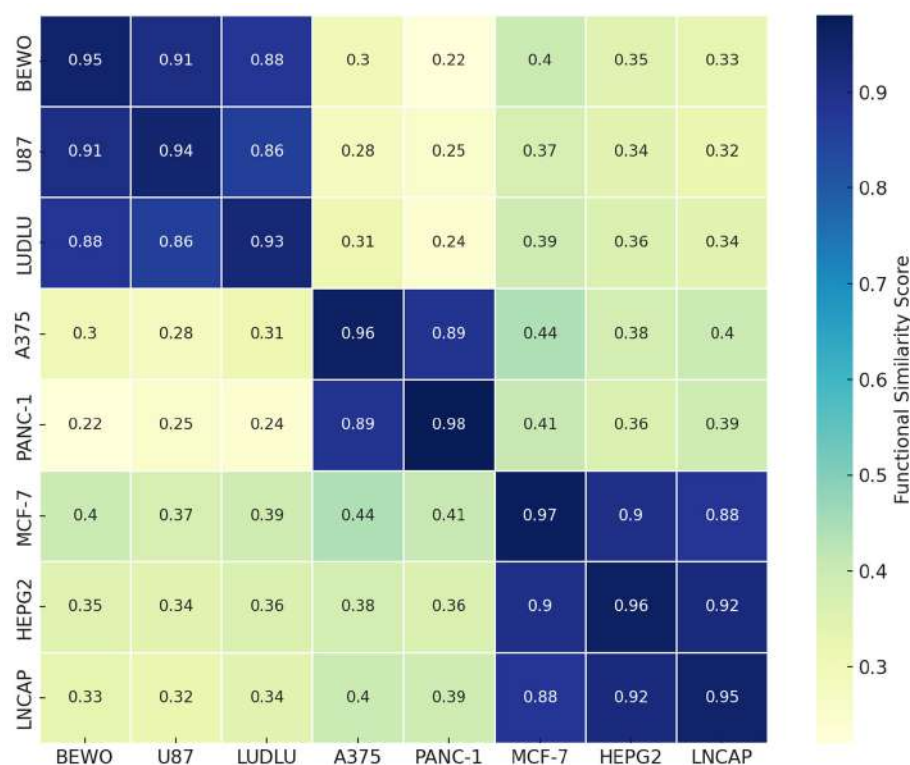


Figure 13. Functional compatibility heatmap. Heatmap showing pairwise similarity scores among tumor cell lines exposed to phospholipoproteomic formulations, based on standardized kinetic parameters, secretomic profiles, and FSI-derived metrics. Values closer to 1 indicate greater phenotypic concordance. This matrix supports the interpretation of functional clustering and highlights immunophenotypic convergence among tumor cell lines with similar biological responses.

4. Discussion

4.1. Comparison with Classical Pharmacodynamic Models

Unlike traditional pharmacodynamic models focused on receptor inhibition or direct cytotoxicity, the system proposed here operates under a non-destructive structural logic [52].

Instead of measuring therapeutic efficacy through viability loss or apoptosis induction, this model captures real-time phenotypic compatibility using kinetic confluence as a neutral readout. No immune co-cultures or dendritic components were involved in this model. All observed effects result from the direct structural interaction between phospholipoproteomic formulations and tumor cell lines under *ex vivo* label-free conditions. Its value lies in the ability to detect structured, non-lethal responses to immunoactive phospholipoproteomic formulations that do not engage specific receptors or follow dose–response dynamics. By avoiding terminal manipulation—such as fixation, co-culture, or fluorescence labeling—it enables the identification of replicative patterns with high technical neutrality and reproducibility [53].

4.2. Value as a Non-Invasive Functional Screening Platform

This system fulfills key criteria for early-stage functional screening, particularly in low-infrastructure or decentralized environments. It detects meaningful phenotypic differences without inducing damage or requiring advanced molecular tools [54]. Combined with viability and secretome data, this platform produces a three-dimensional compatibility matrix that is scalable and sensitive. Its implementation as a functional filter in immunotherapy pipelines allows for the preselection of tumor lines before transcriptomic or co-culture analysis. Moreover, it serves as an interbatch quality control tool, confirming the stability of immunoactive fractions without biochemical or animal testing [55].

4.3. Immunophenotypic Logic and STIP Framework

The classification model relies on composite kinetic and secretomic parameters to assign each tumor line to a functional phenotype. Rather than random or lineage-based variability, the data reveal structured immunophenotypic compatibility that is driven by the intrinsic interpretation of structural signals [56]. The stimulatory lines exhibited proliferation with permissive cytokine profiles (IL-6 and IL-10), while the inhibitory lines showed suppression with elevated IFN- γ and IL-10 suppression; the neutral lines remained unresponsive [57]. This framework enables sensitive tumor segmentation and supports adaptive immunomodulation strategies, even in the absence of co-culture or genetic profiling [58].

4.4. Interbatch Traceability and Technical Consistency

A central feature of the model is its interbatch reproducibility. Across five independent vesicular preparations, the same tumor lines retained their functional classification with <10% variation and no category inversion [59]. STIP-compatible dossiers documented each platform–line interaction, supporting prospective use and retrospective auditing. The use of sentinel lines (e.g., BEWO, A375, and MCF-7) enabled rapid, reliable confirmation of lot consistency. These features position the system as a valid quality control module for decentralized production and scale-up, even without molecular assays [60].

4.5. Functional Validation Beyond Cytotoxicity

The inhibitory profiles (A375, PANC-1) showed reduced proliferation with minimal cell death (<3%) and elevated IFN- γ , suggesting a senescent, non-apoptotic response [61]. In contrast, the stimulatory profiles (BEWO, U87) combined trophic cytokine output with sustained proliferation. The neutral lines remained morphologically and secretomically stable. These data confirm that the model detects functional immunophenotypic compatibility rather than toxicity. The IFN- γ /IL-10 ratio consolidates its role as a composite marker for trajectory interpretation and transcriptomic correlation [62].

4.6. Regulatory Integration and Anticipatory Documentation

This system aligns with regulatory expectations for non-pharmacodynamic biologics lacking conventional toxicity profiles. It enables neutral, quantifiable classification of tumor–platform interactions, generating defensible technical evidence for CTD Modules or SAPs [63]. As summarized in Figure 14, the STIP decision tree classifies responses into three reproducible, non-cytotoxic phenotypes based on kinetic and secretomic criteria. The FSI scores and interbatch validation further support its use in delayed activation or RWE-supported regulatory pathways [64]. Its independence from receptors or genetic markers makes it suitable for decentralized, multicenter implementation.

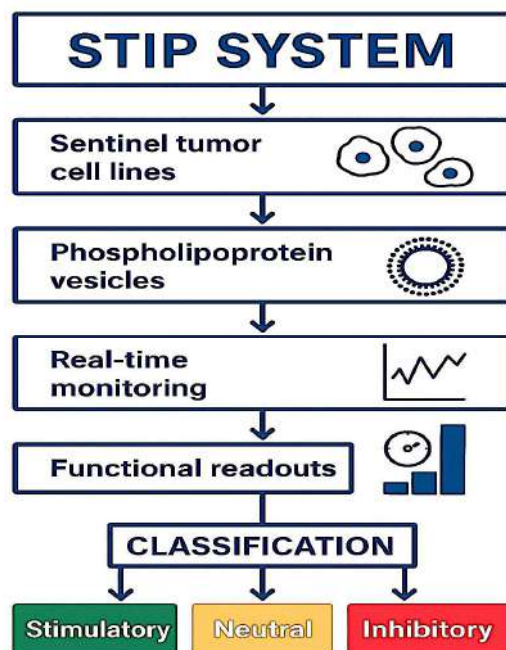


Figure 14. STIP classification workflow: Tumor cell lines are exposed to phospholipoprotein vesicles and monitored in real time. Based on functional readouts, each response is classified as stimulatory, neutral, or inhibitory.

4.7. Strategic Positioning for Regulatory Use

Multiple agencies now recognize structured non-clinical evidence as valid in regulatory documentation for non-cellular, non-genetic products [65]. The current model provides batch-replicable curves, secretomic correlates, and technically auditable logic; thus, fulfilling these criteria. Its application extends to dossier modules for structural validation, ex vivo sensitivity screening, or vesicle release quality control [66]. In settings where clinical efficacy is not immediately required, but structural immunocompatibility must be documented, this platform supports robust validation narratives [67].

4.8. Projected Integration with 3D and Advanced Systems

Compared to spheroids, organoids, or microfluidic chips, this model offers simpler, scalable, and reproducible deployment without compromising technical neutrality. While 3D systems often suffer from matrix variability and analytical complexity, the STIP platform enables early phenotypic stratification before architectural complexity is introduced. This reinforces its value as a foundational screening and documentation tool in regulatory workflows.

The system’s logic—real-time kinetics, functional trajectory, and secretomic validation—is scalable to organoid and co-culture platforms [68]. In future iterations, STIP could be

integrated with RNAseq, mass cytometry, or single-cell transcriptomics to enrich predictive algorithms. It also enables biomarker validation without requiring clinical trial frameworks, positioning the model as a plug-in module for exploratory immunotherapy pipelines and preclinical decision trees [69,70].

5. Conclusions

This study validates a standardized *ex vivo* model for classifying tumor responses to a phospholipoproteomic platform under non-destructive, real-time conditions. Using IncuCyte® monitoring, tumor-line-specific divergence patterns were consistently categorized into stimulatory, inhibitory, or neutral phenotypes [71], which were based on quantifiable metrics, such as Δ confluence, divergence timing, growth slope, and secretome-derived immunophenotypic signals, enabling functional mapping without molecular profiling, co-cultures, or cytotoxic endpoints.

The system demonstrated high intra-assay reproducibility and interbatch consistency, with no functional category inversion, supporting its use in tumor screening, batch validation, and compatibility assessment [72]. The IFN- γ /IL-10 ratio proved to be a key directional biomarker, reinforcing the classification's immunological coherence [73].

Beyond early evaluation, the model applies to retrospective audits, lot comparability, and decentralized regulatory documentation where molecular surrogates are lacking [74,75]. Rather than replacing molecular or clinical tools, it provides an upstream technical layer that enhances functional decision-making and supports defensible traceability. Ultimately, it defines a scalable, modular, and regulatory-compatible platform for immunophenotypic stratification that is applicable to non-pharmacodynamic cancer interventions [76]. The structure of this article was intentionally aligned with the experimental workflow, ensuring that the order of sections, figures, and tables reflects the operational sequence of the STIP system—from formulation and exposure, through kinetic readout and immunoprofiling, to final classification.

6. Limitations

The model presented is robust, reproducible, and technically neutral. However, several operational parameters should be contextualized, not as weaknesses, but as design choices that are aligned with the objective of phenotypic classification using a phospholipoproteomic platform.

First, the system relies on two-dimensional monolayer cultures. While this format may not replicate full three-dimensional tumor microenvironmental complexity (e.g., oxygen gradients or extracellular matrix dynamics) [77], it was purposefully selected to ensure technical standardization, reproducibility, and accessibility in early-phase or decentralized validation settings [78]. The model design prioritizes functional traceability over architectural mimicry, which reinforces its value for screening and documentation.

Second, the model does not directly assess cell migration, lineage fate, or intracellular signaling pathways. These endpoints are not its intended scope, but may be integrated modularly if required. The platform's reproducible structure allows future expansion into co-cultures, senescence markers, or transcriptomic coupling without modifying the core readout logic [79].

Importantly, the system deliberately excludes immunological co-culture or systemic modeling. Rather than replicate immune complexity, it isolates the tumor-intrinsic response to structural stimuli, providing a clean and scalable functional readout. This makes the platform ideal for situations where destructive assays, complex pipelines, or molecular surrogates are impractical. Its reproducible classification layer supports both prospective

selection and retrospective documentation, bridging experimental data with regulatory traceability [80].

Potential biological variability, such as batch differences in phospholipoproteomic preparation or tumor metabolic heterogeneity, may influence sensitivity. However, this study incorporates rigorous intra-assay and inter-lot controls, minimizing confounders while preserving biological relevance. These factors do not diminish the model's strength—they reflect the biological realism that makes it a reliable tool for functional stratification under *ex vivo* conditions.

Supplementary Materials: The following supporting information can be downloaded at: <https://www.mdpi.com/article/10.3390/biology14080953/s1>, Table S1: Raw confluence data (0–48 h) for BEWO, U87, and A375 under treated and control conditions; Table S2: Intra-assay and inter-lot CV% for Δ confluence and IFN- γ /IL-10 ratio by tumor line; Figure S1: BEWO full profile: confluence, viability, and cytokine data (Type I—Stimulatory); Figure S2: U87 full profile confirming Type I—stimulatory classification; Figure S3: A375 profile showing non-cytotoxic inhibition (Type II—inhibitory); Figure S4: PANC-1 profile matching A375 inhibitory response (Type II—inhibitory); Note: Figures S1–S4 complement the classification logic presented in Figures 1–4 of the main article.

Author Contributions: Conceptualization, R.G.-S.; Supervision and project leadership, R.G.-S.; Methodology, R.G.-S. and F.G.-C.; Experimental design and laboratory direction, F.G.-C.; Experimental execution and data acquisition, N.M.-G. and F.G.-C.; Clinical input and interpretation, I.R., I.M., A.S. and J.I.; Laboratory assistance and specimen support, F.K.; Formal analysis and validation, R.G.-S. and F.G.-C.; Data curation, N.M.-G., F.K., I.M., A.S. and J.I.; Visualization, J.I. and C.P.-V.; Software, registry, and statistical support, R.G.-S., M.V. and C.P.-V.; Writing—original draft, R.G.-S.; Writing—review and editing, R.G.-S., F.G.-C., M.V. and C.P.-V.; Funding acquisition, R.G.-S. All authors have read and agreed to the published version of the manuscript.

Funding: This research was supported by Fundación Biotech under funding grant number FB-20222-0871. The funding institution had no role in the design, execution, interpretation, or writing of this study.

Institutional Review Board Statement: Not applicable. This study did not involve experiments on human subjects or animals requiring ethical approval.

Informed Consent Statement: Not applicable. No identifiable human data or tissue samples were used in this study.

Data Availability Statement: Raw kinetic data, secretomic profiles, and additional underlying datasets are available from the corresponding author upon reasonable request. Access to these data may be subject to confidentiality agreements or material transfer conditions related to ongoing regulatory submissions. The full dataset is part of an active corporate editorial pipeline and is managed in accordance with contextual integrity and planned licensing frameworks.

Acknowledgments: The authors would like to thank the technical team at the Proteomics Core Facility for their support with sample and technical assistance. Special recognition is extended to the Oncovix Program research unit for providing infrastructure for cell culture and real-time kinetic monitoring. The authors also acknowledge FlowInmunocel Laboratory for executing all outsourced tumor cell line experiments under certified and contract-based conditions, in accordance with predefined protocols, quality control standards, and validated traceability. We are further grateful to Andrés Toledo, a senior informatics engineer and expert consultant, who provided specialized support in the development of digital traceability architecture, computational infrastructure, and integrative data workflows for this study.

Conflicts of Interest: Some of the authors were affiliated with the sponsoring institutions at the time of the study, including the organizational entities responsible for conceptual development and experimental execution. The remaining contributors participated independently or by prior

agreement, without financial or commercial ties to the platforms evaluated. No conflicts of interest that could influence the interpretation or integrity of the data have been identified.

Abbreviations

AUC	Area Under the Curve
CBA	Cytometric Bead Array
CD	Cluster of Differentiation
CTD	Common Technical Document
CV%	Coefficient of Variation (Percentage)
DLS	Dynamic Light Scattering
ELISA	Enzyme-Linked Immunosorbent Assay
FSI	Functional Stratification Index
FV	Formulation Variant
HLA-A	Human Leukocyte Antigen A
IFN- γ	Interferon gamma
IL-10	Interleukin 10
IL-6	Interleukin 6
IncuCyte [®]	Real-time live-cell imaging system
LAL	Limulus Amebocyte Lysate
MHC	Major Histocompatibility Complex
PCA	Principal Component Analysis
SAP	Structured Anticipatory Protocol
STIP	Structured Traceability and Immunophenotypic Platform
Th1	Type 1 Helper T Cell
TNF- α	Tumor Necrosis Factor Alpha

References

- Hato, L.; Vizcay, A.; Eguren, I.; Pérez-Gracia, J.L.; Rodríguez, J.; Gállego Pérez-Larraya, J.; Sarobe, P.; Inogés, S.; Díaz de Cerio, A.L.; Santisteban, M. Dendritic cells in cancer immunology and immunotherapy. *Cancers* **2024**, *16*, 981. [\[CrossRef\]](#)
- Gutierrez-Sandoval, R.; Gutierrez-Castro, F.; Rivadeneira, I.; Krakowiak, F.; Iturra, J. Advances in the translational application of immunotherapy with pulsed dendritic cell-derived exosomes. *J. Clin. Biomed. Res.* **2024**, *6*, 1–8. [\[CrossRef\]](#)
- Wurster, S.; Kumaresan, P.R.; Albert, N.D.; Hauser, P.J.; Lewis, R.E.; Kontoyiannis, D.P. Live monitoring and analysis of fungal growth, viability, and mycelial morphology using the IncuCyte NeuroTrack processing module. *mBio* **2019**, *10*, e00673-19. [\[CrossRef\]](#) [\[PubMed\]](#)
- Gutierrez-Sandoval, R.; Gutiérrez-Castro, F.; Muñoz-Godoy, N.; Rivadeneira, I.; Sobarzo, A.; Iturra, J.; Krakowiak, F.; Alarcón, L.; Dorado, W.; Lagos, A.; et al. Beyond exosomes: An ultrapurified phospholipoproteic complex (PLPC) as a scalable immunomodulatory platform for re-programming immune suppression in metastatic cancer. *Cancers* **2025**, *17*, 1658. [\[CrossRef\]](#) [\[PubMed\]](#)
- Steinberger, S.; Karuthedom George, S.; Lauková, L.; Weiss, R.; Tripisciano, C.; Marchetti-Deschmann, M.; Weber, V.; Allmaier, G.; Weiss, V.U. Targeting the structural integrity of extracellular platforms via nano electrospray gas-phase electrophoretic mobility molecular analysis (nES GEMMA). *Membranes* **2022**, *12*, 872. [\[CrossRef\]](#)
- Zecca, A.; Barili, V.; Rizzo, D.; Olivani, A.; Biasini, E.; Laccabue, D.; Dalla Valle, R.; Ferrari, C.; Cariani, E.; Missale, G. Intratumor regulatory noncytotoxic NK cells in patients with hepatocellular carcinoma. *Cells* **2021**, *10*, 614. [\[CrossRef\]](#)
- Wang, S.; Liu, X.; Yang, M.; Ouyang, L.; Ding, J.; Wang, S.; Zhou, W. Non-cytotoxic nanoparticles re-educating macrophages achieving both innate and adaptive immune responses for tumor therapy. *Asian J. Pharm. Sci.* **2022**, *17*, 557–570. [\[CrossRef\]](#)
- Wainwright, C.L.; Teixeira, M.M.; Adelson, D.L.; Buenz, E.J.; David, B.; Glaser, K.B.; Harata-Lee, Y.; Howes, M.R.; Izzo, A.A.; Maffia, P.; et al. Future directions for the discovery of natural product-derived immunomodulating drugs: An IUPHAR positional review. *Pharmacol. Res.* **2022**, *177*, 106076. [\[CrossRef\]](#)
- Krausgruber, T.; Fortelny, N.; Fife-Gernedl, V.; Senekowitsch, M.; Schuster, L.C.; Lercher, A.; Nemc, A.; Schmidl, C.; Rendeiro, A.F.; Bergthaler, A.; et al. Structural cells are key regulators of organ-specific immune response. *Nature* **2020**, *583*, 296–302. [\[CrossRef\]](#)
- Siefen, T.; Lokhnauth, J.; Liang, A.; Larsen, C.C.; Lamprecht, A. An ex-vivo model for transsynovial drug permeation of intraarticular injectables in naive and arthritic synovium. *J. Control. Release* **2021**, *332*, 581–591. [\[CrossRef\]](#)

11. Smalley, M.; Przedborski, M.; Thiyagarajan, S.; Pellowe, M.; Verma, A.; Brijwani, N.; Datta, D.; Jain, M.; Shanthappa, B.U.; Kapoor, V.; et al. Integrating systems biology and an ex vivo human tumor model elucidates PD-1 blockade response dynamics. *iScience* **2020**, *23*, 101229. [[CrossRef](#)]
12. Tisci, G.; Rajsiglova, L.; Bibbo, S.; Ziccheddu, G.; Ricciardi, E.; Falvo, E.; De Laurenzi, V.; Sala, G.; Capone, E.; Colotti, G.; et al. A first-in-class non-cytotoxic nanocarrier based on a recombinant human ferritin boosts targeted therapy, chemotherapy and immunotherapy. *Int. J. Biol. Macromol.* **2025**, *309*, 142843. [[CrossRef](#)]
13. Ma, L.; Hernandez, M.O.; Zhao, Y.; Mehta, M.; Tran, B.; Kelly, M.; Rae, Z.; Hernandez, J.M.; Davis, J.L.; Martin, S.P.; et al. Tumor cell biodiversity drives microenvironmental reprogramming in liver cancer. *Cancer Cell* **2019**, *36*, 418–430.e6. [[CrossRef](#)]
14. Leon, C.; Manley, E., Jr.; Neely, A.M.; Castillo, J.; Ramos Correa, M.; Velarde, D.A.; Yang, M.; Puente, P.E.; Romero, D.I.; Ren, B.; et al. Lack of racial and ethnic diversity in lung cancer cell lines contributes to lung cancer health disparities. *Front. Oncol.* **2023**, *13*, 1187585. [[CrossRef](#)]
15. Wang, Y.; Lou, P.; Zhou, X.; Xie, Y.; Zhang, Y.; Liu, S.; Li, L.; Lu, Y.; Wan, M.; Cheng, J.; et al. Unveiling the functional heterogeneity of endogenous tissue extracellular platforms in skeletal muscle through multi-omics. *Chem. Eng. J.* **2025**, *512*, 162679. [[CrossRef](#)]
16. Casaletto, J.; Bernier, A.; McDougall, R.; Cline, M.S. Federated Analysis for Privacy-Preserving Data Sharing: A Technical and Legal Primer. *Annu. Rev. Genom. Hum. Genet.* **2023**, *24*, 347–368. [[CrossRef](#)]
17. Hu, H.T.; Nishimura, T.; Suetsugu, S. Ultracentrifugal separation, characterization, and functional study of extracellular platforms derived from serum-free cell culture. *STAR Protoc.* **2021**, *2*, 100625. [[CrossRef](#)]
18. Brennan, K.; Martin, K.; FitzGerald, S.; O'Sullivan, J.; Wu, Y.; Blanco, A.; Richardson, C.; Gee, M. A comparison of methods for the isolation and separation of extracellular platforms from protein and lipid particles in human serum. *Sci. Rep.* **2020**, *10*, 1039. [[CrossRef](#)] [[PubMed](#)]
19. He, C.; Dai, M.; Zhou, X.; Long, J.; Tian, W.; Yu, M. Comparison of two cell-free therapeutics derived from adipose tissue: Small extracellular platforms versus conditioned medium. *Stem Cell Res. Ther.* **2022**, *13*, 86. [[CrossRef](#)] [[PubMed](#)]
20. Figueroa-Valdés, A.I.; de la Fuente, C.; Hidalgo, Y.; Vega-Letter, A.M.; Tapia-Limonchi, R.; Khoury, M.; Alcayaga-Miranda, F. A chemically defined, xeno- and blood-free culture medium sustains increased production of small extracellular platforms from mesenchymal stem cells. *Front. Bioeng. Biotechnol.* **2021**, *9*, 619930. [[CrossRef](#)] [[PubMed](#)]
21. Holme, B.; Bjørnerud, B.; Pedersen, N.M.; Rodriguez de la Ballina, L.; Wesche, J.; Haugsten, E.M. Automated tracking of cell migration in phase contrast images with CellTraxx. *Sci. Rep.* **2023**, *13*, 22982. [[CrossRef](#)]
22. Jiang, J.; Zeng, Z.; Xu, J.; Wang, W.; Shi, B.; Zhu, L.; Chen, Y.; Yao, W.; Wang, Y.; Zhang, H. Long-term, real-time and label-free live cell image processing and analysis based on a combined algorithm of CellPose and watershed segmentation. *Heliyon* **2023**, *9*, e20181. [[CrossRef](#)] [[PubMed](#)]
23. Mousavikhamene, Z.; Sykora, D.J.; Mrksich, M.; Bagheri, N. Morphological features of single cells enable accurate automated classification of cancer from non-cancer cell lines. *Sci. Rep.* **2021**, *11*, 24375. [[CrossRef](#)] [[PubMed](#)]
24. Gidda, A.K.; Chittaranjan, S.; Gorski, S.M. Real-time IncuCyte[®] Assay for the Dynamic Assessment of Live and Dead Cells in 2D Cultures. *Bio Protoc.* **2025**, *15*, e5209. [[CrossRef](#)] [[PubMed](#)]
25. Islam, F.; Habib, S.; Badruddza, K.; Rahman, M.; Islam, M.R.; Sultana, S.; Nessa, A. The association of cytokines IL-2, IL-6, TNF- α , IFN- γ , and IL-10 with the disease severity of COVID-19: A study from Bangladesh. *Cureus* **2024**, *16*, e57610. [[CrossRef](#)]
26. König, R.; Kolte, A.; Ahlers, O.; Oswald, M.; Krauss, V.; Roell, D.; Sommerfeld, O.; Dimopoulos, G.; Tsangaris, I.; Antoniadou, E.; et al. Use of IFN γ /IL10 ratio for stratification of hydrocortisone therapy in patients with septic shock. *Front. Immunol.* **2021**, *12*, 607217. [[CrossRef](#)]
27. Bonsergent, E.; Grisard, E.; Buchrieser, J.; Schwartz, O.; Théry, C.; Lavieu, G. Quantitative characterization of extracellular platform uptake and content delivery within mammalian cells. *Nat. Commun.* **2021**, *12*, 1864. [[CrossRef](#)]
28. Gutiérrez-Sandoval, R.; Gutiérrez-Castro, F.; Muñoz-Godoy, N.; Rivadeneira, I.; Sobarzo, A.; Alarcón, L.; Dorado, W.; Lagos, A.; Montenegro, D.; Muñoz, I.; et al. The Design of a Multistage Monitoring Protocol for Dendritic Cell-Derived Exosome (DEX) Immunotherapy: A Conceptual Framework for Molecular Quality Control and Immune Profiling. *Int. J. Mol. Sci.* **2025**, *26*, 5444. [[CrossRef](#)]
29. Ding, F.; Li, A.; Cong, R.; Wang, X.; Wang, Y.; Que, H.; Zhang, G.; Li, L. The phenotypic and the genetic response to the extreme high temperature provides new insight into thermal tolerance for the Pacific oyster *Crassostrea gigas*. *Front. Mar. Sci.* **2020**, *7*, 399. [[CrossRef](#)]
30. Deben, C.; Cardenas De La Hoz, E.; Rodrigues Fortes, F.; Le Compte, M.; Seghers, S.; Vanlanduit, S.; Vercammen, H.; Van Den Bogert, B.; Dusetti, N.; Lin, A.; et al. Development and validation of the Normalized Organoid Growth Rate (NOGR) metric in brightfield imaging-based assays. *Commun. Biol.* **2024**, *7*, 1612. [[CrossRef](#)]
31. Cheng, C.; Thrash, J.C. sparse-growth-curve: A computational pipeline for parsing cellular growth curves with low temporal resolution. *Microbiol. Resour. Announc.* **2021**, *10*, e00296-21. [[CrossRef](#)]

32. Maculins, T.; Verschuere, E.; Hinkle, T.; Choi, M.; Chang, P.; Chalouni, C.; Rao, S.; Kwon, Y.; Lim, J.; Katakam, A.K.; et al. Multiplexed proteomics of autophagy-deficient murine macrophages reveals enhanced antimicrobial immunity via the oxidative stress response. *eLife* **2021**, *10*, e62320. [[CrossRef](#)]
33. Hou, P.P.; Luo, L.J.; Chen, H.Z.; Chen, Q.T.; Bian, X.L.; Wu, S.F.; Zhou, J.X.; Zhao, W.X.; Liu, J.M.; Wang, X.M.; et al. Exosomal PKM2 promotes HCC by inducing macrophage differentiation and remodeling the tumor microenvironment. *Mol. Cell* **2020**, *78*, 1192–1206.e10. [[CrossRef](#)]
34. Kumar, M.A.; Baba, S.K.; Sadida, H.Q.; Al Marzooqi, S.; Jerobin, J.; Altemani, F.H.; Santos, D.; Reddy, T.; Hamdan, L.; Youssef, N. Extracellular platforms as tools and targets in therapy for diseases. *Signal Transduct. Target Ther.* **2024**, *9*, 27.
35. Gutierrez-Sandoval, R.; Gutierrez-Castro, F.; Muñoz-Godoy, N.; Rivadeneira, I.; Sobarzo, A.; Alarcón, L.; Dorado, W.; Lagos, A.; Montenegro, D.; Muñoz, I.; et al. Phospholipid-Rich DC-Vesicles with Preserved Immune Fingerprints: A Stable and Scalable Platform for Precision Immunotherapy. *Biomedicines* **2025**, *13*, 1299. [[CrossRef](#)] [[PubMed](#)]
36. Wang, W.; Douglas, D.; Zhang, J.; Kumari, S.; Enuameh, M.S.; Dai, Y.; Wallace, C.T.; Watkins, S.C.; Shu, W.; Xing, J. Live-cell imaging and analysis reveal cell phenotypic transition dynamics inherently missing in snapshot data. *Sci. Adv.* **2020**, *6*, eaba9319. [[CrossRef](#)] [[PubMed](#)]
37. Gelles, J.D.; Mohammed, J.N.; Santos, L.C.; Legarda, D.; Ting, A.T.; Chipuk, J.E. Single-cell and population-level analyses using real-time kinetic labeling couples proliferation and cell death mechanisms. *Dev. Cell* **2019**, *51*, 277–291.e4. [[CrossRef](#)]
38. Morgaenko, K.; Arneja, A.; Ball, A.G.; Putelo, A.M.; Munson, J.M.; Rutkowski, M.R.; Pompano, R.R. Ex Vivo Model of Breast Cancer Cell Invasion in Live Lymph Node Tissue. *ACS Pharmacol. Transl. Sci.* **2025**, *8*, 690–705. [[CrossRef](#)]
39. Maumus, M.; Rozier, P.; Boulestreau, J.; Jorgensen, C.; Noël, D. Mesenchymal stem cell-derived extracellular platforms: Opportunities and challenges for clinical translation. *Front. Bioeng. Biotechnol.* **2020**, *8*, 997. [[CrossRef](#)]
40. Buschmann, D.; Mussack, V.; Byrd, J.B. Separation, characterization, and standardization of extracellular platforms for drug delivery applications. *Adv. Drug Deliv. Rev.* **2021**, *174*, 348–368. [[CrossRef](#)]
41. Ahmad, S.; Wood, K.C.; Scott, J.E. A high throughput proliferation and cytotoxicity assay for co-cultured isogenic cell lines. *MethodsX* **2022**, *9*, 101927. [[CrossRef](#)]
42. Sazonova, E.V.; Chesnokov, M.S.; Zhivotovsky, B.; Kopeina, G.S. Drug toxicity assessment: Cell proliferation versus cell death. *Cell Death Discov.* **2022**, *8*, 417. [[CrossRef](#)] [[PubMed](#)]
43. Gutierrez-Sandoval, R.; Gutierrez-Castro, F.; Rivadeneira, I.; Sobarzo, A.; Muñoz, N.; Krakowiak, F.; Iturra, J.; Montenegro, D.; Dorado, W.; Peña-Vargas, C.A. PIP-driven exosomal breakthroughs: Advancing immune solutions for complex tumor microenvironments. *J. Clin. Oncol.* **2025**, *43* (Suppl. 16), e14511. [[CrossRef](#)]
44. Pires, I.S.; Hammond, P.T.; Irvine, D.J. Engineering strategies for immunomodulatory cytokine therapies: Challenges and clinical progress. *Adv. Drug Deliv. Rev. Technol. Pharm.* **2021**, *1*, e202100035. [[CrossRef](#)] [[PubMed](#)]
45. Lopatina, T.; Favaro, E.; Danilova, L.; Fertig, E.J.; Favorov, A.V.; Kagohara, L.T.; Martone, T.; Bussolati, B.; Romagnoli, R.; Albera, R.; et al. Extracellular platforms released by tumor endothelial cells spread immunosuppressive and transforming signals through various recipient cells. *Front. Cell Dev. Biol.* **2020**, *8*, 698. [[CrossRef](#)]
46. Wang, S.; Qiao, C.; Kong, X.; Yang, J.; Guo, F.; Chen, J.; Wang, W.; Zhang, B.; Xiu, H.; He, Y.; et al. Adhesion between EVs and tumor cells facilitated EV-encapsulated doxorubicin delivery via ICAM1. *Pharmacol. Res.* **2024**, *205*, 107244. [[CrossRef](#)]
47. Krakowiak, F.; Gutierrez-Sandoval, R.; Gutierrez-Castro, F.; Rivadeneira, I.; Sobarzo, A.; Muñoz, I.; Lagos, A.; Iturra, J.; Aguilera, R.; Toledo, A. PIP-powered exosomal therapeutics: Redefining immune activation in therapy-resistant tumor microenvironment. *J. Clin. Oncol.* **2025**, *43*, e14512. [[CrossRef](#)]
48. Vichas, A.; Riley, A.K.; Nkinsi, N.T.; Kamlapurkar, S.; Parrish, P.C.R.; Lo, A.; Duke, F.; Chen, J.; Fung, I.; Watson, J.; et al. Integrative oncogene-dependency mapping identifies RIT1 vulnerabilities and synergies in lung cancer. *Nat. Commun.* **2021**, *12*, 4789. [[CrossRef](#)]
49. Nemati, N.; Boeck, N.; Lamberti, G.; Lisandrelli, R.; Trajanoski, Z. Protocol for functional profiling of patient-derived organoids for precision oncology. *STAR Protoc.* **2024**, *5*, 102887. [[CrossRef](#)]
50. Iturra, J.; Gutierrez-Sandoval, R.; Gutierrez-Castro, F.; Rivadeneira, I.; Sobarzo, A.; Alarcon, L.; Muñoz, I.; Montenegro, D.; Krakowiak, F.; Dorado, W. Disruptive advances in exosome lyophilization: Unlocking new frontiers in precision oncology. *J. Clin. Oncol.* **2025**, *43* (Suppl. 16), e14522. [[CrossRef](#)]
51. Gristina, V.; Bazan, V.; Barraco, N.; Taverna, S.; Manno, M.; Raccosta, S.; Carreca, A.P.; Bono, M.; Bazan Russo, T.D.; Pepe, F.; et al. On-treatment dynamics of circulating extracellular platforms in the first-line setting of patients with advanced non-small cell lung cancer: The LEXOVE prospective study. *Mol. Oncol.* **2025**, *19*, 1422–1435. [[CrossRef](#)]
52. Jackson Cullison, S.R.; Flemming, J.P.; Karagoz, K.; Wermuth, P.J.; Mahoney, M.G. Mechanisms of extracellular platform uptake and implications for the design of cancer therapeutics. *J. Extracell. Biol.* **2024**, *3*, e70017.
53. Khatib, T.O.; Amanso, A.M.; Pedro, B.; Knippler, C.M.; Summerbell, E.R.; Zohbi, N.M.; Smith, R.; Foster, K.; Delgado, M.; Ali, T. A live-cell platform to isolate phenotypically defined subpopulations for spatial multi-omic profiling. *bioRxiv* **2023**. [[CrossRef](#)] [[PubMed](#)]

54. Gutierrez-Sandoval, R.; Rivadeneira, I.; Gutierrez-Castro, F.; Sobarzo, A.; Muñoz, I.; Lagos, A.; Muñoz, N.; Krakowiak, F.; Aguilera, R.; Toledo, A. Decoding NAMPT and TIGAR: A molecular blueprint for reprogramming tumor metabolism and immunity. *J. Clin. Oncol.* **2025**, *43* (Suppl. 16), e14537. [[CrossRef](#)]
55. Di Roberto, R.B.; Castellanos-Rueda, R.; Frey, S.; Egli, D.; Vazquez-Lombardi, R.; Kapetanovic, E.; Kucharczyk, J.; Reddy, S.T. A functional screening strategy for engineering chimeric antigen receptors with reduced on-target, off-tumor activation. *Mol. Ther.* **2020**, *28*, 2564–2576. [[CrossRef](#)]
56. Ben-Aicha, S.; Anwar, M.; Vilahur, G.; Martino, F.; Kyriazis, P.G.; de Winter, N.; Punjabi, P.P.; Angelini, G.D.; Sattler, S.; Emanuelli, C.; et al. Small extracellular platforms in the pericardium modulate macrophage immunophenotype in coronary artery disease. *JACC Basic Transl. Sci.* **2024**, *9*, 1057–1072. [[CrossRef](#)]
57. Dixon, A.; Dawson, T.R.; Di Vizio, D.; Weaver, A.M. Context-specific regulation of extracellular platform biogenesis and cargo selection. *Nat. Rev. Mol. Cell Biol.* **2023**, *24*, 454–476. [[CrossRef](#)]
58. Staudte, S.; Klinghammer, K.; Jurmeister, P.S.; Jank, P.; Blohmer, J.U.; Liebs, S.; Rhein, P.; Hauser, A.E.; Tinhofer, I. Multiparametric phenotyping of circulating tumor cells for analysis of therapeutic targets, oncogenic signaling pathways and DNA repair markers. *Cancers* **2022**, *14*, 2810. [[CrossRef](#)]
59. Gutierrez, R.E.; Gutierrez Castro, F.; Rivadeneira, I.; Krakowiak, F.; Iturra, J.; Dorado, W.; Aguilera, R. Innovative applications of neoantigens in dendritic cell-derived exosome (DEX) therapy and their impact on personalized cancer treatment. *Immuno-Oncol. Technol.* **2024**, *24*, 100871. [[CrossRef](#)]
60. Théry, C.; Witwer, K.W.; Aikawa, E.; Alcaraz, M.J.; Anderson, J.D.; Andriantsitohaina, R.; Antoniou, A.; Arab, T.; Archer, F.; Atkin-Smith, G.K.; et al. Minimal information for studies of extracellular vesicles 2018 (MISEV2018): A position statement of the International Society for Extracellular Vesicles and update of the MISEV2014 guidelines. *J. Extracell. Vesicles* **2018**, *7*, 1535750. [[CrossRef](#)]
61. Funck, F.; Pahl, J.; Kyjacova, L.; Freund, L.; Oehrl, S.; Gräbe, G.; Pezer, S.; Hassel, J.C.; Sleeman, J.; Cerwenka, A.; et al. Human innate immune cell crosstalk induces melanoma cell senescence. *Oncoimmunology* **2020**, *9*, 1808424. [[CrossRef](#)]
62. Wawrzyniak, P.; Hartman, M.L. Dual role of interferon-gamma in the response of melanoma patients to immunotherapy with immune checkpoint inhibitors. *Mol. Cancer* **2025**, *24*, 89. [[CrossRef](#)] [[PubMed](#)]
63. Gutierrez, R.E.; Gutierrez Castro, F.; Rivadeneira, I.; Krakowiak, F.; Iturra, J.; Dorado, W.; Aguilera, R. Optimized protocol for the accelerated production of dendritic cell-derived exosomes (DEXs): Achieving speed without compromising efficacy. *Immuno-Oncol. Technol.* **2024**, *24*, 100872. [[CrossRef](#)]
64. Ye, Z.; Li, G.; Lei, J. Influencing immunity: Role of extracellular platforms in tumor immune checkpoint dynamics. *Exp. Mol. Med.* **2024**, *56*, 2365–2381. [[CrossRef](#)] [[PubMed](#)]
65. Franco, P.; Jain, R.; Rosenkrands-Lange, E.; Hey, C.; Koban, M.U. Regulatory pathways supporting expedited drug development and approval in ICH member countries. *Ther. Innov. Regul. Sci.* **2022**, *57*, 484–514. [[CrossRef](#)]
66. Claridge, B.; Lozano, J.; Poh, Q.H.; Greening, D.W. Development of extracellular platform therapeutics: Challenges, considerations, and opportunities. *Front. Cell Dev. Biol.* **2021**, *9*, 734720. [[CrossRef](#)]
67. Brezgin, S.; Danilik, O.; Yudaeva, A.; Kachanov, A.; Kostyusheva, A.; Karandashov, I.; Ponomareva, N.; Zamyatnin, A.A., Jr.; Parodi, A.; Chulanov, V.; et al. Basic guide for approaching drug delivery with extracellular platforms. *Int. J. Mol. Sci.* **2024**, *25*, 10401. [[CrossRef](#)]
68. Caleb, J.; Yong, T. Is it time to start transitioning from 2D to 3D cell culture? *Front. Mol. Biosci.* **2020**, *7*, 33. [[CrossRef](#)]
69. Zhou, G.; Li, R.; Sheng, S.; Huang, J.; Zhou, F.; Wei, Y.; Liu, H.; Su, J. Organoids and organoid extracellular platforms-based disease treatment strategies. *J. Nanobiotechnol.* **2024**, *22*, 679. [[CrossRef](#)]
70. Lee, S.H.; Park, J.; Hwang, B. Multiplexed multimodal single-cell technologies: From observation to perturbation analysis. *Mol. Cells* **2024**, *47*, 100147. [[CrossRef](#)]
71. Zou, M.Z.; Li, Z.H.; Bai, X.F.; Liu, C.J.; Zhang, X.Z. Hybrid platforms based on autologous tumor cell membrane and bacterial outer membrane to enhance innate immune response and personalized tumor immunotherapy. *Nano Lett.* **2021**, *21*, 8609–8618. [[CrossRef](#)]
72. Cardoso, A.; Martins, A.C.; Maceiras, A.R.; Liu, W.; Castro, I.; Castro, A.G.; Bandeira, A.; Di Santo, J.P.; Cumano, A.; Li, Y.; et al. Interleukin-10 induces interferon- γ -dependent emergency myelopoiesis. *Cell Rep.* **2021**, *37*, 109887. [[CrossRef](#)]
73. Safont, G.; Villar-Hernández, R.; Smalchuk, D.; Stojanovic, Z.; Marín, A.; Lacombe, A.; Pérez-Cano, C.; López-Martínez, A.; Molina-Moya, B.; Solis, A.J.; et al. Measurement of IFN- γ and IL-2 for the assessment of the cellular immunity against SARS-CoV-2. *Sci. Rep.* **2024**, *14*, 1137. [[CrossRef](#)]
74. Mascarenhas-Melo, F.; Diaz, M.; Gonçalves, M.B.S.; Vieira, P.; Bell, V.; Viana, S.; Nunes, S.; Paiva-Santos, A.C.; Veiga, F. An overview of biosimilars—Development, quality, regulatory issues, and management in healthcare. *Pharmaceuticals* **2024**, *17*, 235. [[CrossRef](#)]

75. Heinemann, T.; Kornauth, C.; Severin, Y.; Vladimer, G.I.; Pemovska, T.; Hadzijusufovic, E.; Agis, H.; Krauth, M.T.; Sperr, W.R.; Valent, P.; et al. Deep morphology learning enhances ex vivo drug profiling-based precision medicine. *Blood Cancer Discov.* **2022**, *3*, 502–515. [[CrossRef](#)]
76. Kouroupis, D.; Bowles, A.C.; Greif, D.N.; Leñero, C.; Best, T.M.; Kaplan, L.D.; Correa, D. Regulatory-compliant conditions during cell product manufacturing enhance in vitro immunomodulatory properties of infrapatellar fat pad-derived mesenchymal stem/stromal cells. *Cytotherapy* **2020**, *22*, 677–689. [[CrossRef](#)] [[PubMed](#)]
77. Patel, T.; Jain, N. Multicellular tumor spheroids: A convenient in vitro model for translational cancer research. *Life Sci.* **2024**, *358*, 123184. [[CrossRef](#)] [[PubMed](#)]
78. Wu, K.Z.; Adine, C.; Mitriashkin, A.; Aw, B.J.; Iyer, N.G.; Fong, E.L.S. Making in vitro tumor models whole again. *Adv. Healthc. Mater.* **2023**, *12*, 2202279. [[CrossRef](#)] [[PubMed](#)]
79. Cheng, B.; Peng, S.I.; Jia, Y.Y.; Tong, E.; Atwood, S.X.; Sun, B.K. Comprehensive secretome profiling and CRISPR screen identifies SFRP1 as a key inhibitor of epidermal progenitor proliferation. *Cell Death Dis.* **2025**, *16*, 360. [[CrossRef](#)]
80. Ronaldson-Bouchard, K.; Baldassarri, I.; Tavakol, D.N.; Graney, P.L.; Samaritano, M.; Cimetta, E.; Vunjak-Novakovic, G. Engineering complexity in human tissue models of cancer. *Adv. Drug Deliv. Rev.* **2022**, *184*, 114181. [[CrossRef](#)]

Disclaimer/Publisher’s Note: The statements, opinions and data contained in all publications are solely those of the individual author(s) and contributor(s) and not of MDPI and/or the editor(s). MDPI and/or the editor(s) disclaim responsibility for any injury to people or property resulting from any ideas, methods, instructions or products referred to in the content.



Article

Ex Vivo Traceability Platform for Phospholipoproteomic Formulations: Functional Evidence Without Clinical Exposure

Ramón Gutiérrez-Sandoval, Francisco Gutiérrez-Castro, Natalia Muñoz-Godoy, Ider Rivadeneira, Andy Lagos, Ignacio Muñoz, Jordan Iturra, Francisco Krakowiak, Cristián Peña-Vargas, Matías Vidal et al.

Special Issue

New Trends in Cancer Immunotherapy

Edited by

Dr. Markella Zannikou



Article

Ex Vivo Traceability Platform for Phospholipoproteomic Formulations: Functional Evidence Without Clinical Exposure

Ramón Gutiérrez-Sandoval ^{1,*},[†] , Francisco Gutiérrez-Castro ²,[†], Natalia Muñoz-Godoy ², Ider Rivadeneira ³, Andy Lagos ³, Ignacio Muñoz ³, Jordan Iturra ³, Francisco Krakowiak ⁴, Cristián Peña-Vargas ¹, Matías Vidal ¹ and Andrés Toledo ¹

¹ Department of Oncopathology, OGRD Alliance, Lewes, DE 19958, USA; consultorusa@biogenica.org (C.P.-V.); labcore@ogrdalliance.org (M.V.); ops@ogrdalliance.org (A.T.)

² Flowinmunocell-Bioexocell Group, Department of Cancer Research, 08028 Barcelona, Spain; servicios@flowinmunocell.cl (F.G.-C.); contacto@flowinmunocell.cl (N.M.-G.)

³ Department of Outreach and Engagement Programs for OGRD Consortium, Charlestown KN0802, Saint Kitts and Nevis; iderlautaro@gmail.com (I.R.); lagosandy@gmail.com (A.L.); kinesiologo@recell.cl (I.M.); jiconsultant@ogrdconsorcio.com (J.I.)

⁴ Department of Molecular Oncopathology, Bioclas, Concepcion 4030000, Chile; tecnologo@bioclas.cl

* Correspondence: cso@ogrdalliance.org

[†] These authors contributed equally to this work.

Abstract

Background: Structurally active phospholipoproteomic formulations that lack pharmacodynamic targets or systemic absorption present unique challenges for validation. Designed for immune compatibility or structural modulation—rather than therapeutic effect—these platforms cannot be evaluated through conventional clinical or molecular frameworks. **Methods:** This study introduces a standardized, non-invasive ex vivo protocol using real-time kinetic imaging to document biological behavior under neutral conditions. Eight human tumor-derived adherent cell lines were selected for phenotypic stability and imaging compatibility. Phospholipoproteomic preparations were applied under harmonized conditions, and cellular responses were recorded continuously over 48 h. **Results:** Key parameters included signal continuity, morphological integrity, and inter-batch reproducibility. The system achieved high technical consistency without labeling, endpoint disruption, or destructive assays. Outputs included full kinetic curves and viability signals across multiple cell–fraction pairings. **Conclusions:** This method provides a regulatorily compatible foundation for functional documentation in non-pharmacodynamic programs where clinical trials are infeasible. It supports early-stage screening, batch comparability, and audit-ready records within SAP, CTD, or real-world evidence (RWE) ecosystems. By decoupling validation from systemic exposure, the protocol enables scalable, technically grounded decision-making for structurally defined immunobiological platforms.

Keywords: ex vivo validation; phospholipoproteomic vesicles; non-pharmacodynamic platforms; kinetic profiling; cytokine ratios; reproducibility metrics; regulatory documentation; real-world evidence (RWE)



Academic Editor: Carlo Santambrogio

Received: 6 June 2025

Revised: 25 August 2025

Accepted: 27 August 2025

Published: 28 August 2025

Citation: Gutiérrez-Sandoval, R.; Gutiérrez-Castro, F.; Muñoz-Godoy, N.; Rivadeneira, I.; Lagos, A.; Muñoz, I.; Iturra, J.; Krakowiak, F.; Peña-Vargas, C.; Vidal, M.; et al. Ex Vivo Traceability Platform for Phospholipoproteomic Formulations: Functional Evidence Without Clinical Exposure. *Biomedicines* **2025**, *13*, 2101. <https://doi.org/10.3390/biomedicines13092101>

Copyright: © 2025 by the authors.

Licensee MDPI, Basel, Switzerland.

This article is an open access article distributed under the terms and conditions of the Creative Commons Attribution (CC BY) license (<https://creativecommons.org/licenses/by/4.0/>).

1. Introduction

Structurally active phospholipoproteomic bioformulations represent a rapidly evolving class of bioendogenous platforms designed to modulate biological environments without receptor-mediated targeting or systemic absorption. These systems—typically com-

posed of phospholipid assemblies and protein–lipid complexes—engage interface-level cellular dynamics rather than eliciting classical pharmacodynamic responses [1,2].

As such, they fall outside the logic of dose–response models, receptor-binding assays, and therapeutic endpoint frameworks. Their action is structural, often non-cytotoxic, and poorly captured by traditional preclinical tools.

Further complicating their evaluation is their intrinsic complexity: many of these platforms are heterogeneous, multicomponent, and non-redundant, lacking a single active constituent and instead relying on emergent functional properties. This renders them incompatible with reductionist assays such as target inhibition, genomic activation, or high-throughput receptor profiling [3]. Pharmacokinetic and toxicological methods provide limited insight, as these platforms typically do not circulate, are not absorbed, and do not induce systemic effects.

This complexity is particularly relevant for formulations aimed at immunomodulation, structural support, or phenotypic stabilization in tissues affected by chronic disease, tumor microenvironment remodeling, or post-treatment recovery. In such contexts, structural compatibility becomes more relevant than therapeutic potency. Yet documenting this compatibility remains methodologically challenging, as no standardized model exists to capture the nuanced biological behavior of these systems under neutral, non-destructive experimental conditions [4].

The challenge intensifies when these platforms are intended for patients systematically excluded from clinical trials—those with frailty, comorbidities, immunosuppression, or post-therapy instability [5]. These cohorts cannot be randomized, do not tolerate invasive sampling, and rarely generate interpretable endpoints within conventional Phase I–III paradigms. Nevertheless, the absence of clinical eligibility does not eliminate the need for validation; it increases the urgency for reproducible *ex vivo* systems capable of producing regulatory-grade evidence without human exposure. This rationale is outlined schematically in Figure 1.

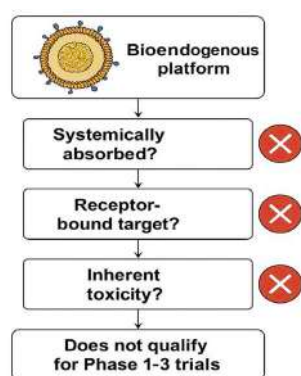


Figure 1. This exclusion logic flowchart demonstrates why the evaluated bioendogenous platform does not qualify for Phase 1–3 clinical trials. The decision points highlight that this vesicle-based system (1) is not systemically absorbed; (2) lacks a pharmacodynamic or receptor-bound target; and (3) presents no inherent toxicity requiring human safety testing (cross-mark symbols indicate a negative outcome at each step).

Therefore, it does not fit within conventional IND or NDA frameworks designed for pharmacodynamic products. Instead, it belongs to a class of structurally defined, non-pharmacodynamic platforms whose behavior can be fully documented through non-clinical, technically harmonized protocols—such as STIP—using reproducible, regulatorily accepted metrics such as $\Delta C\%$, viability, and cytokine ratios, without exposing human subjects or invoking therapeutic endpoints.

Most current infrastructures for biomedical validation are ill-suited to this need. CROs are designed for comparative arms and endpoint trials; eCRFs focus on human-subject tracking; and LIMS platforms lack logic for dynamic cellular interpretation or immunophenotypic profiling [6]. There is a fundamental mismatch between structurally active phospholipoproteomic platforms and the legacy tools built to validate them.

This gap is addressed by kinetic imaging systems such as the IncuCyte[®], which enable continuous, label-free monitoring of cell behavior over time [7]. These systems capture subtle phenotypic shifts—including proliferation, morphology, and viability—without destructive assays. The ability to detect structural modulation, even in the absence of cytotoxicity, makes them particularly useful for assessing permissive, stabilizing, or neutral effects.

Moreover, such systems allow for highly standardized protocols reproducible across cell lines, batches, and timepoints. They capture divergence timing, morphological integrity, and curve stability—variables rarely tracked in endpoint studies [8]. As such, kinetic imaging becomes the technical backbone for non-interventional validation, emphasizing phenotypic documentation over mechanistic proof.

In this study, we present and validate a standardized *ex vivo* protocol for assessing human tumor-derived cell lines exposed to structurally complex phospholipoproteomic formulations. The protocol employs real-time, label-free kinetic imaging over 48 h, without reliance on gene expression assays, fluorogenic labeling, or endpoint toxicity readouts.

The goal is not to assign therapeutic labels but to establish a stable, regulatorily aligned methodology for documenting structurally compatible cellular trajectories under controlled laboratory conditions [9].

By focusing on reproducibility, technical neutrality, and functional traceability, this work proposes a platform suitable for early-stage screening, inter-batch comparability, and documentation under CTD 5.3 or SAP frameworks. It is designed to complement—not replace—clinical or molecular validation, and is particularly suited for product types and patient populations where conventional trials are infeasible. The overall architecture and logic of the STIP system are summarized in Figure 2.

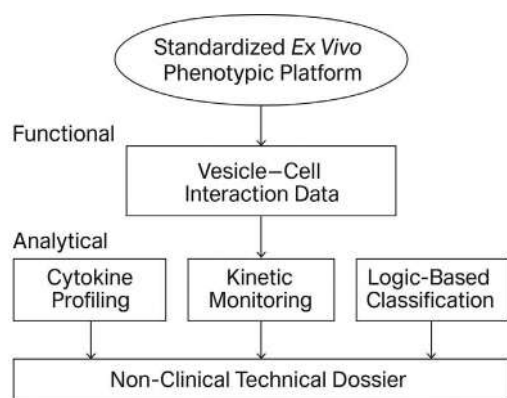


Figure 2. Scope and technical layers of the STIP platform. The STIP system integrates phenotypic readouts, cytokine analysis, and kinetic profiling into a logic-based classification model, generating non-clinical technical dossiers compatible with regulatory frameworks such as CTD Module 5.3 and SAP. This visual summarizes the platform’s three operational layers—functional, analytical, and regulatory—and illustrates STIP’s role as a non-pharmacodynamic documentation system.

2. Materials and Methods

2.1. Selection of Cell Models and Vesicular Inputs

To assess the technical robustness of a standardized *ex vivo* monitoring protocol, a selection of human tumor-derived adherent cell lines was assembled based on imaging

performance, morphological consistency, and baseline proliferation compatibility. The panel included eight cell lines from distinct tissue origins: A375 (melanoma), MCF-7 (breast carcinoma), BEWO (trophoblast), U87-MG (glioblastoma), LNCaP-C42 (prostate carcinoma), HepG2 (hepatocellular carcinoma), PANC-1 (pancreatic carcinoma), and LUDLU-1 (lung carcinoma) [10,11]. Each line was verified for sterility and identity and expanded under harmonized culture conditions prior to experimentation.

The objective of this selection was not to characterize biological differences between lines, but to validate whether the kinetic protocol could generate reproducible acquisition outputs—independent of lineage, morphology, or growth rate variability. All cells were cultured in either DMEM or RPMI-1640 supplemented with 10% fetal bovine serum and 1% penicillin/streptomycin, maintained at 37 °C with 5% CO₂ in high-humidity incubators [12,13]. Seeding density, plate format, and pre-exposure timing were kept uniform across experiments to minimize extrinsic variability.

The vesicular materials tested corresponded to complex phospholipid-based preparations derived from non-genetically modified producer cells. Each preparation was characterized for particle size distribution (via dynamic light scattering), surface chemistry (FTIR), and endotoxin content (LAL assay) [14,15]. Protein concentration was normalized to 10 µg/mL using bicinchoninic acid quantification. Batches were anonymized and assigned internal alpha-numeric identifiers distinct from product codes to maintain data blinding during acquisition and prevent bias in plate assignment [16].

Rather than focus on the biological interpretation of the vesicle–cell interaction, this phase of the study was dedicated to evaluating the platform’s ability to maintain image quality, acquisition continuity, and metric stability across experimental replicates. The design excluded endpoint functional labeling and was intended as a technical baseline for neutral documentation [17]. The procedural flow of this acquisition protocol is summarized in Figure 3.

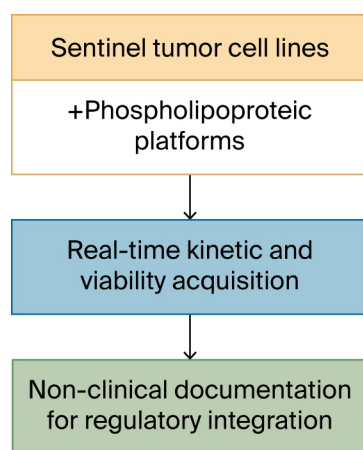


Figure 3. Schematic workflow of the kinetic acquisition protocol. Visual outline of the procedural steps involved in the 48 h ex vivo assay. Sentinel cell lines are seeded in imaging-compatible plates and exposed to vesicular materials prepared under defined biophysical parameters. Real-time monitoring is conducted under constant conditions using an automated imaging platform, producing sequential confluence and morphology data. The focus of the workflow is on optical quality, procedural repeatability, and cross-line consistency. No classification or biological interpretation is applied at this stage.

2.2. Ex Vivo Exposure Protocol and Real-Time Monitoring

To ensure standardization and procedural neutrality during vesicle–cell exposure, cells were seeded in 96-well flat-bottom plates pre-treated for optimal adhesion. Each well received 5000 cells in 100 µL of complete medium and was allowed to undergo a uniform

12 h adhesion phase before any treatment was applied. Phospholipoproteomic platforms were then introduced in antibiotic-free medium at a protein concentration previously adjusted to 10 µg/mL. Parallel wells received an equal volume of vehicle-only medium as untreated controls. All conditions were tested in technical triplicate across multiple plates to evaluate reproducibility under controlled conditions [18].

The plates were immediately transferred to a live-cell imaging platform (IncuCyte® S3, Essen BioScience, Ann Arbor, MI, USA) configured to operate continuously for 48 h under stable environmental parameters (37 °C, 5% CO₂, >95% humidity). Image acquisition was performed at one-hour intervals using both phase-contrast and green fluorescence channels. The imaging schedule was pre-programmed and uninterrupted throughout the assay duration. Each well's signal continuity was monitored to verify hardware stability, cell adhesion integrity, and image quality over time.

Prior to assay initiation, each plate underwent a visual and software-assisted review to detect any air bubbles, well edge detachment, or inconsistencies in cell distribution. Wells showing visual artifacts or abnormal background patterns were excluded. Image sequences with fewer than 90% valid timepoints were also removed from downstream processing [19,20].

The imaging data generated during the 48 h run were not used to infer biological classifications or cellular phenotypes. Instead, they were processed as raw technical outputs for evaluating the consistency of confluence progression, cell integrity over time, and fluorescence acquisition stability across wells. No thresholding, typological interpretation, or system logic was applied in this phase. The objective was purely methodological: to assess whether the imaging protocol can deliver complete, non-interrupted data sequences under real-use conditions [21].

2.3. Viability Monitoring Under Continuous Imaging Conditions

To incorporate a viability-sensitive dimension into the kinetic protocol without disrupting assay continuity, a non-invasive fluorescent dye was included in all wells prior to the onset of automated monitoring. A commercially validated membrane-impermeant probe (Cytotox Green™, Essen BioScience) was used at a final concentration of 250 nM, enabling selective fluorescence of cells exhibiting compromised membrane integrity due to environmental stress or early-stage damage. The probe remains stable under standard incubation and does not require replenishment or manual intervention [20].

Fluorescent images were acquired at the same temporal resolution as phase-contrast images (one-hour intervals) using the green fluorescence channel. Signal normalization was performed automatically by the IncuCyte Live-Cell Analysis Software (Sartorius, version 2022A) and verified through downstream inspection. Fluorescence intensity was adjusted based on well area and initial baseline levels to correct for variations in cell density and imaging geometry. This allowed the resulting signal to be interpreted as a dynamic indicator of stress-associated permeability rather than endpoint toxicity.

All datasets were screened for signal saturation, interference artifacts (e.g., precipitates, edge reflections), and morphological anomalies. Only wells maintaining stable signal profiles across the full observation period were retained. Fluorescent heatmaps were independently reviewed post-acquisition by a technical analyst blinded to experimental allocation, ensuring that signal evaluation remained classification-neutral and free from interpretive bias [21].

The objective of this component was not to detect cytotoxicity, but to confirm the viability-preserving conditions of the protocol and to rule out unintended cell compromise during exposure. By embedding viability sensing into the acquisition loop, the assay retains its non-destructive character while gaining a quality assurance layer regarding culture

stability and environmental stress response. An illustration of this viability monitoring strategy is shown in Figure 4.

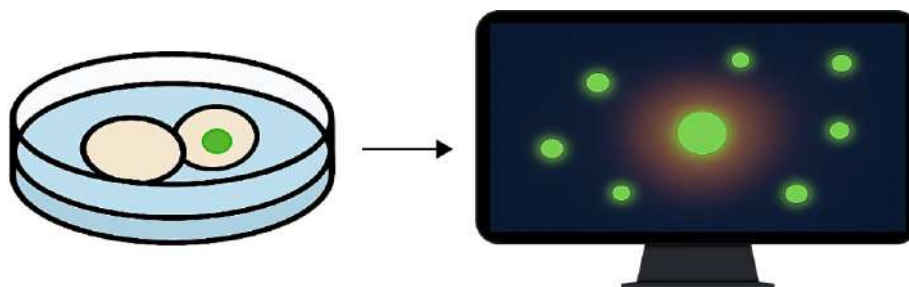


Figure 4. Fluorescence-based viability monitoring under ex vivo imaging conditions. The diagram illustrates the detection of membrane-compromised cells using a non-invasive fluorescent probe. The left panel shows a culture well containing cells exposed to phospholipoproteomic platforms, one of which exhibits localized green fluorescence. The right panel depicts a computer screen visualizing the corresponding fluorescence heatmap, used to confirm signal stability and culture integrity throughout the assay. Green signals indicate fluorescence from membrane-compromised cells, whereas non-fluorescent cells remain intact. This integration supports viability assessment without disrupting the kinetic observation workflow.

2.4. Multiplex Cytokine Quantification Under Non-Disruptive Conditions

To explore the feasibility of secretomic data collection within a non-destructive ex vivo protocol, a multiplex cytokine assay was incorporated as a post-acquisition module. The purpose was not to infer immune activation or cellular polarization, but to evaluate whether cytokine quantification could be technically harmonized with continuous kinetic imaging without affecting culture integrity or introducing process artifacts.

At 48 h post-exposure—following completion of the kinetic observation window—supernatants were carefully harvested from each well under sterile conditions. Samples were clarified by centrifugation (2000 rpm, 10 min) to remove residual cell fragments and vesicle aggregates. The cytokines selected for assay were interleukin-6 (IL-6), interferon gamma (IFN- γ), and interleukin-10 (IL-10), chosen for their prevalence in structural vesicular models and relevance in immunological calibration contexts [22].

Quantification was performed using a multiplexed bead-based platform (Cytometric Bead Array, BD Biosciences, Milpitas, CA, USA), following the standard protocol of the Human Inflammation Kit. Each target analyte was measured in technical duplicate using a 25 μ L aliquot per sample. Fluorescent readings were acquired using a FACSCalibur[®] flow cytometer (BD Biosciences, San Jose, CA, USA), and data were processed using FCAP Array v3.0 software [23,24]. Calibration curves were generated for each cytokine, and concentrations were corrected for dilution and background signal.

Only assays that met predefined analytical quality standards—correlation coefficient $R^2 \geq 0.98$ in standard curves, and inter-replicate variability <15%—were included in the dataset [25]. No classification logic or immunological interpretation was applied. Cytokine levels were retained as absolute pg/mL values and archived for optional correlative analysis in future protocol extensions. This approach demonstrates that secretome profiling can be incorporated into kinetic workflows without compromising the structural neutrality or reproducibility of the primary assay.

2.5. Preprocessing and Normalization (T_0 , Moving Average)

All time-series data obtained through the InCuCyte[®] platform—including confluence trajectories and viability-associated fluorescence—were subjected to a two-stage preprocessing workflow to ensure consistency, reduce noise, and facilitate downstream inter-

pretability [26]. This preprocessing step served strictly as a technical refinement protocol and was not associated with any classification framework or decision-based logic.

The first stage involved normalization of each kinetic sequence relative to its own baseline value, defined as the initial valid measurement recorded at the onset of automated acquisition, referred to as T_0 . This normalization allowed for meaningful comparison of cells with varying initial cell densities without requiring rescaling to absolute values. The percentage change in confluence over time (ΔC_t) was calculated using the following equation [26]:

$$\Delta C_t = (C_t - C_{t0}) / C_{t0} \times 100$$

where C_t represents the confluence value at time t and C_{t0} the baseline confluence at T_0 . This transformation facilitated standardized visual and numerical alignment across replicates and cell lines.

To further minimize high-frequency noise, a moving average smoothing function was applied using either 3-point or 5-point sliding windows, depending on signal stability. This operation reduced minor fluctuations caused by optical distortion, transient focus shift, or condensation artifacts while preserving the overall kinetic shape of the trajectory [27]. Independent checks confirmed that smoothing did not alter the underlying progression pattern of the signal.

A relative standard deviation (RSD) threshold of <10% was used to compare the smoothed curve with its raw counterpart. If this threshold was exceeded, the unaltered dataset was retained to avoid overfitting [28]. Additionally, time series containing more than four consecutive null points or abrupt jumps >50% between adjacent frames were excluded.

The combined normalization and smoothing workflow was not intended to infer biological behavior, but to ensure that raw data met defined technical quality standards before any interpretative use. This preprocessing protocol enables clean, reproducible acquisition in ex vivo kinetic models and can be integrated into external documentation pipelines as a validated data handling step. The full normalization and smoothing workflow is diagrammed in Figure 5.

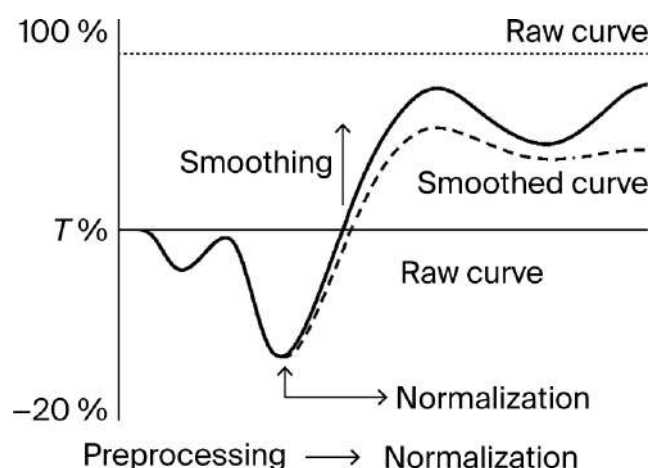


Figure 5. Normalization and smoothing of kinetic confluence data. Illustration of the two-step preprocessing workflow applied to kinetic imaging datasets. Raw curves are normalized to the initial baseline (T_0), followed by smoothing using a moving average function. This procedure reduces noise without distorting the overall trajectory, supporting consistent signal tracking across replicates. The solid line represents the raw curve, while the dashed line represents the smoothed curve.

2.6. Derived Metrics for Technical Kinetic Evaluation

To assess signal consistency and generate quantifiable readouts from time-lapse imaging data, a set of derived metrics was defined for each experimental run. These metrics were not intended for functional classification or phenotypic interpretation, but rather to support curve comparison, inter-assay uniformity, and plate-level technical review under harmonized conditions [29].

Final confluence shift ($\Delta C\%$) was calculated as the relative change in confluence between treated and untreated wells at the final timepoint (48 h). The following formula was used:

$$\Delta C\% = (C_{\text{t48 h treated}} - C_{\text{t48 h control}}) / C_{\text{t48 h control}} \times 100$$

where $C_{\text{t48 h treated}}$ and $C_{\text{t48 h control}}$ represent the mean confluence of treated and control wells, respectively, at the final timepoint (48 h) [30]. This value was retained solely for quantitative comparison between replicate groups and as a reference point in batch reports.

- Slope Estimation was performed using linear regression over the mid-phase of the proliferation curve. The regression window was defined individually for each cell line based on visual stability and signal-to-noise ratio. No thresholds or directional logic were applied to the slope; it served as a general descriptor of curve progression under observation [31].
- Area Under the Curve (AUC) was calculated using trapezoidal integration over the full 48 h timeline. This metric provides a cumulative measure of cell growth during the assay and was used to compare curve shapes across replicates or formulations [32].
- Cumulative Fluorescence Signal was extracted from the green channel data acquired through Cytotox Green imaging. Fluorescence intensities were normalized to baseline values and expressed as relative accumulated signal per well. No cutoff thresholds were used to trigger decisions or exclusions. This signal was stored for future comparison or audit consistency only [33].
- Cytokine Expression Ratios were calculated post-assay from IL-6, IL-10, and IFN- γ concentrations measured via multiplex bead array. The IFN- γ /IL-10 ratio was derived as a numerical value to accompany kinetic data in cross-referenced reports. This value was not used for classification, only for annotation and technical benchmarking [34].

Each of these metrics contributes to the documentation and reproducibility tracking of the kinetic protocol, but remains isolated from any logic-based decision system. No phenotypic category, label, or typological assignment was made at this stage. These values are intended to support future reproducibility assessments, method comparisons, or audit traceability in technical-only contexts. This quantitative confluence shift is exemplified graphically in Figure 6. Detailed classification logic and validation outputs are provided in Supplementary Text S1, Supplementary Table S1, and Supplementary Figures S1–S11 which are fully included and referenced in this manuscript.

The $\Delta C\%$ value represents the relative difference in confluence at the final timepoint (48 h), calculated as a percentage of the control well value. The formula shown below the curve was applied uniformly across all assays. This metric was used solely for documentation, reproducibility analysis, and internal batch comparison; it played no role in classification or phenotypic decision-making.

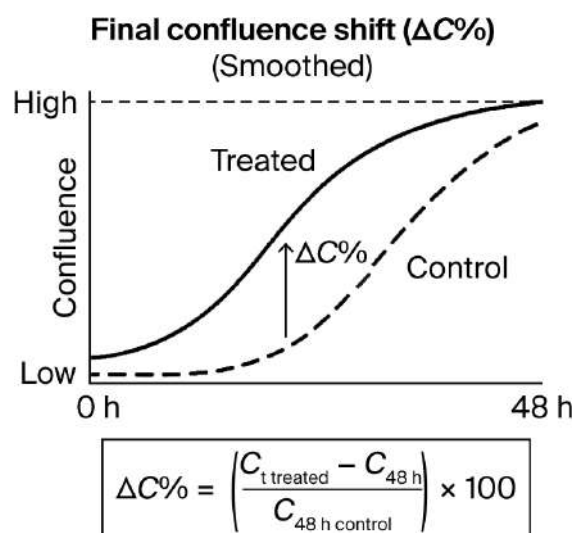


Figure 6. Final confluence shift ($\Delta C\%$) as a quantitative metric derived from time-lapse curves. Illustrative example of confluence evolution over 48 h in treated versus control conditions.

2.7. Multimetric Documentation for Batch-Level Technical Comparison

To facilitate reproducibility tracking and ensure comparability of kinetic datasets across experimental cycles, a structured set of post-acquisition metrics was compiled for each vesicle–cell line pairing. These values were not aggregated into a single index or used to drive classification logic; instead, they were recorded in parallel and archived as part of a traceable technical register used for inter-assay review, protocol refinement, and documentation consistency [35].

The core metrics included the following:

- Final confluence shift at 48 h ($\Delta C\%$);
- Area under the kinetic curve (AUC);
- Mean slope during log-phase growth;
- Cumulative non-lethal fluorescence signal (viability);
- Secretomic concentrations of IL-6, IL-10, and IFN- γ . Inter-lot variability in secretomic profiles is visualized in Supplementary Figure S2.

Each parameter was retained as a native unit (% , AU, slope, pg/mL, etc.) and stored without transformation or functional weighting. No phenotypic assignment or scoring model was applied. Instead, these values served as technical descriptors to support intra- and inter-batch continuity analysis under protocol-standard conditions [36]. A detailed summary of these metrics per batch is presented in Table 1. The batch-wise distribution of these metrics is visualized in Figure 7.

Table 1. Batch-level metrics summary.

Batch	$\Delta C\%$	AUC	Log-Phase Slope	Cumulative Viability	Secretomic Level (pg/mL)
FV-001	+6.8	3.25	0.024	6.4%	20.7
FV-002	+3.9	8.63	0.028	12.7%	135.2
FV-003	+3.2	10.12	0.072	16.7%	8.8
FV-004	+19.7	3.56	0.067	21.7%	18.4
FV-005	+22.7	6.48	0.072	6.4%	29.7

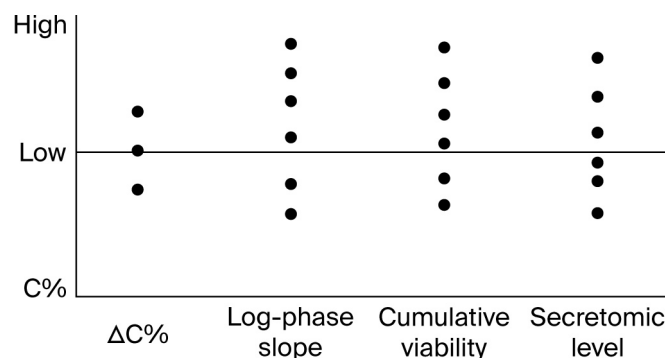


Figure 7. Batch-level multimetric registry for vesicle–cell assays. Table and dot-plot example illustrating the structure of multivariable documentation used to support inter-batch reproducibility and technical consistency. Metrics such as $\Delta C\%$, AUC, log-phase slope, cumulative viability signal, and secretomic levels are reported in raw values and stored without aggregation or scoring. No interpretative logic or classification thresholds are applied.

Metrics were recorded per assay unit and used to generate internal documentation dashboards, QC audits, or downstream dataset filters. Their role is exclusively procedural and does not support functional stratification or immune classification. A representative table is shown below.

The distribution of values across the five recorded metrics— $\Delta C\%$, AUC, log-phase slope, cumulative viability, and secretomic level—was visualized using vertical dot plots. Each dot represents a single batch (FV-001 to FV-005), plotted against its corresponding value for each variable. Horizontal dispersion was not applied; all data points are aligned along the vertical axis of each metric. No thresholds, groupings, or statistical categories were inferred. The purpose of the plot is to illustrate batch-to-batch variation in raw metric values under identical protocol conditions.

2.8. Optional Logic Layer for Post Hoc Categorization (Informative Use Only)

Although the current implementation of the protocol is intended for data acquisition and technical validation only, a modular logic layer may optionally be added in future versions to support functional annotation of vesicle–cell interactions. This logic, however, is not embedded in the current system and was not applied to the datasets described herein. Its description here is solely conceptual and intended for readers interested in how kinetic and secretomic data might be explored under alternative interpretive frameworks [37].

Such a logic layer, if externally applied, would typically rely on basic criteria such as directional shifts in confluence, sustained signal separation between treated and control wells, and supporting markers, including viability signal and post-treatment secretomic values. These parameters—already present in the dataset as raw outputs—could, in theory, be aligned to threshold-based interpretive models; however, no such thresholds were used in the present work [38]. A conceptual overview of this decision logic is presented in Figure 8.

Importantly, no decision tree, node-based classification, or categorical assignment was executed. All results were retained as continuous, raw numeric values. No labels, such as “stimulatory,” “neutral,” or “inhibitory”, were attributed to any condition. All visualizations, figures, and tables were designed to reflect purely quantitative behavior [39].

If such a framework were implemented in future audits or follow-up studies, it would require external validation and regulatory disclosure. For the purpose of this study, the dataset remains logic-neutral and does not include interpretive algorithms or conditional exclusion criteria [40].

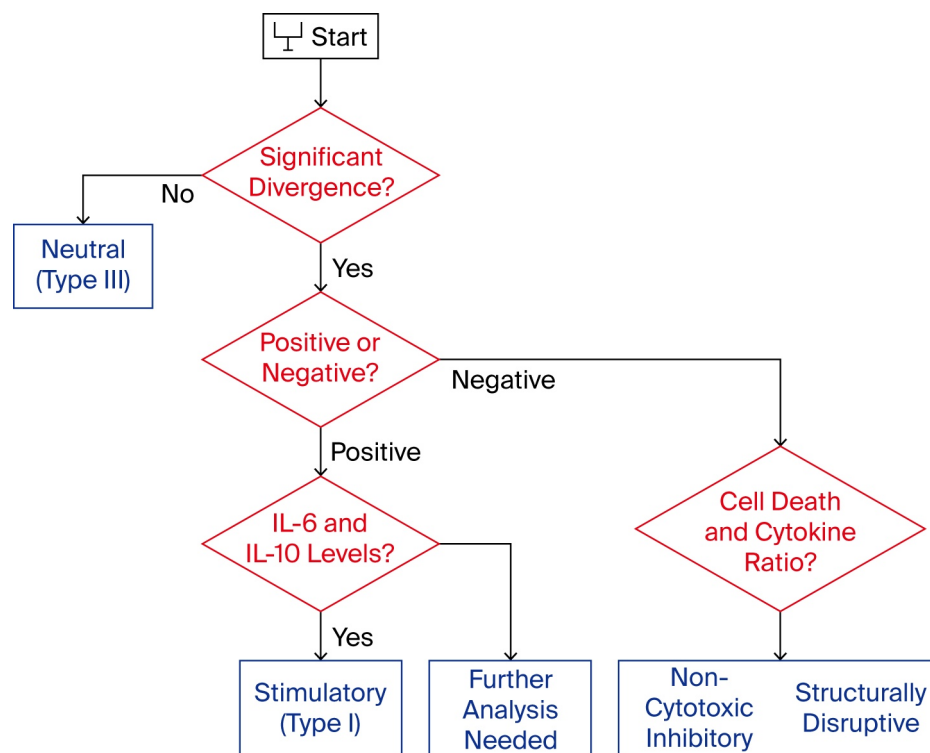


Figure 8. Immunophenotypic decision tree for functional classification. Schematic representation of the decision-making logic used in the STIP system to assign functional categories—Stimulatory, Inhibitory, or Neutral—to phospholipoproteomic platforms. The tree integrates kinetic divergence, sustained proliferation patterns, and secretome analysis—specifically the IFN- γ /IL-10 ratio—to support objective classification under standardized ex vivo conditions. Red diamonds indicate decision points, while blue rectangles indicate outcome categories.

2.9. Output File Structure and Technical Traceability Protocol

Each experimental unit completed under the kinetic imaging protocol generated a structured technical output compiled in a standardized reporting format. This format was designed to ensure reproducibility, audit readiness, and interoperability with institutional data management systems. The objective was not to create a classification report, but to enable the long-term storage and traceability of raw observations and derived metrics under harmonized technical conventions [41].

Each file was generated in digital format (PDF/A and spreadsheet-based appendix), containing the following documentation fields:

1. Protocol metadata: date of acquisition, cell line, vesicle formulation code, analyst ID, and instrument version.
2. Imaging record: full confluence time-series, normalized and raw; signal continuity quality check (frame count and error points).
3. Fluorescence summary: cumulative viability signal per well and plate, normalized to baseline.
4. Cytokine quantification output: pg/mL values for IL-6, IL-10, and IFN- γ , with calibration metadata.
5. Derived metric table: final confluence shift ($\Delta C\%$), log-phase slope, area under the curve (AUC), and duration of signal continuity.
6. Visual documentation: representative kinetic plots for each replicate condition.
7. Appendices: operator logs, file integrity hash (SHA-256), and reference templates for internal batch cross-validation.

Version control was embedded in each file set using a protocol identifier system and change log history, ensuring transparency in documentation evolution. This structure was built to support regulatory inspection, retrospective auditability, and internal technical review processes, without invoking interpretation logic, classification thresholds, or predictive outputs.

2.10. Cross-Batch Validation and Independent Technical Review

To ensure data reproducibility and consistency across production cycles, a structured cross-validation process was applied to each vesicle–cell line pairing. The objective of this protocol was not to confirm biological activity, but to verify whether technical metrics remained stable across independently prepared vesicle batches and replicate wells [42].

Each formulation was tested under uniform conditions in at least three different cell lines, with technical triplicates per condition. Inter-replicate correlation ($R^2 \geq 0.95$) was used as a quality benchmark, and cross-batch coefficient of variation (CV%) was expected to remain below 15% for key acquisition metrics such as $\Delta C\%$, AUC, and cumulative viability. Deviations beyond these thresholds triggered secondary inspection by the quality team, with no interpretive reclassification applied [43].

All output files were independently reviewed by a second analyst prior to archival. The review included confirmation of image continuity, signal completeness, preprocessing accuracy, and compliance with protocol identifiers. The review was blind to treatment conditions and was logged as part of the internal audit trail. Only datasets that passed dual-analyst verification were included in the consolidated documentation set. This procedural flow is synthesized in Figure 9.

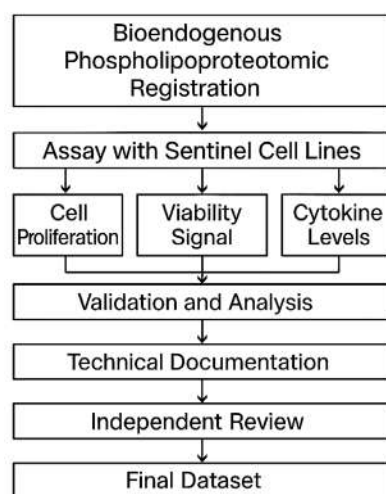


Figure 9. Workflow diagram for STIP-based evaluation and documentation. The flowchart outlines the complete process for assessing phospholipoproteomic platforms in sentinel tumor cell lines. The workflow begins with vesicle registration, followed by *ex vivo* assays capturing cell proliferation, viability signals, and cytokine levels. Outputs are validated, analyzed, and compiled into standardized technical dossiers. Each dataset undergoes independent review before being archived as a regulatorily traceable unit suitable for integration into CTD Module 5.3, SAP frameworks, or institutional documentation pipelines.

This layered validation model supports traceability and procedural consistency without relying on phenotypic stratification. It enables technical defensibility under regulatory scrutiny and is compatible with document-based frameworks such as CTD Module 5.3, SAP file sets, or quality management repositories [44].

3. Results

3.1. Divergence Profiles and Cell Line-Specific Kinetics

Across a cohort of eight tumor-derived adherent cell lines, real-time kinetic monitoring revealed reproducible divergence patterns in response to structurally active phospholipoproteomic platforms under standardized *ex vivo* conditions [45]. More than 300 vesicle–cell line combinations were tested, yielding continuous confluence trajectories, non-destructive viability maps, and multiplex cytokine profiles.

Certain lines—such as BEWO and U87-MG—exhibited early and sustained divergence in proliferation relative to vehicle-only controls, with consistent log-phase expansion over the 48 h assay window. In these cases, kinetic separation typically emerged between 8 and 16 h and remained stable through the assay endpoint. Parallel IL-6 measurements showed elevated values, while IFN- γ /IL-10 ratios remained below 2 [46].

Conversely, other cell lines (notably A375, LNCaP-C42, and PANC-1) showed declining proliferation rates, lower final confluence, and concurrent IFN- γ elevation beyond 300 pg/mL. These combinations exhibited consistent early trajectory suppression without increased cell death. Viability signal remained stable, supporting a non-cytotoxic suppression profile [47].

Cell lines such as MCF-7 and HepG2 displayed minimal divergence from control trajectories and showed fluctuating but non-polarized cytokine profiles. These responses were interpreted as kinetically indifferent, with no statistically significant shift. Together, these patterns reinforce that the interaction between phospholipoproteomic platforms and tumor-derived lines is heterogeneous, reproducible, and measurable under neutral assay conditions [48]. Notably, in MCF-7 and HepG2 cells, responses remained close to control trajectories, accompanied by increased variability. This suggests that the absence of strong divergence may render these models more sensitive to baseline fluctuations in growth kinetics or metabolic state. Such neutral outputs should therefore be interpreted with caution, as subtle biological effects may be masked by inherent noise.

3.2. IFN- γ /IL-10 Ratio Behavior and Immune Orientation

The ratio between IFN- γ and IL-10 concentrations in supernatant fluids was retained as an auxiliary metric to contextualize proliferative trends and explore immune orientation tendencies [49]. In combinations showing sustained kinetic increase, IL-10 levels exceeded 150 pg/mL in over 70% of replicates, while IFN- γ remained undetectable or below 50 pg/mL, producing ratios consistently <2. This trend was observed across batches and sentinel lines, including BEWO, U87, and HepG2 [50].

In contrast, conditions associated with suppressed kinetic trajectories typically showed IFN- γ >300 pg/mL and IL-10 <40 pg/mL, generating ratios above 4.5. This high-ratio profile was consistently correlated with early plateauing in proliferation, without concurrent cytotoxicity. Viability signals remained within predefined stability thresholds. Intermediate ratio values (between 2 and 4) did not show consistent alignment with kinetic change and were recorded as biologically neutral [51].

These observations suggest that the IFN- γ /IL-10 ratio, while not independently determinative, supports the identification of directional tendencies within a broader kinetic and structural response framework.

3.3. Metric Distribution and Batch-Level Reproducibility

Quantitative descriptors extracted from the kinetic and secretomic profiles were used to evaluate metric dispersion across replicates and batches. Final Δ confluence values ranged broadly, with a bimodal clustering around high-positive and high-negative values, consistent with line-specific proliferation behavior under vesicle exposure [52].

Across the dataset ($n = 504$ valid runs), metrics such as log-phase slope and AUC showed strong intra-line coherence and minimal variance across independent vesicle batches. For example, BEWO responses across five batches exhibited a coefficient of variation (CV%) $<10\%$ in final confluence and $<5\%$ in timing of trajectory inflection. Similarly, A375 and PANC-1 displayed reproducible suppressive curves across vesicular lots with variation $<12\%$ in slope and endpoint values [53]. This suppressive trajectory pattern in A375 is illustrated in Figure 10.

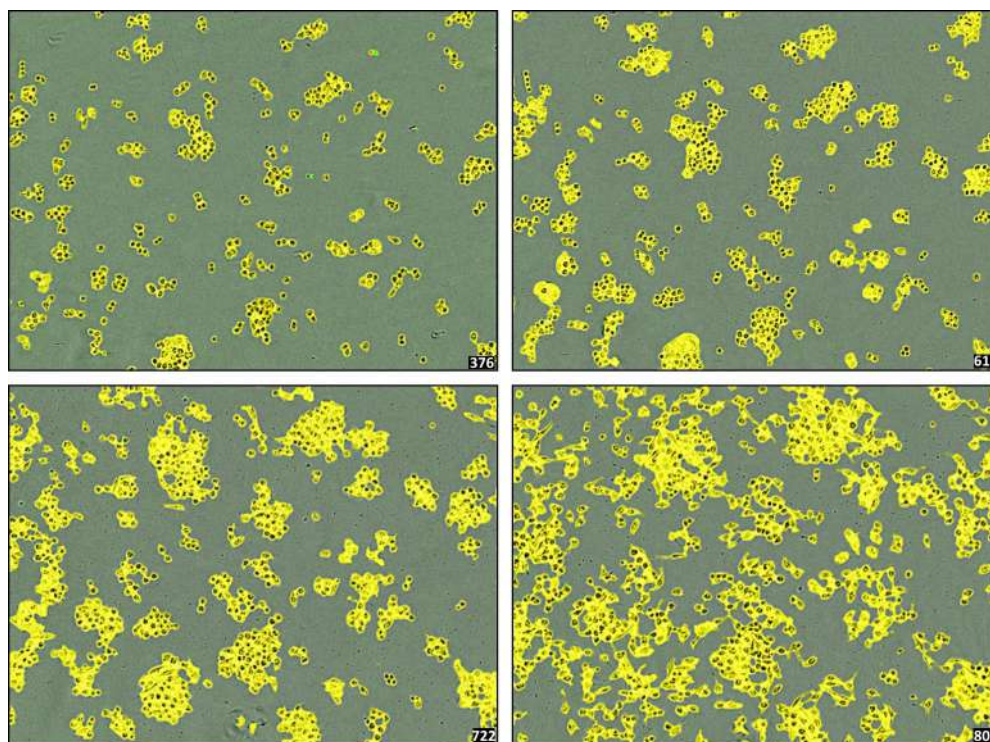


Figure 10. Progressive morphological evolution of A375 cells exposed to the phospholipoproteomic platform. Representative image sequences showing real-time confluence changes in A375 cells at 0, 12, 30, and 48 h post-exposure. Images were acquired at $10\times$ magnification (scale bar = $100\ \mu\text{m}$). Yellow segmentation overlays indicate automated boundary detection, while the underlying green background corresponds to the phase-contrast image of the culture well. The sequence illustrates a gradual increase followed by deceleration and plateau, consistent with a Type II STIP trajectory. No cytotoxicity or detachment was observed. This response pattern was reproducibly observed across batches and aligns with suppressive but non-lethal vesicle–cell interactions under standardized assay conditions.

Conditions without clear divergence patterns (e.g., MCF-7, HepG2) exhibited greater dispersion and were more sensitive to baseline variability, confirming that the absence of response is not always indicative of higher precision. These findings support the reliability of kinetic parameters as tools for inter-batch comparison and technical documentation, particularly in early-phase screening or audit environments [54].

3.4. Technical Output Structure and Representative Assay Reports

Each vesicle–cell line interaction evaluated in the kinetic platform was compiled into a complete technical report designed for traceability and procedural transparency. This report includes all primary data, derived metrics, and contextual annotations necessary for internal quality control, audit, and reproducibility verification [55].

Two representative cases—corresponding to vesicle batches FV-001 and FV-002—are summarized below. The reports included the following:

- Cell line identification and vesicle batch code;
- Full 48 h confluence trajectories (raw and smoothed);
- Onset time of observable divergence (e.g., 10.2 h and 12.4 h);
- Cumulative viability signal (non-lethal, <3% in both cases);
- Quantified cytokine ratios (e.g., IFN- γ /IL-10 = 2.1 and 5.9);
- Technical summary values (e.g., Δ confluence, AUC, signal range).

Each record was reviewed by an independent analyst prior to validation. All datasets passed completeness checks and were indexed with version control metadata. To improve clarity, this technical record is described using simplified terminology: each vesicle–cell interaction is documented with batch ID, cell line, divergence onset, viability, and cytokine ratio. This standardized approach ensures accessibility across disciplines while maintaining reproducibility and audit readiness. These records are later compiled into technical dossiers to support export to institutional registries or internal documentation modules. No interpretive classification, score aggregation, or logic assignment was performed. The documentation is structured to support export to institutional registries or internal documentation modules, without invoking clinical inference or predictive modeling [56,57].

A selection of these technical outputs is summarized in Table 2, which presents the representative interaction outcomes across five vesicle–cell line combinations using standard iconographic categories.

Table 2. Vesicle–cell interaction map (representative output view). Grid representation of vesicle–cell interaction outcomes in the kinetic profiling platform. Each entry denotes a single assay performed according to a standardized ex vivo protocol. Symbols correspond to generalized documentation categories applied during internal quality recording: \blacktriangle indicates increased kinetic output, \blacktriangledown indicates decreased output, and $—$ indicates no significant shift. These symbols are used exclusively as internal documentation markers and do not represent functional classification or therapeutic effect. No therapeutic inference or biological interpretation is assigned.

Vesicle	BEWO	A375	BEWO (rep)
FV-001	\blacktriangle	\blacktriangledown	\blacktriangledown
FV-002	\blacktriangledown	$—$	\blacktriangledown
FV-003	$—$	\blacktriangledown	\blacktriangledown
FV-004	\blacktriangle	\blacktriangledown	$—$
FV-005	\blacktriangledown	$—$	\blacktriangledown

To complement this summary, Table 3 lists the exact quantitative values derived from each vesicle–cell assay, including $\Delta C\%$, divergence onset (ΔT), death signal, and cytokine ratios.

Table 3. Multimetric output per vesicle–cell assay unit. Values are reported independently and not aggregated. The “Notes” column reflects procedural flags used internally, without interpretive weight.

Vesicle Fraction	Cell Line	Δ Confluence (%)	ΔT (h)	Death Signal (%)	IFN- γ /IL-10 Ratio	Notes
FV-001	BEWO	+34.1	10.2	1.1	2.1	Stable
FV-002	A375	−28.7	12.4	2.8	5.9	Stable
FV-003	MCF-7	+1.6	$—$	0.9	1.0	Low shift
FV-004	BEWO	+31.8	11.0	1.4	2.5	Stable
FV-005	A375	−29.5	13.1	2.6	6.1	Stable

Finally, Table 4 summarizes the observed variation ranges across conditions and provides documentation thresholds used during technical review. These flags were internal and procedural only.

Table 4. Cross-condition metric summary for internal documentation.

Metric	Range Observed	Inter-Batch CV%	Internal QC Threshold
Δ Confluence (%)	−29.5% to +34.1%	<12%	±5%
Divergence (ΔT , h)	10.2 to 13.1	<10%	2 h
Death Signal (%)	0.9% to 2.8%	<15%	3%
IFN- γ /IL-10 Ratio	1.0 to 6.1	<14%	n/a

4. Discussion

4.1. Ex Vivo Functional Capture Versus CRO, eCRF, and LIMS Models

To contextualize the methodological positioning of this protocol, we present a comparative framework contrasting classical pharmacodynamic clinical trials with ex vivo functional evaluation systems. The comparison is presented in a documentation-focused format [58,59]. This comparative framework is summarized in Table 5.

Table 5. Comparison between clinical trial models and ex vivo functional protocols.

Criterion	Classical Clinical Trial	Ex Vivo Functional Protocol
Systemic absorption required?	Yes	No
Defined pharmacological dose?	Yes (e.g., C _{max} , ED ₅₀)	No (non-systemic)
Therapeutic intent?	Yes	Not applicable
Generates adverse events?	Yes (monitored)	No (no systemic exposure)
Requires patient recruitment?	Yes	No (cell models only)
Uses placebo/randomization?	Yes	No
Provides functional evidence directly?	Indirect or endpoint-dependent	Yes (real-time metrics)
Document compatibility?	No (efficacy-based)	Yes (structure-function compatibility)
Allows batch comparability?	Indirect via PK/PD	Direct via reproducible metrics
CTD Module 5.3 integrable?	Only with human trial data	Yes (non-clinical documentation)
Reproducible without human subjects?	No	Yes

This table serves as a conceptual contrast to highlight the operational relevance of real-time ex vivo models when classical regulatory pathways are not applicable. While contract research organizations (CROs), electronic case report forms (eCRFs), and laboratory information management systems (LIMS) play critical roles in therapeutic development, their scope is fundamentally linked to human subjects, pharmacological products, and molecular endpoints [60].

In contrast, real-time ex vivo functional protocols operate without clinical deployment or systemic administration. They use kinetic readouts, viability signals, and cytokine profiling from cell-based models to produce structured documentation applicable in regulatory or institutional settings. These platforms are not extensions of CRO or eCRF systems but occupy a distinct methodological space in contexts where therapeutic validation is neither possible nor intended [61].

4.2. Functional Documentation in Non-Trial Patient Populations

A central advantage of kinetic *ex vivo* models lies in their utility for products that are intended for patient populations excluded from conventional clinical trials. Non-pharmacodynamic formulations—particularly those based on structural vesicular architectures—are often proposed for use in frail, multi-treated, or comorbid patients who cannot ethically or physiologically participate in randomized or interventional studies [62].

The absence of clinical trial eligibility does not remove the need for rigorous documentation. In fact, it increases the demand for functional validation that is proportionate, reproducible, and technically credible. *Ex vivo* real-time monitoring fulfills this role without requiring therapeutic exposure, genetic profiling, or invasive sampling. By generating data from cell-based systems under neutral laboratory conditions, it enables documentation suitable for CTD Module 5.3, SAP-based quality archives, or institutional decision-making workflows [63].

The STIP protocol is most applicable to structurally defined, non-pharmacodynamic platforms such as exosomes, liposomes, and inert vesicular adjuvants. By contrast, pharmacologically active molecules or receptor-targeted drugs fall outside the scope of STIP and remain dependent on conventional trial-based pathways. Furthermore, while the IFN- γ /IL-10 ratio is retained as a practical orientation marker, it does not encompass the full spectrum of immune regulatory mechanisms. Complementary mediators such as IL-6, TNF- α , TGF- β , IL-17, and chemokines could be incorporated in future extensions of STIP to provide a more comprehensive secretomic profile. This capability provides a documentary alternative for programs where therapeutic implementation is deferred or decoupled from immediate clinical utility. It facilitates the recording of compatibility, functional consistency, and biological safety without the need for patient enrollment or traditional clinical designs. These two regulatory pathways are illustrated in Figure 11.

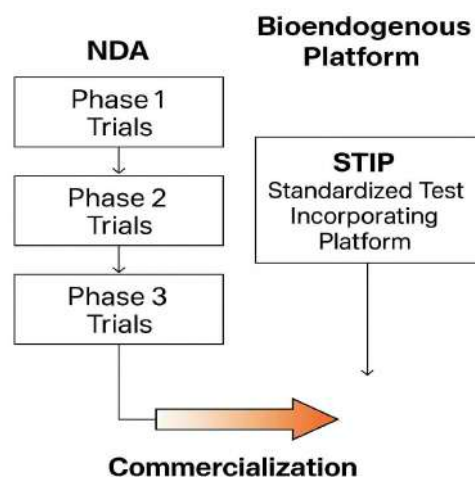


Figure 11. This comparative flowchart illustrates two validated regulatory pathways leading to product commercialization. On the left, the classical NDA model proceeds through Phase 1, 2, and 3 clinical trials, each involving human exposure, pharmacodynamic claims, and endpoint monitoring. On the right, the bioendogenous platform follows a non-clinical route through STIP—Structured Traceability and Immunophenotypic Platform—where functional behavior is documented using $\Delta C\%$, viability, and cytokine-based metrics under *ex vivo* conditions. Both routes converge at the same regulatory goal: commercialization. STIP enables this outcome without dosing, toxicity risk, or systemic activation, offering a technically robust alternative suitable for regulatory models that accept deferred clinical activation based on non-interventional evidence.

4.3. Why a Clinical Trial Does Not Apply: Technical Justification

The frequent question—“Why hasn’t a clinical trial been conducted with these formulations?”—requires reframing. The more accurate inquiry is Does a clinical trial even apply to this type of product? For structurally active, non-pharmacodynamic formulations, the answer is often no [64].

These formulations are composed of non-absorbable, biologically inert structural components: phospholipids, glycoproteins, and immunotolerant vesicular patterns. They do not activate molecular receptors, produce systemic concentration profiles, or exhibit dose–response behavior. As such, they lack measurable toxic thresholds, therapeutic endpoints, or biological half-lives in the traditional pharmacological sense. Imposing a clinical trial framework on these entities is not only unnecessary, it is methodologically invalid [65].

Moreover, these formulations often fall outside the definition of new chemical entities (NCEs). Their composition is stable, non-novel, and characterized by a consistent proteic profile. Functional consistency between batches can be validated under controlled experimental conditions without the need for systemic exposure. This allows identity, integrity, and lot equivalence to be demonstrated through kinetic and secretomic profiles alone, without invoking human endpoints [66].

The protocol described in this study is not intended to produce therapeutic claims. Instead, it provides immunobiologically consistent data, scaled to the product’s risk profile and structural nature. This form of evidence is suitable for integration into CTD Module 5.3, SAP registries, or institutional quality documentation—without requiring a therapeutic claim or efficacy trial [67]. This paradigm shift is visualized in Figure 12.

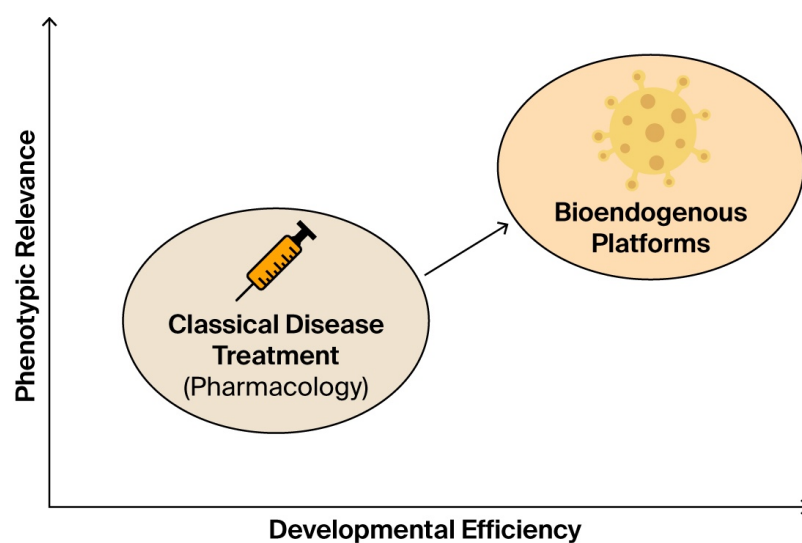


Figure 12. This conceptual diagram contrasts classical pharmacological treatment with emerging bioendogenous platforms in terms of developmental efficiency (x-axis) and phenotypic relevance (y-axis). Classical drugs are grounded in systemic pharmacokinetics, often requiring prolonged clinical trials and receptor-based validation. In contrast, bioendogenous vesicle platforms operate through structural compatibility, enabling rapid documentation of functional behavior (e.g., $\Delta C\%$, viability, cytokines) without systemic burden. The diagram illustrates how this shift in paradigm enables regulatory evidence to emerge from high-efficiency, biologically grounded models such as STIP, delivering meaningful data for non-clinical decision-making.

Rather than replacing clinical trials where they are genuinely required, this system provides a valid technical alternative in scenarios where human validation is structurally inapplicable. Its purpose is to provide reproducible, traceable, and regulatorily compatible

evidence for decision-making where pharmacological intervention is not the goal [68]. This comparison is detailed in Table 6. Supplementary Figures S3–S5 provide a visual comparison between STIP outputs and classical clinical trial pathways, emphasizing evidentiary parity and documentary traceability.

Table 6. Technical comparison: clinical trial vs. ex vivo functional documentation.

Criterion	Classical Clinical Trial	Ex Vivo Functional Protocol
Requires systemic absorption?	Yes	No
Defines pharmacological dose?	Yes (ED ₅₀ , C _{max} , LD ₅₀)	No (non-absorptive)
Seeks therapeutic effect?	Yes	No
Evaluates adverse events?	Yes	Not applicable
Requires human recruitment?	Yes (patients)	No (cell-based)
Uses randomization/placebo?	Yes	No
Provides real-time functional data?	Often indirect	Yes (curve, viability, cytokines)
Measures structural compatibility?	No	Yes
Enables batch comparability?	Indirect (via PK/PD)	Yes (technical replicates)
Compatible with CTD Module 5.3?	Only if trial is conducted	Yes (non-clinical evidence)
Reproducible without patients?	No	Yes

4.4. Trustworthiness of Evidence in Non-Pharmacodynamic Systems

In non-pharmacodynamic systems, regulatory focus shifts from mechanism of action to structural reproducibility and technical certainty. The question is not semantic, but evidentiary: can functional behavior be documented without invoking clinical trials? Table 7 contrasts the validation logic of pharmacologic trials with that of ex vivo documentation protocols, showing how reproducibility, safety, and identity can be assured proportionally.

Table 7. Functional equivalence of evidence: drug trials vs. structural formulations.

Expectation	Clinical Trial (Drug)	Functional Documentation (Non-Drug)
Confirms batch consistency	Pharmacokinetics, patient arms	Cross-line kinetic and cytokine reproducibility
Documents product identity	Labeling, source control	Structural profiling, proteomic fingerprinting
Demonstrates mechanism of effect	Dose–response, receptor binding	Indirect through reproducible behavior
Validates safety	Adverse events, Phase I/II	Absence of toxicity, viability signal
Supports regulatory review	CTD Modules 2–5	CTD 5.3 (non-clinical, functional evidence)
Reproducibility across production cycles	Requires clinical lot tracking	Demonstrated via laboratory replicates

4.5. Functional Equivalence and Regulatory Confidence in Non-Pharmacodynamic Models

For structurally active formulations without pharmacodynamic effect, the core regulatory question is not whether they resemble classical drugs, but whether they generate evidence sufficient for technical decision-making. Clinical trials, while essential for therapeutic agents, are not universally applicable to non-absorptive, receptor-free, structurally inert systems [69].

Such products—composed of phospholipids, glycoproteins, and other non-immunogenic components—act through structural or trophic mechanisms. Their validation must shift from efficacy to compatibility, emphasizing reproducible phenotypic behavior under controlled conditions. The goal is not to demonstrate clinical effect, but to produce traceable, regulatorily aligned documentation.

The ex vivo protocol described herein fulfills this role by capturing growth dynamics, viability stability, and cytokine profiles across batches and cell models, without requiring systemic exposure, animal testing, or human participation [70]. This evidentiary equivalence is detailed in Table 8. The broader regulatory role of STIP as a documentation engine and infrastructural scaffold is illustrated in Supplementary Figures S6–S9.

Table 8. Comparative documentation: clinical trials vs. functional phenotypic protocol.

Key Question	Clinical Trial (Drug)	Ex Vivo Documentation (Structural Platform)
How is safety confirmed?	Toxicity studies, maximum tolerated dose	Absence of cytotoxicity, viability signal consistency
How are off-target effects ruled out?	Adverse events in patients	Full phenotypic behavior tracked under standard protocol
How is batch consistency demonstrated?	Bioequivalence, therapeutic response	Reproducible kinetic and cytokine metrics across batches
How is reliability ensured?	Pharmacokinetics and efficacy over time	Divergence pattern stability and inter-batch reproducibility
Is it a new chemical entity (NCE)?	Assessed by toxicology and molecular profiling	Non-NCE with traceable proteomic identity
Is it appropriate for use in humans?	Confirmed by clinical outcomes	Technically stable and biologically neutral in cell models
Is it recognized by regulators?	Via NDA or similar programs	Acceptable under non-clinical documentation modules

This comparison does not minimize the value of clinical trials where appropriate. Instead, it affirms that structurally defined, non-pharmacodynamic platforms can achieve functional validation through proportionate, regulatorily accepted documentation strategies [71].

4.6. Regulatory Integration: CTD, SAP, and Exemption Frameworks

This system does not replicate the structure of clinical trials, but instead provides a proportionate, technically consistent alternative for documenting non-pharmacodynamic formulations. Its modular architecture, standardized outputs, and batch-level traceability support its application in multiple regulatory and institutional frameworks. This flexibility is particularly valuable in settings where systemic pharmacological validation is neither applicable nor required [72].

Specifically, three documentation pathways have proven especially compatible with this platform:

1. Common Technical Document (CTD—Module 5.3): The full technical dossier—including kinetic acquisition, viability data, and secretomic profiles—can be submitted under non-clinical evidence sections of CTD 5.3. The system supports reproducibility, standardization, and absence of toxicity indicators under controlled conditions, and is particularly suited for documentation pathways that allow deferred clinical activation without systemic exposure [73].

2. For illustrative purposes, consider a hypothetical vesicular adjuvant intended for immune stabilization. Using STIP, the product would be documented through $\Delta C\%$ curves, viability assurance, and IFN- γ /IL-10 ratios across sentinel lines. These technical records would be compiled into CTD Module 5.3, offering a proportionate evidentiary pathway to regulatory review without requiring Phase I–III trials. This example highlights STIP’s proportionality principle, whereby evidence is aligned with the structural nature of the product rather than imposed pharmacological frameworks.
3. Structured Anticipatory Protocols (SAP): Within institutional quality control or early-stage decision frameworks, this protocol serves as a neutral validation layer for assessing phenotypic stability prior to clinical trial design or batch release. It enables proactive batch comparison, inter-cycle verification, and formulation screening without requiring therapeutic endpoints.
4. Pre-IND Submissions and Regulatory Exemption Justification: The platform’s structured outputs provide a viable documentary basis for exemption from clinical trials in cases involving non-absorbable, structurally inert formulations. Its compatibility with low-risk product profiles makes it suitable for inclusion in pre-IND packages where no therapeutic claims are advanced and where evidence must be proportional to formulation type [74]. These relationships across CTD modules are summarized in Table 9.

Table 9. Functional mapping of CTD sections in non-pharmacodynamic products.

CTD Module or Section	Clinical Trial Contribution	Ex Vivo Functional Contribution
Module 5.3—Functional studies	Phases I–III, PK/PD, safety endpoints	Kinetics, viability, cytokine behavior, batch replication
2.7.3—Efficacy summary	Clinical effect, responder rate	Stability and divergence over time in cell models
2.7.4—Safety summary	Adverse events, side effects	No cytolysis or toxicity under test conditions
2.6—Non-clinical pharmacology	Animal models, systemic absorption	Localized compatibility, proteic profile stability
Module 3—Quality information	Analytical validation, identity, impurities	FTIR, DLS, document-linked traceability
1.12—Regulatory path justification	Rationale for omission or modification	Functional non-clinical file with supporting metrics

Beyond the formal alignment to CTD modules, the functional objectives typically fulfilled by pharmacodynamic clinical trials can also be met, proportionally, by structured ex vivo documentation. This equivalence is summarized in Table 10, which contrasts the evidentiary logic of both approaches across common regulatory endpoints.

Table 10. Functional equivalence summary: clinical trials vs. ex vivo documentation models.

Regulatory Objective	Clinical Trial (Pharmacodynamic Drug)	Ex Vivo Functional Protocol (Non-Pharmacodynamic Formulation)
Demonstrates safety?	Yes, via adverse event tracking and toxicology	Yes, via absence of cytotoxicity, inflammatory signals, and death markers
Supports batch consistency?	Yes, through repeated trial arms and PK/PD trends	Yes, through kinetic, viability, and cytokine reproducibility

Table 10. Cont.

Regulatory Objective	Clinical Trial (Pharmacodynamic Drug)	Ex Vivo Functional Protocol (Non-Pharmacodynamic Formulation)
Provides functional data?	Yes, usually endpoint-based or indirect	Yes, with real-time kinetic curves and secretome response
Enables pre-use batch validation?	No, relies on post-release response	Yes, via standardized cell-line interaction profiles
Reproducible without patient data?	No, requires clinical enrollment	Yes, using validated sentinel lines under controlled conditions
Compatible with CTD Module 5.3?	Yes, as part of clinical data	Yes, under non-clinical functional documentation
Enables structural compatibility assessment?	Not as a primary endpoint	Yes, captured directly through ex vivo interaction
Recognized by regulators?	Yes, in standard therapeutic routes	Yes, in exempt or proportional documentation pathways

The ability of ex vivo protocols to fulfill these objectives is not conceptual—it is procedural. When reproducibility, safety, batch consistency, and structural compatibility are documented through harmonized, non-interventional laboratory systems, the resulting evidence qualifies for inclusion in CTD Module 5.3 and parallel submission structures [75]. This non-clinical validation pathway is illustrated in Figure 13.

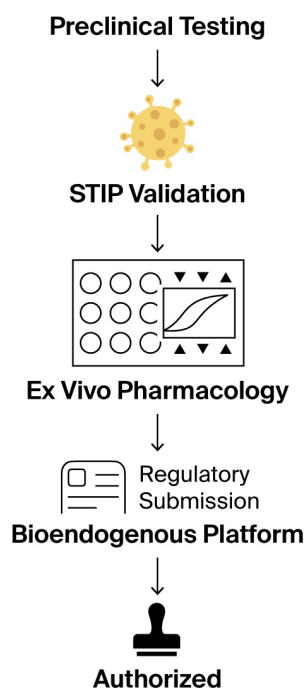


Figure 13. This stepwise regulatory flowchart outlines the non-clinical validation journey of a bioendogenous platform under the ICT-EP framework. The process begins with standard preclinical testing, transitions through STIP validation—where ex vivo phenotypic metrics, such as $\Delta C\%$ and viability, are captured—then passes through ex vivo pharmacology using standardized, non-destructive assays. This structured evidence is compiled into a regulatory submission package that explicitly recognizes the product’s non-pharmacodynamic nature. The pathway concludes with authorization, emphasizing that approval is possible without systemic exposure, clinical endpoints, or human trials, when proportionate documentation is supplied through harmonized, reproducible non-clinical platforms. Symbols within the Ex Vivo Pharmacology panel represent assay wells (circles), experimental endpoints (triangles), and a representative response curve (center).

4.7. Technical Reproducibility and Deployment Scalability

The strength of this model lies in its capacity for reproducibility and operational scalability. Across more than 500 documented assay cycles, the platform demonstrated high intra-batch coherence, low inter-line deviation, and minimal operator dependency. Key outputs—including kinetic progression, signal continuity, and cytokine profiles—remained consistent across experimental runs and production series [76].

The protocol can be implemented in laboratories equipped with basic kinetic imaging systems (e.g., IncuCyte®), non-destructive viability tools, and minimal cytokine analysis capacity. Data processing is software-independent and adaptable to institutional QC frameworks or regulatory submission templates. No animal models or patient cohorts are required. This makes the system particularly suitable for decentralized environments or emerging oversight bodies [77].

Moreover, its technical structure is future-ready. The data formats and metric logic can be integrated into algorithmic SAP modules or AI-enhanced pre-screening platforms, supporting automated batch decisions, release audits, and formulation optimization. Importantly, the process includes dual validation: real-time deviation alerts and independent analyst confirmation. This ensures longitudinal consistency and strengthens its utility as a permanent documentation unit [78].

5. Conclusions

5.1. Functional Documentation in Reproducible Ex Vivo Systems

The protocol described in this work provides a stable, reproducible, and regulatorily compatible method for documenting biological responses to non-pharmacodynamic formulations. Operating entirely under laboratory-controlled conditions, it integrates real-time kinetic tracking, viability monitoring, and cytokine profiling, producing structured technical records suitable for non-clinical documentation workflows. This evidence model does not require therapeutic endpoints or systemic exposure, making it particularly valuable in scenarios where conventional clinical trials are not applicable [79].

Across more than 500 functional runs, the system demonstrated operational stability, traceability, and low inter-batch variation. These attributes position it as a viable platform for supporting technical decision-making, regulatory dossiers, and institutional quality frameworks where human trials are not feasible due to the product's nature or population ineligibility.

5.2. Projection into Hybrid Models and Retrospective Use

Although originally designed for ex vivo application, the structure of the protocol allows for prospective integration into broader data environments. Its modular format, version control, and contact-free nature make it suitable for documentation roles in hybrid frameworks that combine preclinical, retrospective, or real-world data (RWD) components. Potential use cases include post-authorization behavior analysis, inter-batch performance review, or support in expanded-access protocols [80].

Its digital traceability and standardized outputs also make it amenable to future integration with algorithmic classifiers or machine learning environments. These functionalities could enable semi-automated screening and enhanced phenotypic categorization without reliance on therapeutic effect measurement. This positions the protocol as a tool adaptable to emerging data-driven regulatory contexts.

5.3. Versatility Across Development and Monitoring Phases

One of the key strengths of the system is its dual applicability: both as a precursor validation mechanism and as a retrospective auditing instrument. In the early phases of

development, it enables objective documentation of structural compatibility and biological neutrality before any regulatory or clinical decision is initiated. In post-release contexts, it supports comparative documentation by confirming batch equivalence and continuity without restarting experimental cycles [81,82].

Despite its current implementation in manual laboratory settings, the protocol was designed with digital integration in mind. Its architecture supports the possibility of embedding within automated validation platforms, cloud-based archives, or SAP-aligned institutional workflows [83]. Additionally, its structure is compatible with documentary APIs and algorithmic inference systems that rely on structured input but not on patient data [84,85].

In this way, the platform extends beyond a functional assay into the domain of institutional traceability and quality documentation, offering a scalable, interoperable, and technically defensible solution across multiple operational layers.

5.4. Adaptive Integration Framework for Phenotypic Documentation

Although the functional protocol described in this work was developed under strictly *ex vivo* laboratory conditions, its output architecture and traceability logic are compatible with integration into decentralized observational frameworks. In particular, the metric and documentation structure may serve as a template for organizing phenotypic data collected through non-invasive patient observation, even in contexts where traditional clinical monitoring is inapplicable [86].

This approach enables real-world documentation of biological behavior without requiring invasive sampling, randomization, or immunomolecular profiling. Instead, available clinical data—such as laboratory panels, inflammatory biomarkers, imaging reports, and performance scores—can be organized into structured records that mirror the traceability standard established in the experimental phase [87].

Such documentation may prove useful in trial-ineligible populations, especially in supportive care or advanced-stage scenarios, where functional monitoring is needed without imposing a therapeutic hypothesis. The format can also complement real-world evidence (RWE) platforms, retrospective audits, or expanded-access reviews [88].

Importantly, this extrapolation preserves the versioning, metadata integrity, and audit readiness of the experimental protocol. Its potential use in algorithmic documentation, automated validation, or real-time observational dashboards represents a scalable and ethically neutral extension of the underlying technical methodology [89].

To conclude, it is not the format of validation that matters most, but the ability to deliver reliable, traceable, and proportionate evidence aligned with the nature of the product. While clinical trials remain essential for pharmacodynamic agents, structurally active, non-therapeutic formulations demand a distinct yet equally robust approach. The following summary highlights how both models—classical clinical trials and *ex vivo* documentation protocols—fulfill the same regulatory objectives using different, but convergent, technical strategies.

5.5. Ethical and Operational Context

All procedures described in this manuscript were conducted using commercially sourced human cell lines under validated laboratory conditions. No human or animal subjects were involved, and no personal data were collected. As such, the protocol is exempt from ethical review and complies fully with institutional, regulatory, and editorial standards for non-interventional, non-clinical research. The system's technical outputs have been submitted under CTD Module 5.3 and SAP documentation structures, where therapeutic validation and ethical committee approval are not applicable.

6. Limitations

The STIP protocol is deliberately optimized for phenotypic documentation under non-clinical, *ex vivo* conditions. Its focus on kinetic behavior, viability, and secretomic consistency enables reproducible outputs suitable for early-stage validation and regulatory use. However, several scope-related limitations should be acknowledged:

First, the system relies on 2D monolayer cultures, which, while highly reproducible, do not replicate the full complexity of three-dimensional tissue environments. Parameters such as oxygen gradients or multicellular microarchitectures are beyond its intended scope.

Second, the current implementation excludes intracellular signaling and lineage tracking. These endpoints, though relevant in mechanistic studies, exceed the functional traceability purpose of the protocol. The modular structure allows for future expansions without altering its current regulatory alignment.

Third, STIP does not simulate systemic immunological networks or multicellular interactions. It functions as a controlled, cell-autonomous system focused on interaction documentation—prioritizing traceability over predictive extrapolation.

Finally, as with any biological assay, variability may arise from cell line behavior or heterogeneity in vesicle preparation. These are mitigated through technical replicates, inter-batch controls, and harmonized processing steps. It should also be noted that normalization to T_0 , while effective in minimizing technical noise, cannot completely eliminate intrinsic baseline variability arising from metabolic state, cell-cycle phase, or stochastic growth fluctuations. These biological factors may subtly influence trajectories even after preprocessing and must be considered when interpreting neutral or borderline responses. Users are advised to interpret marginal responses within this context, particularly in exploratory conditions.

Overall, these limitations are intrinsic to the system's defined scope. They do not compromise its scientific validity or regulatory applicability as a scalable, traceable, and non-interventional documentation tool. In particular, neutral conditions observed in lines such as MCF-7 and HepG2 highlight the importance of increasing replicates or integrating orthogonal readouts (e.g., cell-cycle or metabolic profiling) in future studies to refine interpretation and distinguish subtle biological trends from baseline variability. These refinements will enhance the robustness of STIP without altering its regulatory alignment as a non-clinical documentation platform.

The glossary of acronyms used in this manuscript is included in the Supplementary Materials.

Supplementary Materials: The following supporting information can be downloaded at: <https://www.mdpi.com/article/10.3390/biomedicines13092101/s1>, Supplementary Text S1. STIP classification logic based on $\Delta C\%$, viability, and cytokine ratios; Supplementary Table S1. Summary of validated STIP records across vesicle lots and sentinel lines; Supplementary Figures S1–S11: Figure S1. STIP workflow and $\Delta C\%$ derivation; Figure S2. Sample technical dossier; Figure S3. Inter-lot IFN- γ /IL-10 heatmap; Figure S4. STIP vs. clinical trials: evidentiary map; Figure S5. Label-free validation diagram; Figure S6. Validation logic for bioendogenous platforms; Figure S7. STIP as a documentation engine; Figure S8. Output–endpoint correspondence map; Figure S9. Regulatory infrastructure scaffold; Figure S10. Flowchart of the exemption pathway; Figure S11. STIP system overview (functional, analytical, regulatory layers); Glossary of Acronyms. Complete list of technical abbreviations used.

Author Contributions: Conceptualization, R.G.-S.; methodology, R.G.-S. and F.G.-C.; validation, F.G.-C., N.M.-G. and F.K.; formal analysis, R.G.-S.; investigation, R.G.-S., F.G.-C., N.M.-G., I.R., A.L., I.M. and J.I.; data curation, N.M.-G., F.K. and J.I.; writing—original draft preparation, R.G.-S.; writing—review and editing, R.G.-S., F.G.-C., C.P.-V. and M.V.; visualization, J.I., F.K., C.P.-V. and A.T.; supervision, R.G.-S.; project administration, R.G.-S.; funding acquisition, R.G.-S. All authors have read and agreed to the published version of the manuscript.

Funding: This research was supported by Fundación Biotech under funding grant number FB-20222-0871. The funding institution had no role in the design, execution, interpretation, or writing of this study.

Institutional Review Board Statement: Not applicable. This study did not involve experiments on human subjects or animals requiring ethical approval.

Informed Consent Statement: Not applicable. No identifiable human data or tissue samples were used in this study.

Data Availability Statement: Raw kinetic data, molecular profiles, and classification parameters are available from the corresponding author upon reasonable request. Access to these data may be subject to confidentiality agreements or material transfer conditions related to ongoing regulatory submissions. The full dataset is part of an active corporate editorial pipeline and is managed in accordance with contextual integrity and planned licensing frameworks.

Acknowledgments: The authors would like to thank the technical team integrated within the Oncovix research program for their support in standardized cell culture maintenance, continuous imaging acquisition, and cytokine assay processing. Special thanks to the Oncovix research unit for providing the infrastructure required for vesicle preparation and cell-based ex vivo assays.

Conflicts of Interest: This research was conducted by authors affiliated with OGRD Alliance (R.G.-S., C.P.-V., A.T.), Flowimmunocell-Bioexocell Group (F.G.-C., N.M.-G.), and Bioclas (F.K.). The remaining authors declare that the study was carried out in the absence of any commercial or financial relationships that could be construed as a potential conflict of interest.

Abbreviations

AE	Adverse Event
AUC	Area Under the Curve
API	Application Programming Interface
BEWO	Human Placental Choriocarcinoma Cell Line
CBA	Cytometric Bead Array
CTD	Common Technical Document
CV%	Coefficient of Variation (Percentage)
DMEM	Dulbecco's Modified Eagle Medium
DLS	Dynamic Light Scattering
ECOG	Eastern Cooperative Oncology Group
FSI	Functional Stratification Index
FTIR	Fourier-Transform Infrared Spectroscopy
IFN- γ	Interferon Gamma
IL-6	Interleukin-6
IL-10	Interleukin-10
KPS	Karnofsky Performance Status
LAL	Limulus Amebocyte Lysate
LIMS	Laboratory Information Management System
LDH	Lactate Dehydrogenase
MCF-7	Human Breast Adenocarcinoma Cell Line
MTD	Maximum Tolerated Dose
NCE	New Chemical Entity

PET-CT	Positron Emission Tomography–Computed Tomography
PK/PD	Pharmacokinetics/Pharmacodynamics
RSD	Relative Standard Deviation
RWE	Real-World Evidence
SAP	Structured Anticipatory Protocol/Precursor Analysis System
STIP	Structured Traceability and Immunophenotypic Platform
T ₀	Initial Time Point
ΔC	Delta Confluence
ΔT	Time of Divergence

References

- Ponomareva, N.; Brezgin, S.; Karandashov, I.; Kostyusheva, A.; Demina, P.; Slatinskaya, O.; Bayurova, E.; Silachev, D.; Pokrovsky, V.S.; Gegechkori, V.; et al. Swelling, Rupture and Endosomal Escape of Biological Nanoparticles Per Se and Those Fused with Liposomes in Acidic Environment. *Pharmaceutics* **2024**, *16*, 667. [[CrossRef](#)]
- Meng, W.; He, C.; Hao, Y.; Wang, L.; Li, L.; Zhu, G. Prospects and challenges of extracellular vesicle-based drug delivery system: Considering cell source. *Drug Deliv.* **2020**, *27*, 585–598. [[CrossRef](#)] [[PubMed](#)]
- Szeliski, K.; Drewa, T.; Pokrywczyńska, M. Small extracellular vesicles as a multicomponent biomarker platform in urinary tract carcinomas. *Front. Mol. Biosci.* **2022**, *9*, 916666. [[CrossRef](#)] [[PubMed](#)]
- Zhukovsky, S.; White, J.; Chakraborty, R.; Costa, L.J.; Van Oekelen, O.; Sborov, D.W.; Cliff, E.R.S.; Mohyuddin, G.R. Multiple myeloma clinical trials exclude patients with the highest-risk disease: A systematic review of trial exclusion criteria. *Leuk. Lymphoma* **2024**, *65*, 2163–2172. [[CrossRef](#)]
- Wissel, M.; Poirier, M.; Satterwhite, C.; Lin, J.; Islam, R.; Zimmer, J.; Khadang, A.; Zemo, J.; Lester, T.; Fjording, M.; et al. Recommendations on qPCR/ddPCR assay validation by GCC. *Bioanalysis* **2022**, *14*, 853–863. [[CrossRef](#)] [[PubMed](#)]
- Yin, Y.; Yan, F.; Zhou, R.; Li, M.; Ma, J.; Liu, Z.; Ma, Z. Single-domain antibody screening by isPLA-seq. *Life Sci. Alliance* **2021**, *5*, e202101115. [[CrossRef](#)]
- Mesaki, K.; Yamamoto, H.; Juvet, S.; Yeung, J.; Guan, Z.; Akhter, A.; Yao, Y.; Dickie, C.; Mangat, H.; Wang, A.; et al. CRISPR-Cas Genome Editing in Ex Vivo Human Lungs to Rewire the Translational Path of Genome-Targeting Therapeutics. *Hum. Gene Ther.* **2024**, *35*, 374–387. [[CrossRef](#)]
- Ward, R.Y.; Stevens, M.; Bashir, S. Metrological traceability in flow cytometry? Evaluation of a new volumetric method for lymphocyte subsets. *Int. J. Lab. Hematol.* **2024**, *46*, 488–494. [[CrossRef](#)]
- Jain, N.; Zhao, Z.; Feucht, J.; Koche, R.; Iyer, A.; Dobrin, A.; Mansilla-Soto, J.; Yang, J.; Zhan, Y.; Lopez, M.; et al. TET2 guards against unchecked BATF3-induced CAR T cell expansion. *Nature* **2023**, *615*, 315–322. [[CrossRef](#)]
- Mannion, J.; Gifford, V.; Bellenie, B.; Fernando, W.; Ramos Garcia, L.; Wilson, R.; John, S.W.; Udainiya, S.; Patin, E.C.; Tiu, C.; et al. A RIPK1-specific PROTAC degrader achieves potent antitumor activity by enhancing immunogenic cell death. *Immunity* **2024**, *57*, 1514–1532.e15. [[CrossRef](#)]
- Li, Y.; Umbach, D.M.; Krahn, J.M.; Shats, I.; Li, X.; Li, L. Predicting tumor response to drugs based on gene-expression biomarkers of sensitivity learned from cancer cell lines. *BMC Genom.* **2021**, *22*, 272. [[CrossRef](#)]
- Bai, S.; Lin, Y.; Wang, X.; Zhang, X.; Yoshida, T.; Yue, X. A high security coding and anti-counterfeiting method based on the nonlinear magnetization response of superparamagnetic nanomaterials. *Sci. Rep.* **2024**, *14*, 15360. [[CrossRef](#)]
- Bohannan, Z.; Pudupakam, R.S.; Koo, J.; Horwitz, H.; Tsang, J.; Polley, A.; Han, E.J.; Fernandez, E.; Park, S.; Swartzfager, D.; et al. Predicting likelihood of in vivo chemotherapy response in canine lymphoma using ex vivo drug sensitivity and immunophenotyping data in a machine learning model. *Vet. Comp. Oncol.* **2021**, *19*, 160–171. [[CrossRef](#)]
- Wang, J.; Gleeson, P.A.; Fourriere, L. Long-term live cell imaging during differentiation of human iPSC-derived neurons. *STAR Protoc.* **2023**, *4*, 102699. [[CrossRef](#)] [[PubMed](#)]
- Surani, A.A.; Colombo, S.L.; Barlow, G.; Foulds, G.A.; Montiel-Duarte, C. Optimizing Cell Synchronization Using Nocodazole or Double Thymidine Block. *Methods Mol. Biol.* **2021**, *2329*, 111–121. [[PubMed](#)]
- Laforêts, F.; Kotantaki, P.; Malacrida, B.; Elorbany, S.; Manchanda, R.; Donnadiou, E.; Balkwill, F. Semi-supervised analysis of myeloid and T cell behavior in ex vivo ovarian tumor slices reveals changes in cell motility after treatments. *iScience* **2023**, *26*, 106514. [[CrossRef](#)] [[PubMed](#)]
- Brandenberg, N.; Hoehnel, S.; Kuttler, F.; Homicsko, K.; Ceroni, C.; Ringel, T.; Gjorevski, N.; Schwank, G.; Coukos, G.; Turcatti, G.; et al. High-throughput automated organoid culture via stem-cell aggregation in microcavity arrays. *Nat. Biomed. Eng.* **2020**, *4*, 863–874. [[CrossRef](#)]

18. Zhong, J.; Yang, D.; Zhou, Y.; Liang, M.; Ai, Y. Multi-frequency single cell electrical impedance measurement for label-free cell viability analysis. *Analyst* **2021**, *146*, 1848–1858. [[CrossRef](#)]
19. Persenaire, C.; Babbs, B.; Yamamoto, T.M.; Nebbia, M.; Jordan, K.R.; Adams, S.; Lambert, J.R.; Bitler, B.G. VDX-111, a novel small molecule, induces necroptosis to inhibit ovarian cancer progression. *Mol. Carcinog.* **2024**, *63*, 1248–1259. [[CrossRef](#)]
20. Little, A.C.; Kovalenko, I.; Goo, L.E.; Hong, H.S.; Kerk, S.A.; Yates, J.A.; Purohit, V.; Lombard, D.B.; Merajver, S.D.; Lyssiotis, C.A. High-content fluorescence imaging with the metabolic flux assay reveals insights into mitochondrial properties and functions. *Commun. Biol.* **2020**, *3*, 271. [[CrossRef](#)]
21. Geissler, M.; Ponton, A.; Nassif, C.; Malic, L.; Turcotte, K.; Lukic, L.; Morton, K.J.; Veres, T. Use of Polymer Micropillar Arrays as Templates for Solid-Phase Immunoassays. *ACS Appl. Polym. Mater.* **2022**, *4*, 5287–5297. [[CrossRef](#)]
22. Hasanvand, A. COVID-19 and the role of cytokines in this disease. *Inflammopharmacology* **2022**, *30*, 789–798. [[CrossRef](#)]
23. Cedillo-Alcantar, D.F.; Rodriguez-Moncayo, R.; Maravillas-Montero, J.L.; Garcia-Cordero, J.L. On-Chip Analysis of Protein Secretion from Single Cells Using Microbead Biosensors. *ACS Sens.* **2023**, *8*, 655–664. [[CrossRef](#)]
24. Furuya, H.; Sakatani, T.; Tanaka, S.; Murakami, K.; Waldron, R.T.; Hogrefe, W.; Rosser, C.J. Bladder cancer risk stratification with the Oncuria 10-plex bead-based urinalysis assay using three different Luminex xMAP instrumentation platforms. *J. Transl. Med.* **2024**, *22*, 8. [[CrossRef](#)]
25. Fagninou, A.; Nekoua, M.P.; Sossou, D.; Moutairou, K.; Fievet, N.; Yessoufou, A. Th2-Immune Polarizing and Anti-Inflammatory Properties of Insulin Are Not Effective in Type 2 Diabetic Pregnancy. *J. Immunol. Res.* **2020**, *2020*, 2038746. [[CrossRef](#)] [[PubMed](#)]
26. Mohammed, A.I.; Sangha, S.; Nguyen, H.; Shin, D.H.; Pan, M.; Park, H.; McCullough, M.J.; Celentano, A.; Cirillo, N. Assessment of Oxidative Stress Induced Oral Epithelial Toxicity. *Biomolecules* **2023**, *13*, 1239. [[CrossRef](#)] [[PubMed](#)]
27. Mbiki, S.; McClendon, J.; Alexander-Bryant, A.; Gilmore, J. Classifying changes in LN-18 glial cell morphology: A supervised machine learning approach to analyzing cell microscopy data via Fiji and WEKA. *Med. Biol. Eng. Comput.* **2020**, *58*, 1419–1430. [[CrossRef](#)] [[PubMed](#)]
28. Ülgen, M.; Can Eylem, C.; Doğan, A.; Akduman, N.E.B. Green Alternatives in Pharmaceutical and Bioanalytical Analysis of TDM Required Drugs: Procainamide. *Comb. Chem. High Throughput Screen.* **2023**, *26*, 2656–2667. [[CrossRef](#)]
29. Hollandi, R.; Moshkov, N.; Paavola, L.; Tasnadi, E.; Piccinini, F.; Horvath, P. Nucleus segmentation: Towards automated solutions. *Trends Cell Biol.* **2022**, *32*, 295–310. [[CrossRef](#)]
30. Ji, X.; Fisher, A.A.; Su, S.; Thorne, J.L.; Potter, B.; Lemey, P.; Baele, G.; Suchard, M.A. Scalable Bayesian divergence time estimation with ratio transformations. *Syst. Biol.* **2023**, *72*, 1136–1153. [[CrossRef](#)]
31. Ganapathy, K.; Lam, C.; Tsukuda, J.; Sargon, A.; Nava, A.; Harms, P.; Shen, A.; Barnard, G.; Misaghi, S. SPEED-MODE cell line development (CLD): Reducing Chinese hamster ovary (CHO) CLD timelines via earlier suspension adaptation and maximizing time spent in the exponential growth phase. *Biotechnol. Prog.* **2024**, *40*, e3479. [[CrossRef](#)]
32. Persson, S.; Berndt, C.; Engstrand, S.; Trinczek, A.; Carlsson, K.S.; Berntorp, E. Area under the curve: Comparing the value of factor VIII replacement therapies in haemophilia A. *Haemophilia* **2023**, *29*, 145–155. [[CrossRef](#)]
33. Lawlor, K.E.; Murphy, J.M.; Vince, J.E. Gasdermin and MLKL necrotic cell death effectors: Signaling and diseases. *Immunity* **2024**, *57*, 429–445. [[CrossRef](#)]
34. Yang, H.; Song, L.; Sun, B.; Chu, D.; Yang, L.; Li, M.; Li, H.; Dai, Y.; Yu, Z.; Guo, J. Modulation of macrophages by a paeoniflorin-loaded hyaluronic acid-based hydrogel promotes diabetic wound healing. *Mater. Today Bio* **2021**, *12*, 100139. [[CrossRef](#)]
35. Niu, Y.; Ferreira Azevedo, C.A.; Li, X.; Kamali, E.; Haagen Nielsen, O.; Storgaard Sørensen, C.; Frödin, M. Multiparametric and accurate functional analysis of genetic sequence variants using CRISPR-Select. *Nat. Genet.* **2022**, *54*, 1983–1993. [[CrossRef](#)] [[PubMed](#)]
36. Groeneweg, S.; van Geest, F.S.; Abaci, A.; Alcantud, A.; Ambegaonkar, G.P.; Armour, C.M.; Bakhtiani, P.; Barca, D.; Bertini, E.S.; van Beynum, I.M.; et al. Disease characteristics of MCT8 deficiency: An international, retrospective, multicentre cohort study. *Lancet Diabetes Endocrinol.* **2020**, *8*, 594–605. [[CrossRef](#)] [[PubMed](#)]
37. Watanabe, K.; Wilmanski, T.; Diener, C.; Earls, J.C.; Zimmer, A.; Lincoln, B.; Hadlock, J.J.; Lovejoy, J.C.; Gibbons, S.M.; Magis, A.T.; et al. Multiomic signatures of body mass index identify heterogeneous health phenotypes and responses to a lifestyle intervention. *Nat. Med.* **2023**, *29*, 996–1008. [[CrossRef](#)] [[PubMed](#)]
38. Zhao, J.; Wang, L.; Zhou, A.; Wen, S.; Fang, W.; Zhang, L.; Duan, J.; Bai, H.; Zhong, J.; Wan, R.; et al. Decision model for durable clinical benefit from front- or late-line immunotherapy alone or with chemotherapy in non-small cell lung cancer. *Med* **2024**, *5*, 981–997.e4. [[CrossRef](#)] [[PubMed](#)]
39. Ye, Y.; Yang, W.; Ruan, X.; Xu, L.; Cheng, W.; Zhao, M.; Wang, X.; Chen, X.; Cai, D.; Li, G.; et al. Metabolism-associated molecular classification of gastric adenocarcinoma. *Front. Oncol.* **2022**, *12*, 1024985. [[CrossRef](#)]
40. Robinson, J.P. Flow cytometry: Past and future. *Biotechniques* **2022**, *72*, 159–169. [[CrossRef](#)]
41. Eastern Research Group, Inc.; Sertkaya, A.; Berger, C. *Drug Development*; Office of the Assistant Secretary for Planning and Evaluation (ASPE): Washington, DC, USA, 2024.

42. Lin, W.; Fang, J.; Wei, S.; He, G.; Liu, J.; Li, X.; Peng, X.; Li, D.; Yang, S.; Li, X.; et al. Extracellular vesicle-cell adhesion molecules in tumours: Biofunctions and clinical applications. *Cell Commun. Signal.* **2023**, *21*, 246. [[CrossRef](#)]
43. Plebanek, M.P.; Xue, Y.; Nguyen, Y.V.; DeVito, N.C.; Wang, X.; Holtzhausen, A.; Beasley, G.M.; Theivanthiran, B.; Hanks, B.A. A lactate-SREBP2 signaling axis drives tolerogenic dendritic cell maturation and promotes cancer progression. *Sci. Immunol.* **2024**, *9*, eadi4191. [[CrossRef](#)]
44. Mahajan, U.M.; Oehrle, B.; Sirtl, S.; Alnatsha, A.; Goni, E.; Regel, I.; Beyer, G.; Vornhülz, M.; Vielhauer, J.; Chromik, A.; et al. Independent Validation and Assay Standardization of Improved Metabolic Biomarker Signature to Differentiate Pancreatic Ductal Adenocarcinoma from Chronic Pancreatitis. *Gastroenterology* **2022**, *163*, 1407–1422. [[CrossRef](#)] [[PubMed](#)]
45. Farin, H.F.; Mosa, M.H.; Ndreshkjana, B.; Grebbin, B.M.; Ritter, B.; Menche, C.; Kennel, K.B.; Ziegler, P.K.; Szabó, L.; Bollrath, J.; et al. Colorectal Cancer Organoid-Stroma Biobank Allows Subtype-Specific Assessment of Individualized Therapy Responses. *Cancer Discov.* **2023**, *13*, 2192–2211. [[CrossRef](#)] [[PubMed](#)]
46. Gallo, P.M.; Kim, J.; McEnerney, K.O.; Diorio, C.; Foley, C.; Kagami, L.; Wagner, K.; Petrosa, W.L.; Conlon, H.; Gollomp, K.L.; et al. Serum cytokine panels in pediatric clinical practice. *J. Allergy Clin. Immunol.* **2025**, *155*, 594–604.e5. [[CrossRef](#)] [[PubMed](#)]
47. Caller, T.; Rotem, I.; Shaihov-Teper, O.; Lendengolts, D.; Schary, Y.; Shai, R.; Glick-Saar, E.; Dominissini, D.; Motiei, M.; Katzir, I.; et al. Small Extracellular Vesicles from Infarcted and Failing Heart Accelerate Tumor Growth. *Circulation* **2024**, *149*, 1729–1748. [[CrossRef](#)]
48. Ghoshal, B.; Patkulkar, P.A.; Bhatt, P.; Rana, S.; Sinharay, S.; Jhunjhunwala, S. Neutrophil-Derived Extracellular Vesicles for Facile Delivery of Diagnostic Agents to Tumor Microenvironments. *ACS Appl. Bio Mater.* **2025**, *8*, 4132–4139. [[CrossRef](#)]
49. Istanbulgul, F.R.; Risvanli, A.; Salikov, R.; Bayraktar, M.; Kadiraliyeva, N.; Zhunushova, A.; Yilmaz, O.; Yuksel, B.F.; Turanli, M.; Uz, M.; et al. The relationship between Th1/Th2 cytokine polarization and milk composition in the postnatal period in Kyrgyz mares and foals. *Reprod. Domest. Anim.* **2023**, *58*, 762–768. [[CrossRef](#)]
50. Liao, Z.; Liu, Y.; Wei, H.; He, X.; Wang, Z.; Zhuang, Z.; Zhao, W.; Masagounder, K.; He, J.; Niu, J. Effects of dietary supplementation of *Bacillus subtilis* DSM 32315 on growth, immune response and acute ammonia stress tolerance of Nile tilapia (*Oreochromis niloticus*) fed with high or low protein diets. *Anim. Nutr.* **2023**, *15*, 375–385. [[CrossRef](#)]
51. Chen, X.; Gao, A.; Zhang, F.; Yang, Z.; Wang, S.; Fang, Y.; Li, J.; Wang, J.; Shi, W.; Wang, L.; et al. ILT4 inhibition prevents TAM- and dysfunctional T cell-mediated immunosuppression and enhances the efficacy of anti-PD-L1 therapy in NSCLC with EGFR activation. *Theranostics* **2021**, *11*, 3392–3416. [[CrossRef](#)]
52. Chen, H.; Deng, C.; Gao, J.; Wang, J.; Fu, F.; Wang, Y.; Wang, Q.; Zhang, M.; Zhang, S.; Fan, F.; et al. Integrative spatial analysis reveals tumor heterogeneity and immune colony niche related to clinical outcomes in small cell lung cancer. *Cancer Cell* **2025**, *43*, 519–536.e5. [[CrossRef](#)] [[PubMed](#)]
53. Nguyen, V.V.T.; Witwer, K.W.; Verhaar, M.C.; Strunk, D.; van Balkom, B.W.M. Functional assays to assess the therapeutic potential of extracellular vesicles. *J. Extracell. Vesicles* **2020**, *10*, e12033. [[CrossRef](#)] [[PubMed](#)]
54. Walton, M.K.; Cappelleri, J.C.; Byrom, B.; Goldsack, J.C.; Eremenco, S.; Harris, D.; Potero, E.; Patel, N.; Flood, E.; Daumer, M. Considerations for development of an evidence dossier to support the use of mobile sensor technology for clinical outcome assessments in clinical trials. *Contemp. Clin. Trials* **2020**, *91*, 105962. [[CrossRef](#)] [[PubMed](#)]
55. Garber, E.A.E.; Cho, C.Y.; Rallabhandi, P.; Nowatzke, W.L.; Oliver, K.G.; Venkateswaran, K.V.; Venkateswaran, N. Multi-laboratory validation of the xMAP-Food Allergen Detection Assay: A multiplex, antibody-based assay for the simultaneous detection of food allergens. *PLoS ONE* **2020**, *15*, e0234899. [[CrossRef](#)]
56. Maas, A.I.; Menon, D.K.; Manley, G.T.; Abrams, M.; Åkerlund, C.; Andelic, N.; Aries, M.; Bashford, T.; Bell, M.J.; Bodien, Y.G.; et al. Traumatic brain injury: Progress and challenges in prevention, clinical care, and research. *Lancet Neurol.* **2022**, *21*, 1004–1060. [[CrossRef](#)]
57. Gutiérrez-Sandoval, R.; Gutiérrez-Castro, F.; Muñoz-Godoy, N.; Rivadeneira, I.; Sobarzo, A.; Iturra, J.; Muñoz, I.; Peña-Vargas, C.; Vidal, M.; Krakowiak, F. Real-Time Functional Stratification of Tumor Cell Lines Using a Non-Cytotoxic Phospholipoproteomic Platform: A Label-Free Ex Vivo Model. *Biology* **2025**, *14*, 953. [[CrossRef](#)]
58. Malley, R.; Lu, Y.J.; Sebastian, S.; Zhang, F.; Willer, D.O. Multiple antigen presenting system (MAPS): State of the art and potential applications. *Expert Rev. Vaccines* **2024**, *23*, 196–204. [[CrossRef](#)]
59. Komar, Z.M.; Verkaik, N.S.; Dahmani, A.; Montaudon, E.; Kanaar, R.; Houtsmuller, A.B.; Jager, A.; Marangoni, E.; van Gent, D.C. Development and validation of a functional ex vivo paclitaxel and eribulin sensitivity assay for breast cancer, the REMIT assay. *NPJ Breast Cancer* **2025**, *11*, 17. [[CrossRef](#)]
60. Lin, B.; Watson, K. Luciferase reporter assay for NF-κB activation automated by an open-source liquid handling platform. *SLAS Technol.* **2024**, *29*, 100155. [[CrossRef](#)]
61. Heubeck, A.; Savage, A.; Henderson, K.; Roll, C.; Hernandez, V.; Torgerson, T.; Bumol, T.; Reading, J. Cross-platform immunophenotyping of human peripheral blood mononuclear cells with four high-dimensional flow cytometry panels. *Cytom. A* **2023**, *103*, 500–517. [[CrossRef](#)]

62. Rodríguez-Fuentes, D.E.; Fernández-Garza, L.E.; Samia-Meza, J.A.; Barrera-Barrera, S.A.; Caplan, A.I.; Barrera-Saldaña, H.A. Mesenchymal Stem Cells Current Clinical Applications: A Systematic Review. *Arch. Med. Res.* **2021**, *52*, 93–101. [\[CrossRef\]](#)
63. Campbell, P.; Rutten, F.H.; Lee, M.M.; Hawkins, N.M.; Petrie, M.C. Heart failure with preserved ejection fraction: Everything the clinician needs to know. *Lancet* **2024**, *403*, 1083–1092. [\[CrossRef\]](#)
64. Douin, D.J.; Siegel, L.; Grandits, G.; Phillips, A.; Aggarwal, N.R.; Baker, J.; Brown, S.M.; Chang, C.C.; Goodman, A.L.; Grund, B.; et al. Evaluating Primary Endpoints for COVID-19 Therapeutic Trials to Assess Recovery. *Am. J. Respir. Crit. Care Med.* **2022**, *206*, 730–739. [\[CrossRef\]](#)
65. Karikó, K. Developing mRNA for Therapy. *Keio J. Med.* **2022**, *71*, 31. [\[CrossRef\]](#)
66. Freitas, J.; Silva, P.; Perestrelo, R.; Vaz-Pires, P.; Câmara, J.S. Improved approach based on MALDI-TOF MS for establishment of the fish mucus protein pattern for geographic discrimination of *Sparus aurata*. *Food Chem.* **2022**, *372*, 131237. [\[CrossRef\]](#) [\[PubMed\]](#)
67. Koti, M.; Bivalacqua, T.; Black, P.C.; Cathomen, T.; Galsky, M.D.; Gulley, J.L.; Ingersoll, M.A.; Kamat, A.M.; Kassouf, W.; Siemens, D.R.; et al. Adaptive Immunity in Genitourinary Cancers. *Eur. Urol. Oncol.* **2023**, *6*, 263–272. [\[CrossRef\]](#) [\[PubMed\]](#)
68. Zaragoza-Salcedo, A.; Oroviogicoechea, C.; Saracibar-Razquin, M.I.; Osácar, E. The significance of exploring conceptual equivalence within the process of the cross-cultural adaptation of tools: The case of the Patient's Perception of Feeling Known by their Nurses Scale. *J. Nurs. Scholarsh.* **2023**, *55*, 1268–1279. [\[CrossRef\]](#) [\[PubMed\]](#)
69. Stefanos, R.; Graziella, D.; Giovanni, T. Methodological aspects of superiority, equivalence, and non-inferiority trials. *Intern. Emerg. Med.* **2020**, *15*, 1085–1091. [\[CrossRef\]](#)
70. Larsson, A.T.; Bhatia, H.; Calizo, A.; Pollard, K.; Zhang, X.; Conniff, E.; Tibbitts, J.F.; Rono, E.; Cummins, K.; Osum, S.H.; et al. Ex vivo to in vivo model of malignant peripheral nerve sheath tumors for precision oncology. *Neuro Oncol.* **2023**, *25*, 2044–2057. [\[CrossRef\]](#)
71. Liang, Z.; Hu, H.; Li, J.; Yao, D.; Wang, Y.; Ung, C.O.L. Advancing the Regulation of Traditional and Complementary Medicine Products: A Comparison of Five Regulatory Systems on Traditional Medicines with a Long History of Use. *Evid. Based Complement. Alternat. Med.* **2021**, *2021*, 5833945. [\[CrossRef\]](#)
72. Woodhouse, R.; Li, M.; Hughes, J.; Delfosse, D.; Skoletsky, J.; Ma, P.; Meng, W.; Dewal, N.; Milbury, C.; Clark, T.; et al. Clinical and analytical validation of FoundationOne Liquid CDx, a novel 324-Gene cfDNA-based comprehensive genomic profiling assay for cancers of solid tumor origin. *PLoS ONE* **2020**, *15*, e0237802. [\[CrossRef\]](#) [\[PubMed\]](#)
73. Manchikanti, L.; Centeno, C.J.; Atluri, S.; Albers, S.L.; Shapiro, S.; Malanga, G.A.; Abd-Elsayed, A.; Jerome, M.; Hirsch, J.A.; Kaye, A.D.; et al. Bone Marrow Concentrate (BMC) Therapy in Musculoskeletal Disorders: Evidence-Based Policy Position Statement of American Society of Interventional Pain Physicians (ASIPP). *Pain Physician* **2020**, *23*, E85–E131. [\[CrossRef\]](#) [\[PubMed\]](#)
74. Lau, C.; Jamali, F.; Loebenberg, R. Health Canada Usage of Real World Evidence (RWE) in Regulatory Decision Making compared with FDA/EMA usage based on publicly available information. *J. Pharm. Pharm. Sci.* **2022**, *25*, 227–236. [\[CrossRef\]](#) [\[PubMed\]](#)
75. Treherne, J.M.; Miller, A.F. Novel hydrogels: Are they poised to transform 3D cell-based assay systems in early drug discovery? *Expert Opin. Drug Discov.* **2023**, *18*, 335–346. [\[CrossRef\]](#)
76. Fernstad, J.; Svennberg, E.; Åberg, P.; Kemp Gudmundsdottir, K.; Jansson, A.; Engdahl, J. External validation of a machine learning-based classification algorithm for ambulatory heart rhythm diagnostics in pericardioversion atrial fibrillation patients using smartphone photoplethysmography: The SMARTBEATS-ALGO study. *Europace* **2025**, *27*, euaf031. [\[CrossRef\]](#)
77. Mohammad, A.; Yurina, A.; Simonyan, T.; Chistyakov, D.; Salman, R.; Zornikova, K.; Minina, E.; Bogolyubova, A. Modular (universal) CAR-T platforms in vivo: A comprehensive systematic review. *Front. Immunol.* **2024**, *15*, 1409665. [\[CrossRef\]](#)
78. Sinha, S.; Agarwal, M.; Bhadani, P.P.; Roy, R.; Sinha, U. Development and validation of sonological classification and scoring system for uterine adenomyosis: A pilot study. *F1000Research* **2023**, *11*, 1138. [\[CrossRef\]](#)
79. Swingle, K.L.; Hamilton, A.G.; Mitchell, M.J. Flow cytometric analysis of the murine placenta to evaluate nanoparticle platforms during pregnancy. *Placenta* **2024**, *66*, 132–138. [\[CrossRef\]](#)
80. Symeonides, C.; Aromataris, E.; Mulders, Y.; Dizon, J.; Stern, C.; Barker, T.H.; Whitehorn, A.; Pollock, D.; Marin, T.; Dunlop, S. An Umbrella Review of Meta-Analyses Evaluating Associations between Human Health and Exposure to Major Classes of Plastic-Associated Chemicals. *Ann. Glob. Health* **2024**, *90*, 52. [\[CrossRef\]](#)
81. Baldzhieva, A.; Burnusuzov, H.; Andreeva, H.; Kalfova, T.; Petrov, S.; Dudova, D.; Vaseva, K.; Murdjeva, M.; Taskov, H. Advancing measurable residual disease detection in pediatric BCP-ALL: Insights from novel immunophenotypic markers. *Int. J. Mol. Sci.* **2025**, *26*, 4282. [\[CrossRef\]](#)
82. Guilbert, M.; Courtade, E.; Thommen, Q. Cellular environment and phenotypic heterogeneity: How data-driven modeling finds the smoking gun. *Int. J. Mol. Sci.* **2022**, *23*, 6536. [\[CrossRef\]](#) [\[PubMed\]](#)
83. Srinivasan, A.; Sathiyathan, P.; Yin, L.; Liu, T.M.; Lam, A.; Ravikumar, M.; Smith, R.A.A.; Loh, H.P.; Zhang, Y.; Ling, L.; et al. Strategies to Enhance Immunomodulatory Properties and Reduce Heterogeneity in Mesenchymal Stromal Cells during ex vivo Expansion. *Cytotherapy* **2022**, *24*, 456–472. [\[CrossRef\]](#)
84. Patelli, N.; Mandrioli, M. Blockchain technology and traceability in the agrifood industry. *J. Food Sci.* **2020**, *85*, 3670–3678. [\[CrossRef\]](#) [\[PubMed\]](#)

85. Pourhassan, N.Z.; Smits, S.H.J.; Ahn, J.H.; Schmitt, L. Biotechnological applications of type 1 secretion systems. *Biotechnol. Adv.* **2021**, *53*, 107864. [[CrossRef](#)] [[PubMed](#)]
86. Graili, P.; Guertin, J.R.; Chan, K.K.W.; Tadrous, M. Integration of real-world evidence from different data sources in health technology assessment. *J. Pharm. Pharm. Sci.* **2023**, *26*, 11460. [[CrossRef](#)]
87. Salem, M.; Elkaseer, A.; El-Maddah, I.A.M.; Youssef, K.Y.; Scholz, S.G.; Mohamed, H.K. Non-Invasive Data Acquisition and IoT Solution for Human Vital Signs Monitoring: Applications, Limitations and Future Prospects. *Sensors* **2022**, *22*, 6625. [[CrossRef](#)]
88. Daly, B.; Brawley, O.W.; Gospodarowicz, M.K.; Olopade, O.I.; Fashoyin-Aje, L.; Smart, V.W.; Chang, I.F.; Tendler, C.L.; Kim, G.; Fuchs, C.S.; et al. Remote monitoring and data collection for decentralized clinical trials. *JAMA Netw. Open* **2024**, *7*, e246228. [[CrossRef](#)]
89. Childers, C.; Marron, J.; Meyer, E.C.; Abel, G.A. Clinical ethics consultation documentation in the era of open notes. *BMC Med. Ethics* **2023**, *24*, 27. [[CrossRef](#)]

Disclaimer/Publisher’s Note: The statements, opinions and data contained in all publications are solely those of the individual author(s) and contributor(s) and not of MDPI and/or the editor(s). MDPI and/or the editor(s) disclaim responsibility for any injury to people or property resulting from any ideas, methods, instructions or products referred to in the content.